

---

# Copper-Containing Ionic Liquids for the Separation of Carbon Monoxide from Gas Mixtures



The  
University  
Of  
Sheffield.

**Liam James Woodhead**

A Thesis Submitted for the Degree of Doctor of Philosophy

Department of Chemistry

University of Sheffield

September 2019

---

## Summary

**Chapter 1** introduces the usefulness of CO as a feedstock for industrial catalytic reactions and outlines some of the current CO purification techniques. The use of copper(I) salts in ILs as a purification technology is explored and the reversible binding of CO to Cu(I) is discussed. The aims of the project are outlined.

**Chapter 2** reports the methods used to synthesise various ionic liquids and copper(I) salts and their subsequent combination to form the target copper(I)-containing ILs. The methodology of the instrumentation was recorded and characterisation details obtained.

**Chapter 3** details the synthesis of copper(I)-containing ILs from 1-alkyl-3-methyl imidazolium salts with weakly coordinating anions. Their physical properties such as density and viscosity are assessed and reversible reactions with CO are demonstrated using high-pressure infrared spectroscopy. The formation of copper monocarbonyl and dicarbonyl complexes formed is discussed.

**Chapter 4** outlines the synthesis of copper(I)-containing ILs based on imidazolium cations functionalised with ether or highly fluorinated substituents. Properties such as viscosity, density and CO uptake of these systems are compared to the non-functionalised analogues.

**Chapter 5** describes the use of copper-containing ILs with weakly coordinating anions to separate CO from gas mixtures containing H<sub>2</sub> and N<sub>2</sub>. Comparisons to the free halide systems are drawn and

---

implications for potential commercial use are discussed. Their ability to separate CO from other gases such as CH<sub>4</sub> and CO<sub>2</sub> is also discussed with reference to literature solubility data.

**Chapter 6** explores the use of high-boiling point co-solvents (e.g. dimethyl malonate or dimethyl glutarate) in conjunction with the copper-containing ILs to reduce the viscosity of the mixture. The stability of the copper species and the effect on properties such as viscosity, copper concentration and density are investigated. The use of these mixtures to separate CO from H<sub>2</sub> and N<sub>2</sub> is explored.

**Chapter 7** gives the overall conclusions to the project and suggestions for future work.

**Appendices** include supplementary spectroscopic and experimental data.

---

## Acknowledgements

I am extremely grateful to my supervisor Dr. Anthony Haynes for the opportunity to work in his group and for all the support and guidance throughout the project.

I would also like to thank my industrial supervisor Dr. Dave Law for the advice and to all of my BP colleagues who sat in on meetings for the interesting discussions.

A massive thank you to all the staff in the department for their invaluable assistance throughout my project. I'd like to thank Rob Hanson for help with gas chromatography, Simon Thorpe for mass spectrometry, Stephen Atkin for elemental analysis, Keith Owen and Richard Wilkinson for help managing the CO systems and Pete and Nick in stores who always had time for a chat.

To the Haynes group members Dave Griffin and Sam Ivko, the fellow founding members of the Burritrio, thank you for the chemistry support but more importantly the friendship. D35 always had the biggest tunes and bantz whilst also a place to discuss our next sdm and our collective love of scented candles. Name a more iconic trio, I'll wait.

I am forever thankful for the friends made along the way or the 'PhDivas': Alex James could make any song his, James Railton (even though you dropped me), Phil Reeve (Phil Reeve), Jenna Spencer-Briggs, Sally Morton, Andy Saddlecakes, Heather Carson (Keith), Stephen Doddy, once rage cage has been experienced, it bonds for life, Matt Dwyer, Tom Roseveare, Jon Shewring, Liam Marshall and Eren Slate. Thanks to all the tea at 3 people for the much needed break and to the Tuesday footballers (Vamonos la Crystal Phallus!).

Lastly, I'd like to thank my family. Alice has provided nothing but love and support throughout and I look forward to the next chapter. Paul, my best friend and the best brother a guy could ask for. Finally, to mum and dad, thanks for all the tremendous support throughout, I hope I have done you proud.

---

## Abbreviations

---

Chemicals	
DBE	Dibasic Ester
DMG	Dimethyl Glutarate
DMM	Dimethyl Malonate
DMSO	Dimethyl sulfoxide
NBS	N-bromosuccinimide
tol	Toluene

---

Ionic Liquid Cations	
$[C_n\text{mim}]^+$	1-alkyl-3-methylimidazolium
$[C_3O_1\text{mim}]^+$	1-(2-methoxyethyl)-3-methylimidazolium
$[C_2(O_1C_2)_2\text{mim}]^+$	1-(2,2-diethoxyethyl)-3-methylimidazolium
$[C^F_4C_2\text{mim}]^+$	1-(1,1,1,2,2,3,3,4,4-nonafluorohexyl)-3-methylimidazolium
$[C^F_6C_2\text{mim}]^+$	1-(1,1,1,2,2,3,3,4,4,5,5,6,6-tridecafluorooctyl)-3-methylimidazolium

---

Ionic Liquid Anions	
$\text{AcO}^-$	Acetate
$\text{TFA}^-$	Trifluoroacetate
$\text{OTf}^-$	Trifluoromethane sulfonate
$\text{NTf}_2^-$	bis(trifluoromethane)sulfonimide

---

Alkyl Groups	
Me	Methyl
Et	Ethyl

---

Bu	n-Butyl
Hex	n-Hexyl
Instrumentation	
ATR	Attenuated Total Reflectance
CIR	Cylindrical Internal Reflectance
ES-MS	Electrospray Mass Spectrometry
FTIR	Fourier Transform Infrared
GC	Gas Chromatography
HPIR	High Pressure Infrared
IR	Infrared
NMR	Nuclear Magnetic Resonance
TCD	Thermal Conductivity Detector
TOF	Time-of-flight
General	
eq	Equivalent
equ	Equilibrium
IL	Ionic Liquids
MOF	Metal Organic Framework
RTIL	Room Temperature Ionic Liquids
Quantitative Parameters	
$K_H$	Henry's Law Constant
$\eta$	Viscosity
$\nu(\text{CO})$	Carbonyl Stretching Frequency
ppm	Parts per million
$\rho$	Density

---

---

NMR Spectroscopy

---

s	Singlet
d	Doublet
t	Triplet
q	Quartet
qu	Quintet
m	multiplet
tt	triplet of triplets

---

---

<b>1. Introduction .....</b>	<b>1</b>
1.1 Carbon Monoxide Applications in Catalysis.....	2
1.2 Routes to Carbon Monoxide Production .....	5
1.3 Established Processes for CO Purification .....	6
1.3.1 Cryogenic Distillation .....	6
1.3.2 Separation by Absorption .....	7
1.4 Solid-State CO Adsorption .....	10
1.4.1 CO Purification using Zeolites .....	10
1.4.2 CO Purification using Metal-Organic Frameworks.....	11
1.4.3 CO Purification using Activated Carbons .....	11
1.5 Ionic Liquids .....	12
1.5.1 Typical Ionic Liquids .....	13
1.5.2 General Properties of Ionic Liquids.....	15
1.5.3 Solubility of Gases in Ionic Liquids .....	18
1.6 Copper(I) Carbonyl Chemistry.....	20
1.7 Copper-Containing Ionic Liquids and Deep Eutectic Mixtures .....	22
1.8 Recent developments in CO separation using Cu(I) containing ionic liquids.....	25
1.9 Potential use of Copper Containing Ionic Liquids in a Large Scale Process for CO Purification .	30
1.10 Project Aims .....	31
1.11 References .....	33
<b>2. Experimental.....</b>	<b>40</b>
2.1 Instrumentation .....	41

---

2.2 Viscosity measurements .....	41
2.3 Low Pressure CO Absorption Studies.....	42
2.4 High Pressure CO Absorption Studies .....	42
2.5 Gas Enrichment Studies .....	44
2.6 Gas Chromatography Measurements.....	45
2.7 Solvents and Reagents .....	45
2.8 Gaseous Reagents .....	46
2.9 Synthetic Procedures .....	46
2.9.1 Synthesis of 1-alkyl-3methylimidazolium Halide Salts.....	46
2.9.2 Synthesis of Non-Halide Ionic Liquids .....	55
2.9.3 Synthesis of Copper(I) Salts.....	72
2.9.4 Synthesis of Copper-Containing Ionic Liquids <sup>1,18</sup> .....	73
[C <sub>6</sub> mim][CuBr <sub>2</sub> ] <sup>1</sup> .....	74
[C <sub>3</sub> O <sub>1</sub> mim][CuBr <sub>2</sub> ].....	74
[C <sub>2</sub> (O <sub>1</sub> C <sub>2</sub> ) <sub>2</sub> mim][CuBr <sub>2</sub> ] .....	74
2.9.5 Synthesis of Copper-Containing Ionic Liquid/Dibasic Ester Mixtures.....	77
2.10 References .....	81
<b>3. Copper-Containing Ionic Liquids with Weakly Coordinating Anions .....</b>	<b>83</b>
3.1 Introduction .....	84
3.2 Synthesis of Ionic Liquid Precursors.....	84
3.3 Synthesis of Copper(I) Precursors .....	85
3.4 Synthesis of Copper(I) Containing Ionic Liquids.....	86

---

3.5 Density Measurements .....	91
3.6 Viscosity Measurements .....	92
3.7 Low-Pressure CO Reactions .....	99
3.8 <i>In Situ</i> High Pressure Infrared Studies of OTf <sup>-</sup> and NTf <sub>2</sub> <sup>-</sup> Systems .....	101
3.8.1 Absorption of CO by [C <sub>n</sub> mim][Cu(NCMe)(OTf)(X)] Ionic Liquids .....	102
3.8.2 CO Uptake at equilibrium.....	107
3.8.3 Rate of CO Uptake.....	111
3.8.4 Speciation of Copper Carbonyl Complexes .....	113
3.9 Conclusions .....	119
3.10 References .....	120
<b>4. Functionalised Imidazolium Ionic Liquids.....</b>	<b>122</b>
4.1 Introduction .....	123
4.2 Synthesis and Characterisation of Functionalised Imidazolium Ionic Liquids .....	123
4.3 Copper-Containing Functionalised Imidazolium Ionic Liquids.....	127
4.4 Density Measurements .....	129
4.5 Viscosity Measurements .....	130
4.6 Low-Pressure CO Reactions .....	132
4.7 <i>In Situ</i> High-Pressure Infrared Studies .....	133
4.7.1 [C <sub>n</sub> mim][CuBr <sub>2</sub> ] .....	134
4.7.2 [C <sub>n</sub> mim][Cu(NCMe)(OTf) <sub>2</sub> ].....	136
4.7.3 [C <sub>n</sub> mim][Cu(NCMe)(OTf)(NTf <sub>2</sub> )] .....	138
4.8 Conclusions .....	141

---

4.9	References .....	143
<b>5.</b>	<b>Separation of CO from N<sub>2</sub> and H<sub>2</sub> Using Copper(I) Containing Ionic Liquids.....</b>	<b>145</b>
5.1	Introduction .....	146
5.2	Analysis of composition of gas mixtures.....	146
5.3	CO Enrichment Studies using Copper(I) Containing Ionic Liquids.....	149
5.4	Enrichment Studies Using [C <sub>2</sub> mim][Cu(NCMe)(OTf)(NTf <sub>2</sub> )] .....	150
5.4.1	CO Enrichment from CO/N <sub>2</sub> .....	150
5.4.2	CO Enrichment from CO/H <sub>2</sub> .....	156
5.5	Enrichment Studies Using [C <sub>6</sub> mim][Cu(NCMe)(OTf) <sub>2</sub> ] .....	159
5.5.1	CO Enrichment from CO/N <sub>2</sub> .....	159
5.5.2	CO Enrichment from CO/H <sub>2</sub> .....	161
5.6	Comparisons with Halide Ionic Liquids and Implications for Commercial Use.....	161
5.7	CO Enrichment Studies Using Functionalised Imidazolium Copper Containing Ionic Liquids ..	165
5.7.2	CO Enrichment from CO/X <sub>2</sub> .....	165
5.8	Discussion of Potential Separation of CO/X mixtures.....	167
5.9	Conclusions .....	170
5.9	References .....	171
<b>6.</b>	<b>Ionic Liquid Co-Solvent Mixtures .....</b>	<b>172</b>
6.1	Introduction .....	173
6.2	Copper Containing Ionic Liquid / Dibasic Ester Co-Solvent Mixtures .....	174
6.2.1	Synthesis and Copper Stability.....	174
6.2.2	Density Measurements .....	176

---

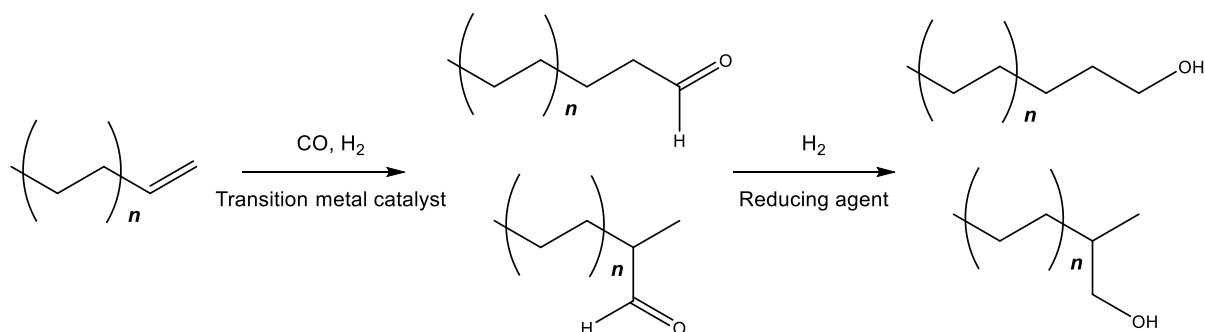
6.2.3 Viscosity Measurements .....	177
6.2.4 Low-Pressure CO Reactions .....	181
6.2.5 <i>In Situ</i> High-Pressure Infrared Studies .....	183
6.2.6 [C <sub>6</sub> mim][CuBr <sub>2</sub> ].DMG vs [C <sub>n</sub> mim][Cu(NCMe)(OTf)(X)].DMG vs co-mixtures.....	193
6.3 Enrichment Studies Using [C <sub>6</sub> mim][CuBr <sub>2</sub> ].DMM Mixtures .....	194
6.3.1 CO Enrichment from CO/X <sub>2</sub> .....	194
6.4 CO Enrichment Using [C <sub>n</sub> mim][Cu(NCMe)(OTf)(X)].DMM Where X = OTf, NTf <sub>2</sub> .....	195
6.4.1 CO/X <sub>2</sub> Separations.....	195
6.5 Conclusions .....	198
6.6 References .....	200
<b>7. Overall Conclusions and Future Work.....</b>	<b>201</b>
7.1 Conclusions .....	202
7.2 Future Work .....	203
<b>8. Appendix.....</b>	<b>205</b>
8.1 Sample IR Spectra .....	206
8.1.1 Neat Copper-Containing Ionic Liquids .....	206
8.1.2. Copper-Containing Ionic Liquid/DBE Mixtures .....	216
8.2 HPIR Spectra.....	217
8.3 CO/X <sub>2</sub> Enrichment Data.....	221

# 1. Introduction

## 1.1 Carbon Monoxide Applications in Catalysis

Carbon monoxide is an essential starting material in the synthesis of some large-scale, high-value compounds, including aldehydes,<sup>1</sup> alcohols, isocyanates<sup>2</sup> and acetic acid.<sup>3</sup> Moreover, in some cases, it is essential that a pure CO feedstock is used as impurities can lead to side reactions or lower CO partial pressures, which lead to a loss in efficiency.

Scheme 1.1 gives an outline of the hydroformylation process, in which aldehydes and/or alcohols are produced from the reaction of alkenes with CO and H<sub>2</sub> using a homogeneous transition-metal catalyst such as cobalt or rhodium. The long-chain alcohol products are utilised in the detergent industry. Catalyst poisons for such a process are oxygen and carbon dioxide, the latter being a common gas that would be present if the CO was obtained from flue gases, meaning that a purification step would be required.



**Scheme 1.1.** Hydroformylation of alkenes.

Methanol is produced industrially through the catalytic conversion of synthesis gas, a gaseous mixture of H<sub>2</sub> and CO. The catalyst used is typically Cu/ZnO at around 300 °C and 100 bar pressure.<sup>4-6</sup> Methanol is consumed at an estimated rate of 100 Mt per year,<sup>7,8</sup> including as a reactant in the production of formaldehyde, MTBE (methyl tert-butyl ether) and acetic acid, with the latter also requiring CO as a feedstock which will be examined later in this section.

The Fischer-Tropsch process is another chemical reaction which utilises CO and H<sub>2</sub> and converts them into long chain hydrocarbons.<sup>9,10</sup> Various metals show activity towards the hydrogenation of CO particularly those from groups VIII and IX with the most common commercial catalysts being based on iron or cobalt. Although ruthenium is shown to be the most active Fischer-Tropsch catalyst, its high price has limited its use in practical Fischer-Tropsch processes.

Phosgene is an important industrial reagent used in the preparation of other organic compounds such as isocyanates. It is produced by passing a pure CO feedstock and Cl<sub>2</sub> gas over an activated charcoal catalyst (Scheme 1.2). Isocyanates are precursors to numerous polymers, including polyurethane foam, of which 17.9 million tonnes are consumed annually.<sup>11</sup>



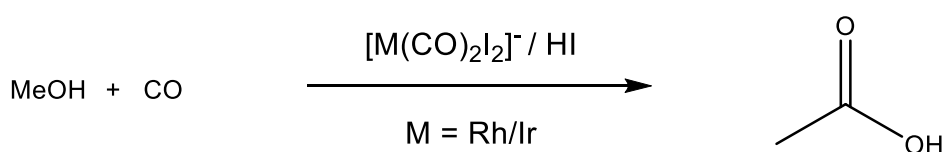
**Scheme 1.2.** Reaction scheme for the production of phosgene.

Methanol carbonylation to form acetic acid is another process which requires a pure CO feedstock to operate. The acetic acid product has a wide range of applications, from a raw material used in vinyl acetate monomer synthesis, to being a solvent in the synthesis of terephthalic acid. Global consumption of acetic acid is approximately 12.9 million tonnes per year and thus acetic acid synthesis is an important reaction.<sup>12</sup>

Commercialisation of methanol carbonylation to form acetic acid was first developed by BASF in the early 1960s using an iodide-promoted cobalt-based process.<sup>13</sup> The process required high temperatures and pressures (230 °C and 6.0 – 8.0 MPa) and gave a selectivity of 90 % based on the methanol reactant.

Improvement upon the BASF process came through the Monsanto process<sup>14–16</sup> developed in 1966 and later the Cativa process developed by BP in 1996. Scheme 1.3 shows the scheme for both catalysts

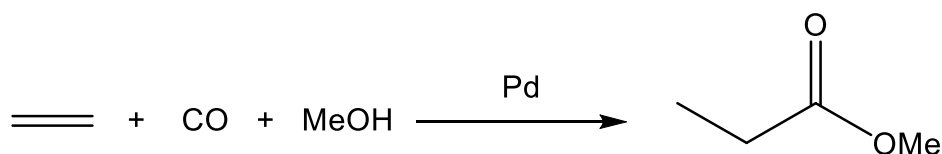
which are based on  $[M(\text{CO})_2\text{I}_2]^-$ , where  $M = \text{Rh}$  or  $\text{Ir}$ .<sup>17,18</sup> The Monsanto process used a rhodium catalyst which gave acetic acid with a selectivity of >99 % based on methanol. However, based on CO, selectivity was about 85 % owing to the competing water-gas shift reaction. Moreover, much milder conditions relative to the BASF process were possible through using the heavier group 9 metals. The Cativa process uses an iridium/iodide catalyst and offered significant improvements over Monsanto, most predominantly catalyst stability, high rate of reaction and improved yield based on carbon monoxide.<sup>3,19</sup>



**Scheme 1.3.** Reaction scheme for the metal catalysed carbonylation of methanol to produce acetic acid.

Low partial pressure of CO has a negative effect on the reaction rate of this process, and gas impurities such as  $\text{H}_2$  can lead to side reactions. Such observations highlight the importance of using a pure CO feedstock.

Methoxycarbonylation of alkenes in the Lucite process (or alkynes to form methacrylates) are other examples of processes which require a pure CO feedstock.<sup>20-22</sup> Scheme 1.4 shows how palladium is used as the transition metal catalyst in the commercialised Lucite process.



**Scheme 1.4.** Reaction scheme for the formation of methyl propionate in the Lucite process.

## 1.2 Routes to Carbon Monoxide Production

For most commercial processes, CO originates from syngas, which is produced synthetically from fossil fuels, mostly natural gas. Although mainly composed of a mixture of CO and H<sub>2</sub>, impurities such as CO<sub>2</sub> and H<sub>2</sub>O are common as well as CH<sub>4</sub> or N<sub>2</sub>. Such industrial routes to syngas are steam-methane reformation (eq 1) and the partial oxidation of methane (eq 2).



Another source of CO is to recover it from flue gases of industrial processes. These usually contain large amounts and varying compositions of CO<sub>2</sub> and N<sub>2</sub> depending on which process it has been sourced from.<sup>23</sup> Blast furnace gas generated from the reduction of iron ore with coke to produce metallic iron typically offers 20 % CO for recovery. Moreover, the converter gas created from pig iron during the steel production process has large amounts of CO, in excess of 65 %. The tail gas from yellow phosphorus also contains large amounts of CO, 90 – 95 %<sup>24</sup> and therefore these processes exhibit an opportunity to capture CO to become economically viable for use.<sup>25</sup> Table 1.1 presents a summary of the flue gas composition of some industrial processes. In addition, CO is a toxic gas and therefore, from an environmental point of view, it is imperative the CO is not released into the atmosphere.

**Table 1.1.** Volume % of high CO containing flue gases of some industrial processes. COG = Coke oven gas; BFG = Blast furnace gas; CG = Converter gas

Gas	Iron and Steel Manufacturing <sup>25</sup>			Carbon Black	Yellow Phosphorus <sup>24</sup>
	COG	BFG	CG		
CO	6	20	65+	6 – 12	90 – 95
H <sub>2</sub>	50 – 60	2 – 5	1	6 – 14	3 – 5
CO <sub>2</sub>	2	12	15 – 20	1.5 – 4	2 – 4
CH <sub>4</sub>	15 - 50	0.2		0.1 – 0.8	0.4
N <sub>2</sub>		balance	15 – 20	32 – 46	3 – 5
H <sub>2</sub> O				29 - 50	

Overall therefore, when pure CO is required for reasons outlined in the previous section, invariably it needs to be separated from gases such as N<sub>2</sub>, CO<sub>2</sub> and H<sub>2</sub> as well as other impurities such as CH<sub>4</sub>, O<sub>2</sub> and H<sub>2</sub>O.

### 1.3 Established Processes for CO Purification

#### 1.3.1 Cryogenic Distillation

Cryogenic distillation is a common and widespread method to separate gas mixtures. It works by cooling gases down to their liquid phase, with separation being dependent on the differences in boiling point of the components. Operation consequently requires high energy consumption due to the cryogenic temperatures. This method is common when separating CO from mixtures with H<sub>2</sub> and leads to high purity of each.<sup>26,27</sup> Syngas purification is possible via this method with CO<sub>2</sub>, CH<sub>4</sub> and H<sub>2</sub>O being

relatively easily removed due to the low temperatures coupled with acid gas removal systems and gas scrubbers when necessary.

Separation of CO/N<sub>2</sub> mixtures is poor via this method as the boiling points of the respective gases only differ by about 5 K. Depending on the source of syngas feedstock, the N<sub>2</sub> concentration could vary quite a lot and if the desired application cannot operate with such levels of N<sub>2</sub> present, further processing is required to reduce the N<sub>2</sub> concentration.

### 1.3.2 Separation by Absorption

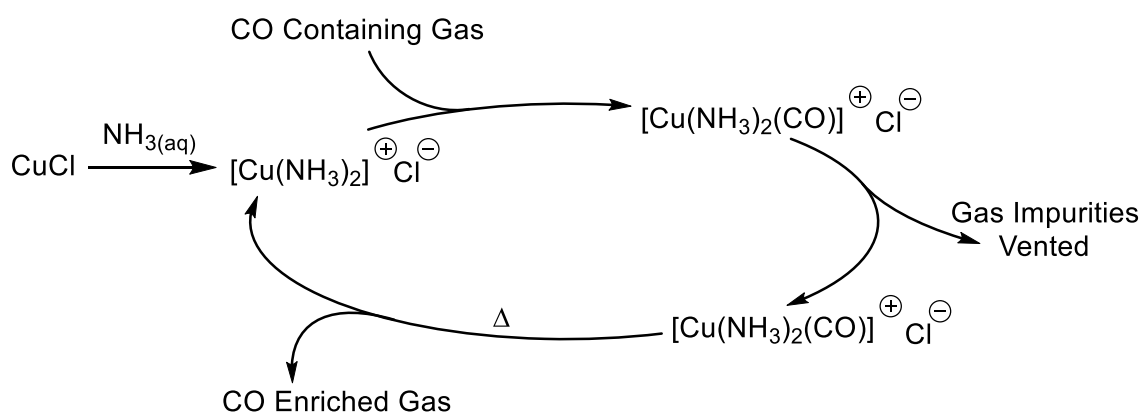
An alternative to cryogenic distillation methods is the reversible adsorption of CO to transition metals, particularly copper. These processes rely on the specific interactions that CO makes with transition metals. Figure 1.1 illustrates how CO gives weak  $\sigma$  donation to the metal, while synergistic back donation arises from the filled metal d-orbitals donating electron density into the empty  $\pi^*$  orbitals of the CO ligand. This helps to strengthen the metal-carbon bond but weaken the carbon-oxygen bond. Since the carbon-oxygen bond is very sensitive to the amount of back-donation, and CO gives a strong characteristic absorption due to the C-O stretching vibration, the use of infrared spectroscopy is a useful tool to probe such species. Copper carbonyl complexes and why copper is regularly the transition metal of choice will be discussed in more detail in section 1.6.



**Figure 1.1.** Orbital interactions involved in the binding of CO to transition metals.

**Ammoniacal Copper Liquor Process**

Scheme 1.5 shows the overall cycle for the ammoniacal copper liquor process, which is an example of a liquid-phase CO absorption process.<sup>28</sup> Aqueous NH<sub>3</sub> is the solvent, which dramatically increases the solubility of copper salts over water alone, due to the formation of cationic complexes such as Cu(NH<sub>3</sub>)<sub>2</sub><sup>+</sup>. The copper source is usually CuCl.



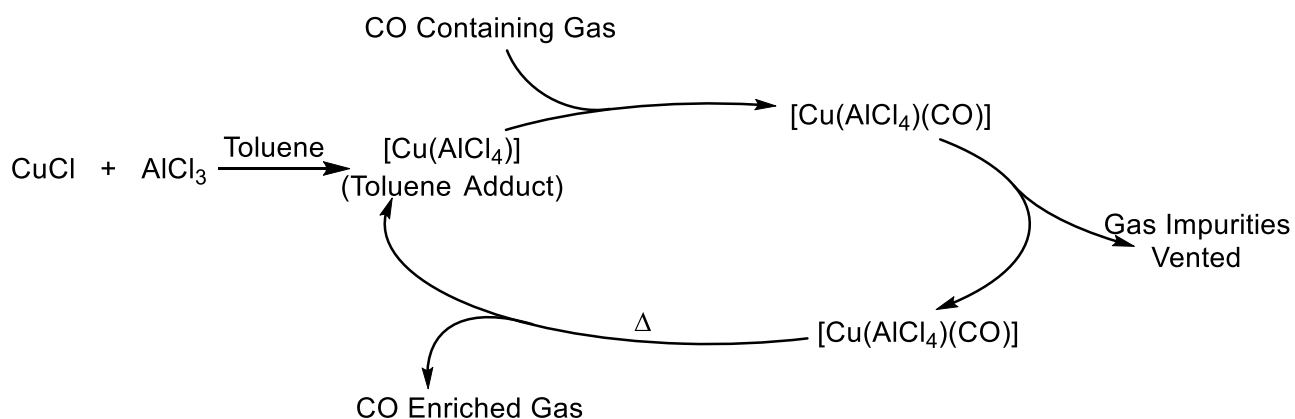
**Scheme 1.5.** Ammoniacal copper liquor cycle used for the purification of CO containing gas mixtures.

The CO is introduced into the solution and is selectively bound from the other gas to form a metal carbonyl. The gas impurities are then vented from the system. Finally, by applying heat to the solution, the metal-carbon bond is broken and the CO can be collected as an enriched gas source.

Issues with this approach are that the aqueous ammonia solution is inherently corrosive and therefore requires expensive, non-corrosive elements to be required when designing the plant. Moreover, during the desorption step, the vapour pressure at this temperature is significant and therefore the CO can be contaminated by H<sub>2</sub>O or NH<sub>3</sub> which requires a further scrubber to be used in order to give pure CO.

**The COSORB Process**

The COSORB process is another example of a liquid-based CO absorption process which was developed by Tenneco Chemicals in the early 1970s. In this process, the organic solvent is toluene and the active copper species is formed from CuCl and AlCl<sub>3</sub>.<sup>29</sup> Scheme 1.6 demonstrates the overall cycle which is analogous to the ammoniacal copper liquor process. The recovery of CO can be >99 % and the purity usually greater than 98 mol %.<sup>30</sup>



**Scheme 1.6.** COSORB cycle for the purification of CO containing gas mixtures.

Some common impurities found in flue gases such as H<sub>2</sub>O and H<sub>2</sub>S are detrimental to this process so must be removed in pre-treatment.<sup>31</sup> The presence of H<sub>2</sub>O and H<sub>2</sub>S leads to detrimental side reactions as well as the formation of HCl. Therefore, expensive anti-corrosive metals need to be employed and moreover, the acidic conditions lead to the disproportionation of the Cu<sup>+</sup> and loss of efficiency. As for the ammoniacal copper liquor process, the solvent can evaporate during the desorption step and contaminate the output CO gas.

Other systems have been developed based on the COSORB system such as COSORB II<sup>TM</sup> and COPure<sup>SM</sup>.<sup>32,33</sup> The COPure<sup>SM</sup> technology is claimed to be able to separate CO from gas mixtures containing CH<sub>4</sub> and N<sub>2</sub>, but also CO<sub>2</sub> which is particularly impressive given that CO<sub>2</sub> is considerably more soluble than CO in most common organic solvents.

## 1.4 Solid-State CO Adsorption

It is also possible to separate CO from gas mixtures through adsorption rather than absorption. Adsorption processes use porous, solid-state materials such as: zeolites, metal-organic frameworks (MOFs), activated carbons and activated alumina. They have emerged as potential promising targets for gas separations and storage due to their high porosity, large surface area and tuneable properties.

### 1.4.1 CO Purification using Zeolites

Zeolites are solid-state porous materials based on aluminosilicates with excellent chemical and thermal stability.<sup>34</sup> These materials have been proposed for CO purification with exchange of the metal cations to alkali metals or alkali earth metals which help to improve CO uptake and selectivity.<sup>35-37</sup> The uptake of CO was found to decrease as the cation size was increased going down the group for the alkali metals. This was attributed to the weakened electrostatic interaction of the CO with the metal ion due to the increased cation radius. It was also noted that the alkali earth metals proved to be more receptive to CO uptake over alkali metals.<sup>36</sup>

Wang *et al.* used zeolite-Y-supported CuCl to purify CO containing gas mixtures.<sup>38</sup> The zeolite was prepared by dispersing a monolayer of CuCl<sub>2</sub> which was then activated by reducing Cu(II) to Cu(I) at 663 K with CO. The resulting material showed high CO adsorption, as well as high selectivities with

respect to other gases such as N<sub>2</sub>, CH<sub>4</sub> and CO<sub>2</sub>. The reversibility of CO binding was also shown to be good as the heat of adsorption,  $\Delta H$ , was recorded at -43 kJ mol<sup>-1</sup>. Compared to the established COSORB process, which has a  $\Delta H$  of -67 kJ mol<sup>-1</sup>, indicates the CO complexation is more labile.<sup>39</sup>

#### 1.4.2 CO Purification using Metal-Organic Frameworks

Metal-organic frameworks (MOFs) are crystalline materials made up of inorganic metal nodes and organic linkers.<sup>40-43</sup> As for the liquid phase CO separation technologies, chemical complexation to copper(I) has been exploited in order to capture CO.

One route for CO separation has been to synthesise MOFs and then introduce CO adsorption sites, such as copper(I), by metal impregnation to increase the CO adsorption capacity.<sup>44,45</sup> Wang *et al.* used the COSORB solution as a way to post synthetically introduce copper(I) sites into a MIL-101 MOF. The MOF was treated with the COSORB solution and the toluene was removed under vacuum to leave the AlCuCl<sub>4</sub> impregnated inside the pores. Like its liquid-phase analogue, the impregnated MOF showed excellent selectivity for binding CO over N<sub>2</sub> whilst also showing improved stability. Not only does the introduction of copper(I) help to preferentially bind CO, but the presence of the AlCuCl<sub>4</sub> in the pore reduces the volume available for common gas impurities such as N<sub>2</sub>. This is another factor in determining the improved selectivity of CO/N<sub>2</sub> mixtures.

#### 1.4.3 CO Purification using Activated Carbons

Activated carbon (AC) is a form of carbon which has been processed to increase the surface area of the available pores, which is useful for gas adsorption.<sup>46</sup> Li *et al.* impregnated AC with aqueous solutions of copper(II) chloride and copper(II) carboxylate which could then be reduced to Cu(I).<sup>47</sup> The

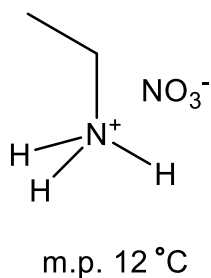
result was that highly dispersed CuCl on AC allowed for a stoichiometric amount of CO to coordinate to the copper(I). This enabled high adsorption capacity of CO and good CO selectivities to be achieved from gas mixtures containing CO<sub>2</sub>, CH<sub>4</sub> and N<sub>2</sub> by pressure swing adsorption.

## 1.5 Ionic Liquids

As previously mentioned, a drawback to some of the established CO purification methods is the contamination of the output CO gas by the volatile solvent. ILs are a class of compound which have a negligible vapour pressure due to electrostatic interactions between the component ions. Therefore, use of an IL solvent medium would eliminate this problem.

ILs are liquids that are composed completely of ions, in common with simple salts (e.g. NaCl) when heated to high temperatures. ILs are generally defined as salts having a melting point below 100 °C. This is usually achieved by using cations which are large, unsymmetrical, able to delocalise charge and have conformational flexibility. These criteria are employed to disrupt packing efficiency which leads to small lattice enthalpy.<sup>48</sup> An increase in entropy when going from solid to liquid also supports the preference for the liquid phase.

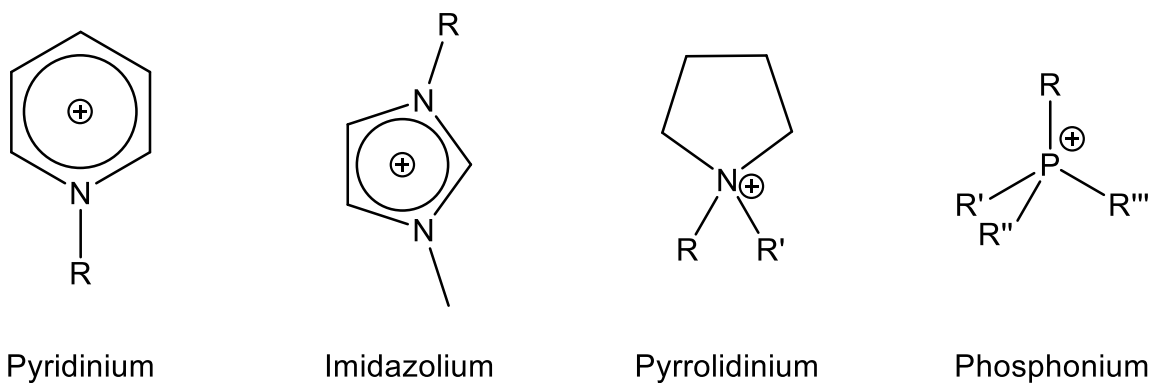
Over the last decade, literature on ILs has surged. At the turn of the century, ILs could be reviewed in a paper containing just over a hundred references,<sup>49</sup> but their potential in catalysis and separation, lubricants, fuel cells, extractants and many more applications have made them very attractive. ILs that are liquid at ambient temperature are known as room temperature ILs, RTILs. The first truly RTIL was ethyl ammonium nitrate, synthesised in 1914 shown in figure 2.<sup>50</sup>



**Figure 1.2.** Ethyl ammonium nitrate the first synthesised RTIL.

### 1.5.1 Typical Ionic Liquids

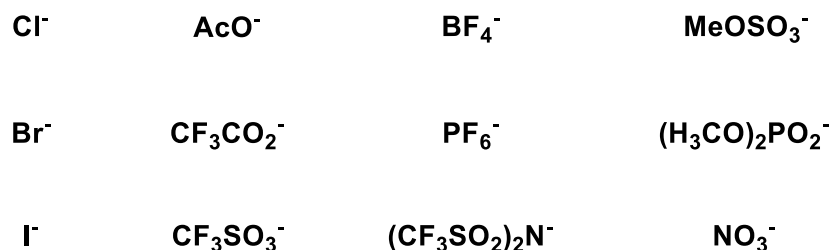
Figure 1.3 presents some typical ILs which are based on unsymmetrical cations such as imidazolium, ammonium and pyrrolidinium.



**Figure 1.3.** Common cations used in ILs

The potential for diversity in the R group and functionalisation means that the cation can be tailored to provide certain properties to meet the required needs. For example, increasing the alkyl chain length can improve the solubility of less polar compounds in ILs.

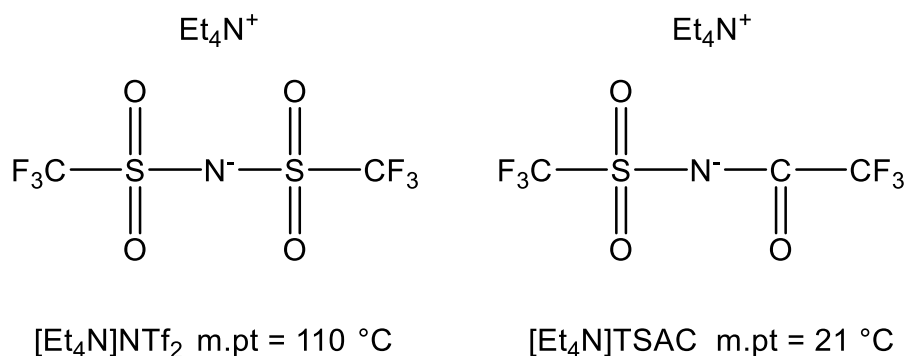
Anions, in contrast to the cations can be either organic or inorganic. Types of anions range from simple halides to larger species, as illustrated in Figure 1.4.



**Figure 1.4.** Examples of common anions used in ILs

Careful consideration of the anion is needed depending on the type of IL required. Increasingly, anions that contain carbon-fluorine bonds are popular. These types of anion are stable to hydrolysis, which makes them desirable in industrial applications.<sup>51</sup> They also tend to be weakly nucleophilic, which aids in depressing the melting point.

Varying the anion, analogously to the cation, has a significant effect on the melting points of ILs. The melting point generally decreases as the size of the anion increases, assuming the charge is consistent between anions. For example, the melting points of  $[\text{C}_2\text{mim}][\text{Cl}]$  and  $[\text{C}_2\text{mim}][\text{CF}_3\text{CO}_2]$  are 87 °C and -14 °C respectively. As for the cations, unsymmetrical anions can depress the melting point remarkably, although examples are less common in literature. Matsumoto *et al.* worked on ILs with unsymmetrical amide anions e.g.  $[\text{Et}_4\text{N}][\text{TSAC}]$ , (Figure 1.5), which showed a remarkably lower melting point than the more symmetrical  $[\text{Et}_4\text{N}]\text{NTf}_2$ .<sup>52</sup>



**Figure 1.5.** Example of unsymmetrical anion used by Matsumoto et al.

### 1.5.2 General Properties of Ionic Liquids

A notable property of ILs is their negligible vapour pressure.<sup>53, 54</sup> Due to long-range coulombic attractions it is very unfavourable for any of the ions to escape into the gas phase. This is one of the main reasons ILs have the potential in a variety of areas such as gas separation.

One of the shortcomings of ILs is their relatively high viscosity, especially for ILs containing halide ions. It is particularly problematic when using ILs in electrochemistry applications as this relies on the ease of mobility of the ions.<sup>55</sup> Viscosities of ILs can be up to 3 orders of magnitude greater than for common solvents, although careful choice of anion and cation can alleviate this. Prominently in the literature, dialkylimidazolium cations provide the lowest viscosity. In addition, reducing the length of the alkyl chain decreases the viscosity. The positive correlation between alkyl chain length and viscosity is attributed to the increase of van der Waals forces.<sup>56</sup> Table 1.2 gives the viscosities of some common 1-alkyl-3-methylimidazolium ILs, C<sub>n</sub>mim, where C<sub>n</sub> refers to the length of the 1-alkyl chain. Some common molecular solvents are also included for comparison. The data illustrates how changing the anion can have a dramatic effect on the viscosity of ILs.

**Table 1.2.** Effect of changing chain length and anion on the viscosity of ILs at 298 K.<sup>57, 58, 59</sup>

Ionic Liquid	Viscosity, $\eta$ / mPa.s
[C <sub>2</sub> mim][BF <sub>4</sub> ]	43
[C <sub>4</sub> mim][BF <sub>4</sub> ]	154
[C <sub>4</sub> mim][PF <sub>6</sub> ]	371
[C <sub>4</sub> mim][NTf <sub>2</sub> ]	69
[C <sub>4</sub> mim][Cl]	1701
Water	1
DMSO	2

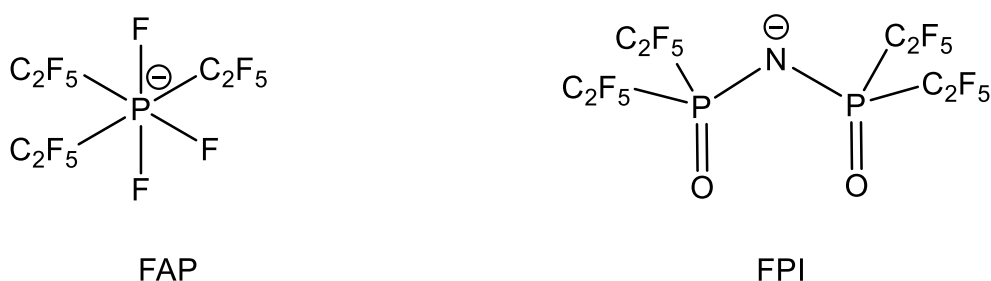
The trend of decreasing viscosity for anions  $\text{Cl}^- > \text{PF}_6^- > \text{BF}_4^- > \text{NTf}_2^-$  was accredited to 'hole theory'. Abbott first applied hole theory to ILs where the size of the anion is inversely proportional to viscosity.<sup>60</sup> However, this does not comprehensively explain the behaviour of all ILs. Another contributing factor is ion pairing. The ability to delocalise charge and in addition, not support hydrogen bonding, leads to low viscosity ILs. This is the reason  $\text{NTf}_2^-$  ILs are generally not particularly viscous.

Another property characteristic to ILs is their hygroscopicity. This feature is usually undesirable, but inevitable as ILs are molten salts. It is particularly troublesome in synthesis as any exposure to air will lead to water absorption. The absorbed water can be removed to a certain extent, but there will always be some remaining. Water contents at saturation and after drying for some ILs are shown in Table 1.3.

**Table 1.3.** Anion effects on hydrophobicity of ILs.<sup>57</sup>

Ionic Liquid	Saturated Water Content / ppm	Residual Water Content After Drying / ppm
[C <sub>4</sub> mim][BF <sub>4</sub> ]	Miscible	4530
[C <sub>4</sub> mim][PF <sub>6</sub> ]	11700	590
[C <sub>4</sub> mim][NTf <sub>2</sub> ]	3280	474
[C <sub>4</sub> mim][Cl]	Miscible	2200
[C <sub>6</sub> mim][FAP]	2030	10 - 15

The identity of the anion is usually the deciding factor regarding hydrophobicity of ILs. The more basic the anion, the more soluble it is in water. The cation typically does not play a significant role in determining this. However, there is a slight secondary effect where shorter alkyl chains or the introduction of functional groups can enhance water solubility.<sup>61</sup> Hydrophilic anions are halides or other species capable of hydrogen bonding. Many of the hydrophobic anions are highly fluorinated to help with the immiscibility with water. Work by Ignat'ev *et al.* developed anions such as tris(perfluoroalkyl)trifluorophosphate (FAP), bis[bis(pentafluoroethyl)phosphinyl]imide (FPI), shown in Figure 1.6, which showed high hydrophobicity.<sup>62, 63</sup> ILs containing these anions also showed very low viscosities.

**Figure 1.6.** Examples of hydrophobic anions.

The FAP anion is particularly interesting as it is an improvement on the simpler  $\text{PF}_6^-$  anion. One of the issues with ILs is their hydrolytic stability. ILs often contain fluorine substituents to help with water immiscibility, but when exposed to water, these can degrade into HF. As well as destroying the solvent, HF is extremely corrosive and therefore potentially hazardous to surroundings. The  $\text{PF}_6^-$  anion is unstable due to hydrolysis of P-F bonds, but C-F bonds less prone to hydrolysis than P-F or B-F bonds. Therefore, substituting fluorine atoms for perfluoroalkyl groups looks a promising method to increase hydrolytic stability.

### 1.5.3 Solubility of Gases in Ionic Liquids

The solubility of CO in ILs has had some research but not to the same extent as for  $\text{CO}_2$ . Other useful solubility data when discussing CO separation is that for  $\text{CH}_4$ ,  $\text{H}_2\text{S}$ ,  $\text{H}_2$  and  $\text{N}_2$  as these are gases commonly present in gas mixtures with CO.<sup>64</sup>

The overall maximum gas absorption capacity of ILs is increased as the incompatibility of the anion and cation increases. Short-range repulsion of their ionic shells allows for more gas to be absorbed. Studies show that both the cation and anion have effects on gas solubility, although the anion generally provides the largest effect.<sup>65</sup> Generally, ILs containing the anion  $\text{NTf}_2^-$  exhibit the largest gas solubility. Since the  $\text{NTf}_2^-$  anion is relatively large, it weakens the electrostatic interactions leading to an increased solubility.<sup>66</sup> In much the same way, ILs containing cations with longer alkyl chains demonstrate larger gas capacities.<sup>67</sup>

The general trend for solubility of gases in ILs is  $\text{CO}_2 \sim \text{N}_2\text{O} \gg \text{CH}_4 > \text{CO} \sim \text{N}_2 \sim \text{H}_2$ . This is shown through measurements of Henry's law constants which states that at a constant temperature, the amount of a given gas that dissolves in a given type and volume of liquid is directly proportional to the partial pressure of that gas in equilibrium with that liquid.<sup>68</sup> The mathematical expression for Henry's law

volatility is shown in equation 3 where  $P_{\text{gas}}$  is the partial pressure of gas above the solution and  $x_L$  is the mole fraction of gas in solution. Therefore, the smaller the Henry's law volatility,  $k_H$ , the more soluble a gas is in that liquid.

$$K_H = \frac{P_{\text{gas}}}{x_L} \quad (\text{eq 3})$$

The value of  $k_H$  for  $\text{CO}_2$  in ILs is generally one or two orders of magnitude smaller than that of CO and reinforces the superior solubility  $\text{CO}_2$  has compared to CO.<sup>69, 70</sup> Solubility data on gases other than  $\text{CO}_2$  in ILs are unfortunately limited. There are however, several papers outlining the solubility of carbon monoxide in different ILs.<sup>71</sup> Some Henry's Law constants are shown in Table 1.4 for the IL  $[\text{C}_4\text{mim}]\text{BF}_4$  which highlights the high physical solubility of  $\text{CO}_2$  relative to CO,  $\text{N}_2$  and  $\text{H}_2$  which have similar solubilities.

**Table 1.4.** Henry's law constants for different gases in the IL  $[\text{C}_4\text{mim}]\text{BF}_4$  at 298 K.<sup>70</sup>

Gas	Henry's Law Constant, $K_H$ / MPa
CO	172
$\text{H}_2$	204
$\text{N}_2$	179
$\text{CO}_2$	6
$\text{H}_2\text{S}$	2

A study by Raeissi *et al.* reported the temperature dependence of gas solubility in the IL  $[\text{C}_4\text{mim}]\text{NTf}_2$ .<sup>72</sup>  $\text{CO}_2$  solubility decreased with increasing temperature whereas for  $\text{H}_2$  solubility increased with temperature. This was explained by the small intermolecular forces between  $\text{H}_2$  and the IL. This gives

it characteristics of a perfect gas i.e. completely non-interacting, point-sized molecules. This facet of H<sub>2</sub> solubility means that separation of H<sub>2</sub> from more strongly interacting gases, like CO<sub>2</sub>, should be undertaken at relatively low temperatures in order to achieve the best selectivity.

## 1.6 Copper(I) Carbonyl Chemistry

As noted in section 1.3.2, methods for CO absorption by liquids typically exploit copper(I). This is usually the transition metal of choice for the separation of CO due to it being to the right of the d-block and so has a relatively high electronegativity. This results in the back-bonding component of the metal-carbonyl interaction being relatively weak and so copper(I) complexes typically bind CO reversibly.

Table 1.5 shows how this weak Cu-CO bond is apparent when comparing infrared spectroscopic data for copper(I) carbonyls with that of other transition metal carbonyls. The  $\nu(\text{CO})$  values observed reflect the strength of metal-CO  $\pi$ -backdonation. The  $\nu(\text{CO})$  values of the copper(I) complexes are not too dissimilar to that of free CO at 2143 cm<sup>-1</sup> which supports the idea that the amount of back-bonding is limited. Some metal carbonyl complexes can exhibit  $\nu(\text{CO})$  values above 2143 cm<sup>-1</sup> which are known as non-classical metal carbonyls. Typically, the metal-carbonyl interaction in such adducts is dominated by  $\sigma$ - and electrostatic interactions, with minimal or no  $\pi$ -backbonding.<sup>73,74</sup> Cations such as copper(I) and silver(I) are particularly adept at forming metal-carbonyls, which can be described as being non-classical.<sup>75</sup>

**Table 1.5.** Typical  $\nu(\text{CO})$  stretching values for a variety of metal carbonyls.<sup>76–78</sup>

Metal Carbonyl	$\nu(\text{CO}) / \text{cm}^{-1}$
$\text{Cr}(\text{CO})_6$	2000
$\text{Ni}(\text{CO})_4$	2057
$\text{Fe}(\text{CO})_5$	2034, 2013
$\text{Mn}_2(\text{CO})_{10}$	2044, 2013, 1983
$\text{Cu}(\text{CO})\text{Cl}$	2127
$\text{Cu}(\text{CO})\text{CF}_3\text{CO}_2$	2155
$\text{Cu}(\text{CO})\text{CF}_3\text{SO}_3$	2128
$\text{Cu}(\text{CO})\text{AsF}_6$	2178
$\text{Ag}(\text{CO})\text{SbF}_6$	2185

Moreover, because metal carbonyls show strong IR absorptions in a region which is usually clear, IR spectroscopy is a useful tool to investigate the CO uptake of Cu-containing materials.

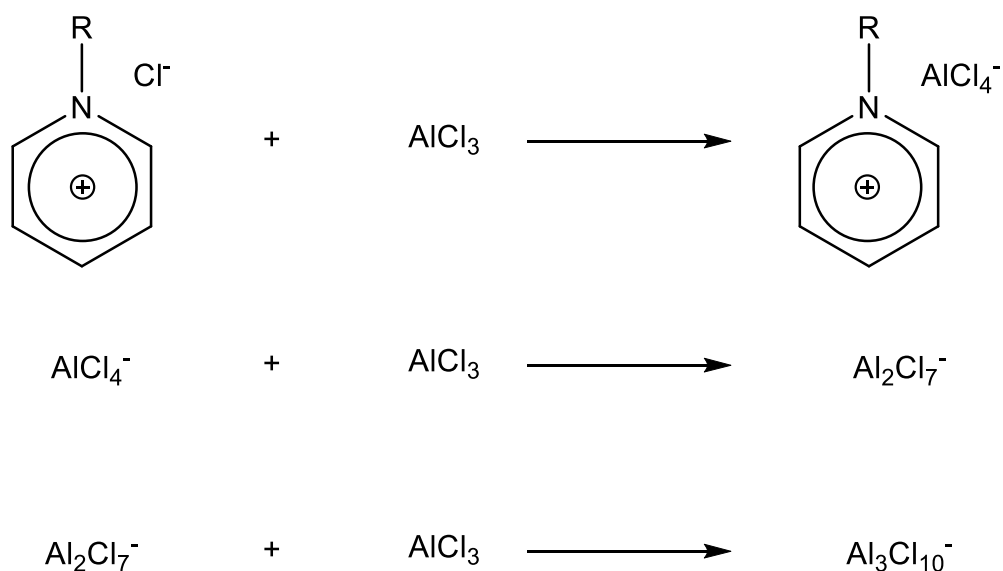
Table 1.6 shows spectroscopic data demonstrating copper(I) polycarbonyls are also possible when paired with weakly coordinating anions such as  $\text{OTf}$ ,  $\text{NTf}_2$  and  $\text{AsF}_6$ . Copper(I) monocarbonyls using more basic anions such as  $\text{Cl}^-$  or  $^-\text{OC}(\text{CH}_3)_3$  do not exhibit an affinity for forming dicarbonyls, even at high pressures.<sup>79,80</sup> This is unusual, as one would predict substituting a more basic anion would induce more  $\pi$ -backbonding and strengthen the dicarbonyl species  $\text{Cu}(\text{CO})_2\text{X}$ . Therefore, it appears that copper(I) polycarbonyls are ‘non-classical’ by nature, given their  $\nu(\text{CO}) > 2143 \text{ cm}^{-1}$ . Copper(I) tricarbonyls and even tetracarbonyls have been reported in the literature but have not yet been exploited for commercial use. Nevertheless, copper(I) polycarbonyls are an interesting prospect especially concerning CO uptake and separation technologies.

**Table 1.6.**  $\nu(\text{CO})$  stretching values for a variety of copper polycarbonyls.<sup>81</sup>

Metal Carbonyl	$\nu(\text{CO}) / \text{cm}^{-1}$
$\text{Cu}(\text{CO})_2\text{OTf}$	2143, 2171
$\text{Cu}(\text{CO})_2\text{AsF}_6$	2164, 2177
$\text{Cu}(\text{CO})_2\text{NTf}_2$	2158, 2184
$\text{Cu}(\text{CO})_3\text{NTf}_2$	2172, 2190
$[\text{Cu}(\text{CO})_4][\text{Al}(\text{OC}(\text{CF}_3)_3)_4]$	2196

### 1.7 Copper-Containing Ionic Liquids and Deep Eutectic Mixtures

Addition of a metal halide salt to a halide-containing IL results in the formation of a binary mixture. These molten salt mixtures are classically comprised of pyridinium or imidazolium halides with aluminium halides.<sup>82, 83</sup> The potential aggregates achievable by  $\text{AlCl}_3$  are shown in Scheme 1.7.

**Scheme 1.7.** The speciation in chloroaluminate ILs.

Melts of this type are easily prepared and are highly tuneable depending on the amount of  $\text{AlCl}_3$  added. Moreover, they exhibit a significant depression in melting point and viscosity whilst displaying an increase in conductivity.<sup>84</sup> Pyridinium halide salts are mostly solids at room temperature, however adding an equivalent of  $\text{AlCl}_3$  creates a system where the melting point is well below  $0\text{ }^\circ\text{C}$ . This is referred to as a deep-eutectic mixture.

Aluminium is not the only metal that can be integrated into IL systems. Other transition metals such as tin, nickel and cobalt have been reported, as well as non-transition metals such as germanium.<sup>85, 86</sup> All of these types of systems have been widely used for catalytic reactions. For example, the chloroaluminate(III) ILs have received a lot of attention in Friedel-Crafts acylation reactions as well as alkylation of benzene.<sup>87</sup> The application of chlorostannate(II) ILs in hydrogenation and hydroformylation reactions is recognised as the first use of an IL in transition metal catalysis.<sup>88</sup>

Similarly to the aluminium based systems, copper can be incorporated to achieve a deep eutectic mixture. The first reported case reacted triethylammonium chloride with copper(I) chloride to produce a liquid salt with the composition  $[\text{NEt}_3\text{H}][\text{CuCl}_2]$ .<sup>89</sup> These systems also demonstrated that higher aggregates of copper and chloride were possible when different  $[\text{NEt}_3\text{H}]\text{Cl} : \text{CuCl}$  ratios were used. A 1:1 mixture gives the  $[\text{CuCl}_2]^-$  anion, however if excess  $\text{CuCl}$  is added then the major anionic species has a higher Cu:Cl ratio for example  $[\text{Cu}_2\text{Cl}_3]^-$ . Conversely, a mixture with a deficient amount of  $\text{CuCl}$  added will result in the major anionic species in the mixture having a lower Cu:Cl ratio for example  $[\text{CuCl}_3]^{2-}$ .

Deep eutectic mixtures formed from  $[\text{C}_n\text{mim}]\text{Cl}$  and  $\text{CuCl}$  display low melting points, similar to the chloroaluminate(III) systems.<sup>90</sup> Figure 1.7 shows how a 1:1  $\text{CuCl}$  to  $[\text{C}_2\text{mim}]\text{Cl}$  ratio gives a minimum in viscosity, corresponding to the major copper species being  $[\text{CuCl}_2]^-$  as shown in Scheme 1.8.<sup>91</sup> Low viscosity is beneficial for a gas separation process using a liquid absorbent. These ILs have a relatively high concentration of copper(I), making them potentially attractive for application in CO purification. Another advantage is the relative stability of the  $\text{Cu}^+$  cation which can undergo disproportionation to

Cu metal and  $\text{Cu}^{2+}$  in common organic solvents. One notable issue associated in these systems however, is their hygroscopic nature. Absorption of water from the atmosphere can lead to a pathway to degradation.<sup>92</sup>

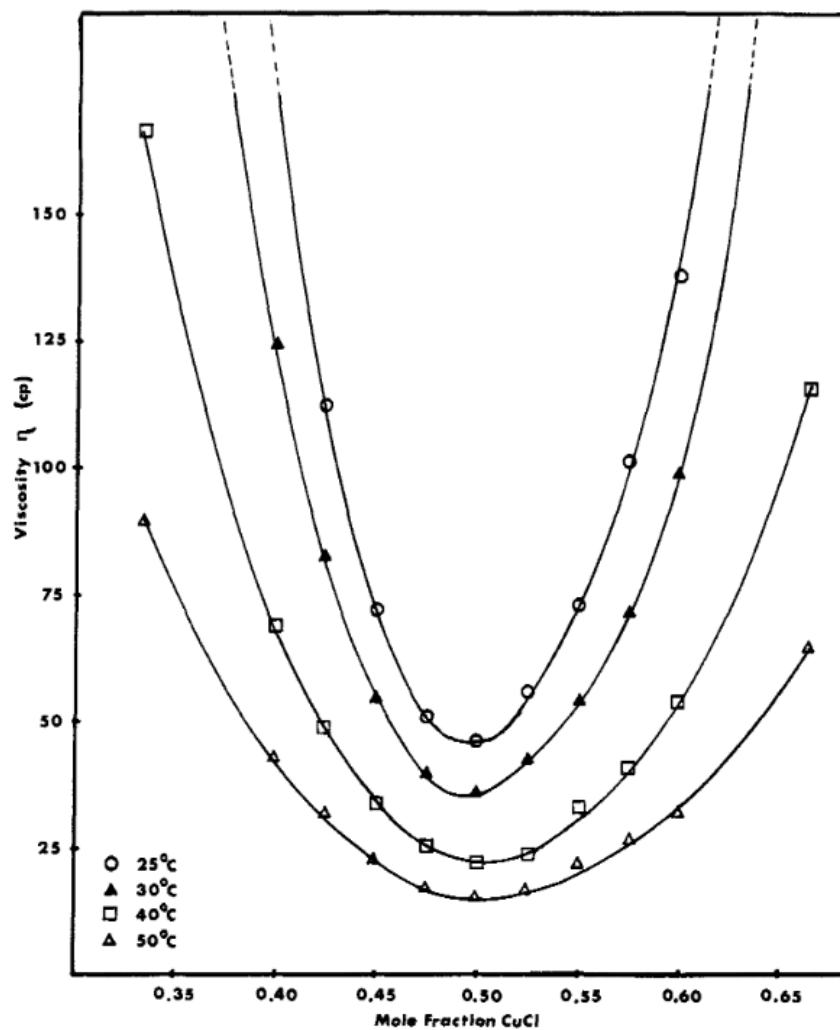
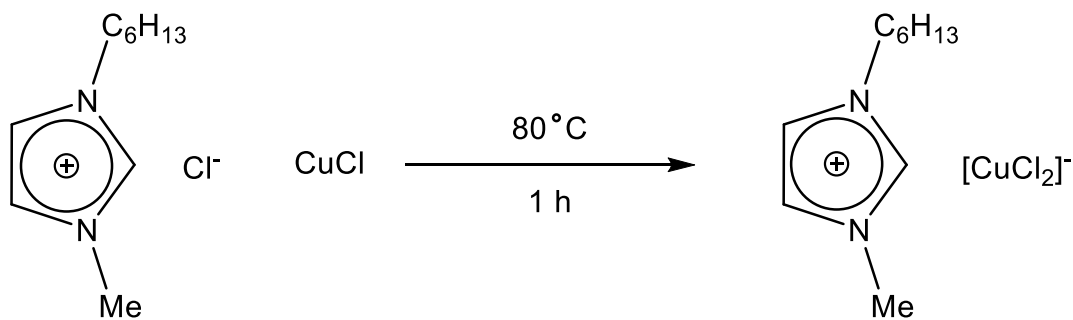


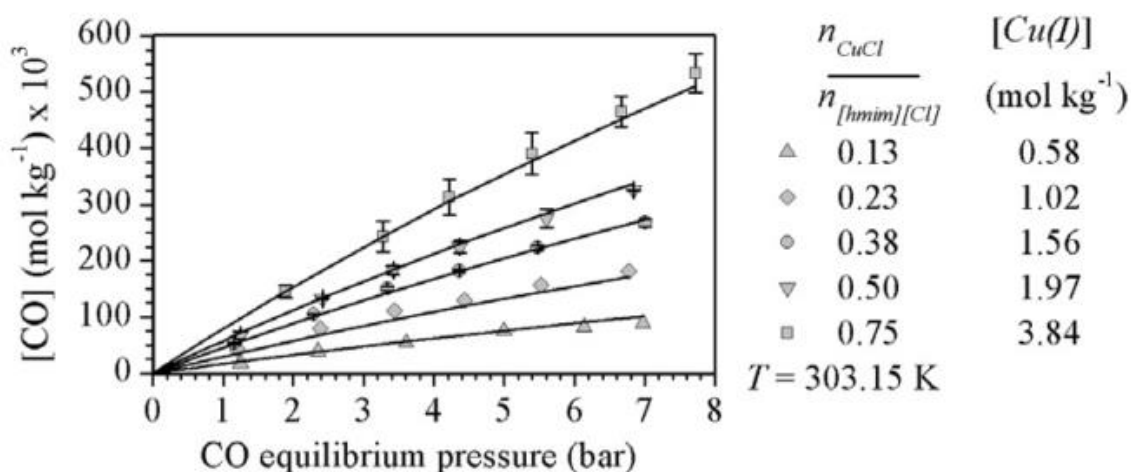
Figure 1.7. Viscosity isotherms for  $\text{CuCl}/[\text{C}_2\text{mim}][\text{Cl}]$  melts.<sup>91</sup>



**Scheme 1.8.** Incorporation of copper(I) into an IL.

### 1.8 Recent developments in CO separation using Cu(I) containing ionic liquids

A number of recent studies have investigated CO absorption by copper-containing ILs. In 2012 Urriaga *et al.* reported the dramatically improved solubility of CO in a cuprous IL.<sup>93</sup> Figure 1.8 shows how the CO uptake by [C<sub>6</sub>mim]Cl increased on addition of different proportions of CuCl. By contrast, the solubility of N<sub>2</sub> remained low, which supports the idea that these systems could be utilised in preferential absorption of CO from CO/N<sub>2</sub> gas mixtures.

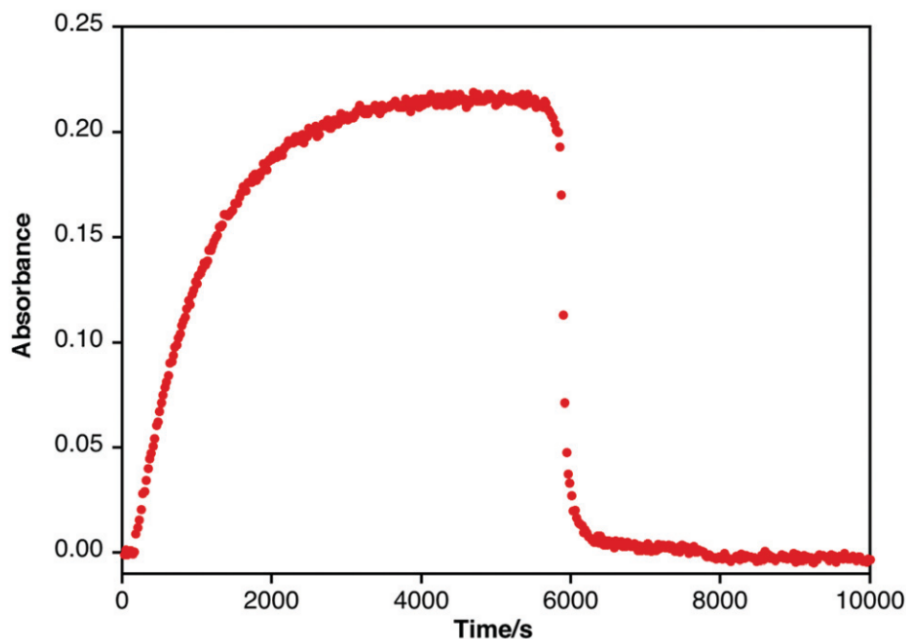


**Figure 1.8.** Solubility of CO in [C<sub>6</sub>mim][Cl] with different proportions of CuCl at varying pressure and constant temperature 303.15 K.<sup>93</sup>

Equilibrium constants for the complexation between CO and copper(I) showed a temperature dependence. The enthalpy of complexation was calculated to have a negative value of  $\Delta H_r = -13.4 \text{ kJ mol}^{-1}$  and demonstrates the formation of the copper(I) carbonyl is exothermic and so the solubility of CO in the IL medium will decrease as temperature increases.

Urriaga *et al.* have since turned their attention to integrating this system into semi-permeable membranes.<sup>94, 95, 96, 97</sup> Since the permeabilities of CO and N<sub>2</sub> in non-cuprous ILs are comparable due to the similar molecular sizes and critical temperatures, it was hoped that incorporating copper(I) would aid in separation. Although this was the case, the selectivity for CO from CO/H<sub>2</sub> mixtures decreased since the CO permeability became comparable to that of H<sub>2</sub>. It was therefore proposed that this system could be employed for the simultaneous recovery of H<sub>2</sub> and CO from N<sub>2</sub> enriched gas streams.

In a previous PhD project in the Haynes group in Sheffield, Repper investigated the reversible absorption of CO by ILs prepared from 1:1 mixtures of [C<sub>n</sub>mim]X and CuX (X = Cl, Br, I). High-pressure IR spectroscopy was used to monitor the formation of copper(I) carbonyl species.<sup>98</sup> Typically, a single  $\nu(\text{CO})$  band was observed around  $2080 \text{ cm}^{-1}$ , assigned to formation of a monocarbonyl complex, [CuX<sub>2</sub>(CO)]. Figure 1.9 shows how the CO uptake was reversible and the CO could be liberated quickly on heating to 100 °C and purging the cell with N<sub>2</sub>. After several absorption/desorption cycles the system maintained its CO absorption ability with no evidence of decomposition of the cuprous IL.



**Figure 1.9.** Plot of the growth of the  $\nu(\text{CO})$  band at  $2076\text{ cm}^{-1}$  when  $[\text{C}_6\text{mim}][\text{CuCl}_2]$  is exposed to 20 bar pressure of CO at 298 K and a stir rate of 428 rpm. Sample was purged with  $\text{N}_2$  and heated to  $100\text{ }^\circ\text{C}$  at approximately 6000 s with decay of  $\nu(\text{CO})$  signal.<sup>98</sup>

The work done by Repper was primarily undertaken using imidazolium cations and halide anions. It was found that ILs containing chloride anions absorbed the most CO with iodide the least (assuming that the extinction coefficients of the  $\nu(\text{CO})$  bands for the  $[\text{CuX}_2(\text{CO})]^-$  complexes do not differ significantly). This was consistent with the relative strength of Cu-CO binding, indicated by the  $\nu(\text{CO})$  frequencies for  $[\text{CuX}_2(\text{CO})]^-$ . It was also shown that increasing the chain length on the imidazolium cation increased the equilibrium  $\nu(\text{CO})$  intensity.

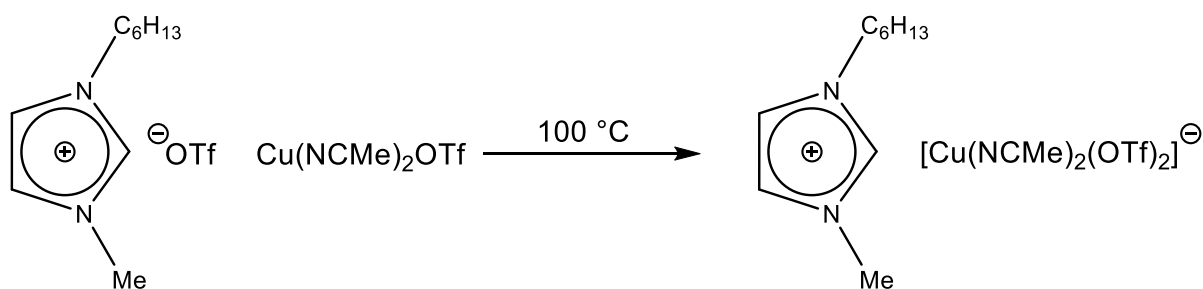
Repper also studied the enrichment of CO from gas mixtures, by measuring the composition of the gas desorbed from copper-containing ILs. Table 1.7 shows the results of CO enrichment experiments that were performed for 1:1  $\text{CO}:\text{N}_2$  and  $\text{CO}:\text{H}_2$  mixtures. In both cases it was shown that this method is very promising in CO enrichment even after only one absorption/desorption cycle.

**Table 1.7.** Enrichment results from initial 8 bar of pressure using [C<sub>6</sub>mim][CuCl<sub>2</sub>].

50:50 mixture of gases	CO enrichment after 1 step / %
CO:H <sub>2</sub>	93
CO:N <sub>2</sub>	>99

The better separation achieved for the CO:N<sub>2</sub> mixtures was accounted for by the higher physical solubility of H<sub>2</sub> relative to N<sub>2</sub> and CO. Extending from this, it was concluded that there could be some potential for separation of CO:CH<sub>4</sub> gas mixtures, although this may be less effective since CH<sub>4</sub> has a higher physical solubility than H<sub>2</sub>. Separation of CO:CO<sub>2</sub> gas mixtures, however, was not thought to be viable because of the extremely high physical solubility of CO<sub>2</sub> in these ILs.

Although these copper-containing ILs have some promising properties, there are also a few shortcomings which need to be addressed. The use of free halides in ILs is cause for concern in an industrial process as these can react with water to form corrosive acids. This would require expensive anti-corrosive metals to be employed. In the PhD thesis of Repper, attempts to use ILs with other anions, such as acetate (OAc<sup>-</sup>) and trifluoromethane sulfonate, (triflate, OTf<sup>-</sup>) were explored.<sup>99</sup> The copper species used to incorporate into the acetate ILs was copper(I) acetate, analogous to the halides. However for the triflate ILs, copper(I) triflate was too unstable and therefore two acetonitrile ligands were included in order to stabilise the copper(I) species, as shown in Scheme 1.9. The formation of the melt is done in the same manner as described earlier.

**Scheme 1.9.** Proposed structure of the triflate based system with copper(I) incorporation by Repper.

In both cases, the viscosity was lower than the ILs with halide anions. The acetate and triflate derivatives showed significantly better uptake of CO over the corresponding halides. Again, after several absorption/desorption cycles there seemed to be no decomposition of the IL.

The higher CO binding affinity observed for the triflate system is counter intuitive when considering the high  $\nu(\text{CO})$  stretching frequency of around  $2114\text{ cm}^{-1}$  that was recorded. Temperatures exceeding  $100\text{ }^\circ\text{C}$  and longer time periods  $\sim 30$  minutes were required to remove the chemisorbed CO.

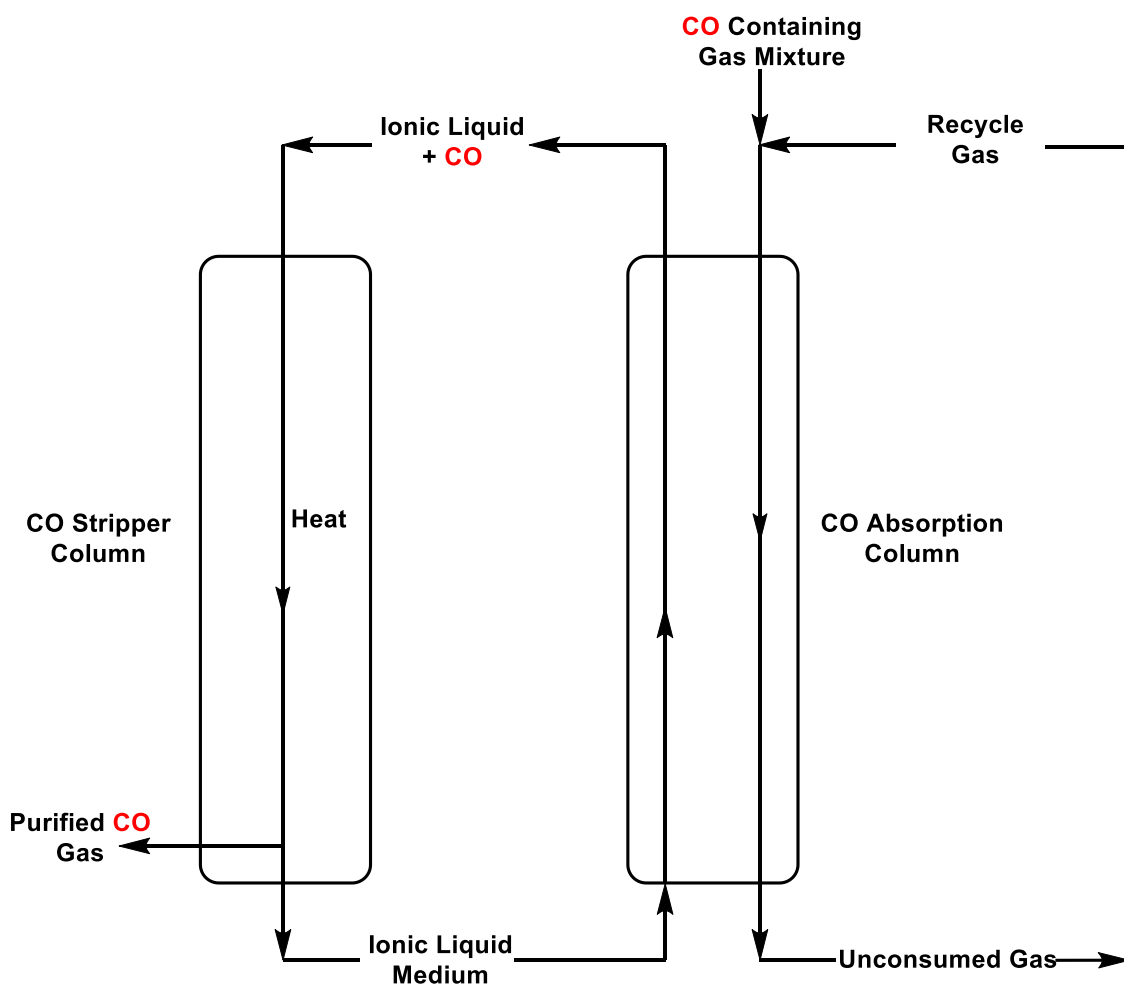
Urriaga *et al.* also investigated the use of copper-containing ILs with other anions such as thiocyanate, ( $\text{SCN}^-$ ) and bis(trifluoromethylsulfonyl)imide ( $\text{NTf}_2^-$ ).<sup>100,101</sup> The  $\text{SCN}^-$  based systems did not show any particular improvement in viscosity or selectivity with gases such as  $\text{N}_2$  or  $\text{H}_2$  however, the maximum amount of  $\text{CuSCN}$  added was only 30 mol%.

The  $\text{NTf}_2^-$  anion was employed in a composite poly(IL)-IL membrane. The IL monomer (1-vinyl-3-butylimidazolium) $\text{NTf}_2$  was used to fabricate the poly(IL) membrane and different amounts of  $[\text{C}_4\text{mim}]\text{Cl}$  and  $\text{CuCl}$  were added to form the chlorocuprate anion  $[\text{CuCl}_2]^-$ . Unfortunately, the expected improvement in transport of CO through the membrane was not observed, although it was noted that the selectivity with respect to other light gases such as  $\text{CO}_2$ ,  $\text{N}_2$  and  $\text{H}_2$  could be altered.

More recently Tu *et al.* reported a self-enhancement of CO reversible absorption in protic chlorocuprate ILs based on trialkyl ammonium cations.<sup>102</sup> The enhanced CO uptake was reported to occur during a phase change from a liquid to a liquid-solid mixture and was further enhanced when the material solidified. They claimed the causation of this enhancement was due to the formation of  $\text{Cu}(\text{CO})_2^+$  and  $\text{Cu}(\text{CO})_3^+$  based on peaks observed in the FTIR spectrum at  $2029\text{ cm}^{-1}$  and  $1980\text{ cm}^{-1}$ . Although, this interpretation is suspect as  $\nu(\text{CO})$  dicarbonyl bands usually shift to higher wavenumbers compared to the monocarbonyl peak, which in this case was  $2069\text{ cm}^{-1}$ .

## **1.9 Potential use of Copper Containing Ionic Liquids in a Large Scale Process for CO Purification**

As mentioned above, one drawback to ILs is their relatively high viscosity. Although improvements have been made, even the least viscous IL would still possess a viscosity an order of magnitude higher than common molecular solvents such as water or dichloromethane. Figure 1.10 shows a possible process design for purification of CO using a liquid phase absorbent. This would involve the solvent being pumped in one direction with the CO containing gas mixture passing in the opposite direction through the CO absorption column. It is important to minimise the viscosity, as this will affect how easily the solvent can flow through the column, as well as how much energy will be required to ensure sufficient mixing.



**Figure 1.10.** A Process diagram outlining a potential absorption/stripper column for the purification of CO from CO containing gas mixtures by copper containing ILs.

## 1.10 Project Aims

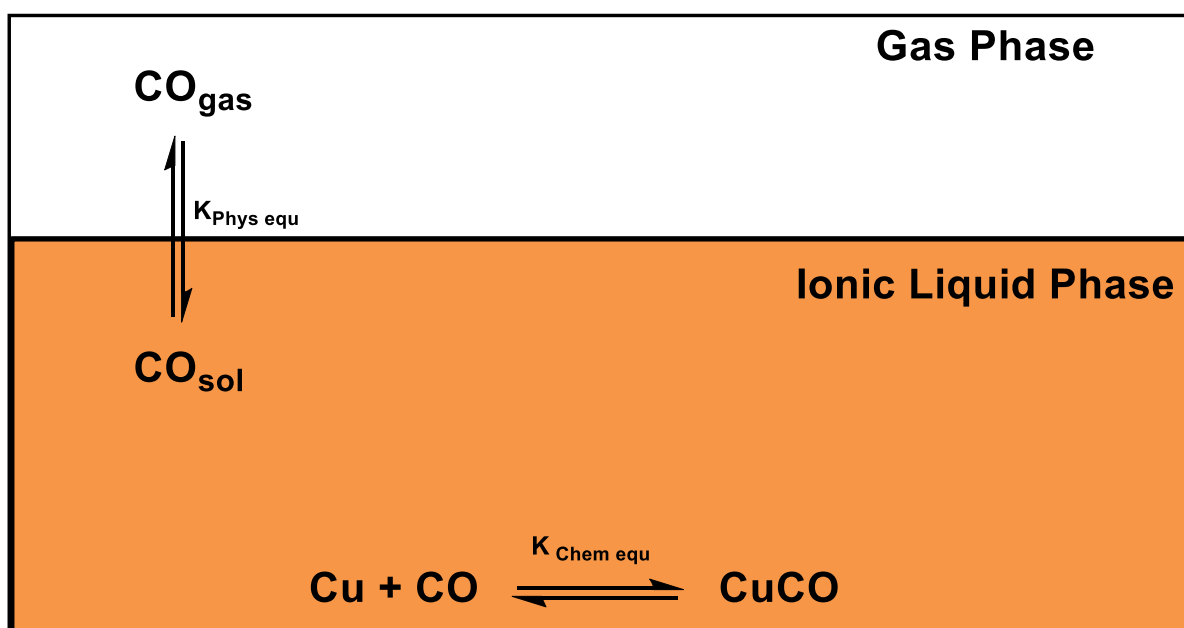
The use of copper-containing ILs has been shown to effectively enrich CO from mixtures containing gases such as  $N_2$  and  $H_2$ . However, there are some notable shortcomings and some improvements in CO selectivity which would be desirable.

To this end this project aimed to expand the scope of the IL anions in order to circumvent the corrosive nature of the free halide systems and also reduce viscosity. Moreover, functionalising the cation with groups such as ethers and alcohols could also be a way to reduce the viscosity and improve CO

selectivity. Therefore, the initial focus of this project was to extend the previous work in the group by Repper, to investigate the CO uptake properties and viscosities of a range of ILs with different combinations of cation and anion.

Further reductions in viscosity could be achieved by blending the copper-containing IL with a high boiling point molecular solvent. This part of the project aimed to investigate the ability of such 'diluted' systems to separate CO from gas mixtures, as well as establishing the stability of the copper species.

Overall, the total CO uptake by copper-containing ILs will be the sum of the physical solubility of the CO into the IL, defined by Henry's law constants, and the chemical complexation of the CO to the copper as depicted in Scheme 1.10. Both aspects will be influenced by careful choice of IL and copper source used.



**Scheme 1.10.** Physical CO solubility equilibrium and CO binding equilibrium to show the pathway total CO uptake.

Previous work on CO absorption by copper-containing ILs has indicated formation of copper monocarbonyl species. It was therefore aimed to identify systems that bind more than one CO at each copper centre, thereby enhancing CO uptake. This may be favoured by ILs with weakly coordinating anions.

## 1.11 References

- 1 J. Falbe, *Carbon Monoxide in Organic Synthesis*, Springer Berlin Heidelberg, 1970.
- 2 K. Weissermel and H.-J. Arpe, *Industrial Organic Chemistry*, 1997.
- 3 A. Haynes, *Adv. Catal.*, 2010, **53**, 1–45.
- 4 J. Strunk, K. Kähler, X. Xia and M. Muhler, *Surf. Sci.*, 2009, **603**, 1776–1783.
- 5 K. C. Waugh, *Catal. Today*, 1992, **15**, 51–75.
- 6 H. T. Luk, C. Mondelli, D. C. Ferré, J. A. Stewart and J. Pérez-Ramírez, *Chem. Soc. Rev.*, 2017, **46**, 1358–1426.
- 7 S. N. Khadzhiev, N. V. Kolesnichenko and N. N. Ezhova, *Pet. Chem.*, 2016, **56**, 77–95.
- 8 X. Zhen and Y. Wang, *Renew. Sustain. Energy Rev.*, 2015, **52**, 477–493.
- 9 A. Y. Khodakov, W. Chu and P. Fongarland, *Chem. Rev.*, 2007, **107**, 1692–1744.
- 10 M. E. Dry, *Catal. Today*, 2002, **71**, 227–241.
- 11 M. I. LLP, in *Global Polyurethanes Market Segmented by Application, Industry and Geography Trends and Forecasts 2015-2020*, 2016.
- 12 K. Wakatsuki, in *Chemicals Committee Meeting at APIC 2015*, 2015, pp. 1–24.
- 13 C. M. Thomas and G. Süß-Fink, *Coord. Chem. Rev.*, 2003, **243**, 125–142.
- 14 R. T. Eby and T. C. Singleton, *Appl. Ind. Catal*, 1971, **483**, 275.
- 15 J. F. Roth, J. H. Craddock, A. Hershman and F. E. Paulik, *Chem. Technol.*, 1971, 600.
- 16 F. E. Paulik and J. F. Roth, *Chem. Commun.*, 1968, 1578–1579.

- 
- 17 P. M. Maitlis, A. Haynes, G. J. Sunley and M. J. Howard, *J. Chem. Soc. Dalton. Trans.*, 1996, 2187–2196.
- 18 G. J. Sunley and D. J. Watson, *Catal. Today*, 2000, **58**, 293–307.
- 19 A. Haynes, *Comprehensive Inorganic Chemistry II*, 2013, vol. 6.01.
- 20 S. O. Akiri and S. O. Ojwach, *Inorg. Chim. Acta*, 2019, **489**, 236–243.
- 21 L. Crawford, D. J. Cole-Hamilton and M. Bü, *Organometallics*, 2015, **34**, 438–449.
- 22 X.-F. Wu, X. Fang, L. Wu, R. Jackstell, H. Neumann and M. Beller, *Acc. Chem. Res.*, 2014, **47**, 1041–1053.
- 23 T. C. Drage, C. E. Snape, L. A. Stevens, J. Wood, J. Wang, A. I. Cooper, R. Dawson, X. Guo, C. Satterley and R. Irons, *J. Mater. Chem.*, 2012, **22**, 2815–2823.
- 24 K. Li, X. Song, P. Ning, H. Yi, X. Tang and C. Wang, *Energy Technol.*, 2015, **3**, 136–144.
- 25 Blast Furnace, Coke Gas and Converter Gas for Power Production, <https://www.clarke-energy.com/steel-production-gas/>, (accessed 28 January 2019).
- 26 T. Shenoy, *US Pat.*, 4,217,759, 1980, Union Carbide Corporation.
- 27 R. Fabian, *US Pat.*, 4,478,621, 1984, Linde Aktiengesellschaft.
- 28 A. Kohl and F. Riesenfeld, *AIChE J.*, 1985, **32**, 1404–1404.
- 29 J. A. Hogendoorn, W. P. M. van Swaaij and G. F. Versteeg, *Chem. Eng. J. Biochem. Eng. J.*, 1995, **59**, 243–252.
- 30 D. J. Haase and D. G. Walker, *Chem. Eng. Prog.*, 1974, **70**, 74–77.
- 31 J. A. Hogendoorn, W. P. M. van Swaaij and G. F. Versteeg, *Chem. Eng. J. Biochem. Eng. J.*, 1995, **59**, 243–252.

- 32 A. Keller and R. Schendel, The use of COSORB II to recover high purity carbon monoxide from a feed gas, <http://www.rschendel.com/PDF/COSORB.pdf>, (accessed 26 June 2019).
- 33 COSTELLO | COPure Carbon Monoxide Purification | Carbon Monoxide Removal | Carbon Monoxide Recovery, <http://www.rccostello.com/copure.html>, (accessed 5 February 2019).
- 34 J. Kärger, D. M. Ruthven and D. N. Theodorou, *Chemie Ing. Tech.*, 2013, **83**, 1779–1780.
- 35 R. S. Pillai, G. Sethia and R. V. Jasra, *Ind. Eng. Chem. Res.*, 2010, **49**, 5816–5825.
- 36 G. Sethia, R. S. Somani and H. Chand Bajaj, *RSC Adv.*, 2015, **5**, 12773–12781.
- 37 A. Stanislaus, M. J. B. Evans and R. F. Mann, *J. Phys. Chem.*, 1972, **76**, 2349–2352.
- 38 F. Gao, Y. Wang and S. Wang, *Chem. Eng. J.*, 2016, **290**, 418–427.
- 39 R. V. Gholap and R. V. Chaudhari, *Can. J. Chem. Eng.*, 2009, **70**, 505–510.
- 40 K. Sumida, D. L. Rogow, J. A. Mason, T. M. McDonald, E. D. Bloch, Z. R. Herm, T.-H. Bae and J. R. Long, *Chem. Rev.*, 2012, **112**, 724–781.
- 41 M. P. Suh, H. J. Park, T. K. Prasad and D.-W. Lim, *Chem. Rev.*, 2012, **112**, 782–835.
- 42 S. Qiu, M. Xue and G. Zhu, *Chem. Soc. Rev.*, 2014, **43**, 6116.
- 43 J.-R. Li, J. Sculley and H.-C. Zhou, *Chem. Rev.*, 2012, **112**, 869–932.
- 44 Y. Wang, C. Li, F. Meng, S. Lv, J. Guo, X. Liu, C. Wang and Z. Ma, *Front. Chem. Sci. Eng.*, 2014, **8**, 340–345.
- 45 J. Peng, S. Xian, J. Xiao, Y. Huang, Q. Xia, H. Wang and Z. Li, *Chem. Eng. J.*, 2015, **270**, 282–289.
- 46 M. Rafatullah, O. Sulaiman, R. Hashim and A. Ahmad, *J. Hazard. Mater.*, 2010, **177**, 70–80.
- 47 J. Ma, L. Li, J. Ren and R. Li, *Sep. Purif. Technol.*, 2010, **76**, 89–93.

- 48 I. Crossing, J. M. Slattery, C. Daguinet, P. J. Dyson, A. Oleinikova and H. Weingärtner, *J. Am. Chem. Soc.*, 2006, **128**, 13427–34.
- 49 T. Welton, *Chem. Rev.*, 1999, **99**, 2071–2084.
- 50 P. Walden, *Bull. Acad. Imper. Sci. St. Petersburg.*, 1914, **8**, 405–422.
- 51 J. S. Wilkes, *Green Chem.*, 2002, **4**, 73–80.
- 52 H. Matsumoto, H. Kageyama and Y. Miyazaki, *Chem. Commun.*, 2002, 1726–1727.
- 53 K. R. Holbrey, J. D., Seddon, *Clean Prod. Proc.*, 1999, **1**, 223–236.
- 54 J. D. Holbrey, *Chim. Oggi*, 2004, **22**, 35–37.
- 55 A. P. Abbott, *Chem. Phys. Chem.*, 2004, **5**, 1242.
- 56 Y. Yoshida, O. Baba and G. Saito, *J. Phys. Chem. B*, 2007, **111**, 4742–9.
- 57 J. G. Huddleston, A. E. Visser, W. M. Reichert, H. D. Willauer, G. A. Broker and R. D. Rogers, *Green Chem.*, 2001, **3**, 156–164.
- 58 Y. S. Nanayakkara, H. Moon, T. Payagala, A. B. Wijeratne, J. A. Crank, P. S. Sharma and D. W. Armstrong, *Anal. Chem.*, 2008, **80**, 7690–8.
- 59 H. Shirota, T. Mandai, H. Fukazawa and T. Kato, *J. Chem. Eng. Data*, 2011, **56**, 2453–2459.
- 60 A. P. Abbott, G. Capper and S. Gray, *Chemphyschem*, 2006, **7**, 803–6.
- 61 J. P. Hallett and T. Welton, *Chem. Rev.*, 2011, **111**, 3508–76.
- 62 N. V. Ignat'ev, M. Finze, J. A. P. Sprenger, C. Kerpen, E. Bernhardt and H. Willner, *J. Fluor. Chem.*, 2015, **177**, 46–54.
- 63 N. V. Ignat'ev, U. Welz-Biermann, A. Kucheryna, G. Bissky and H. Willner, *J. Fluor. Chem.*,

- 2005, **126**, 1150–1159.
- 64 F. Llovell, M. B. Oliveira, J. A. P. Coutinho and L. F. Vega, *Catal. Today*, 2015, **255**, 87–96.
- 65 E. J. Cadena, C.; Anthony, J.L.; Shah, J.K.; Morrow, T.I.; Brennecke, J.F. and Maginn, *J. Am. Chem. Soc.*, 2004, **126**, 5300–5308.
- 66 M. F. Costa Gomes, *J. Chem. Eng. Data*, 2007, **52**, 472–475.
- 67 J. F. Aki, S. N. V. K.; Mellein, B. R.; Saurer, E. M. and Brennecke, *J. Phys. Chem. B*, 2004, **108**, 20355–20365.
- 68 S. Zumdahl, *Chemistry*, Houghton Mifflin Company, Boston, MA, 5th edn., 2000.
- 69 J. Blath, M. Christ, N. Deubler, T. Hirth and T. Schiestel, *Chem. Eng. J.*, 2011, **172**, 167–176.
- 70 J. Jacquemin, M. F. Costa Gomes, P. Husson and V. Majer, *J. Chem. Thermodyn.*, 2006, **38**, 490–502.
- 71 C. A. Ohlin, P. J. Dyson and G. Laurency, *Chem. Commun.*, 2004, **9**, 1070–1071.
- 72 S. Raeissi and C. J. Peters, *AIChE J.*, 2012, **58**, 3553–3559.
- 73 R. D. Pike, *Organometallics*, 2012, **31**, 7647–7660.
- 74 M. Fianchini, T. R. Cundari, N. J. DeYonker and H. V. R. Dias, *Dalton. Trans.*, 2009, **1**, 2085.
- 75 S. H. Strauss, *Dalton. Trans.*, 2000, **1**, 1–6.
- 76 J. J. Rack, J. D. Webb and S. H. Strauss, *Inorg. Chem.*, 1996, **35**, 277–278.
- 77 N. J. Alben, J. O.; Yen, L.; Farrier, *J. Am. Chem. Soc.*, 1970, **92**, 4475.
- 78 M. Bochmann, *Organometallics*, Oxford University Press, 1994.
- 79 T. Tsuda, H. Habu, S. Horiguchi and T. Saegusa, *J. Am. Chem. Soc.*, 1974, 5930–5931.

- 80 M. Håkansson, S. Jagner and S. F. A. Kettle, *Spectrochim. Acta Part A Mol. Spectrosc.*, 1992, **48**, 1149–1152.
- 81 Oleg G. Polyakov, Svetlana M. Ivanova, Christine M. Gaudinski, Susie M. Miller, A. Oren P. Anderson and S. H. Strauss, *Organometallics*, 1999, **18**, 3769–3771.
- 82 J. S. Wilkes, J. A. Levisky, R. A. Wilson and C. L. Hussey, *Inorg. Chem.*, 1982, **21**, 1263–1264.
- 83 R. J. Gale and R. A. Osteryoung, *Inorg. Chem.*, 1979, **18**, 1603–1605.
- 84 J. A. Boon, J. A. Levisky, J. L. Pflug and J. S. Wilkes, *J. Org. Chem.*, 1986, **51**, 480–483.
- 85 G. W. Parshall, *J. Am. Chem. Soc.*, 1972, **94**, 8716.
- 86 T. Hitchcock, P. B.; Seddon, K. R.; Welton, *Dalton. Trans.*, 1993, 2639.
- 87 T. Welton, *Coord. Chem. Rev.*, 2004, **248**, 2459–2477.
- 88 G. W. Parshall, *J. Am. Chem. Soc.*, 1972, **94**, 8716.
- 89 G. Yoke III, J. T.; Weiss, J. F.; Tollin, *Inorg. Chem.*, 1963, **2**, 1210.
- 90 J. T. Bolkan, S. A.; Yoke III, *J. Chem. Eng. Data*, 1986, **31**, 194.
- 91 S. A. Bolkan and J. T. Yoke, *J. Chem. Eng. Data*, 1986, **31**, 194–197.
- 92 T. Wasserscheid, P., Welton, *Ionic Liquids in Synthesis*, WILEY-VCH Verlag GmbH, Weinheim, Germany, 2nd edn., 2007.
- 93 O. C. David, G. Zarca, D. Gorri, A. Urriaga and I. Ortiz, *Sep. Purif. Technol.*, 2012, **97**, 65–72.
- 94 G. Zarca, I. Ortiz and A. Urriaga, *Chem. Eng. Res. Des.*, 2014, **92**, 764–768.
- 95 G. Zarca, I. Ortiz and A. Urriaga, *Desalin. Water Treat.*, 2014, **56**, 3640–3646.
- 96 G. Zarca, I. Ortiz and A. Urriaga, *J. Memb. Sci.*, 2013, **438**, 38–45.

- 97 G. Zarca, M. Fernández, A. Santamaría, I. Ortiz and A. Urriaga, *Sep. Purif. Technol.*, 2015, **155**, 96–100.
- 98 S. E. Repper, A. Haynes, E. J. Ditzel and G. J. Sunley, *Dalton. Trans.*, 2017, **46**, 2821–2828.
- 99 S. Repper PhD Thesis, University of Sheffield, 2014.
- 100 G. Zarca, W. J. Horne, I. Ortiz, A. Urriaga and J. E. Bara, *J. Memb. Sci.*, 2016, **515**, 109–114.
- 101 G. Zarca, I. Ortiz and A. Urriaga, *Sep. Purif. Technol.*, 2018, **196**, 47–56.
- 102 Z.-H. Tu, Y.-Y. Zhang, Y.-T. Wu, X.-B. Hu, R. Li, *Chem. Commun*, 2019, **55**, 3390.

## **2. Experimental**

## 2.1 Instrumentation

Infrared solution-spectra and thin-film spectra were recorded using either a Nicolet Magna-IR 560 FTIR spectrometer or a Nicolet Magna-IR 380 FTIR spectrometer, using Omnic software. Standard solution cells with CaF<sub>2</sub> windows were used for IR spectroscopy with a path length of 0.5 mm. Thin film spectra were obtained using NaCl plates. High-pressure IR spectra were recorded using a Perkin Elmer Spectrum GX FTIR spectrometer controlled by both Spectrum and Timebase software. A resolution of 2 cm<sup>-1</sup> was used for both high-pressure and solution-cell spectra.

Gas chromatographs were collected using a Perkin Elmer Arnel autosystem XL fitted with a thermal conductivity detector. H<sub>2</sub> was used as the carrier gas for CO, N<sub>2</sub> and O<sub>2</sub> quantification. N<sub>2</sub> was used as the carrier gas for H<sub>2</sub> quantification.

<sup>1</sup>H, <sup>13</sup>C, <sup>19</sup>F and <sup>31</sup>P NMR spectra were recorded using a Bruker AC400 spectrometer with the solvent as the internal standard. Elemental analyses were performed using a Perkin Elmer 2400 automated vario MICRO cube CHNS analyser. Mass spectra were obtained by electrospray ionisation using a Waters LCT time of flight (TOF) instrument.

## 2.2 Viscosity measurements

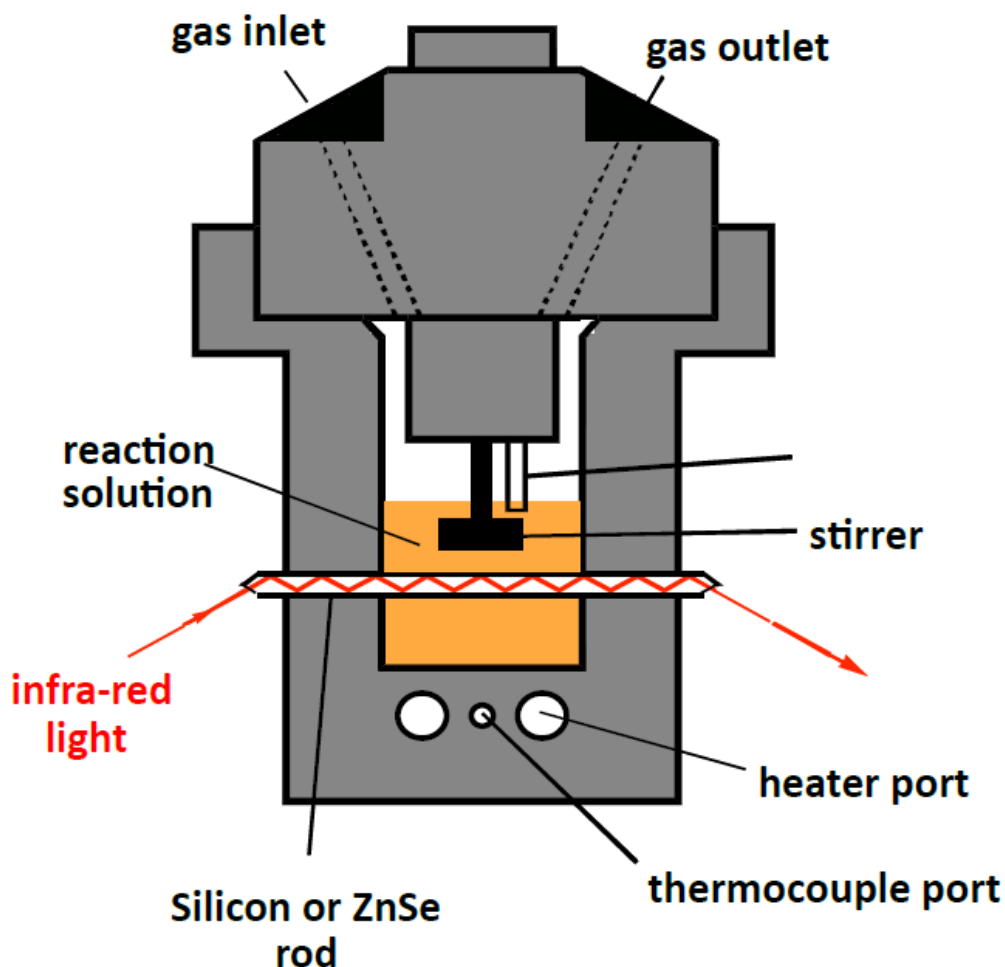
Viscosity data was recorded using a controlled stress rheometer (AR-G2, TA Instruments) using a cone and plate geometry of 40 mm diameter and a cone angle of 2°. Samples of liquid were equilibrated to the desired temperature for 5 minutes, and the shear rate was exponentially increased from 10 to 1000 s<sup>-1</sup> by continuous ramp step over a 5 minute period. Due to the air sensitivity and hygroscopic nature of ionic liquids, each measurement was performed on a new sample. All measurements were done at atmospheric pressure.

### 2.3 Low Pressure CO Absorption Studies

Approximately 1 g of the copper-containing ionic liquid was put into a Schlenk tube under N<sub>2</sub>. A background scan of the liquid was then recorded on the FTIR by thin film. Carbon monoxide was then bubbled into the liquid through a Pasteur pipette secured into a rubber seal attached to a quick fit adaptor. After bubbling CO for approximately 10-15 minutes, a sample was taken and analysed by FTIR to determine copper-carbonyl formation from the presence of any  $\nu$  (CO) bands.

### 2.4 High Pressure CO Absorption Studies

High-pressure in-situ studies on the absorption of CO by copper containing ionic liquids were carried out using a cylindrical internal reflectance (CIR) cell (Figure 2.1).<sup>1,2</sup> Spectra were collected using a Perkin Elmer GX FTIR Spectrometer where the mercury cadmium telluride (MCT) detector is cooled with liquid N<sub>2</sub>. The base of the cell was secured and the cell aligned to optimise the IR energy throughput by adjusting the tilt table and focusing mirrors. Heating of the cell to the required temperature was done using two heating rods inserted into ports in the base of the cell. The temperature was set using a controller linked to a thermocouple inserted into a thermocouple port. The cell was usually operated between 1-20 bar of pressure and between 20-140 °C.



**Figure 2.1.** Diagram of the CIR cell used in high pressure in-situ IR studies.

The cell was loaded with approximately 8 cm<sup>3</sup> or 10 cm<sup>3</sup> of the relevant liquid depending on the experiment, the cell lid was tightened and a motor attached with a spinning rod attached to an impeller immersed in the liquid. A flow of N<sub>2</sub> was then purged through the cell for approximately 10 minutes. A rotation setting of 30 on the dial equates to approximately 215 rpm. A 256 scan background was taken over the range 4000-1000 cm<sup>-1</sup> after the cell had been sealed under N<sub>2</sub>.

For the absorption studies, the cell equilibrated to 20 °C, unless stated otherwise, and the stir rate set to the required level. The cell was then purged and refilled with CO several times to the desired pressure and sealed.

Spectra were taken continuously throughout the experiment. Timebase software was used to generate absorbance vs time plots for  $\nu(\text{CO})$  absorptions. The data were exported to Microsoft Excel as a .CSV file to create graphs.

## 2.5 Gas Enrichment Studies

These studies were also performed using the CIR cell. In a typical experiment either 8 cm<sup>3</sup> or 10 cm<sup>3</sup> of copper-containing ionic liquid was loaded into the cell, and then pressurised with either a CO/H<sub>2</sub> or CO/N<sub>2</sub> gas mixture at 10 bar total pressure. The CO mixtures were 50:50 CO:X<sub>2</sub> (X<sub>2</sub> = N<sub>2</sub> or H<sub>2</sub>) from a pre-made cylinder purchased from BOC. The absorption of CO was tracked by monitoring the intensity of the  $\nu(\text{CO})$  band. As CO was absorbed, the pressure dropped and the headspace was repressurised up to 10 bar and left to absorb several times, until no further drop in pressure was recorded. The repressurisation was done in stages in order to limit diffusion effects that could occur if the line was left open to the cylinder. Once equilibrium was reached, as determined from a plateau in the  $\nu(\text{CO})$  band intensity, stirring was stopped and the headspace vented before being resealed. The cell was then heated to between 80 °C – 140 °C, depending on the experiment, and the absorbed gas was driven back into the headspace. This new headspace was then sampled and the procedure repeated as many times as necessary.

A sample of this gas was then collected in a pre-evacuated Schlenk tube and a 100  $\mu\text{L}$  syringe was then used to extract a sample from the Schlenk tube and injected into the GC. By integrating the area under each peak, the amount of each gas present can be calculated by comparing with calibration plots which are given in chapter 5.2.

## 2.6 Gas Chromatography Measurements

Analysis of gas compositions was done using a Perkin-Elmer Autosystem XL gas chromatograph equipped with thermal conductivity detector (TCD). Separation of gases was provided by a Restek RT-M porous layer sieve (5 Å) column with a 30 m length and a diameter of 0.53 mm. Injection of a sample was done by a 100 µL manual gas-tight syringe directly into the column.

For the CO, N<sub>2</sub> and O<sub>2</sub> analysis, a hydrogen carrier gas was used at a flow rate of 5 mL min<sup>-1</sup>. The oven was set to 100 °C as was the TCD temperature, with a bridge current range setting of 3 and positive polarity.

For H<sub>2</sub> analysis, a nitrogen carrier gas was used at a flow rate of 5 mL min<sup>-1</sup>. The oven was set to 30 °C and the TCD temperature was set to 100 °C, with a bridge current range setting of 2 and negative polarity.

## 2.7 Solvents and Reagents

All standard reagents were supplied by Sigma-Aldrich Chemicals Ltd and used as supplied, unless stated otherwise. Lithium trifluoromethanesulfonate, 2-bromoethyl methyl ether, 1,1,1,2,2,3,3,4,4,5,5,6,6-tridecafluorooctanol and 1,1,1,2,2,3,3,4,4,5,5,6,6-tridecafluorooctyl iodide were purchased from Florochem Ltd.

The solvents dichloromethane, toluene and acetonitrile were obtained from a Grubbs solvent purification system in which the solvents were degassed prior to being passed through activated alumina and a supported copper catalyst to remove protic contaminants and trace oxygen respectively. These solvents were stored under N<sub>2</sub> in either round bottom flasks or conical flasks with side-arm attachments. Solvents were used within 24 hours of collection from the dry solvent system. Other solvents were purchased either from Fisher Scientific or Sigma Aldrich, (HPLC grade unless otherwise stated) and were used without further purification

## 2.8 Gaseous Reagents

Carbon monoxide (99.9% CP Grade), CO/N<sub>2</sub> and CO/H<sub>2</sub> 50:50 gas mixtures were purchased from BOC and used directly from their cylinders. Nitrogen used as an inert atmosphere was supplied by an in-house generator.

## 2.9 Synthetic Procedures

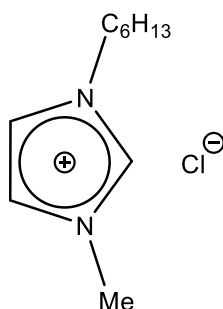
Unless stated otherwise, all synthetic reactions were carried out using a Schlenk line, in which a two way tap was fitted such that one way connected to an inert atmosphere (N<sub>2</sub>) and the other to a high vacuum. Glassware was dried in an oven at 120 °C before use and degassed using three inert gas/vacuum cycles. Solvents were transferred between containers using either a syringe fitted with a secure Luerlock needle, which had been degassed at least three times by purging with N<sub>2</sub>, or a cannula which was purged with a flow of N<sub>2</sub>, for at least 1 minute prior to use.

### 2.9.1 Synthesis of 1-alkyl-3methylimidazolium Halide Salts

Procedures of this type were performed by adding 1-methyl imidazole (~ 50 mmol) to a dried round bottom flask under a N<sub>2</sub> atmosphere. The appropriate alkyl halide was added, in the case of chloride and bromide 1.1 equivalents were added, and the reaction mixture heated to 80 °C overnight. With regards to the iodide salts, 1 equivalent of the alkyl iodide was added dropwise at 0 °C and the flask wrapped with foil to prevent the light-induced formation of I<sub>2</sub>. Again, the reaction mixture was stirred overnight.

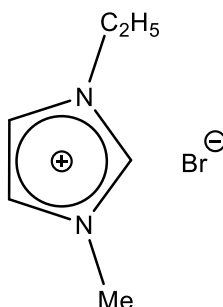
Once the reaction had completed, assessed by <sup>1</sup>H NMR, any unreacted alkyl halide was removed under reduced pressure at 80 °C for at least 4 hours.

The products synthesised were obtained as hygroscopic solids or liquids and in most cases yields of at least 90 %. These salts were analysed by  $^1\text{H}$  NMR spectroscopy,  $^{13}\text{C}$  NMR spectroscopy,  $^{19}\text{F}$  NMR spectroscopy where appropriate and electrospray mass spectrometry ( $\text{ES}^+$  and  $\text{ES}^-$ ).

**1-hexyl-3-methylimidazolium chloride [C<sub>6</sub>mim]<sup>+</sup>Cl<sup>-</sup>**

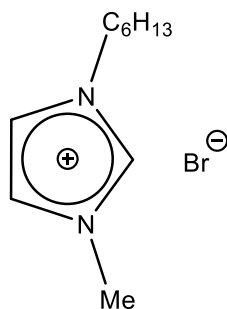
1-methyl imidazole (4.0 ml, 50 mmol) and 1-chlorohexane (7.5 ml, 55 mmol) were subjected to the procedure described above to isolate 1-hexyl-3-methylimidazolium chloride as a pale yellow viscous liquid (12.35 g, 50 mmol, 100 %).

**<sup>1</sup>H NMR (400 MHz, CDCl<sub>3</sub>)** δ 10.50 (1H, s) 7.65 (s, 1H), 7.46 (1H, s), 4.22 (2H, t, 7.5 Hz), 4.05 (3H, s), 1.80 – 1.61 (2H, m), 1.15-1.30 (6H, m), 0.75 (3H, t, 7.0 Hz); **<sup>13</sup>C NMR (101 MHz, CDCl<sub>3</sub>)** δ 137.5, 123.8, 121.9, 49.8, 36.3, 30.9, 30.1, 25.7, 22.2, 13.8; **TOF MS (ES<sup>+</sup>):** m/z 167 ([C<sub>6</sub>mim]<sup>+</sup>).

**1-ethyl-3-methylimidazolium bromide [C<sub>2</sub>mim]<sup>+</sup>Br<sup>-</sup>**

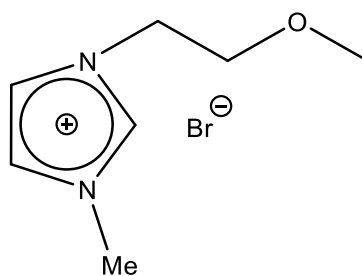
1-methyl imidazole (4.0 ml, 50 mmol) and 1-bromoethane (4.1 ml, 55 mmol) were subjected to the procedure described above to isolate 1-ethyl-3-methylimidazolium bromide as a white solid (9.75 g, 50 mmol, 100 %).

**<sup>1</sup>H NMR (400 MHz, CDCl<sub>3</sub>)** δ 10.30 (s, 1H), 7.58 (s, 1H), 7.57 (s, 1H), 4.40 (q, *J* = 7.5 Hz, 2H), 4.10 (s, 3H), 1.58 (t, *J* = 7.5 Hz, 3H); **<sup>13</sup>C NMR (101 MHz, CDCl<sub>3</sub>)** δ 136.5, 123.6, 122.0, 45.0, 36.5, 15.6; **TOF MS (ES<sup>+</sup>)** m/z 111 ([C<sub>2</sub>mim]<sup>+</sup>), (ES<sup>-</sup>); m/z 79 ([Br]<sup>-</sup>).

**1-hexyl-3-methylimidazolium bromide [C<sub>6</sub>mim]Br<sup>4</sup>**

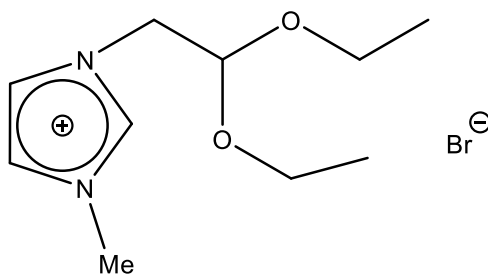
1-methyl imidazole (4.0 ml, 50 mmol) and 1-bromohexane (7.7 ml, 55 mmol) were subjected to the procedure described above to isolate 1-hexyl-3-methylimidazolium bromide as a brown viscous liquid (12.35 g, 50 mmol, 100 %).

**<sup>1</sup>H NMR (400 MHz, CDCl<sub>3</sub>)** δ 10.11 (s, 1H), 7.61 (s, 1H), 7.44 (s, 1H), 4.19 (t, *J* = 7.5 Hz, 2H), 3.99 (s, 3H), 1.85 – 1.64 (m, 2H), 1.29 – 1.02 (m, 6H), 0.72 (t, *J* = 7.0 Hz, 3H); **<sup>13</sup>C NMR (101 MHz, CDCl<sub>3</sub>)** δ 137.0, 123.7, 122.0, 50.0, 36.8, 31.0, 30.3, 25.5, 22.1, 13.9; **TOF MS (ES<sup>+</sup>)**; *m/z* 167 ([C<sub>6</sub>mim]<sup>+</sup>), (ES<sup>-</sup>); *m/z* 79 ([Br<sup>-</sup>]).

**1-(2-Methoxyethyl)-3-methylimidazolium bromide [C<sub>3</sub>O<sub>1</sub>mim]Br<sup>5</sup>**

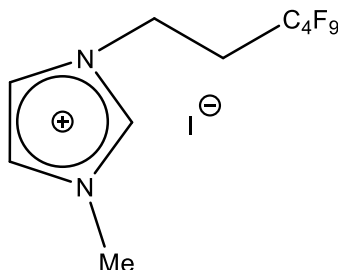
1-methyl imidazole (4.0 ml, 50 mmol) and 2-bromoethyl methyl ether (5.2 ml, 55 mmol) were subjected to the procedure described above, but heated to 40 °C instead overnight, to isolate 1-(2-methoxyethyl)-3-methylimidazolium bromide as a pale yellow solid (10.62 g, 48 mmol, 96 %).

**<sup>1</sup>H NMR (400 MHz, CDCl<sub>3</sub>)** δ 9.76 (s, 1H), 7.53 (s, 1H), 7.51 (s, 1H), 4.40 (t, *J* = 6.0 Hz, 2H), 3.93 (s, 3H), 3.57 (t, *J* = 6.0 Hz, 2H), 3.17 (s, 3H); **<sup>13</sup>C NMR (101 MHz, CDCl<sub>3</sub>)** δ 137.0 (s), 123.3 (s), 123.0 (s), 70.0 (s), 58.9 (s), 49.6 (s), 36.6 (s).; **TOF MS (ES<sup>+</sup>)**; *m/z* 141 ([C<sub>3</sub>O<sub>1</sub>mim]<sup>+</sup>), (ES<sup>-</sup>); *m/z* 79 ([Br<sup>-</sup>]).

**1-(2,2-diethoxyethyl)-3-methylimidazolium bromide [C<sub>2</sub>(O<sub>1</sub>C<sub>2</sub>)<sub>2</sub>mim]<sup>+</sup>Br<sup>-</sup>**

1-methyl imidazole (4.0 ml, 50 mmol) and 1-Bromo-2,2-diethoxyethane (8.3 ml, 55 mmol) were subjected to the procedure described above, but heated for 48 hours instead, to isolate 3-(2,2-diethoxyethyl)-1-methylimidazolium bromide as a dark brown solid (13.40 g, 48 mmol, 96 %).

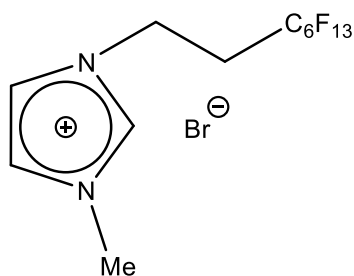
**<sup>1</sup>H NMR (400 MHz, CDCl<sub>3</sub>)** δ 9.62 (s, 1H), 7.48 (s, 1H), 7.29 (s, 1H), 4.56 (t, *J* = 4.0 Hz, 1H), 4.20 (d, *J* = 4.0 Hz, 2H), 3.83 (s, 3H), 3.52 – 3.41 (m, 2H), 3.41 – 3.27 (m, 2H), 0.89 (t, *J* = 7.0 Hz, 6H); **<sup>13</sup>C NMR (101 MHz, CDCl<sub>3</sub>)** δ 137.3 (s), 123.4 (s), 123.0 (s), 99.2 (s), 63.8 (s), 51.5 (s), 36.5 (s), 14.9 (s). **TOF MS (ES<sup>+</sup>);** *m/z* 199 ([C<sub>2</sub>(O<sub>1</sub>C<sub>2</sub>)<sub>2</sub>mim]<sup>+</sup>), (**ES<sup>+</sup>**); *m/z* 79 ([Br]<sup>-</sup>).

**1-(1,1,1,2,2,3,3,4,4-nonafluorohexyl)-3-methylimidazolium iodide [C<sup>F</sup><sub>4</sub>C<sub>2</sub>mim]<sup>+</sup>I<sup>-</sup>**

1-methyl imidazole (4.0 ml, 50 mmol) and 1,1,1,2,2,3,3,4,4-nonafluorohexyl iodide (10.6 ml, 55 mmol) were added to a glass microwave vial (35 ml) and heated in a microwave reactor to 120 °C for 20 minutes. Once cooled to room temperature, the mixture was diluted with dichloromethane (100 ml) and water (100 ml) was added. Three layers formed and the bottom two layers were collected and the aqueous layer was washed with further amounts of dichloromethane (2 x 25 ml). The organic layers were combined and the dichloromethane removed under reduced pressure to yield 1-(1,1,1,2,2,3,3,4,4-nonafluorohexyl)-3-methylimidazolium iodide as a pale yellow waxy solid (15.5 g, 34 mmol, 68 %).

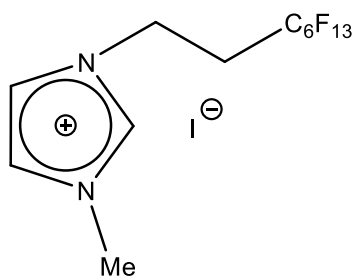
**<sup>1</sup>H NMR (400 MHz, DMSO-d<sup>6</sup>)** δ 9.32 (s, 1H), 7.93 (s, 1H), 7.77 (s, 1H), 4.59 (t, *J* = 7.0 Hz, 2H), 3.89 (s, 3H), 3.02 (tt, *J* = 19.5, 7.0 Hz, 2H); **<sup>13</sup>C NMR (101 MHz, DMSO-d<sup>6</sup>)** δ 137.7 (s), 124.1 (s), 122.9 (s), 121.7 – 120.2 (m), 119.7 – 117.6 (m), 115.8 – 114.7 (m), 111.4 – 108.1 (m), 41.7 (t, *J* = 11.0 Hz), 36.2 (s), 30.4 (t, *J* = 20.5 Hz); **<sup>19</sup>F NMR (377 MHz, DMSO-d<sup>6</sup>)** δ -80.4, -113.7, -124.0, -125.7; **TOF MS (ES<sup>+</sup>)**; *m/z* 329 ([C<sup>F</sup><sub>4</sub>C<sub>2</sub>mim]<sup>+</sup>), (ES<sup>+</sup>); *m/z* 127 ([I<sup>-</sup>]);



**1-(1,1,1,2,2,3,3,4,4,5,5,6,6-tridecafluorooctyl)-3-methylimidazolium bromide [C<sub>6</sub>F<sub>13</sub>mim]<sup>+</sup>Br<sup>-</sup>**


1-methylimidazole (1.0 ml, 12 mmol) and 1,1,1,2,2,3,3,4,4,5,5,6,6-tridecafluorooctyl bromide (3.2 ml, 13 mmol) were subjected to the procedure described above to isolate 1-(1,1,1,2,2,3,3,4,4,5,5,6,6-tridecafluorooctyl)-3-methylimidazolium bromide as a dark brown viscous liquid (1.79 g, 4 mmol, 35 %)

<sup>1</sup>H NMR (400 MHz, DMSO-d<sup>6</sup>) δ 10.19 (s, 1H), 7.82 (s, 1H), 7.60 (s, 1H), 4.76 (t, *J* = 6.5 Hz, 2H), 4.01 (s, 3H) 2.86 (t, *J* = 6.5 Hz, 2H); <sup>13</sup>C NMR (101 MHz, DMSO-d<sup>6</sup>) δ 137.6 (s), 124.3 (s), 123.3 (s), 121.7 – 119.3 (m), 119.0 – 117.5 (m), 116.4 – 114.5 (m), 114.1 – 112.1 (m), 111.5 – 109.7 (m), 109.2 – 106.7 (m), 41.5 (s), 36.5 (s), 30.2 (t, *J* = 20.5 Hz); <sup>19</sup>F NMR (377 MHz, DMSO-d<sup>6</sup>) δ -81.7, -113.9, -122.4, -123.3, -124.1, -126.9; TOF MS (ES<sup>+</sup>); *m/z* 429 ([C<sub>6</sub>F<sub>13</sub>mim]<sup>+</sup>), (ES<sup>+</sup>); *m/z* 79 ([Br]<sup>-</sup>); Elemental, calculated for C<sub>12</sub>H<sub>10</sub>N<sub>2</sub>F<sub>13</sub>Br C 28.11 % H 2.01 % N 5.56 % Br 15.69 %, Found C 26.04 % H 2.84 % N 5.88 % Br 19.27 %.

**1-(1,1,1,2,2,3,3,4,4,5,5,6,6-tridecafluorooctyl)-3-methylimidazolium iodide [C<sub>6</sub>F<sub>13</sub>C<sub>2</sub>mim]<sup>+</sup>I<sup>-</sup>**

1-methylimidazole (4.0 ml, 50 mmol) and 1,1,1,2,2,3,3,4,4,5,5,6,6-tridecafluorooctyl iodide (13.8 ml, 55 mmol) were subjected to the procedure described above. The crude mixture was further purified via flash column chromatography (silica gel, 60 % chloroform in acetonitrile) to isolate 1-(1,1,1,2,2,3,3,4,4,5,5,6,6-tridecafluorooctyl)-3-methylimidazolium iodide as a dark brown viscous liquid (2.171 g, 4 mmol, 39 %).

**<sup>1</sup>H NMR (400 MHz, DMSO-d<sub>6</sub>)** δ 10.13 (s, 1H), 7.65 (s, 1H), 7.49 (s, 1H), 4.87 (t, *J* = 6.5 Hz, 2H), 4.10 (s, 3H), 2.98 (t, *J* = 6.5 Hz, 2H); **<sup>13</sup>C NMR (101 MHz, DMSO-d<sub>6</sub>)** δ 137.7 (s), 124.1 (s), 122.9 (s), 121.7 – 119.8 (m), 119.1 – 117.5 (m), 116.3 – 114.9 (m), 114.1 – 112.1 (m), 111.5 – 109.7 (m), 109.2 – 106.7 (m), 41.7 (s), 36.5 (s), 30.6 (t, *J* = 20.5 Hz). **<sup>19</sup>F NMR (377 MHz, DMSO-d<sub>6</sub>)** δ -78.4, -81.5, -114.0, -122.2, -123.7, -123.9, -126.8; **TOF MS (ES<sup>+</sup>)**; *m/z* 429 ([C<sub>6</sub>F<sub>13</sub>C<sub>2</sub>mim]<sup>+</sup>), **(ES<sup>-</sup>)**; *m/z* 127 ([I]<sup>-</sup>).

## 2.9.2 Synthesis of Non-Halide Ionic Liquids

### *Anion Exchange by Anion Exchange Column*

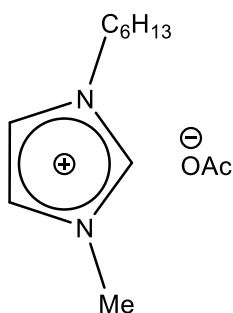
The following ionic liquids were prepared via anion exchange from either the bromide or iodide precursor using anion exchange resin. The procedure is adapted from that reported by Dinares *et al.*<sup>9</sup>

Anion exchange resin, in this case Amberlyst A-26 (OH-form), was loaded into a sintered column to a depth of about 15 cm. Methanol was poured over until it just covered the top of the resin and a separate methanolic solution of the relevant acid (AcOH or CF<sub>3</sub>COOH ~ 2 M concentration, 50 ml) was poured into the column and eluted slowly until dryness. The reaction proceeds with a change of colour in the resin from pink to yellow, which is indicative of the neutralisation reaction occurring, and the loading of the conjugate base of the acid being loaded onto the column. Once completed, the column was then washed with methanol until the eluent was no longer acidic, typically about 150 ml of methanol was used.

The resin was then recovered with methanol, just enough to cover, and a methanolic solution of a halide salt (15 g in about 50 ml of methanol) was poured into the column and eluted slowly over about a 4 hour period. After elution, the column was washed with further with methanol, approximately 4 x 50 ml, and the solvent removed under reduced pressure. The procedure was repeated until no trace of the halide was detected, by mass spectrometry. Typically, this required 2 – 3 runs of the column. Once confident there was no residual halide, the product was dried under vacuum at 80 °C for at least 6 hours. These salts were analysed by <sup>1</sup>H NMR spectroscopy, <sup>13</sup>C NMR spectroscopy, <sup>19</sup>F NMR spectroscopy where appropriate, electrospray mass spectrometry (ES<sup>+</sup> and ES<sup>-</sup>) and CHNS elemental analysis. Some elemental analyses are slightly different to that predicted. This was owed to the

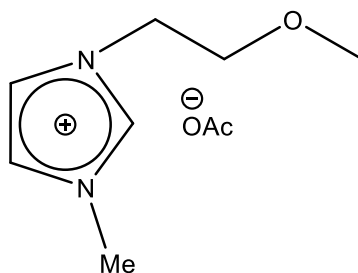
hygroscopic nature of these compounds. Incorporation of water whilst waiting to be analysed is the most likely cause of the disparity.

**1-hexyl-3-methylimidazolium acetate [C<sub>6</sub>mim]OAc<sup>10</sup>**



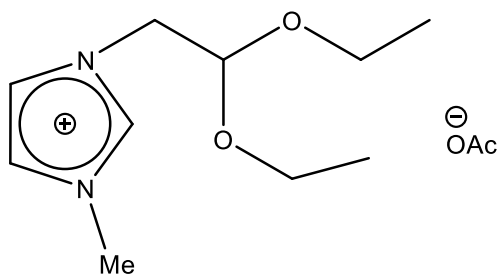
1-hexyl-3-methylimidazolium bromide (12.3 g, 50 mmol) was subjected to the procedure described above. The column required 2 runs to isolate 1-hexyl-3-methylimidazolium acetate as a pale yellow liquid (8.5 g, 38 mmol, 75 %).

<sup>1</sup>H NMR (400 MHz, CDCl<sub>3</sub>) δ 10.40 (s, 1H), 7.25 (s, 1H), 7.11 (s, 1H), 3.88 (t, J = 7.5 Hz, 2H), 3.66 (s, 3H), 1.57 (s, 3H), 1.53 – 1.38 (m, 2H), 1.03 – 0.78 (m, 6H), 0.46 (t, J = 6.5 Hz, 3H); <sup>13</sup>C NMR (101 MHz, CDCl<sub>3</sub>) δ 176.5 (s), 139.3 (s), 123.3 (s), 121.5 (s), 49.5 (s), 35.9 (s), 30.8 (s), 29.9 (s), 25.5 (s), 24.4 (s), 22.1 (s), 13.64 (s); TOF MS (ES<sup>+</sup>); m/z 167 ([C<sub>6</sub>mim]<sup>+</sup>); Elemental, calculated for C<sub>12</sub>H<sub>22</sub>N<sub>2</sub>O<sub>2</sub> C 63.69 % H 9.80 % N 12.38 % Br 0.00 %, Found C 61.91 % H 9.41 % N 11.56 % Br < 0.3 %

**1-(2-Methoxyethyl)-3-methylimidazolium acetate [C<sub>3</sub>O<sub>1</sub>mim]OAc<sup>10</sup>**

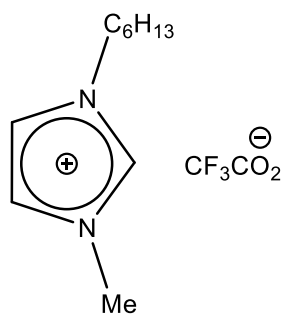
1-(2-Methoxyethyl)-3-methylimidazolium bromide (15 g, 68 mmol) was subjected to the procedure described above. The column required 3 runs to isolate 1-(2-Methoxyethyl)-3-methylimidazolium acetate as a yellow viscous liquid (10.20 g, 51 mmol, 75%).

**<sup>1</sup>H NMR (400 MHz, CDCl<sub>3</sub>)** δ 9.56 (s, 1H), 7.48 (s, 2H), 4.39 (t, *J* = 4.5 Hz, 2H), 3.92 (s, 3H), 3.60 (t, *J* = 4.5 Hz, 2H), 3.19 (s, 3H), 1.89 (s, 3H); **<sup>13</sup>C NMR (101 MHz, CDCl<sub>3</sub>)** δ 174.3 (s), 136.8 (s), 123.2 (s), 123.1 (s), 70.1 (s), 58.9 (s), 49.6 (s), 36.6 (s), 21.1 (s); **TOF MS (ES<sup>+</sup>)**; *m/z* 141 ([C<sub>3</sub>O<sub>1</sub>mim]<sup>+</sup>); **Elemental calculated for C<sub>9</sub>H<sub>16</sub>N<sub>2</sub>O<sub>3</sub>** C 53.99 % H 8.05 % N 13.99 % Br 0.00 % **Found** C 51.54 % H 8.55 % N 13.11 % Br < 0.3 %

**1-(2,2-diethoxyethyl)-3-methylimidazolium acetate**  $[\text{C}_2(\text{O}_1\text{C}_2)_2\text{mim}]\text{OAc}^{10}$ 

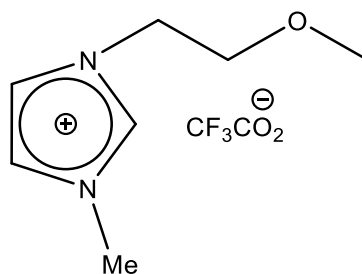
1-(2,2-diethoxyethyl)-3-methylimidazolium bromide (15 g, 54 mmol) was subjected to the procedure described above. The column required 3 runs to isolate 1-(2,2-diethoxyethyl)-3-methylimidazolium acetate as a dark brown viscous liquid (12.20 g, 47 mmol, 88 %)

**<sup>1</sup>H NMR (400 MHz, CDCl<sub>3</sub>)** δ 9.53 (s, 1H), 7.47 (s, 1H), 7.37 (s, 1H), 4.70 (t, *J* = 4.0 Hz, 1H), 4.32 (d, *J* = 4.0 Hz, 2H), 3.94 (s, 3H), 3.68 – 3.55 (m, 2H), 3.55 – 3.38 (m, 2H), 1.91 (s, 3H), 1.04 (t, *J* = 7.0 Hz, 6H);  
**<sup>13</sup>C NMR (101 MHz, CDCl<sub>3</sub>)** δ 174.3 (s), 137.5 (s), 123.6 (s), 123.0 (s), 99.3 (s), 64.0 (s), 51.7 (s), 36.6 (s), 21.0 (s), 15.0 (s).; **TOF MS (ES<sup>+</sup>)**; *m/z* 199 ([C<sub>2</sub>(O<sub>1</sub>C<sub>2</sub>)<sub>2</sub>mim]<sup>+</sup>). **Elemental, calculated for C<sub>12</sub>H<sub>22</sub>N<sub>2</sub>O<sub>4</sub>** C 55.81 % H 8.59 % N 10.85 % Br 0.00 %, **Found** C 51.88 % H 8.06 % N 8.31 % Br < 0.3 %.

**1-hexyl-3-methylimidazolium trifluoroacetate [C<sub>6</sub>mim] CF<sub>3</sub>CO<sub>2</sub><sup>10</sup>**

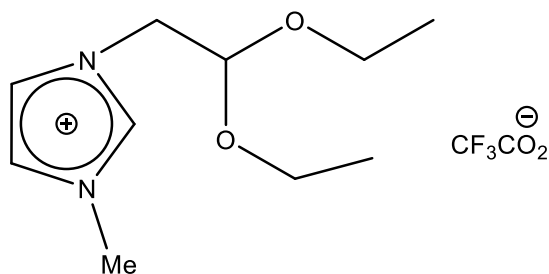
1-hexyl-3-methylimidazolium bromide (15 g, 61 mmol) was subjected to the procedure described above. The column required 3 runs to isolate 1-hexyl-3-methylimidazolium trifluoroacetate as a pale yellow viscous liquid (12.98 g, 46 mmol, 76 %).

**<sup>1</sup>H NMR (400 MHz, CDCl<sub>3</sub>)** δ 9.47 (s, 1H), 7.44 (s, 1H), 7.35 (s, 1H), 4.16 (t, *J* = 7.5 Hz, 2H), 3.94 (s, 3H), 1.84 – 1.71 (m, 2H), 1.30 – 1.10 (m, 6H), 0.73 (t, *J* = 7.0 Hz, 3H); **<sup>13</sup>C NMR (101 MHz, CDCl<sub>3</sub>)** δ 158.2 (q, *J* = 40.5 Hz), 136.4 (s), 123.7 (s), 122.1 (s), 114.8 (q, *J* = 286.0 Hz), 50.0 (s), 36.6 (s), 30.9 (s), 29.9 (s), 25.7 (s), 22.1 (s), 13.7 (s); **<sup>19</sup>F NMR (376 MHz, CDCl<sub>3</sub>)** δ -76.2 (s); **TOF MS (ES<sup>+</sup>);** *m/z* 167 ([C<sub>6</sub>mim]<sup>+</sup>), (ES<sup>-</sup>); *m/z* 113 ([CF<sub>3</sub>CO<sub>2</sub>]<sup>-</sup>); **Elemental calculated for C<sub>12</sub>H<sub>19</sub>F<sub>3</sub>N<sub>2</sub>O<sub>2</sub>** C 51.42 % H 6.83 % N 9.99 % Br 0.00 % **Found** C 51.33 % H 6.81 % N 10.16 % Br < 0.3 %

**1-(2-Methoxyethyl)-3-methylimidazolium trifluoroacetate [C<sub>3</sub>O<sub>1</sub>mim]CF<sub>3</sub>CO<sub>2</sub><sup>10</sup>**

1-(2-Methoxyethyl)-3-methylimidazolium bromide (15 g, 68 mmol) was subjected to the procedure described above. The column required 3 runs to isolate 1-(2-Methoxyethyl)-3-methylimidazolium trifluoroacetate as a pale yellow viscous liquid (13.09 g, 52 mmol, 76 %).

**<sup>1</sup>H NMR (400 MHz, CDCl<sub>3</sub>)** δ 9.57 (s, 1H), 7.48 (s, 1H), 7.46 (s, 1H), 4.38 (t, *J* = 5.0 Hz, 2H), 3.92 (s, 3H), 3.60 (t, *J* = 5.0 Hz, 2H), 3.18 (s, 3H); **<sup>13</sup>C NMR (101 MHz, CDCl<sub>3</sub>)** δ 158.0 (q, *J* = 40.5 Hz), 136.8 (s), 123.3 (s), 123.1 (s), 114.8 (q, *J* = 286.5 Hz), 70.0 (s), 58.8 (s), 49.7 (s), 36.6 (s, *J* = 27.5 Hz); **<sup>19</sup>F NMR (377 MHz, CDCl<sub>3</sub>)** δ -76.1 (s); **TOF MS (ES<sup>+</sup>);** *m/z* 141 ([C<sub>3</sub>O<sub>1</sub>mim]<sup>+</sup>), (ES<sup>+</sup>); *m/z* 113 ([CF<sub>3</sub>CO<sub>2</sub>]<sup>-</sup>); **Elemental calculated for C<sub>9</sub>H<sub>13</sub>F<sub>3</sub>N<sub>2</sub>O<sub>3</sub>** C 42.52 % H 5.15 % N 11.02 Br 0.00 % **Found** C 42.19 % H 5.24 % N 11.19 Br < 0.3 %

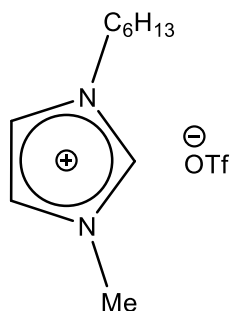
**1-(2,2-diethoxyethyl)-3-methylimidazolium trifluoroacetate**  $[\text{C}_2(\text{O}_1\text{C}_2)_2\text{mim}]\text{CF}_3\text{CO}_2^{-10}$ 


1-(2,2-diethoxyethyl)-3-methylimidazolium bromide (15 g, 54 mmol) was subjected to the procedure described above. The column required 2 runs to isolate 1-(2,2-diethoxyethyl)-3-methylimidazolium trifluoroacetate as a brown viscous liquid (13.56 g, 43 mmol, 82 %).

**$^1\text{H}$  NMR (400 MHz,  $\text{CDCl}_3$ )**  $\delta$  9.06 (s, 1H), 7.29 (s, 1H), 7.27 (s, 1H), 4.57 (t,  $J = 4.0$  Hz, 1H), 4.15 (d,  $J = 4.0$  Hz, 2H), 3.77 (s, 3H), 3.62 – 3.48 (m, 2H), 3.45 – 3.29 (m, 2H), 0.97 (t,  $J = 7.0$  Hz, 6H).  **$^{13}\text{C}$  NMR (101 MHz,  $\text{CDCl}_3$ )**  $\delta$  158.2 (q,  $J = 40.5$  Hz), 137.3 (s), 123.8 (s), 122.9 (s), 117.4 (q,  $J = 288.0$  Hz), 99.2 (s), 64.1 (s), 52.0 (s), 36.6 (s), 14.9 (s).  **$^{19}\text{F}$  NMR (376 MHz,  $\text{CDCl}_3$ )**  $\delta$  -76.2 (s); **TOF MS ( $\text{ES}^+$ )**;  $m/z$  199 ( $[\text{C}_2(\text{O}_1\text{C}_2)_2\text{mim}]^+$ ), ( **$\text{ES}^-$** );  $m/z$  113 ( $[\text{CF}_3\text{CO}_2]^-$ ); **Elemental, calculated for  $\text{C}_{12}\text{H}_{19}\text{N}_2\text{O}_4\text{F}_3$**  C 46.21 % H 5.54 % N 9.00 % Br 0.00 %, **Found** C 46.27 % H 5.50 % N 8.92 % Br < 0.3 %.

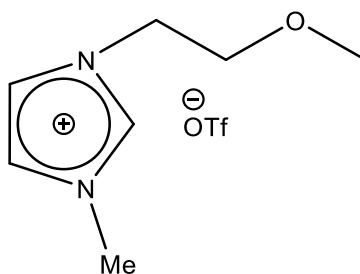
**Anion Exchange by Metathesis**

The following compounds were synthesised using an adapted metathesis method.<sup>11</sup> In general, a sample of the appropriate salt (~ 10 mmol) was dissolved in 1 ml of deionised water under N<sub>2</sub>. To this 1.1 equivalents of lithium bis(trifluoromethylsulfonyl)imide or lithium trifluoromethanesulfonate dissolved in minimum amount of deionised water was added and stirred vigorously at room temperature for several hours. The 2 immiscible layers were separated and the bottom, ionic liquid layer, washed several times with deionised water to remove any residual halide. To remove any water remaining, the product is dried under vacuum of 10<sup>-2</sup> mPa at 80 °C for 4 hours.

**1-hexyl-3-methylimidazolium triflate [C<sub>6</sub>mim]<sup>+</sup>OTf<sup>-</sup>**

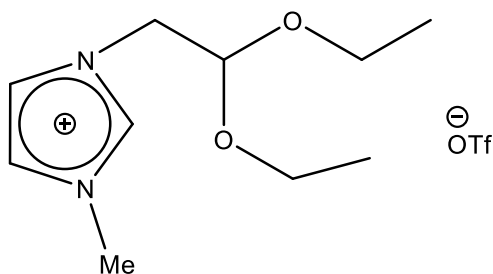
1-hexyl-3-methylimidazolium bromide (12.3 g, 50 mmol) was subjected to the procedure described above to isolate 1-hexyl-3-methylimidazolium triflate as a pale yellow viscous liquid (14.22 g, 45 mmol, 90 %)

**<sup>1</sup>H NMR (400 MHz, CDCl<sub>3</sub>)** δ 8.85 (s, 1H), 7.33 (d, *J* = 8.5 Hz, 2H), 4.05 (t, *J* = 7.5 Hz, 2H), 3.82 (s, 3H), 1.81 – 1.65 (m, 2H), 1.28 – 1.05 (m, 6H), 0.72 (t, *J* = 6.5 Hz, 3H); **<sup>13</sup>C NMR (101 MHz, CDCl<sub>3</sub>)** δ 136.3 (s), 123.8 (s), 122.3 (s), 120.6 (q, *J* = 320.0 Hz), 49.9 (s), 36.1 (s), 30.9 (s), 29.9 (s), 25.6 (s), 22.2 (s), 13.8 (s); **<sup>19</sup>F NMR (377 MHz, CDCl<sub>3</sub>)** δ -78.9; **TOF MS (ES<sup>+</sup>);** *m/z* 167 ([C<sub>6</sub>mim]<sup>+</sup>), (ES<sup>+</sup>); *m/z* 149 ([OTf]<sup>-</sup>); **Elemental calculated for C<sub>11</sub>H<sub>18</sub>N<sub>2</sub>SO<sub>3</sub>F<sub>3</sub>** C 41.62 % H 6.04 % N 8.82 % S 10.09 % Br 0.00 %, **Found** C 41.06 % H 6.05 % N 8.63 % S 10.04 % Br < 0.3 %

**1-(2-Methoxyethyl)-3-methylimidazolium triflate [C<sub>3</sub>O<sub>1</sub>mim]OTf<sup>13</sup>**

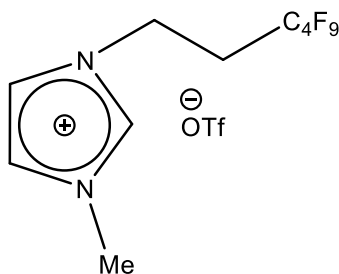
1-(2-Methoxyethyl)-3-methylimidazolium bromide (15 g, 68 mmol) was subjected to the procedure described above to isolate 1-(2-Methoxyethyl)-3-methylimidazolium triflate as a pale yellow viscous liquid (17.40 g, 60 mmol, 89 %).

**<sup>1</sup>H NMR (400 MHz, CDCl<sub>3</sub>)** δ 8.79 (s, 1H), 7.38 (s, 1H), 7.33 (s, 1H), 4.25 (t, *J* = 4.5 Hz, 2H), 3.83 (s, 3H), 3.59 (t, *J* = 4.5 Hz, 2H), 3.22 (s, 3H).; **<sup>13</sup>C NMR (101 MHz, CDCl<sub>3</sub>)** δ 136.5 (s), 123.3 (s), 123.0 (s), 120.5 (q, *J* = 320.0 Hz), 69.7 (s), 58.6 (s), 49.5 (s), 36.1 (s).; **<sup>19</sup>F NMR (377 MHz, CDCl<sub>3</sub>)** δ -78.9 (s).; **TOF MS (ES<sup>+</sup>);** *m/z* 141 ([C<sub>3</sub>O<sub>1</sub>mim]<sup>+</sup>), **(ES<sup>-</sup>);** *m/z* 149 ([OTf]<sup>-</sup>). **Elemental, calculated for C<sub>8</sub>H<sub>13</sub>N<sub>2</sub>SO<sub>4</sub>F<sub>3</sub>** C 33.10 % H 4.50 % N 9.65 % S 11.05 % Br 0.00 %, **Found** C 33.13 % H 4.47 % N 10.15 % S 11.21 % Br < 0.3 %.

**1-(2,2-diethoxyethyl)-3-methylimidazolium triflate [C<sub>2</sub>(O<sub>1</sub>C<sub>2</sub>)<sub>2</sub>mim]OTf**

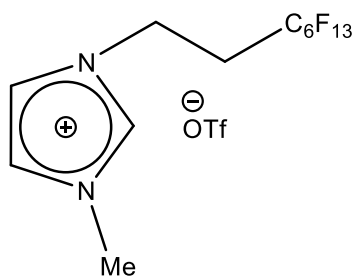
1-(2,2-diethoxyethyl)-3-methylimidazolium bromide (15 g, 54 mmol) was subjected to the procedure described above to isolate 1-(2,2-diethoxyethyl)-3-methylimidazolium triflate as a brown viscous liquid (13.83 g, 40 mmol, 75 %).

**<sup>1</sup>H NMR (400 MHz, CDCl<sub>3</sub>)** δ 8.61 (s, 1H), 7.35 (s, 1H), 7.30 (s, 1H), 4.71 (t, *J* = 4.0 Hz, 1H), 4.23 (d, *J* = 4.0 Hz, 2H), 3.92 (s, 3H), 3.79 – 3.66 (m, 2H), 3.63 – 3.50 (m, 2H), 1.18 (t, *J* = 7.0 Hz, 6H). **<sup>13</sup>C NMR (101 MHz, CDCl<sub>3</sub>)** δ 136.7 (s), 123.9 (s), 122.9 (s), 120.6 (q, *J* = 323.2 Hz), 99.2 (s), 64.2 (s), 52.08 (s), 36.2 (s), 14.9 (s).; **<sup>19</sup>F NMR (376 MHz, CDCl<sub>3</sub>)** δ -79.2 (s); **TOF MS (ES<sup>+</sup>)**; *m/z* 199 ([C<sub>2</sub>(O<sub>1</sub>C<sub>2</sub>)<sub>2</sub>mim]<sup>+</sup>), (**ES<sup>+</sup>**); *m/z* 149 ([OTf]<sup>-</sup>). **Elemental, calculated for C<sub>11</sub>H<sub>19</sub>N<sub>2</sub>SO<sub>5</sub>F<sub>3</sub>** C 38.00% H 5.50 % N 8.00 % S 9.20 % Br 0.00 %, **Found** C 38.08 % H 5.60 % N 8.00 % S 8.40 % Br < 0.3 %.

**1-(1,1,1,2,2,3,3,4,4-nonafluorohexyl)-3-methylimidazolium triflate [ $C^F_4C_2mim$ ]OTf**

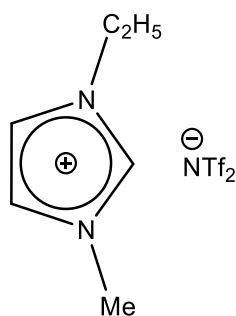
1-(1,1,1,2,2,3,3,4,4-nonafluorohexyl)-3-methylimidazolium iodide (15 g, 68 mmol) was subjected to the procedure described above to isolate 1-(2-Methoxyethyl)-3-methylimidazolium triflate as a pale yellow viscous liquid (17.40 g, 60 mmol, 89 %).

**$^1H$  NMR (400 MHz, DMSO- $d^6$ )**  $\delta$  9.22 (s, 1H), 7.89 (s, 1H), 7.73 (s, 1H), 4.58 (t,  $J$  = 7.0 Hz, 2H), 3.88 (s, 3H), 3.01 (tt,  $J$  = 19.5, 7.0 Hz, 2H);  **$^{13}C$  NMR (101 MHz, DMSO- $d^6$ )**  $\delta$  137.7 (s), 124.1 (s), 122.9 (s), 121.1 (q,  $J$  = 322.0 Hz), 121.7 – 120.2 (m), 119.7 – 117.6 (m), 115.9 – 114.7 (m), 111.6 – 108.3 (m), 41.6 (t,  $J$  = 11.0 Hz), 36.2 (s), 30.4 (t,  $J$  = 20.5 Hz).;  **$^{19}F$  NMR (377 MHz, DMSO- $d^6$ )**  $\delta$  -78.0, -80.8, -113.6, -124.2, -125.9; **TOF MS (ES $^+$ )**;  $m/z$  329 ( $[C^F_4C_2mim]^+$ ), (ES $^+$ );  $m/z$  149 ([OTf] $^-$ ); **Elemental calculated for  $C_{11}H_{10}F_{12}N_2O_3S$**  C 27.63 % H 2.11 % N 5.68 % S 6.70 I 0.00 % **Found** C 27.51 % H 2.45 % N 6.00 % S 6.34 % I < 0.3 %

**1-(1,1,1,2,2,3,3,4,4,5,5,6,6-tridecafluorooctyl)-3-methylimidazolium triflate  $[(C^F_6C_2mim)][OTf]$** 


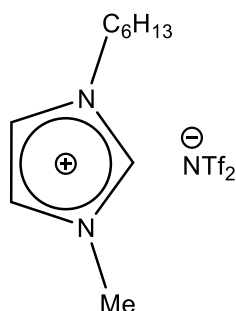
1-(1,1,1,2,2,3,3,4,4,5,5,6,6-tridecafluorooctyl)-3-methylimidazolium iodide (15 g, 27 mmol) was subjected to the procedure described above. The column required 2 runs to isolate 1-(1,1,1,2,2,3,3,4,4,5,5,6,6-tridecafluorooctyl)-3-methylimidazolium triflate as a yellow viscous liquid (12.00 g, 22 mmol, 80 %).

$^1H$  NMR (400 MHz, DMSO- $d_6$ )  $\delta$  8.95 (s, 1H), 7.66 (s, 1H), 7.49 (s, 1H), 4.42 (t,  $J$  = 7.2 Hz, 2H), 3.74 (s, 3H), 2.90 – 2.64 (m, 2H);  $^{13}C$  NMR (101 MHz, DMSO- $d_6$ )  $\delta$  137.7, 124.0, 122.8, 120.6 (q,  $J$  = 320.0 Hz), 120.9 – 119.8 (m), 119.1 – 117.6 (m), 116.3 – 115.1 (m), 114.0 – 112.4 (m), 111.6 – 110.0 (m), 109.4 – 107.3 (m), 41.7, 36.1, 30.5 (t,  $J$  = 20.5 Hz);  $^{19}F$  NMR (377 MHz, DMSO- $d_6$ )  $\delta$  -78.5, -81.7, -114.0, -122.4, -123.5, -123.9, -126.9; TOF MS ( $ES^+$ );  $m/z$  429 ( $[C^F_6C_2mim]^+$ ), ( $ES^-$ );  $m/z$  149 ( $[OTf]^-$ ); Elemental, calculated for  $C_{13}H_{10}N_2SO_3F_{16}$  C 27.01 % H 1.77 % N 4.80 % S 5.45 % Br 0.00 %, Found C 26.97 % H 1.92 % N 4.80 % S 5.64 % Br < 0.3 %.

**1-ethyl-3-methylimidazolium bis(trifluoromethylsulfonyl)imide [C<sub>2</sub>mim]NTf<sub>2</sub><sup>14</sup>**

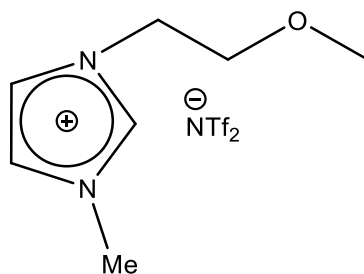
1-ethyl-3-methylimidazolium bromide (12.3 g, 50 mmol) was subjected to the procedure described above to yield 1-ethyl-3-methylimidazolium bis(trifluoromethylsulfonyl)imide as a colourless liquid (16.03 g, 41 mmol, 82 %).

**<sup>1</sup>H NMR (400 MHz, CDCl<sub>3</sub>)** δ 8.47 (s, 1H), 7.29 (s, 1H), 7.24 (s, 1H), 4.11 (q, *J* = 7.5 Hz, 2H), 3.78 (s, 3H), 1.41 (t, *J* = 7.5 Hz, 3H). **<sup>13</sup>C NMR (101 MHz, CDCl<sub>3</sub>)** δ 135.2 (s), 123.6 (s), 121.9 (s), 119.6 (q, *J* = 320.0 Hz), 44.9 (s), 35.9 (s), 14.7 (s); **<sup>19</sup>F NMR (377 MHz, CDCl<sub>3</sub>)** δ -79.6 (s). **TOF MS (ES<sup>+</sup>);** *m/z* 111 ([C<sub>2</sub>mim]<sup>+</sup>), (ES<sup>+</sup>); *m/z* 280 ([NTf<sub>2</sub>]<sup>-</sup>); **Elemental calculated for C<sub>8</sub>H<sub>11</sub>F<sub>6</sub>N<sub>3</sub>O<sub>4</sub>S<sub>2</sub>** C 24.56 % H 2.83 % N 10.74 % S 16.39 % **Found** C 24.57 % H 2.73 % N 10.71 % S 16.72 % Br < 0.3 %.

**1-hexyl-3-methylimidazolium bis(trifluoromethylsulfonyl)imide [C<sub>6</sub>mim]NTf<sub>2</sub><sup>11</sup>**

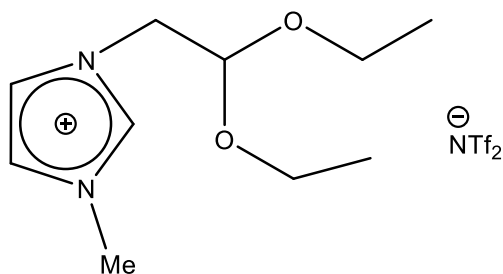
1-hexyl-3-methylimidazolium bromide (12.3 g, 50 mmol) was subjected to the procedure described above to yield 1-hexyl-3-methylimidazolium bis(trifluoromethylsulfonyl)imide as a colourless liquid (18.33 g, 41 mmol, 82 %).

<sup>1</sup>H NMR (400 MHz, CDCl<sub>3</sub>) δ 8.66 (s, 1H), 7.39 (s, 1H), 7.25 (s, 1H), 4.18 – 4.09 (m, 2H), 3.91 (s, 3H), 1.90 – 1.76 (m, 2H), 1.38 – 1.21 (m, 6H), 0.86 (t, J = 7.0 Hz, 3H); <sup>13</sup>C NMR (101 MHz, CDCl<sub>3</sub>) δ 135.7 (s), 123.7 (s), 122.4 (s), 119.7 (q, J = 321.0 Hz), 50.0 (s), 36.1 (s), 30.8 (s), 29.9 (s), 25.6 (s), 22.2 (s), 13.7 (s). <sup>19</sup>F NMR (377 MHz, CDCl<sub>3</sub>) δ -79.2; TOF MS (ES<sup>+</sup>); m/z 167 ([C<sub>6</sub>mim]<sup>+</sup>), (ES<sup>-</sup>); m/z 280 ([NTf<sub>2</sub>]<sup>-</sup>); Elemental, calculated for C<sub>12</sub>H<sub>19</sub>F<sub>6</sub>N<sub>3</sub>O<sub>4</sub>S<sub>2</sub> C 32.21 % H 4.28 % F 25.48 % N 9.39 % O 14.30 % S 14.33 % Br 0.00 % Found C 32.49 % H 4.15 % N 9.50 % S 14.44 Br < 0.3 %

**1-(2-Methoxyethyl)-3-methylimidazolium bis(trifluoromethylsulfonyl)imide [C<sub>3</sub>O<sub>1</sub>mim][NTf<sub>2</sub>]<sup>15</sup>**

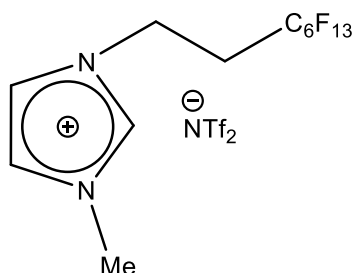
1-(2-Methoxyethyl)-3-methylimidazolium bromide (2.3 g, 10 mmol) was subjected to the procedure described above to yield 1-(2-Methoxyethyl)-3-methylimidazolium bis(trifluoromethylsulfonyl)imide as a pale yellow liquid (3.28 g, 8 mmol, 78 %).

<sup>1</sup>H NMR (400 MHz, CDCl<sub>3</sub>) δ 8.53 (s, 1H), 7.35 (s, 1H), 7.28 (s, 1H), 4.26 (t, *J* = 4.5 Hz, 2H), 3.86 (s, 3H), 3.64 (t, *J* = 4.5 Hz, 2H), 3.29 (s, 3H); <sup>19</sup>F NMR (377 MHz, CDCl<sub>3</sub>) δ -79.4 (s). <sup>13</sup>C NMR (101 MHz, CDCl<sub>3</sub>) δ 136.1 (s), 123.3 (s), 123.1 (s), 119.7 (q, *J* = 321.0 Hz), 69.6 (s), 58.7 (s), 49.7 (s), 36.1 (s). TOF MS (ES<sup>+</sup>); *m/z* 141 ([C<sub>3</sub>O<sub>1</sub>mim]<sup>+</sup>), (ES<sup>+</sup>); *m/z* 280 ([NTf<sub>2</sub>]<sup>-</sup>). Elemental, calculated for C<sub>9</sub>H<sub>13</sub>N<sub>3</sub>O<sub>5</sub>S<sub>2</sub>F<sub>6</sub> C 25.65 % H 3.09 % N 10.00 % S 15.20 % Br 0.00 %, Found C 24.10 % H 2.89 % N 9.51 % S 15.41 % Br 0.3 %.

**1-(2,2-diethoxyethyl)-3-methylimidazolium bis(trifluoromethylsulfonyl)imide [C<sub>2</sub>(O<sub>1</sub>C<sub>2</sub>)<sub>2</sub>mim][NTf<sub>2</sub>]**

1-(2,2-diethoxyethyl)-3-methylimidazolium bromide (2.8 g, 10 mmol) was subjected to the procedure described above to yield 1-(2,2-diethoxyethyl)-3-methylimidazolium bis(trifluoromethylsulfonyl)imide as a brown solid (1.05 g, 2 mmol, 22 %).

**<sup>1</sup>H NMR (400 MHz, CDCl<sub>3</sub>)** δ 8.67 (s, 1H), 7.36 (s, 1H), 7.30 (s, 1H), 4.73 (t, *J* = 4.0 Hz, 1H), 4.26 (d, *J* = 4.0 Hz, 2H), 3.95 (s, 3H), 3.80 – 3.69 (m, 2H), 3.64 – 3.53 (m, 2H), 1.20 (t, *J* = 7.0 Hz, 6H); **<sup>19</sup>F NMR (376 MHz, CDCl<sub>3</sub>)** δ -79.1 (s); **<sup>13</sup>C NMR (101 MHz, CDCl<sub>3</sub>)** δ 136.9 (s), 124.0 (s), 122.9 (s), 119.8 (q, *J* = 321.8 Hz), 99.3 (s), 64.3 (s), 52.1 (s), 36.3 (s), 14.9 (s); **TOF MS (ES<sup>+</sup>)**; *m/z* ([C<sub>2</sub>(O<sub>1</sub>C<sub>2</sub>)<sub>2</sub>mim]<sup>+</sup>) 199, (**ES<sup>-</sup>**); *m/z* 280 ([NTf<sub>2</sub>]<sup>-</sup>); **Elemental, calculated for C<sub>12</sub>H<sub>19</sub>N<sub>3</sub>S<sub>2</sub>O<sub>6</sub>F<sub>6</sub>** C 30.01 % H 3.98 % N 8.73 % S 13.29 %, **Found** C 30.06 % H 3.88 % N 8.72 % S 13.57 % Br < 0.3 %.

**1-(1,1,1,2,2,3,3,4,4,5,5,6,6-tridecafluorooctyl)-3-methylimidazolium****bis(trifluoromethylsulfonyl)imide [C<sup>F</sup><sub>6</sub>C<sub>2</sub>mim][NTf<sub>2</sub>]<sup>16</sup>**

1-(1,1,1,2,2,3,3,4,4,5,5,6,6-tridecafluorooctyl)-3-methylimidazolium iodide (5.6 g, 10 mmol) was subjected to the procedure described above to yield 1-(1,1,1,2,2,3,3,4,4,5,5,6,6-tridecafluorooctyl)-3-methylimidazolium bis(trifluoromethylsulfonyl)imide as a pale yellow liquid (4.18 g, 6 mmol, 59 %).

<sup>1</sup>H NMR (400 MHz, DMSO-d<sup>6</sup>) δ 8.88 (s, 1H), 7.69 (s, 1H), 7.50 (s, 1H), 4.42 (t, *J* = 7.0 Hz, 2H), 3.77 (s, 3H), 2.90 – 2.63 (m, 2H); <sup>13</sup>C NMR (101 MHz, DMSO-d<sup>6</sup>) δ 137.7, 124.0, 122.8, 120.9 – 119.8 (m), 119.9 (q, *J* = 319.0 Hz), 119.1 – 117.6 (m), 116.3 – 115.1 (m), 114.0 – 112.4 (m), 111.6 – 110.0 (m), 109.4 – 107.3 (m), 41.7, 36.1, 30.5 (t, *J* = 20.5 Hz); <sup>19</sup>F NMR (377 MHz, DMSO-d<sup>6</sup>) δ -78.5, -81.7, -114.0, -122.4, -123.5, -123.9, -126.9. **Elemental, calculated for C<sub>14</sub>H<sub>10</sub>N<sub>3</sub>O<sub>4</sub>S<sub>2</sub>F<sub>19</sub>** C 23.7 % H 1.50 % N 5.90 % S 9.00 % Br 0.00 %, **Found** C 22.60 % H 1.67 % N 5.84 % S 10.12 % Br 0.3 %.

### 2.9.3 Synthesis of Copper(I) Salts

#### Copper(I) trifluoroacetate [CuTFA]<sup>17</sup>

Cu<sub>2</sub>O (3 g, 21 mmol) was added to a stirred round bottom flask of toluene (50 ml) under N<sub>2</sub> to form a dark red suspension. Degassed, trifluoroacetic acid (3.2 ml, 4.76 g, 42 mmol) was then added dropwise to the suspension and once completed, the reaction mixture was allowed to stir overnight at room temperature. This procedure produced a colourless solution with some unreacted Cu<sub>2</sub>O which was filtered by canula through celite under N<sub>2</sub>. The solvent was removed under reduced pressure to give a pale green solid which, under further drying under high vacuum, gave the white crystalline solid copper(I) trifluoroacetate (5.56 g, 32 mmol, 75 %).

<sup>19</sup>F NMR (377 MHz, CDCl<sub>3</sub>) δ -73.6; TOF MS (ES<sup>+</sup>); m/z 240 ([Cu<sub>2</sub>TFA]<sup>+</sup>)

#### Bis(acetonitrile)copper(I) triflate [Cu(MeCN)<sub>2</sub>(OTf)]<sup>18</sup>

Cu<sub>2</sub>O (5g, 35 mmol) was added to a stirred round bottom flask of MeCN under N<sub>2</sub> to produce a red suspension. Trifluoromethanesulfonic acid (6 ml, 10.18 g, 68 mmol) was added dropwise at 0 °C and left to stir for 4 hours. The colourless solution produced was filtered through celite and the solvent removed under reduced pressure at 50 °C overnight to give bis(acetonitrile)copper(I) triflate as a white crystalline solid (13.67 g, 46 mmol, 66 %).

<sup>1</sup>H NMR (400 MHz, CDCl<sub>3</sub>) δ 2.15 (s); <sup>13</sup>C NMR (101 MHz, CDCl<sub>3</sub>) δ 120.5 (q, J = 321.0 Hz), 116.8 (s), 1.6 (s); <sup>19</sup>F NMR (377 MHz, CDCl<sub>3</sub>) δ -78.9; TOF MS (ES<sup>+</sup>); m/z 145 ([Cu(MeCN)<sub>2</sub>]<sup>+</sup>), (ES<sup>-</sup>); m/z 149 ([OTf]<sup>-</sup>);

Elemental, calculated for C<sub>5</sub>H<sub>6</sub>CuF<sub>3</sub>N<sub>2</sub>O<sub>3</sub>S C 20.38 % H 2.05 % N 9.51 % S 10.88 % Found C 21.37% H 2.25 % N 10.70 % S 9.99 %

**Synthesis of COSORB solution<sup>19,20</sup>**

CuCl (0.20 g, 2 mmol) was added to a stirred round bottom flask of toluene (20 ml) under N<sub>2</sub>. To this, AlCl<sub>3</sub> (0.26 g, 2 mmol) was added slowly and heated to 40 °C for 4 hours. This procedure produced an intense black suspension with some precipitate at the bottom. The solution was filtered by canula under N<sub>2</sub> to remove the precipitate and stored under an inert atmosphere which gave the basic CuAlCl<sub>4</sub>.tol<sub>2</sub> solution.

**2.9.4 Synthesis of Copper-Containing Ionic Liquids<sup>1,18</sup>**

In a typical procedure, a sample of the salt [Cation]<sup>+</sup>[X]<sup>-</sup> (~ 10 – 15 g) was weighed directly into a dried round bottom flask under N<sub>2</sub>. The sample was then heated to 80 °C for an hour under vacuum to ensure dryness, allowed to cool to room temperature. To this, 1 equivalent of the corresponding CuX salt was added, the only exception were salts with the anion NTf<sub>2</sub><sup>-</sup>, to these salts, [Cu(MeCN)<sub>2</sub>(OTf)] was added. Once added, the mixture was heated to 80 – 100 °C for 1 hour where a melt formed. On cooling of these melts, some exhibited crystallisation to yield a semi-crystalline solid and others remained liquid.

These salts were analysed by <sup>1</sup>H NMR spectroscopy, <sup>13</sup>C NMR spectroscopy, <sup>19</sup>F NMR spectroscopy where appropriate and electrospray mass spectrometry (ES<sup>+</sup> and ES<sup>-</sup>). Density measurements were performed at 20 °C using a 5 ml volumetric flask and balance. The uncertainty in the volume was ±0.025 ml and mass was ±0.0005.

**[C<sub>6</sub>mim][CuBr<sub>2</sub>]<sup>1</sup>**

**<sup>1</sup>H NMR (400 MHz, Acetone-d<sub>6</sub>)** δ 10.23 (s, 1H), 8.19 (s, 1H), 8.10 (s, 1H), 4.50 (t, *J* = 7.5 Hz, 2H), 4.15 (s, 3H), 2.01 – 1.86 (m, 2H), 1.41 – 1.21 (m, 6H), 0.85 (t, *J* = 7.0 Hz, 3H); **<sup>13</sup>C NMR (101 MHz, Acetone-d<sub>6</sub>)** δ 137.4 (s), 123.7 (s), 122.5 (s), 49.2 (s), 35.9 (s), 31.0 (s), 30.2 (s), 25.6 (s), 22.3 (s), 13.5 (s); **TOF MS (ES<sup>+</sup>)**; *m/z* 167 ([C<sub>6</sub>mim]<sup>+</sup>), **(ES<sup>-</sup>)**; *m/z* 223 ([CuBr<sub>2</sub>]).

**[C<sub>3</sub>O<sub>1</sub>mim][CuBr<sub>2</sub>]**

**<sup>1</sup>H NMR (400 MHz, Acetone-d<sub>6</sub>)** δ 9.96 (s, 1H), 7.91 (s, 1H), 7.84 (s, 1H), 4.65 (t, *J* = 4.5 Hz, 2H), 4.12 (s, *J* = 5.5 Hz, 3H), 3.89 – 3.81 (m, 2H), 3.37 (s, 3H); **<sup>13</sup>C NMR (101 MHz, Acetone-d<sub>6</sub>)** δ 137.7 (s), 123.3 (s), 122.9 (s), 70.1 (s), 58.0 (s), 49.2 (s), 35.7 (s); **TOF MS (ES<sup>+</sup>)**; *m/z* 141 ([C<sub>3</sub>O<sub>1</sub>mim]<sup>+</sup>), **(ES<sup>-</sup>)**; *m/z* 223 ([CuBr<sub>2</sub>]).

**[C<sub>2</sub>(O<sub>1</sub>C<sub>2</sub>)<sub>2</sub>mim][CuBr<sub>2</sub>]**

**<sup>1</sup>H NMR (400 MHz, Acetone-d<sub>6</sub>)** δ 10.05 (s, 1H), 8.09 – 7.94 (m, 2H), 5.08 (t, *J* = 5.0 Hz, 1H), 4.60 (d, *J* = 5.0 Hz, 2H), 4.15 (s, 3H), 3.81 – 3.71 (m, 2H), 3.71 – 3.61 (m, 2H), 1.14 (t, *J* = 7.0 Hz, 6H); **<sup>13</sup>C NMR (101 MHz, Acetone-d<sub>6</sub>)** δ 138.1 (s), 123.6 (s), 123.1 (s), 99.7 (s), 63.1 (s), 51.2 (s), 35.9 (s), 14.7 (s); **TOF MS (ES<sup>+</sup>)**; *m/z* 199 ([C<sub>2</sub>(O<sub>1</sub>C<sub>2</sub>)<sub>2</sub>mim]<sup>+</sup>), **(ES<sup>-</sup>)**; *m/z* 223 ([CuBr<sub>2</sub>]).

**[C<sub>6</sub>mim][Cu(NCMe)(OTf)<sub>2</sub>]**

**<sup>1</sup>H NMR (400 MHz, Acetone-d<sub>6</sub>)** δ 8.95 (s, 1H), 7.69 (s, 1H), 7.62 (s, 1H), 4.26 (t, *J* = 7.5 Hz, 2H), 3.96 (s, 3H), 2.01 (s, 3H), 1.96 – 1.80 (m, 2H), 1.39 – 1.18 (m, 6H), 0.83 (t, *J* = 7.0 Hz, 3H); **<sup>13</sup>C NMR (101 MHz, Acetone-d<sub>6</sub>)** δ 136.6 (s), 123.7 (s), 122.4 (s), 120.7 (q, *J* = 319.5 Hz), 117.2 (s), 49.4 (s), 35.7 (s), 30.9 (s), 29.8 (s), 25.4 (s), 22.1 (s), 13.3 (s), 0.4 (s); **<sup>19</sup>F NMR (377 MHz, Acetone-d<sub>6</sub>)** δ -79.2 (s); **TOF MS (ES<sup>+</sup>)**; *m/z* 167 ([C<sub>6</sub>mim]<sup>+</sup>), (ES<sup>-</sup>); *m/z* 361 ([Cu(OTf)<sub>2</sub>]<sup>-</sup>).

**[C<sub>3</sub>O<sub>1</sub>mim][Cu(NCMe)(OTf)<sub>2</sub>]**

**<sup>1</sup>H NMR (400 MHz, CDCl<sub>3</sub>)** δ 8.79 (s, 1H), 7.38 (s, 1H), 7.33 (s, 1H), 4.27 (t, *J* = 4.5 Hz, 2H), 3.85 (s, 3H), 3.61 (t, *J* = 4.5 Hz, 2H), 3.24 (s, 3H), 1.91 (s, 3H); **<sup>13</sup>C NMR (101 MHz, CDCl<sub>3</sub>)** δ 136.6 (s), 123.3 (s), 123.0 (s), 120.5 (q, *J* = 321.0 Hz), 116.8 (s), 69.8 (s), 58.6 (s), 49.6 (s), 36.1 (s), 1.6 (s); **<sup>19</sup>F NMR (376 MHz, CDCl<sub>3</sub>)** δ -78.8 (s); **TOF MS (ES<sup>+</sup>)**; *m/z* 141 ([C<sub>3</sub>O<sub>1</sub>mim]<sup>+</sup>), (ES<sup>-</sup>); *m/z* 361 ([Cu(OTf)<sub>2</sub>]<sup>-</sup>).

**[C<sub>2</sub>(O<sub>1</sub>C<sub>2</sub>)<sub>2</sub>mim][Cu(NCMe)(OTf)<sub>2</sub>]**

**<sup>1</sup>H NMR (400 MHz, CDCl<sub>3</sub>)** δ 8.56 (s, 1H), 7.33 (s, 1H), 7.28 (s, 1H), 4.69 (t, *J* = 4.0 Hz, 1H), 4.20 (d, *J* = 4.0 Hz, 2H), 3.89 (s, 3H), 3.77 – 3.63 (m, 2H), 3.63 – 3.42 (m, 2H), 1.96 (s, 3H), 1.15 (t, *J* = 7.0 Hz, 6H); **<sup>13</sup>C NMR (101 MHz, CDCl<sub>3</sub>)** δ 136.6 (s), 124.0 (s), 123.0(s), 119.8 (q, *J* = 322.0 Hz), 116.7 (s), 99.2 (s), 64.2 (s), 52.0 (s), 36.2 (s), 14.9 (s), 1.6 (s); **<sup>19</sup>F NMR (376 MHz, CDCl<sub>3</sub>)** δ -79.2 (s); **TOF MS (ES<sup>+</sup>)**; *m/z* 199 ([C<sub>2</sub>(O<sub>1</sub>C<sub>2</sub>)<sub>2</sub>mim]<sup>+</sup>), (ES<sup>-</sup>); *m/z* 361 ([Cu(OTf)<sub>2</sub>]<sup>-</sup>).

**[C<sub>2</sub>mim][Cu(NCMe)(OTf)(NTf<sub>2</sub>)]**

**<sup>1</sup>H NMR (400 MHz, Acetone-d<sup>6</sup>)** δ 8.88 (s, 1H), 7.66 (s, 1H), 7.59 (s, 1H), 4.31 (q, *J* = 7.5 Hz, 2H), 3.97 (s, 3H), 2.00 (s, 3H), 1.51 (t, *J* = 7.5 Hz, 3H); **<sup>13</sup>C NMR (101 MHz, Acetone-d<sup>6</sup>)** δ 135.1 (s), 122.5 (s), 120.8 (s), 119.4 (q, *J* = 320.5 Hz), 118.7 (q, *J* = 321.0 Hz), 115.8 (s), 43.5 (s), 34.4 (s), 13.3 (s), -1.0 (s); **<sup>19</sup>F NMR (377 MHz, Acetone-d<sup>6</sup>)** δ -79.2 (s), -79.9 (s); **TOF MS (ES<sup>+</sup>)**; *m/z* 111 ([C<sub>2</sub>mim]<sup>+</sup>), (ES<sup>-</sup>); *m/z* 492 ([Cu(OTf)(NTf<sub>2</sub>)<sup>-</sup>]).

**[C<sub>6</sub>mim][Cu(NCMe)(OTf)(NTf<sub>2</sub>)]**

**<sup>1</sup>H NMR (400 MHz, Acetone-d<sup>6</sup>)** δ 8.94 (s, 1H), 7.70 (s, 1H), 7.63 (s, 1H), 4.30 (t, *J* = 7.5 Hz, 2H), 4.00 (s, 3H), 2.02 (s, 3H), 1.97 – 1.82 (m, 2H), 1.47 – 1.21 (m, 6H), 0.86 (t, *J* = 7.0 Hz, 3H); **<sup>13</sup>C NMR (101 MHz, Acetone-d<sup>6</sup>)** δ 136.5 (s), 123.8 (s), 122.5 (s), 120.6 (q, *J* = 321.0 Hz), 120.0 (q, *J* = 321.0 Hz), 116.9 (s), 49.6 (s), 35.7 (s), 30.9 (s), 29.8 (s), 25.5 (s), 22.1 (s), 13.3 (s), 0.3 (s); **<sup>19</sup>F NMR (376 MHz, Acetone-d<sup>6</sup>)** δ -79.21 (s), -79.92 (s); **TOF MS (ES<sup>+</sup>)**; *m/z* 167 ([C<sub>6</sub>mim]<sup>+</sup>), (ES<sup>-</sup>); *m/z* 492 ([Cu(OTf)(NTf<sub>2</sub>)<sup>-</sup>]).

**[C<sub>3</sub>O<sub>1</sub>mim][Cu(NCMe)(OTf)(NTf<sub>2</sub>)]**

**<sup>1</sup>H NMR (400 MHz, Acetone-d<sup>6</sup>)** δ 9.01 (s, 1H), 7.66 (s, 1H), 7.61 (s, 1H), 4.33 (t, *J* = 5.0 Hz, 2H), 3.85 (s, 3H), 3.67 (t, *J* = 5.0 Hz, 2H), 3.26 (s, 3H), 2.02 (s, 3H); **<sup>13</sup>C NMR (101 MHz, Acetone-d<sup>6</sup>)** δ 135.5 (s), 122.0 (s), 121.3 (s), 119.3 (q, *J* = 323.0 Hz), 118.2 (q, *J* = 321.5 Hz), 116.6 (s), 68.2 (s), 56.6 (s), 47.4 (s), 34.33 (s), -0.4 (s); **<sup>19</sup>F NMR (377 MHz, Acetone-d<sup>6</sup>)** δ -78.6 (s), -79.5 (s). **TOF MS (ES<sup>+</sup>)**; *m/z* 141 ([C<sub>3</sub>O<sub>1</sub>mim]<sup>+</sup>), (ES<sup>-</sup>); *m/z* 492 ([Cu(OTf)(NTf<sub>2</sub>)<sup>-</sup>]).

**[C<sub>2</sub>(O<sub>1</sub>C<sub>2</sub>)<sub>2</sub>mim][Cu(NCMe)(OTf)(NTf<sub>2</sub>)]**

**<sup>1</sup>H NMR (400 MHz, Acetone-d<sup>6</sup>)** δ 8.99 (s, 1H), 7.62 (s, 1H), 7.61 (s, 1H), 4.77 (t, *J* = 4.5 Hz, 1H), 4.27 (d, *J* = 4.5 Hz, 2H), 3.86 (s, 3H), 3.72 – 3.60 (m, 2H), 3.55 – 3.44 (m, 2H), 2.02 (s, 3H), 1.08 (t, *J* = 7.0 Hz, 6H); **<sup>13</sup>C NMR (101 MHz, Acetone-d<sup>6</sup>)** δ 135.6 (s), 121.8 (s), 121.5 (s), 119.5 (q, *J* = 321.5 Hz), 118.5 (q, *J* = 321.5 Hz), 116.2 (s), 97.5 (s), 61.3 (s), 49.3 (s), 34.1 (s), 13.2 (s), -0.7 (s); **<sup>19</sup>F NMR (376 MHz, Acetone-d<sup>6</sup>)** δ -78.5 (s), -79.4 (s).

**2.9.5 Synthesis of Copper-Containing Ionic Liquid/Dibasic Ester Mixtures**

In a typical procedure, a 1:1 molar ratio of copper containing ionic liquid and DMM or DMG was mixed for 30 minutes at room temperature under N<sub>2</sub>, until a homogeneous solution was observed. With regards to the liquids, they were all relatively viscous. The salts were analysed by <sup>1</sup>H NMR spectroscopy, <sup>13</sup>C NMR spectroscopy, <sup>19</sup>F NMR spectroscopy where appropriate and electrospray mass spectrometry (ES<sup>+</sup> and ES<sup>-</sup>). Density measurements were performed at 20 °C using a 5 ml volumetric flask and balance. The uncertainty in the volume was ±0.025 ml and mass was ±0.0005

**[C<sub>6</sub>mim][CuBr<sub>2</sub>].DMM**

**<sup>1</sup>H NMR (400 MHz, Acetone-d<sup>6</sup>)** δ 9.92 (s, 1H), 8.13 (s, 1H), 8.05 (s, 1H), 4.47 (t, *J* = 7.5 Hz, 2H), 4.13 (s, 3H), 3.67 (s, 6H), 3.47 (s, 2H), 1.97 – 1.85 (m, 2H), 1.38 – 1.18 (m, 6H), 0.81 (t, *J* = 6.7 Hz, 3H). **<sup>13</sup>C NMR (101 MHz, Acetone-d<sup>6</sup>)** δ 167.0 (s), 137.2 (s), 123.8 (s), 122.6 (s), 52.1 (s), 49.3 (s), 40.9 (s), 36.3 (s), 31.0 (s), 30.1 (s), 25.6 (s), 22.2 (s), 13.6 (s). **TOF MS (ES<sup>+</sup>);** *m/z* 167 ([C<sub>6</sub>mim]<sup>+</sup>), **(ES<sup>-</sup>);** *m/z* 223 ([CuBr<sub>2</sub>]<sup>-</sup>).

**[C<sub>6</sub>mim][Cu(NCMe)(OTf)<sub>2</sub>].DMM**

**<sup>1</sup>H NMR (400 MHz, Acetone-d<sub>6</sub>)** δ 8.95 (s, 1H), 7.69 (s, 1H), 7.61 (s, 1H), 4.27 (t, *J* = 7.5 Hz, 2H), 3.97 (s, 3H), 3.67 (s, 6H), 3.42 (s, 2H), 2.01 (s, 3H), 1.92 – 1.84 (m, 2H), 1.35 – 1.23 (m, 6H), 0.84 (t, *J* = 7.0 Hz, 3H); **<sup>13</sup>C NMR (101 MHz, Acetone-d<sub>6</sub>)** δ 167.2 (s), 136.6 (s), 123.8 (s), 122.4 (s), 119.7 (q, *J* = 321.5 Hz), 117.2 (s), 51.9 (s), 49.5 (s), 40.6 (s), 35.7 (s), 30.9 (s), 29.8 (s), 25.4 (s), 22.1 (s), 13.3 (s), 0.3 (s); **<sup>19</sup>F NMR (376 MHz, Acetone-d<sub>6</sub>)** δ -79.2 (s); **TOF MS (ES<sup>+</sup>)**; *m/z* 167 ([C<sub>6</sub>mim]<sup>+</sup>), (ES<sup>+</sup>); *m/z* 361 ([Cu(OTf)<sub>2</sub>]<sup>-</sup>).

**[C<sub>2</sub>mim][Cu(NCMe)(OTf)(NTf<sub>2</sub>)].DMM**

**<sup>1</sup>H NMR (400 MHz, Acetone-d<sub>6</sub>)** δ 8.85 (s, 1H), 7.65 (s, 1H), 7.58 (s, 1H), 4.32 (q, *J* = 6.5 Hz, 2H), 3.97 (s, 3H), 3.67 (s, 6H), 3.42 (s, 2H), 2.01 (s, 3H), 1.52 (t, *J* = 6.5 Hz, 3H). **<sup>13</sup>C NMR (101 MHz, Acetone-d<sub>6</sub>)** δ 167.2 (s), 136.15 (s), 123.7 (s), 122.1 (s), 120.8 (q, *J* = 321.0 Hz), 120.1 (q, *J* = 321.0 Hz) 117.1 (s), 51.8 (s), 44.8 (s), 40.5 (s), 35.6 (s), 14.5 (s), 0.2 (s); **<sup>19</sup>F NMR (376 MHz, Acetone-d<sub>6</sub>)** δ -79.3 (s), -79.9 (s); **TOF MS (ES<sup>+</sup>)**; *m/z* 111 ([C<sub>2</sub>mim]<sup>+</sup>), (ES<sup>+</sup>); *m/z* 492 ([Cu(OTf)(NTf<sub>2</sub>)]<sup>-</sup>).

**[C<sub>6</sub>mim][Cu(NCMe)(OTf)(NTf<sub>2</sub>)].DMM**

**<sup>1</sup>H NMR (400 MHz, Acetone)** δ 8.93 (s, 1H), 7.69 (s, 1H), 7.63 (s, 1H), 4.30 (t, *J* = 7.5 Hz, 2H), 4.00 (s, 3H), 3.68 (s, 6H), 3.42 (s, 2H), 2.02 (s, 3H), 1.97 – 1.83 (m, 2H), 1.40 – 1.23 (m, 6H), 0.86 (t, *J* = 7.0 Hz, 3H); **<sup>13</sup>C NMR (101 MHz, Acetone)** δ 167.1 (s), 136.5 (s), 123.8 (s), 122.5 (s), 120.6 (q, *J* = 321.0 Hz), 120.0 (q, *J* = 321.0 Hz), 117.0 (s), 51.8 (s), 49.6 (s), 40.56 (s), 35.7 (s), 30.9 (s), 29.8 (s), 25.5 (s), 22.1 (s), 13.3 (s), 0.3 (s); **<sup>19</sup>F NMR (377 MHz, Acetone)** δ -79.2 (s), -79.9 (s); **TOF MS (ES<sup>+</sup>)**; *m/z* 167 ([C<sub>6</sub>mim]<sup>+</sup>), (ES<sup>+</sup>); *m/z* 492 ([Cu(OTf)(NTf<sub>2</sub>)]<sup>-</sup>).

**[C<sub>6</sub>mim][CuBr<sub>2</sub>].DMG**

**<sup>1</sup>H NMR (400 MHz, Acetone)** δ 9.60 (s, 1H), 7.97 (s, 1H), 7.88 (s, 1H), 4.25 (t, *J* = 7.0 Hz, 2H), 3.92 (s, 3H), 3.51 (s, 6H), 2.28 (t, *J* = 7.5 Hz, 4H), 1.87 – 1.74 (m, 2H), 1.69 (qu, *J* = 7.5 Hz, 2H), 1.33 – 1.03 (m, 6H), 0.74 (t, *J* = 6.5 Hz, 3H); **<sup>13</sup>C NMR (101 MHz, Acetone)** δ 172.8 (s), 136.6 (s), 123.4 (s), 122.2 (s), 51.1 (s), 48.7 (s), 35.8 (s), 32.2 (s), 30.5 (s), 29.5 (s), 25.1 (s), 21.8 (s), 19.7 (s), 13.5 (s); **TOF MS (ES<sup>+</sup>);** *m/z* 167 ([C<sub>6</sub>mim]<sup>+</sup>), (ES<sup>+</sup>); *m/z* 223 ([CuBr<sub>2</sub>]<sup>-</sup>).

**[C<sub>6</sub>mim][Cu(NCMe)(OTf)<sub>2</sub>].DMG**

**<sup>1</sup>H NMR (400 MHz, Acetone-d<sub>6</sub>)** δ 9.08 (s, 1H), 7.74 (s, 1H), 7.68 (s, 1H), 4.17 (t, *J* = 7.5 Hz, 2H), 3.87 (s, 3H), 3.58 (s, 6H), 2.34 (t, *J* = 7.5 Hz, 4H), 2.05 (s, 3H), 1.78 (qu, *J* = 7.5 Hz, 2H), 1.36 – 1.16 (m, 6H), 0.85 (t, *J* = 6.5 Hz, 3H); **<sup>13</sup>C NMR (101 MHz, Acetone-d<sub>6</sub>)** δ 172.8 (s), 136.5 (s), 123.5 (s), 122.2 (s), 120.7 (q, *J* = 322.0 Hz), 117.8 (s), 51.1 (s), 48.8 (s), 35.6 (s), 32.2 (s), 30.5 (s), 29.4 (s), 25.1 (s), 21.8 (s), 19.8 (s), 13.5 (s), 0.9 (s); **<sup>19</sup>F NMR (377 MHz, Acetone-d<sub>6</sub>)** δ -78.6 (s); **TOF MS (ES<sup>+</sup>);** *m/z* 167 ([C<sub>6</sub>mim]<sup>+</sup>), (ES<sup>+</sup>); *m/z* 361 ([Cu(OTf)<sub>2</sub>]<sup>-</sup>).

**[C<sub>2</sub>mim][Cu(NCMe)(OTf)(NTf<sub>2</sub>)].DMG**

**<sup>1</sup>H NMR (400 MHz, Acetone-d<sub>6</sub>)** δ 9.42 (s, 1H), 7.86 (s, 1H), 7.75 (s, 1H), 4.21 (q, *J* = 7.5 Hz, 2H), 3.86 (s, 3H), 3.49 (s, 6H), 2.26 (t, *J* = 7.5 Hz, 4H), 2.02 (s, 3H), 1.66 (qu, *J* = 7.5 Hz, 2H), 1.36 (t, *J* = 7.5 Hz, 3H); **<sup>13</sup>C NMR (101 MHz, Acetone-d<sub>6</sub>)** δ 172.9 (s), 136.2 (s), 123.3 (s), 121.8 (s), 120.5 (q, *J* = 321.5 Hz), 119.5 (q, *J* = 323.0 Hz), 117.8 (s), 51.1 (s), 44.1 (s), 35.6 (s), 32.1 (s), 19.7 (s), 14.9 (s), 1.2 (s); **<sup>19</sup>F NMR (377 MHz, Acetone-d<sub>6</sub>)** δ -78.8 (s), -79.7 (s); **TOF MS (ES<sup>+</sup>);** *m/z* 111 ([C<sub>2</sub>mim]<sup>+</sup>), (ES<sup>+</sup>); *m/z* 492 ([Cu(OTf)(NTf<sub>2</sub>)]<sup>-</sup>).

**[C<sub>6</sub>mim][Cu(NCMe)(OTf)(NTf<sub>2</sub>)].DMG**

**<sup>1</sup>H NMR (400 MHz, Acetone-d<sub>6</sub>)** δ 9.02 (s, 1H), 7.68 (s, 1H), 7.61 (s, 1H), 4.14 (t, *J* = 7.0 Hz, 2H), 3.84 (s, 3H), 3.57 (s, 6H), 2.32 (t, *J* = 7.5 Hz, 4H), 2.01 (s, 3H), 1.87 – 1.70 (m, 4H), 1.35 – 1.17 (m, 6H), 0.83 (t, *J* = 6.0 Hz, 3H); **<sup>13</sup>C NMR (101 MHz, Acetone-d<sub>6</sub>)** δ 172.8 (s), 136.4 (s), 123.5 (s), 122.1 (s), 120.6 (q, *J* = 321.0 Hz), 120.0 (q, *J* = 321.0 Hz) 117.9 (s), 51.0 (s), 48.9 (s), 35.5 (s), 32.2 (s), 30.4 (s), 29.3 (s), 25.0 (s), 21.7 (s), 19.7 (s), 13.4 (s), 0.7 (s); **<sup>19</sup>F NMR (376 MHz, Acetone-d<sub>6</sub>)** δ -78.7 (s), -79.6 (s); **TOF MS (ES<sup>+</sup>)**; *m/z* 167 ([C<sub>6</sub>mim]<sup>+</sup>), **(ES<sup>-</sup>)**; *m/z* 492 ([Cu(OTf)(NTf<sub>2</sub>)]).

## 2.10 References

- 1 S. E. Repper, A. Haynes, E. J. Ditzel and G. J. Sunley, *Dalton. Trans.*, 2017, **46**, 2821–2828.
- 2 Z. Dardas, M. Suer, Y. Ma and W. Moser, *J. Catal.*, 1996, **159**, 204–211.
- 3 J. G. Huddleston, A. E. Visser, W. M. Reichert, H. D. Willauer, G. A. Broker and R. D. Rogers, *Green Chem.*, 2001, **3**, 156–164.
- 4 S. V. Dzyuba and R. A. Bartsch, *J. Heterocycl. Chem.*, 2001, **38**, 265–268.
- 5 S.-W. Wang, W. Liu and R. H. Colby, *Chem. Mater.*, 2011, **23**, 1862–1873.
- 6 S. Leitner, M. List and U. Monkowius, *Zeitschrift für Naturforsch. B*, 2011, **66**, 1255–1260.
- 7 J. M. Breen, S. Olejarz and K. R. Seddon, *ACS Sustain. Chem. Eng.*, 2016, **4**, 387–391.
- 8 R. Appel, *Angew. Chem. Int. Ed. Engl.*, 1975, **14**, 801.
- 9 A. Dinares, I.; Garcia-de-Miguel, C.; Ibanez, *Green Chem.*, 2009, **11**, 1507.
- 10 I. Dinarès, C. Garcia de Miguel, A. Ibáñez, N. Mesquida and E. Alcalde, *Green Chem.*, 2009, **11**, 1507.
- 11 P. Nockemann, E. Beurer, K. Driesen, R. Van Deun, K. Van Hecke, L. Van Meervelt and K. Binnemans, *Chem. Commun.*, 2005, 4354.
- 12 P. Hoang Tran, N. Bich Le Do and T. Ngoc Le, *Tetrahedron Lett.*, 2014, **55**, 205–208.
- 13 Q. Liu, M. H. A. Janssen, F. van Rantwijk and R. A. Sheldon, *Green Chem.*, 2005, **7**, 39.

- 
- 14 G. Sinawang, Y. Kobayashi, Y. Zheng, Y. Takashima, A. Harada and H. Yamaguchi, *Macromolecules*, 2019, **52**, 2932–2938.
  - 15 S. Bulut, P. Eiden, W. Beichel, J. M. Slattery, T. F. Beyersdorff, T. J. S. Schubert and I. Krossing, *ChemPhysChem*, 2011, **12**, 2296–2310.
  - 16 R. P. Singh, R. W. Winter, G. L. Gard, A. Ye Gao and Jean'ne M. Shreeve, *Inorg. Chem.*, 2003, **42**, 6142–6146.
  - 17 M. A. Cotton, F. A.; Dikarev, E. V.; Petrukhina, *Inorg. Chem.*, 2000, **47**, 6072.
  - 18 S. Repper PhD Thesis, University of Sheffield, 2014.
  - 19 J. A. Hogendoorn, W. P. M. van Swaaij and G. F. Versteeg, *Chem. Eng. J. Biochem. Eng. J.*, 1995, **59**, 243–252.
  - 20 R. V. Gholap and R. V. Chaudhari, *Can. J. Chem. Eng.*, 2009, **70**, 505–510.

### **3. Copper-Containing Ionic Liquids with Weakly Coordinating Anions**

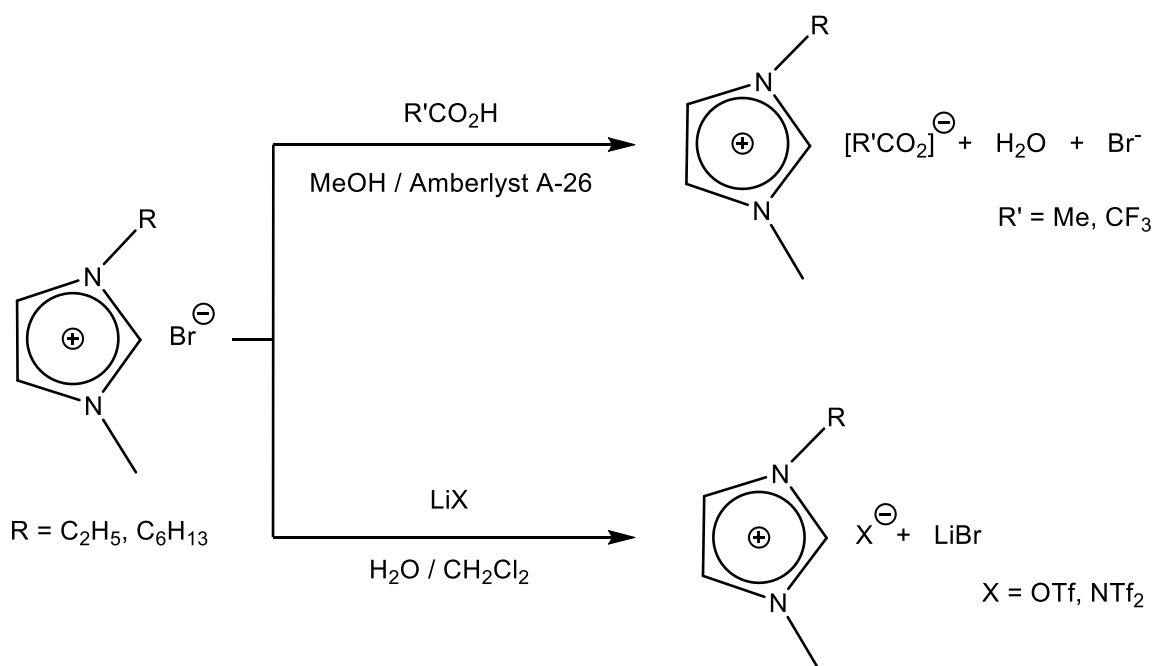
### 3.1 Introduction

Moving away from IL systems with free halides was desirable due to their limitations, as discussed in Chapter 1. The use of copper(I) dihalide ILs could be problematic in a commercial process due to issues with corrosion and high viscosity. Moreover, the copper-halide systems only ever showed evidence of copper monocarbonyls. Using more weakly coordinating anions, may favour the formation of copper-polycarbonyl complexes. If achieved, this would be particularly exciting since even the coordination of a second CO per copper site could enhance CO uptake substantially.

This chapter outlines the synthesis and physical properties of some copper-containing ILs with weakly coordinating anions. Encouragingly, a few promising candidates were found based on trifluoromethane sulfonate (OTf<sup>-</sup>) and bis(trifluoromethylsulfonyl)imide (NTf<sub>2</sub><sup>-</sup>) anions with superior physical properties compared to the halide systems.

### 3.2 Synthesis of Ionic Liquid Precursors

The ILs targeted over the course of this project were entirely based on imidazolium cations, namely 1-alkyl-3-methylimidazolium or [C<sub>n</sub>mim]. Scheme 3.1 shows how the non-halide imidazolium ILs were all produced from the bromide salt precursor via either a metathesis method or by anion exchange with an exchange column. For the more hydrophobic anions, OTf<sup>-</sup> and NTf<sub>2</sub><sup>-</sup>, the metathesis method was exploited as the product was soluble in CH<sub>2</sub>Cl<sub>2</sub> allowing for facile removal of salt by-products. For the more hydrophilic anions, acetate (OAc<sup>-</sup>) and trifluoroacetate (TFA<sup>-</sup>) an anion exchange column had to be used, adapted from a method reported by Ortiz *et. al.*<sup>1,2</sup>



**Scheme 3.1.** Anion exchange techniques used in the synthesis of imidazolium non-halide salts.

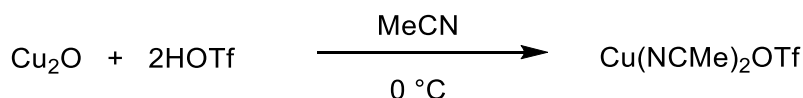
In order to determine whether complete exchange had been achieved, initial qualitative tests were done using mass spectrometry to detect the presence of any residual  $\text{Br}^-$ . Once satisfied that there was no  $\text{Br}^-$ , a quantitative test for  $\text{Br}^-$  was done via elemental analysis. The lower limit for the detection of halides, by mass, is 0.3 %. All ILs analysed were found to be below the 0.3 % limit and therefore deemed sufficient to proceed and labelled halide free. The ILs synthesised were all characterised by  $^1\text{H}$ ,  $^{13}\text{C}$  and  $^{19}\text{F}$  NMR spectroscopy where appropriate, and mass spectrometry to confirm the presence of the desired ions.

### 3.3 Synthesis of Copper(I) Precursors

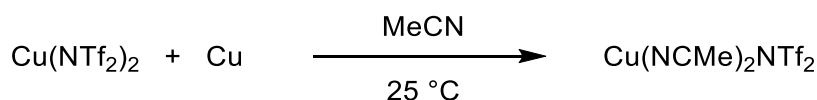
In order to limit complications, it was initially decided to combine each respective imidazolium salt with the corresponding copper(I) salt i.e.  $[\text{C}_n\text{mim}]\text{X} + \text{CuX}$ . This was so there would not be a mixture of

anions present and the copper species would be easier to define. Therefore a number of copper(I) species had to be utilised.

CuOAc was commercially available and found to be very air sensitive, with any exposure to air or moisture causing discolouration. CuTFA was synthesised following literature procedure.<sup>3,4</sup> Attempts to synthesise CuOTf and CuNTf<sub>2</sub> from mesityl copper by an adapted literature procedure were successful on a small scale however, both were difficult to handle and relatively difficult to prepare.<sup>5</sup> Therefore it was decided to use a different copper(I) source. Scheme 3.2 and Scheme 3.3 show the preparation of more air stable copper(I) compounds, which contain acetonitrile ligands complexed to the copper.



**Scheme 3.2.** Synthesis of Cu(NCMe)<sub>2</sub>OTf via acid base reaction of Cu<sub>2</sub>O and HOTf in dry MeCN.<sup>6</sup>



**Scheme 3.3.** Synthesis of Cu(NCMe)<sub>2</sub>NTf<sub>2</sub> by comproportionation reaction of Cu(NTf<sub>2</sub>)<sub>2</sub> and Cu metal in dry MeCN.<sup>7,8</sup>

These Cu(NCMe)<sub>2</sub>X (X = OTf or NTf<sub>2</sub>) type complexes were still air sensitive, but could be manipulated for short periods of time before discolouring to blue.

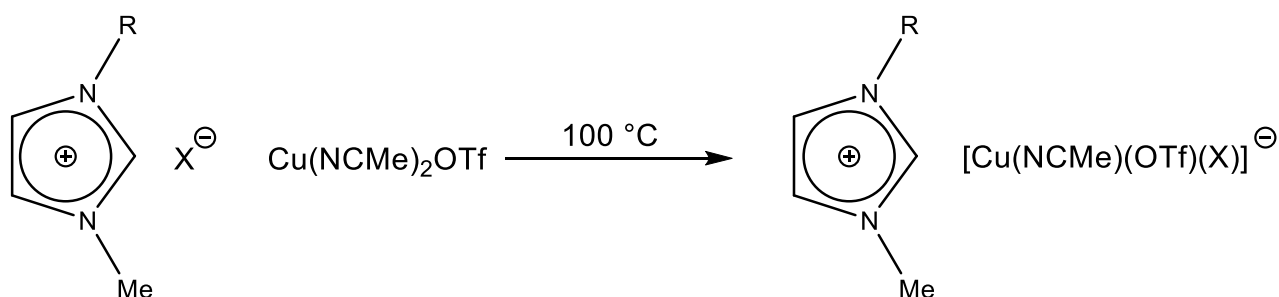
### 3.4 Synthesis of Copper(I) Containing Ionic Liquids

A 1:1 molar ratio of imidazolium salt to corresponding copper(I) salt was used to prepare the Cu(I) containing ILs. Melt reactions were run at 100 °C for 1 hour until a homogeneous mixture was formed.

For the carboxylate systems,  $[C_n\text{mim}][\text{Cu}(\text{O}_2\text{CR})_2]$ , attempts to obtain NMR spectra were unsuccessful due to the high air sensitivity of the product, even when taking great care under an inert atmosphere. Electro spray mass spectrometry did provide evidence for the copper species  $[\text{Cu}(\text{OAc})_2]^-$  ( $m/z$  181) and  $[\text{Cu}(\text{TFA})_2]^-$  ( $m/z$  289).

For the triflyl systems, on cooling to room-temperature the OTf product remained liquid whereas the  $\text{NTf}_2^-$  product solidified. Even when the cation was made more unsymmetrical, by lengthening the alkyl chain from  $\text{C}_2\text{mim}$  to  $\text{C}_6\text{mim}$ , the product was still a solid at room-temperature. However, combination of  $[C_n\text{mim}]\text{NTf}_2$  with  $\text{Cu}(\text{NCMe})_2\text{OTf}$  gave a product that remained liquid at room-temperature (Scheme 3.4). This does, however, result in a system where there is a mixture of  $\text{NTf}_2^-$  and  $\text{OTf}^-$  anions which may complicate determining the copper speciation.

Table 3.1 gives a summary of the physical states of the copper containing salts prepared at 25 °C.



**Scheme 3.4.** Synthesis of  $[C_n\text{mim}][\text{Cu}(\text{NCMe})(\text{OTf})(\text{X})]$  salts ( $R = \text{Et}, \text{C}_6\text{H}_{13}$ ;  $X = \text{OTf}, \text{NTf}_2^-$ )

**Table 3.1.** Physical states of various ILs and copper(I) salts combined to form copper containing salts at 25 °C.

Ionic Liquid	Copper Source	Physical State at 25 °C
$\text{C}_6\text{mimCl}$	$\text{CuCl}$	Liquid

---

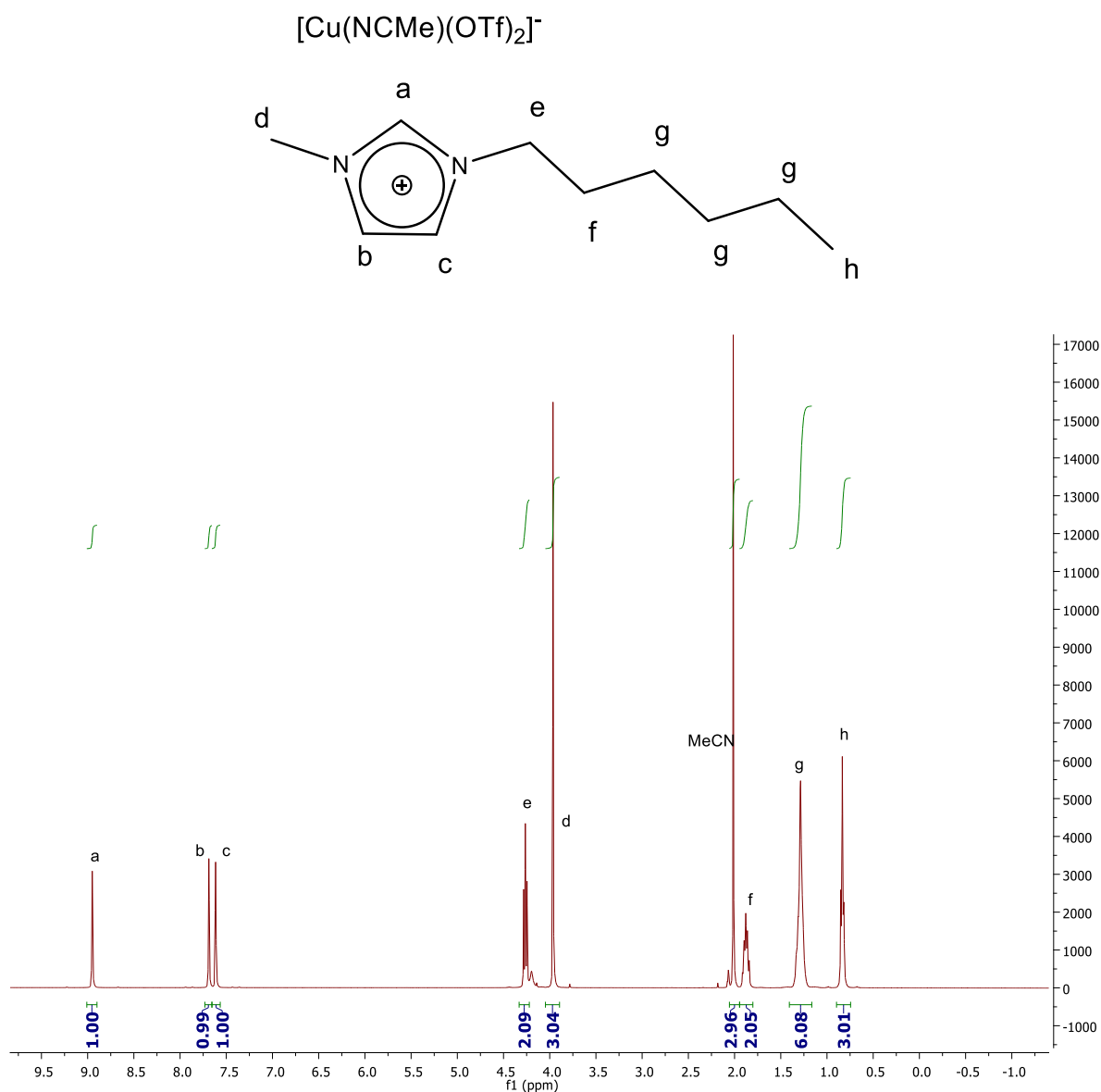
Copper-Containing Ionic Liquids with Weakly Coordinating Anions

---

C <sub>6</sub> mimBr	CuBr	Liquid
C <sub>6</sub> mimOAc	CuOAc	Liquid
C <sub>6</sub> mimTFA	CuTFA	Liquid
C <sub>6</sub> mimOTf	Cu(NCMe) <sub>2</sub> OTf	Liquid
C <sub>2</sub> mimNTf <sub>2</sub>	Cu(NCMe) <sub>2</sub> NTf <sub>2</sub>	Solid
C <sub>6</sub> mimNTf <sub>2</sub>	Cu(NCMe) <sub>2</sub> NTf <sub>2</sub>	Solid
C <sub>2</sub> mimNTf <sub>2</sub>	Cu(NCMe) <sub>2</sub> OTf	Liquid
C <sub>6</sub> mimNTf <sub>2</sub>	Cu(NCMe) <sub>2</sub> OTf	Liquid

---

The copper-containing imidazolium salts synthesised were analysed by <sup>1</sup>H, <sup>13</sup>C and <sup>19</sup>F NMR spectroscopy and mass spectrometry after drying under high vacuum for several hours, at 80 °C.

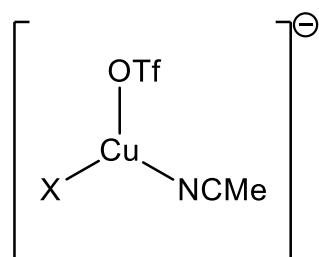


**Figure 3.1.**  $^1\text{H}$  NMR spectrum of  $[\text{C}_6\text{mim}][\text{Cu}(\text{NCMe})(\text{OTf})_2]$  in  $\text{d}^6$  acetone.

Figure 3.1 shows the  $^1\text{H}$  NMR spectrum of the product from combining  $[\text{C}_6\text{mim}]\text{OTf}$  and  $\text{Cu}(\text{NCMe})_2\text{OTf}$ . The signals of the imidazolium ring hydrogens are at a slightly higher chemical shift than in the precursor,  $[\text{C}_6\text{mim}]\text{OTf}$ . Moreover, a peak at 2.1 ppm is consistent with the presence of MeCN. This peak has an integrated intensity of 3, relative to the imidazolium ring protons, showing that there is one MeCN present per imidazolium cation. Presumably the second MeCN from the reactant,  $\text{Cu}(\text{NCMe})_2\text{OTf}$ , is lost when the product is heated under vacuum (MeCN boiling point 82

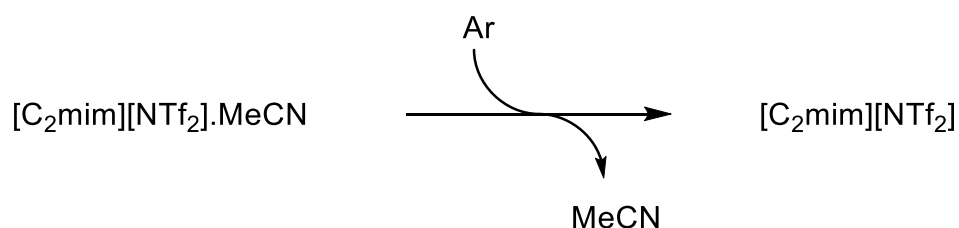
°C). The remaining MeCN is likely acting as a ligand coordinated to the copper. An analogous observation was made for the mixed NTf<sub>2</sub>/OTf anion system.

The positive-ion electrospray mass spectrum recorded from the melt reaction of [C<sub>6</sub>mim]OTf and Cu(NCMe)<sub>2</sub>OTf gave a peak at m/z 167, consistent with the [C<sub>6</sub>mim]<sup>+</sup> cation. The negative ion electrospray mass spectrum gave a peak at m/z 361 with an isotope pattern consistent with [Cu(OTf)<sub>2</sub>]<sup>-</sup>. For the mixed anion system, [C<sub>n</sub>mim]NTf<sub>2</sub> + Cu(NCMe)<sub>2</sub>OTf, the ES<sup>-</sup> mass spectrum showed a peak at m/z 492 which is consistent with [Cu(OTf)(NTf<sub>2</sub>)]<sup>-</sup>. No MeCN was found to be coordinated to the copper. Therefore it may be lost in the mass spectrometer due to the conditions required for analysis. **Figure 3.2** shows the proposed structure of the anion formed on reaction of [C<sub>n</sub>mim]X with Cu(NCMe)<sub>2</sub>OTf.



**Figure 3.2.** Proposed anion formed from the melt reactions of [C<sub>n</sub>mim]X + Cu(NCMe)<sub>2</sub>OTf (X = OTf, NTf<sub>2</sub>)

In a further effort to understand whether acetonitrile is coordinated to the copper, a control experiment was performed by spiking a sample of the IL  $[\text{C}_2\text{mim}][\text{NTf}_2]$  with 1 equivalent of MeCN and then passing a stream of inert gas through the sample (**Scheme 3.5**). After 16 hours the  $^1\text{H}$  NMR spectrum showed no MeCN present, demonstrating that it is volatile enough to be removed under mild conditions.



**Scheme 3.5.** Control experiment showing the removal of MeCN from a sample of  $[\text{C}_2\text{mim}][\text{NTf}_2]$

Next, a stream of inert gas was passed through the IL prepared from  $[\text{C}_2\text{mim}][\text{NTf}_2]$  and  $\text{Cu}(\text{NCMe})_2\text{OTf}$ . The  $^1\text{H}$  NMR spectrum taken showed this was insufficient to remove any of the MeCN as the MeCN peak still integrated to 3. This suggests MeCN is coordinated to the copper centre. The copper-containing ILs of  $\text{OTf}^-$  and  $\text{NTf}_2^-$  were notably more air sensitive than the analogous halide systems and would quickly oxidise to  $\text{Cu}(\text{II})$  if left exposed to air *ca* 10 minutes.

### 3.5 Density Measurements

Table 3.2 gives the density of each IL measured at 20 °C, along with the calculated copper concentration,  $[\text{Cu}]$ . In each case the density of the IL increased when adding a copper(I) salt by about 0.1 g  $\text{cm}^{-3}$ . The only exception was the bromide system which increased dramatically by 0.45 g  $\text{cm}^{-3}$ .

The density also changed when varying the length of the alkyl chain, as longer alkyl chains are known to lower the density of ILs.<sup>9</sup>

**Table 3.2.** Densities of copper containing ILs at 293 K.

Ionic Liquid	Density / g cm <sup>-3</sup>	Copper Containing Ionic Liquid	Density / g cm <sup>-3</sup>	[Cu] / M
C <sub>6</sub> mimCl	1.04	[C <sub>6</sub> mim][CuCl <sub>2</sub> ]	1.10	3.7
C <sub>6</sub> mimBr	1.20	[C <sub>6</sub> mim][CuBr <sub>2</sub> ]	1.65	4.2
C <sub>6</sub> mimOTf	1.31	[C <sub>6</sub> mim][Cu(NCMe)(OTf) <sub>2</sub> ]	1.40	2.5
C <sub>2</sub> mimNTf <sub>2</sub>	1.52	[C <sub>2</sub> mim][Cu(NCMe)(OTf)(NTf <sub>2</sub> )]	1.60	2.5
C <sub>6</sub> mimNTf <sub>2</sub>	1.39	[C <sub>6</sub> mim][Cu(NCMe)(OTf)(NTf <sub>2</sub> )]	1.50	2.1

Copper concentrations are higher for the free halide systems due to their lower molecular weight, even though the OTf<sup>-</sup> and NTf<sub>2</sub><sup>-</sup> ILs had higher densities when compared to the Cl<sup>-</sup> system. Although literature on COSORB solutions is scarce, Hogendoorn *et. al.* reported preparing solutions of CuAlCl<sub>4</sub>.tol<sub>2</sub>, the most concentrated of which had a copper concentration of 1.7 M.<sup>10</sup> Using this value it can be seen that all of the copper-containing ILs reported in Table 3.2 have higher copper concentrations than a typical COSORB solution and hence, have the potential to absorb more CO.

### 3.6 Viscosity Measurements

From a chemical process design perspective, accurate knowledge of the rheology of these solvents is essential as this will determine how much energy is required to overcome its resistance to flow. When running the viscosity measurements, the sample was left between the cone and the plate for 5 minutes to equilibrate to the desired temperature. The viscosity was then measured between a shear

rate of  $10 - 1000 \text{ s}^{-1}$  by continuous ramp step over 5 minutes. This set up was similar to work done by Urtiaga *et. al.* on the viscosity of similar copper-containing ILs.<sup>11</sup>

Initially, tests were done on ILs with known viscosities. Table 3.3 gives the results for some relatively high viscosity ILs, which are in good agreement with those found in the literature. This was encouraging as ILs are known to be very hygroscopic and moisture can have a dramatic effect on their viscosity. The length of time that the sample was exposed to the atmosphere was a lot less than when it was submitted to elemental analysis. Therefore, the sample did not have the opportunity to absorb a lot of moisture from the atmosphere compared to when the elemental analysis results. If the result of the viscosity was very different to the literature, it would point to there being some impurity in the sample, however, all samples tested were in good agreement with the literature. Repeat measurements showed the viscosity results were reproducible within 2 %.

**Table 3.3.** Viscosity measurements compared with literature viscosities of several ILs.

Ionic Liquid	Measured Viscosity / mPa.s	Literature Viscosity / mPa.s	Reference
[C <sub>6</sub> mim]Br	4216	3986	12
[C <sub>6</sub> mim]NTf <sub>2</sub>	76	70	13
[C <sub>6</sub> mim]OTf	201	198	13

Measurements for lower viscosity materials revealed that there was a small discrepancy between measured values and the literature. **Figure 3.3** highlights this discrepancy, which seems to be a systematic over-estimation of about 2 – 3 mPa.s. Therefore, any viscosities measured will be interpreted as the upper limit and in reality may be slightly lower.

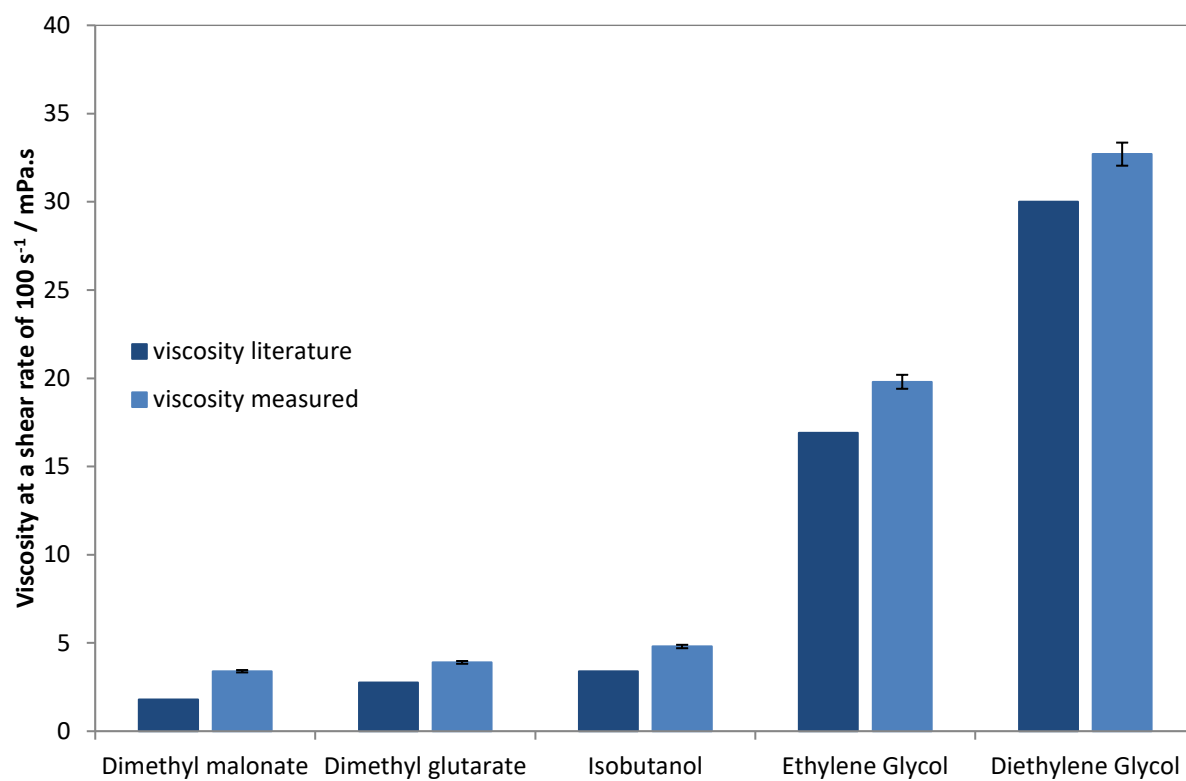


Figure 3.3. Measured viscosities against literature viscosities of some common organic solvents with low viscosity.

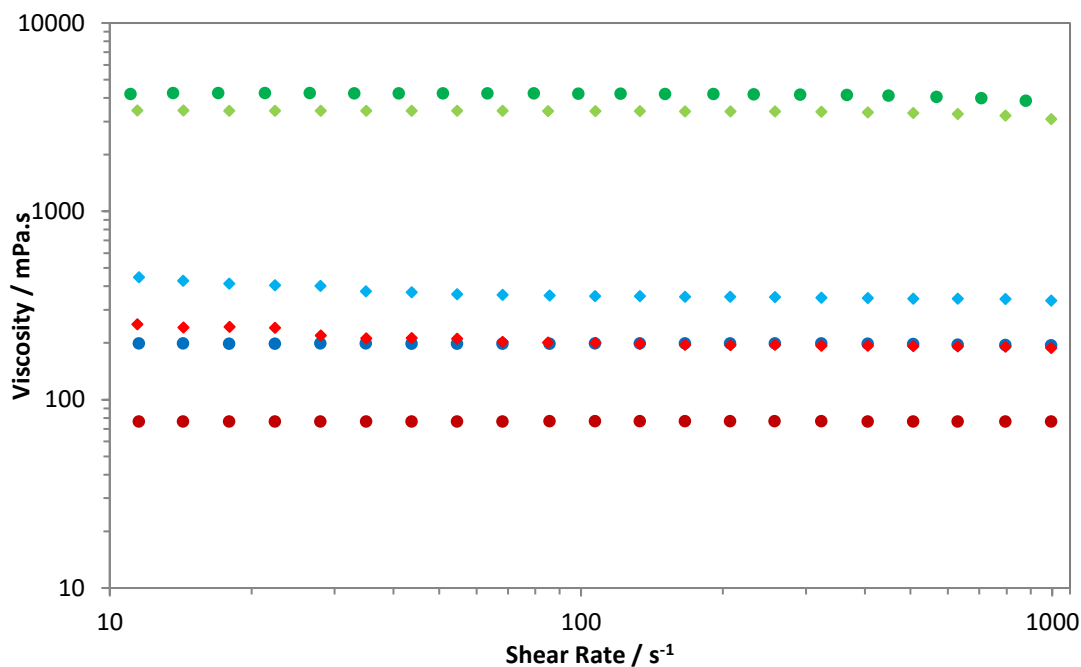
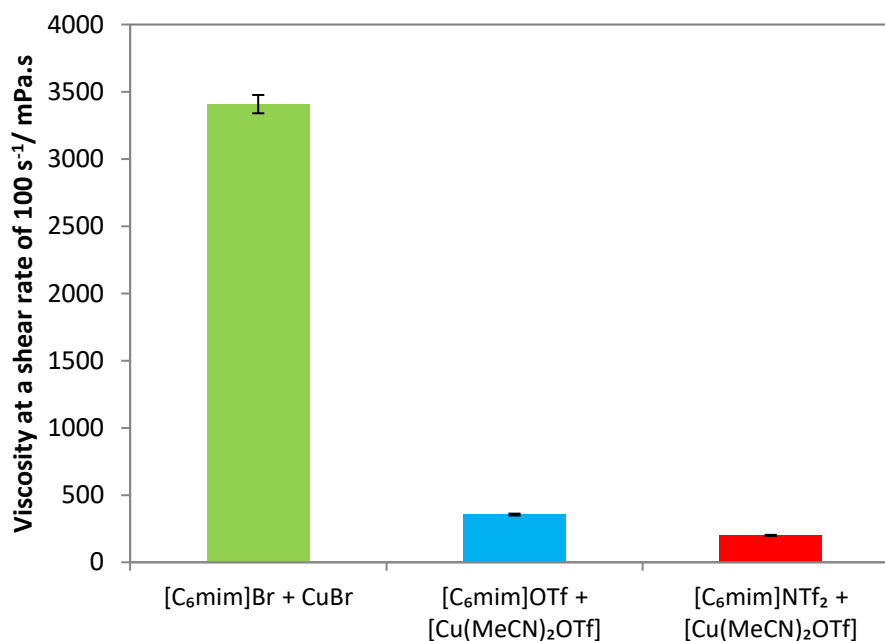


Figure 3.4. Log-log plot of shear viscosity as a function of shear rate at 298.15 K. Circles represent non-copper-containing IL and diamonds represent copper-containing ILs. When Red =  $[C_6mim]NTf_2$ ; Blue =  $[C_6mim]OTf$ ; Green =  $[C_6mim]Br$

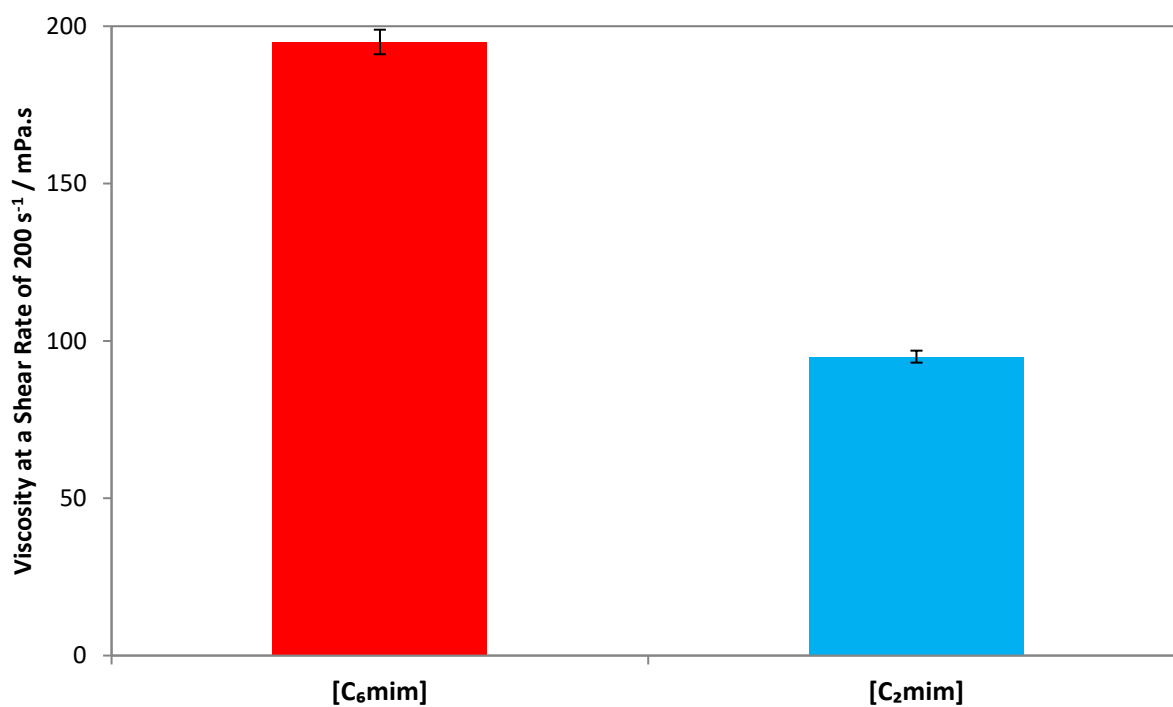
Figure 3.4 shows the effect on viscosity after addition of a copper source to the imidazolium salts, measured at 298 K and between shear rates of 10 – 1000 s<sup>-1</sup>. The constant viscosity independent of stress between the recorded shear rates demonstrates how they behave as a Newtonian fluid. Addition of one equivalent of CuBr to [C<sub>6</sub>mim]Br reduced the viscosity, which is the same observation made when adding CuCl to [C<sub>n</sub>mim]Cl ILs, although the reduction was not as dramatic.<sup>11,14</sup> Conversely, addition of the copper(I) salt, Cu(NCMe)<sub>2</sub>OTf to the ILs containing OTf<sup>-</sup> or NTf<sub>2</sub><sup>-</sup> anions, resulted in a slight increase in viscosity. This result is analogous to that observed when adding LiCl to [C<sub>4</sub>mim]Cl<sup>15</sup> and also by Urutiaga *et.al.* when adding CuSCN to [C<sub>2</sub>mim]SCN.<sup>16</sup>

Figure 3.5 shows the viscosities of the copper-containing ILs at a shear rate of 100 s<sup>-1</sup>. It is notable that the viscosity depends on the anion, following the trend Br<sup>-</sup> >> OTf<sup>-</sup> > NTf<sub>2</sub><sup>-</sup>. This is consistent with the literature where free halide type ILs (Cl<sup>-</sup>, Br<sup>-</sup>) tend to have much higher viscosities and the NTf<sub>2</sub><sup>-</sup> anion is widely known to give low viscosities due to its large size and incorporation of fluorinated side chains.<sup>17</sup>



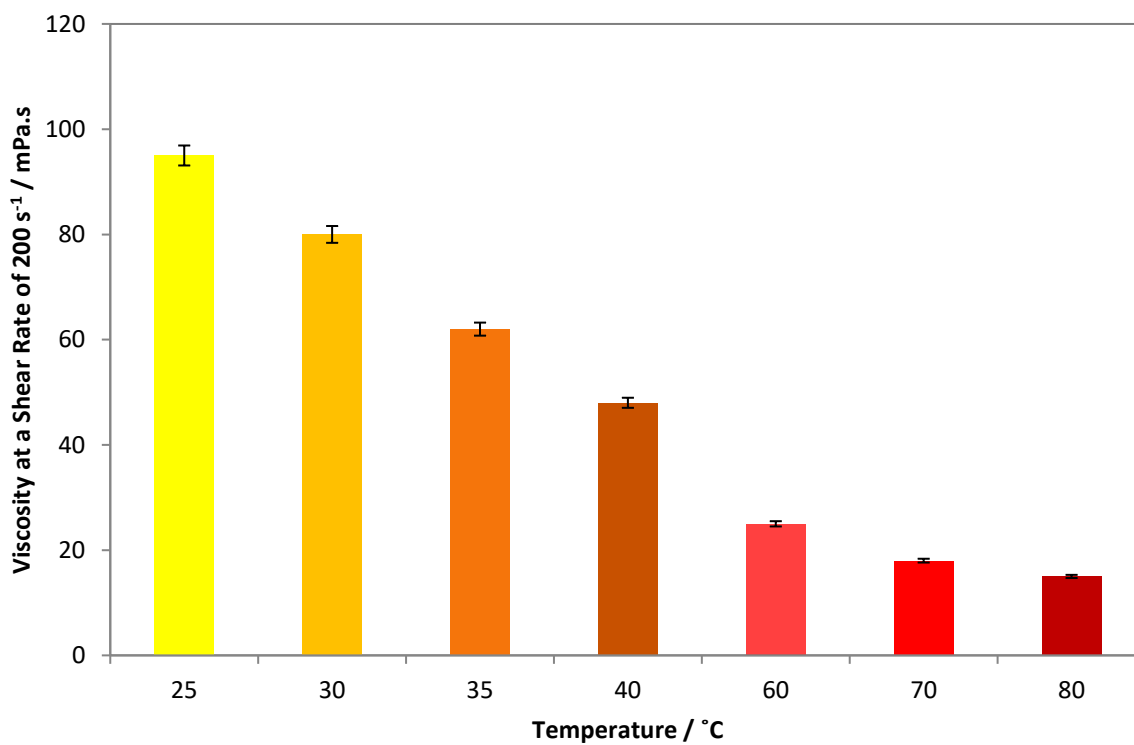
**Figure 3.5.** Viscosities of various copper containing ILs at a shear rate of 100 s<sup>-1</sup> and at 298 K.

Figure 3.6 shows the effect on viscosity of alkyl chain length on the  $C_n\text{mim}$  cation. Moving to a shorter alkyl chain,  $C_6\text{mim}$  to  $C_2\text{mim}$ , is known in the literature to reduce viscosity due to weaker intermolecular van der Waals forces.<sup>18</sup> Figure 3.6 shows how the reduction in alkyl chain length for  $[C_n\text{mim}][\text{Cu}(\text{NCMe})(\text{OTf})(\text{NTf}_2)]$  caused the viscosity to decrease from 195 mPa.s to 95 mPa.s.



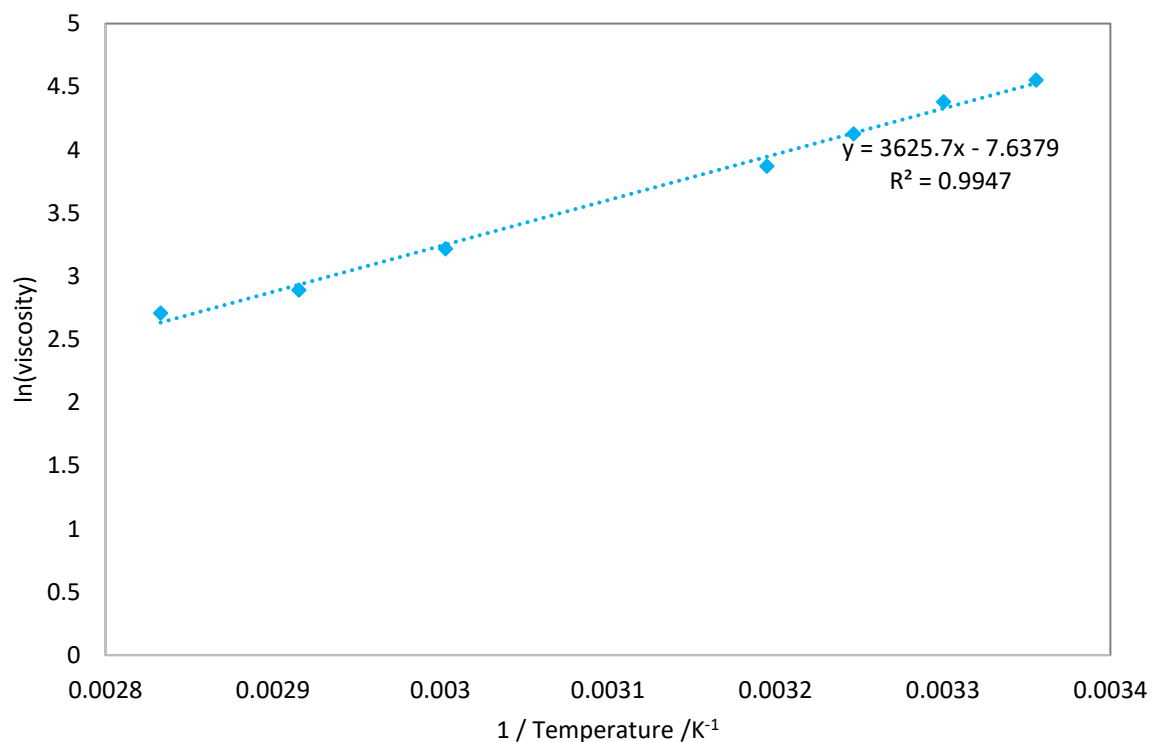
**Figure 3.6.** Effect of alkyl chain length on viscosity of  $[C_n\text{mim}][\text{Cu}(\text{NCMe})(\text{OTf})(\text{NTf}_2)]$  at 298 K.

Figure 3.7 shows the effect of temperature on the viscosity of  $[\text{C}_2\text{mim}][\text{Cu}(\text{NCMe})(\text{OTf})(\text{NTf}_2)]$ . As expected, raising the temperature resulted in a decrease in viscosity. Increasing the temperature by  $15\text{ }^\circ\text{C}$  resulted in a drop in viscosity by about half which shows how a simple change in the conditions can have a dramatic effect on the physical properties of these copper containing ILs.



**Figure 3.7.** Effect of Temperature on Viscosity of the  $[\text{C}_2\text{mim}][\text{Cu}(\text{NCMe})(\text{OTf})(\text{NTf}_2)]$  IL

The viscosity dependency on temperature can be fitted to an empirical model like the Arrhenius equation. Figure 3.8 shows how this effect can be described by the Arrhenius model for the  $[\text{C}_2\text{mim}][\text{Cu}(\text{NCMe})(\text{OTf})(\text{NTf}_2)]$  IL in the range 298 K – 353 K with good agreement. From this analysis, an activation energy of  $30 \text{ kJ mol}^{-1}$  was calculated. Urtiaga *et. al* calculated an activation energy of  $70.6 \text{ kJ mol}^{-1}$  for the copper containing IL  $[\text{C}_6\text{mim}][\text{Cu}(\text{Cl})_x]$ .



**Figure 3.8.** Effect of temperature on viscosity of the  $[\text{C}_2\text{mim}][\text{Cu}(\text{NCMe})(\text{OTf})(\text{NTf}_2)]$  IL and fitted to the Arrhenius model.

### 3.7 Low-Pressure CO Reactions

The reaction of CO with  $[C_n\text{mim}][\text{CuX}_2]$  ILs was initially tested by subjecting the liquid to a stream of CO, at atmospheric pressure, for a few minutes and measuring the IR spectrum of a thin film of the liquid. In each case a single  $\nu(\text{CO})$  absorption was observed consistent with a copper monocarbonyl species. The data are listed in Table 3.4.

**Table 3.4.** IR spectroscopic data for  $\text{Cu}(\text{CO})$  species formed on reaction of CO with  $[C_n\text{mim}][\text{CuX}_2]$ .

Ionic Liquid	$\nu(\text{CO}) / \text{cm}^{-1}$
$[\text{C}_6\text{mim}][\text{CuCl}_2]$	2076 <sup>19</sup>
$[\text{C}_6\text{mim}][\text{CuBr}_2]$	2081 <sup>19</sup>
$[\text{C}_2\text{mim}][\text{CuBr}_2]$	2089
$[\text{C}_6\text{mim}][\text{Cu}(\text{OAc})_2]$	2086
$[\text{C}_6\text{mim}][\text{Cu}(\text{CF}_3\text{CO}_2)_2]$	2099
$[\text{C}_6\text{mim}][\text{Cu}(\text{NCMe})(\text{OTf})_2]$	2114
$[\text{C}_2\text{mim}][\text{Cu}(\text{NCMe})(\text{OTf})(\text{NTf}_2)]$	2122
$[\text{C}_6\text{mim}][\text{Cu}(\text{NCMe})(\text{OTf})(\text{NTf}_2)]$	2122

The  $\text{OAc}^-$  system exhibited a  $\nu(\text{CO})$  value similar to that of the bromide systems, whereas the TFA system gave a higher frequency absorption. Since the copper speciation is thought to be quite similar according to mass spectrometry (i.e.  $[\text{CuX}_2]^-$  where  $X = \text{Cl}, \text{Br}, \text{OAc}, \text{TFA}$ ) the carbonyl complex formed is likely  $[\text{Cu}(\text{CO})\text{X}_2]^-$ . The higher  $\nu(\text{CO})$  value for the TFA system is due to the lower relative basicity of the anion.

Appreciably higher  $\nu(\text{CO})$  values are observed for the ILs containing  $\text{OTf}^-$  and  $\text{NTf}_2^-$  anions suggesting the electron density on the  $\text{Cu}(\text{I})$  centre is lower compared to the free halide systems. The  $\nu(\text{CO})$  value

for the NTf<sub>2</sub> system is also higher due to the NTf<sub>2</sub><sup>-</sup> anion being a much weaker base when compared to other anions, such as OTf<sup>-</sup>, which results in less electron density available on the copper centre.<sup>5</sup> This observation would suggest the anions are interacting with the copper centre. Moreover, the literature  $\nu(\text{CO})$  values for the monocarbonyls Cu(OTf)(CO) and Cu(NTf<sub>2</sub>)(CO) are reported as 2131 cm<sup>-1</sup> and 2161 cm<sup>-1</sup> (Table 3.5) which is higher than the  $\nu(\text{CO})$  values recorded for our systems. This could be consistent with the coordination of a second anion.

**Table 3.5.**  $\nu(\text{CO})$  data for some selected copper(I) carbonyls.<sup>5</sup>

Copper Species	$\nu(\text{CO}) / \text{cm}^{-1}$
[C <sub>6</sub> mim][Cu(NCMe)(OTf) <sub>2</sub> ]	2114
[C <sub>6</sub> mim][Cu(NCMe)(OTf)(NTf <sub>2</sub> )]	2122
CuOTf	2131
CuNTf <sub>2</sub>	2161

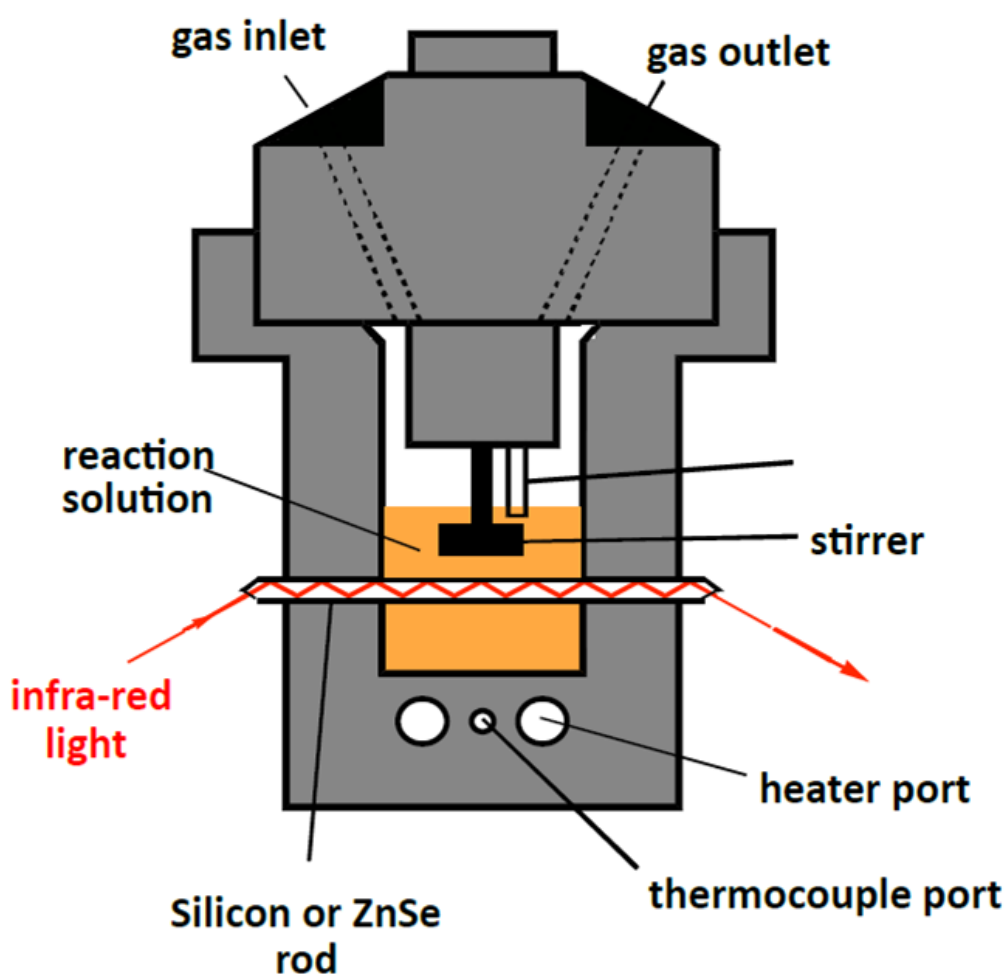
Changing the length of the alkyl chain on the imidazolium species has little effect on  $\nu(\text{CO})$ , which suggests the cation does not affect the electron density on the copper centre.

Further discussion of the copper carbonyl speciation will be given in section 3.8.4 when the results of high pressure CO binding are also taken into account.

As shown by some of the elemental analysis results, these systems are prone to the absorption of water from the atmosphere. With some water potentially present, it is unlikely that it would hinder the CO uptake since water does not compete with binding to the copper sites. Therefore, the effect of having some water present is assumed to be negligible.

### 3.8 *In Situ* High Pressure Infrared Studies of OTf<sup>-</sup> and NTf<sub>2</sub><sup>-</sup> Systems

Figure 3.9 shows the cylindrical internal reflectance (CIR) cell used to monitor the absorption of CO by the copper(I)-containing ILs using in situ high pressure infrared (HPIR) spectroscopy.<sup>20,21</sup> This allows the effects of CO pressure, temperature, and the rate of gas/liquid mixing to be probed, as previously reported by Repper *et.al.*<sup>19</sup>

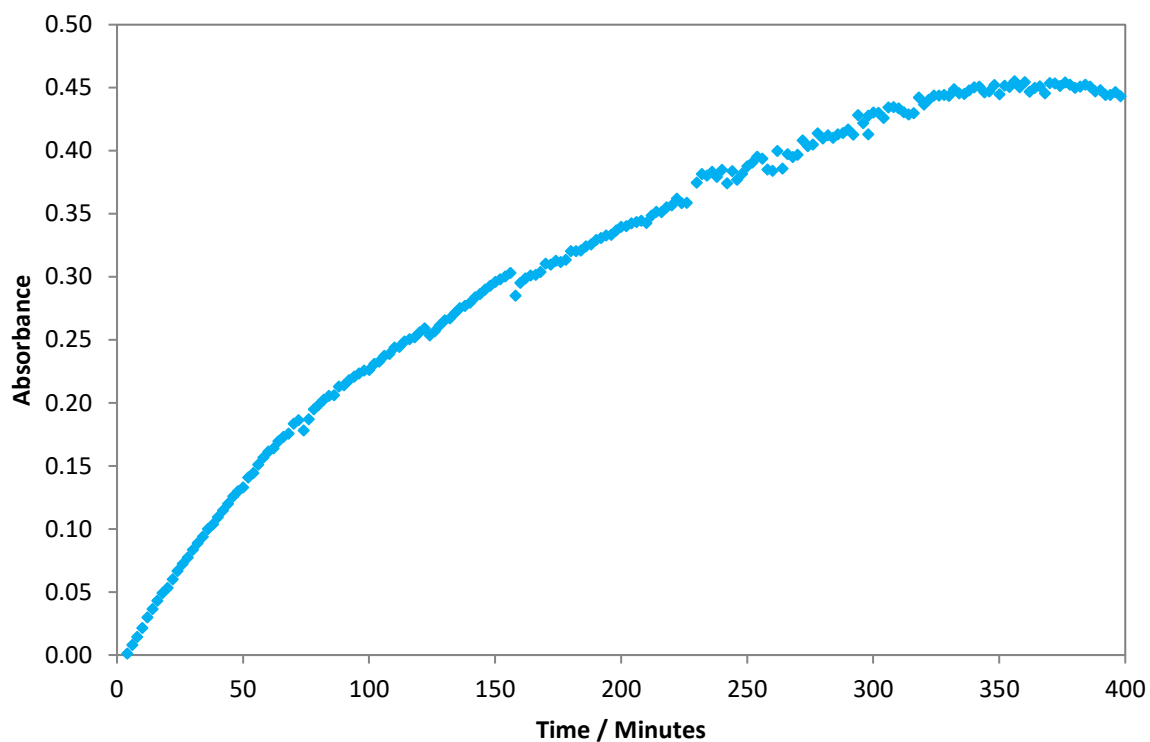


**Figure 3.9.** Diagram of the type of cell used in the high pressure in-situ IR studies.

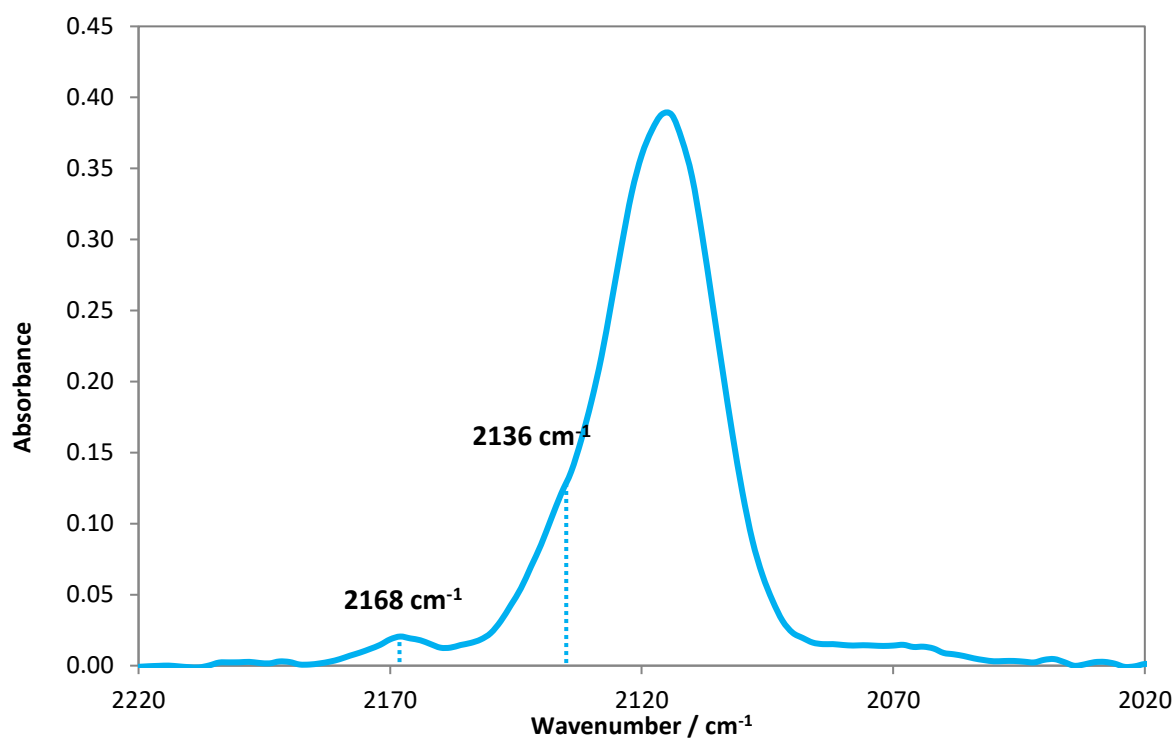
### 3.8.1 Absorption of CO by $[C_n\text{mim}][\text{Cu}(\text{NCMe})(\text{OTf})(\text{X})]$ Ionic Liquids

A sample of about 8 cm<sup>3</sup>  $[\text{C}_6\text{mim}][\text{Cu}(\text{NCMe})(\text{OTf})_2]$  was loaded into the CIR cell and the headspace was pressurised with 12 bar of CO. The absorption of CO was allowed to proceed at 298 K and the growth of a single  $\nu(\text{CO})$  band at 2114 cm<sup>-1</sup> was observed, consistent with that found during the experiment done at 1 bar CO with the same liquid.

Figure 3.10 shows the plot of absorbance against time for the  $\nu(\text{CO})$  band at 2114 cm<sup>-1</sup> during the uptake of CO by  $[\text{C}_6\text{mim}][\text{Cu}(\text{NCMe})(\text{OTf})_2]$ . This is analogous to the observations reported by Repper for halide-based ILs, which showed evidence for formation of monocarbonyl complexes.<sup>6,19</sup> However, it is notable that at around 350 minutes, the absorbance intensity begins to decline slightly which was not observed in any of the halide systems. This coincides with the emergence of a weak band at 2168 cm<sup>-1</sup> and a shoulder at 2136 cm<sup>-1</sup> (Figure 3.11). As the CO pressure increased, the absorptions at 2136 cm<sup>-1</sup> and 2168 cm<sup>-1</sup> continued to grow, whilst the peak at 2114 cm<sup>-1</sup> continued to decrease, suggesting that other copper carbonyl species are forming.

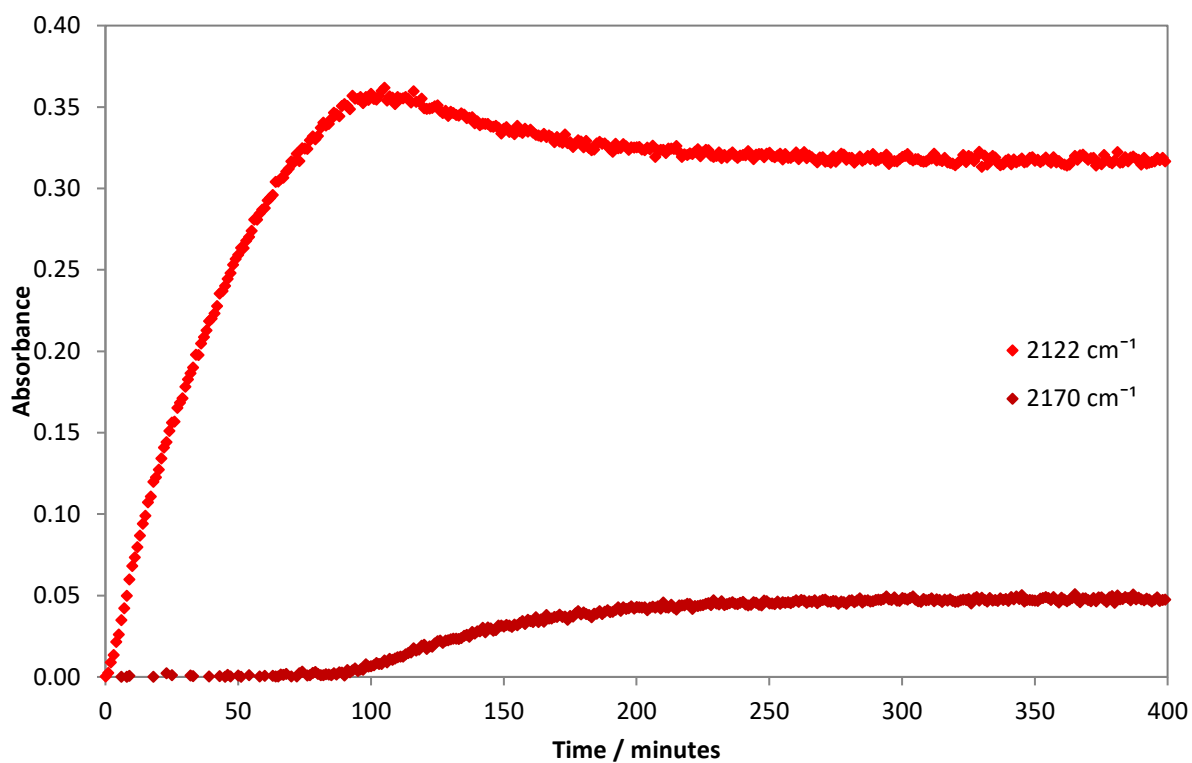


**Figure 3.10.** Plot of absorbance vs. time for the IR band at  $2114\text{ cm}^{-1}$  by  $[\text{C}_6\text{mim}][\text{Cu}(\text{NCMe})(\text{OTf})_2]$  on exposure to 12 bar CO at  $25\text{ }^\circ\text{C}$  and stirrer speed 214 rpm.



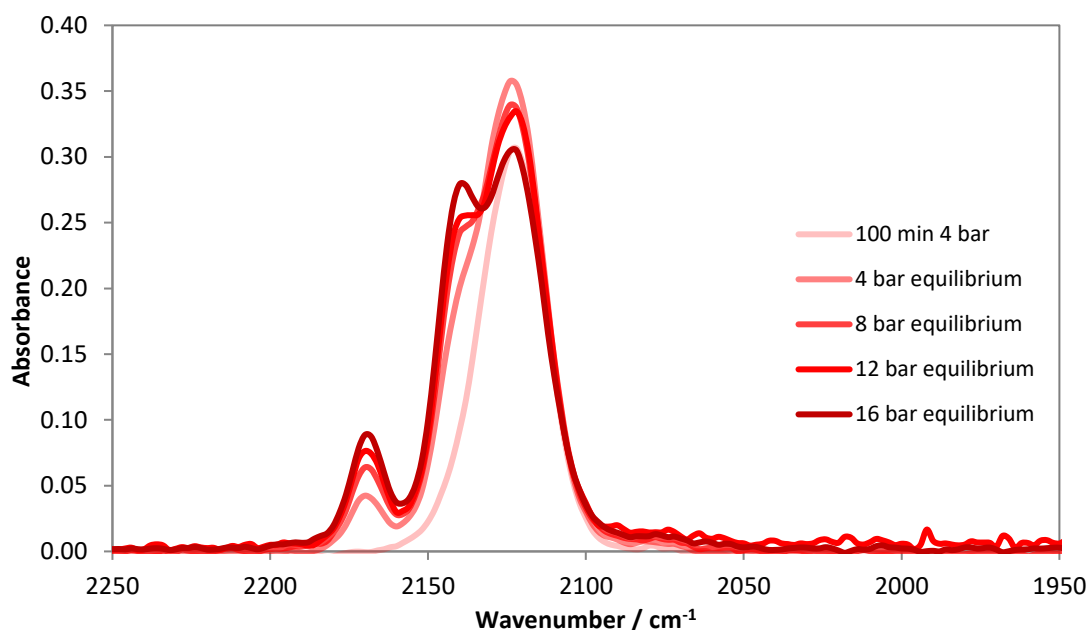
**Figure 3.11.** IR spectrum of  $[\text{C}_6\text{mim}][\text{Cu}(\text{NCMe})(\text{OTf})_2]$  at 16 bar equilibrium CO pressure and  $25\text{ }^\circ\text{C}$ .

The uptake of CO was also investigated using  $[\text{C}_2\text{mim}][\text{Cu}(\text{NCMe})(\text{OTf})(\text{NTf}_2)]$ . Again, the initial growth of a single  $\nu(\text{CO})$  band at  $2122\text{ cm}^{-1}$  was observed which was consistent with that observed during the experiments run at 1 bar CO pressure. Figure 3.12 shows how, after around 100 minutes, the  $\nu(\text{CO})$  band at  $2122\text{ cm}^{-1}$  began to decline whilst absorptions at  $2140\text{ cm}^{-1}$  and  $2170\text{ cm}^{-1}$  began to grow.



**Figure 3.12.** Plot of absorbance vs. time for the initial uptake of CO at  $2122\text{ cm}^{-1}$  and  $2170\text{ cm}^{-1}$  by  $[\text{C}_2\text{mim}][\text{Cu}(\text{NCMe})(\text{OTf})(\text{NTf}_2)]$  on exposure to 12 bar CO at  $25\text{ }^\circ\text{C}$  and stirrer speed 214 rpm.

The growth of the higher frequency bands was more prominent in this case compared to the bis(OTf) system. Figure 3.13 shows a series of IR spectra for  $[\text{C}_2\text{mim}][\text{Cu}(\text{NCMe})(\text{OTf})(\text{NTf}_2)]$  with increasing CO pressure, showing the growth of the absorptions at  $2170$  and  $2140\text{ cm}^{-1}$  as the pressure increases.



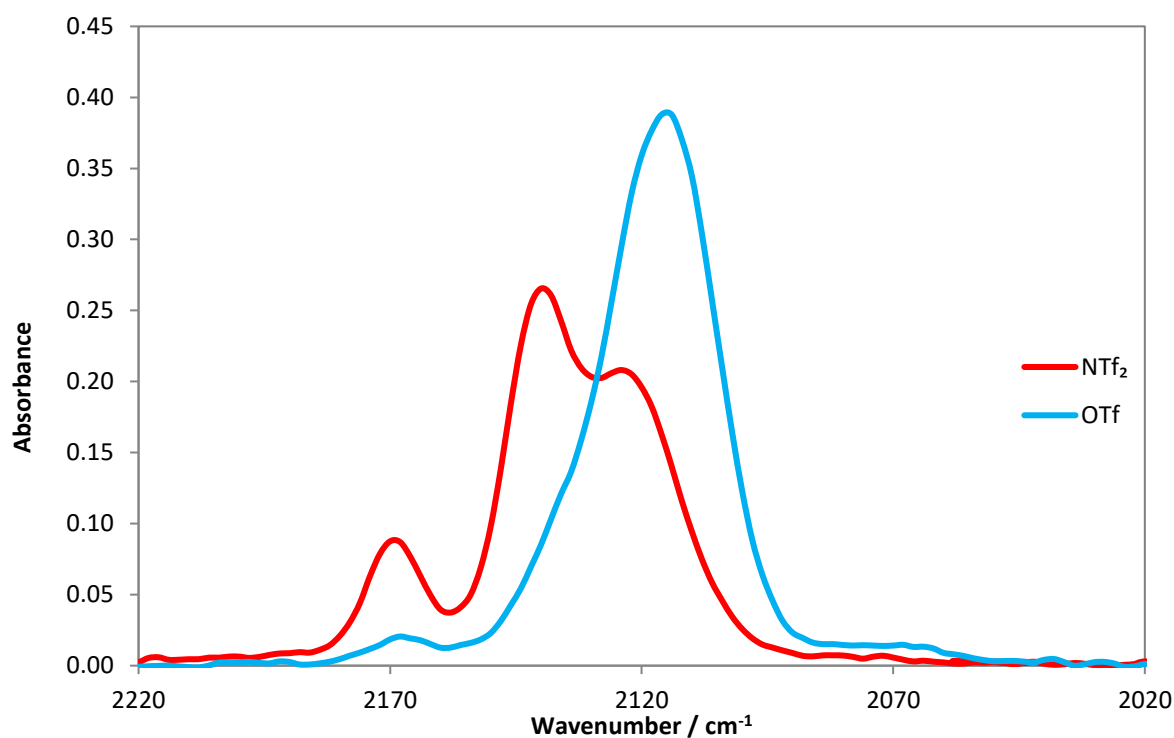
**Figure 3.13.** Series of IR spectra showing the growth and decline of the  $\nu(\text{CO})$  at  $2122\text{ cm}^{-1}$  and the growth of peaks at  $2140\text{ cm}^{-1}$  and  $2170\text{ cm}^{-1}$  as the pressure of CO increased from 4 - 16 bar at  $25\text{ }^{\circ}\text{C}$  for the  $[\text{C}_2\text{mim}][\text{Cu}(\text{NCMe})(\text{OTf})(\text{NTf}_2)]$  IL.

The shift to higher wavenumber, and the relative intensities of the two new peaks, is consistent with the formation of a metal dicarbonyl. Copper dicarbonyls,  $[\text{Cu}(\text{CO})_2\text{NTf}_2]$  and  $[\text{Cu}(\text{CO})_2\text{OTf}]$  are known in the literature<sup>5,22,23</sup> and the frequencies that are recorded in our systems are similar to those attributed to the  $\text{Cu}(\text{CO})_2\text{OTf}$  species (Table 3.6). The relative intensities also match up, with the higher shifted peak at around  $2170\text{ cm}^{-1}$ , showing the weaker intensity of the two.<sup>23</sup> However, in our systems there is an NCMe ligand which may or may not be coordinated at the same time.

**Table 3.6.**  $\nu(\text{CO})$  data for some selected copper(I) dicarbonyls.

Copper Species	$\nu(\text{CO})_2 / \text{cm}^{-1}$
$[\text{C}_6\text{mim}][\text{Cu}(\text{NCMe})(\text{OTf})_2]$	2136, 2168
$[\text{C}_6\text{mim}][\text{Cu}(\text{NCMe})(\text{OTf})(\text{NTf}_2)]$	2140, 2170
CuOTf	2143, 2171
CuNTf <sub>2</sub>	2158, 2184

Moreover, Figure 3.14 shows how comparing the solely OTf system with the system containing NTf<sub>2</sub><sup>-</sup>, it is the latter which gives the much higher preference for the dicarbonyl at a given CO equilibrium pressure, indicating that the presence of NTf<sub>2</sub> makes dicarbonyl formation more amenable. The proposed active copper species will be discussed further in section 3.8.4.



**Figure 3.14.** IR spectra of ILs at 16 bar equilibrium CO pressure and 25 °C showing dicarbonyl formation. Where Red = [C<sub>6</sub>mim][Cu(NCMe)(OTf)(NTf<sub>2</sub>); Blue = [C<sub>6</sub>mim][Cu(NCMe)(OTf)<sub>2</sub>].

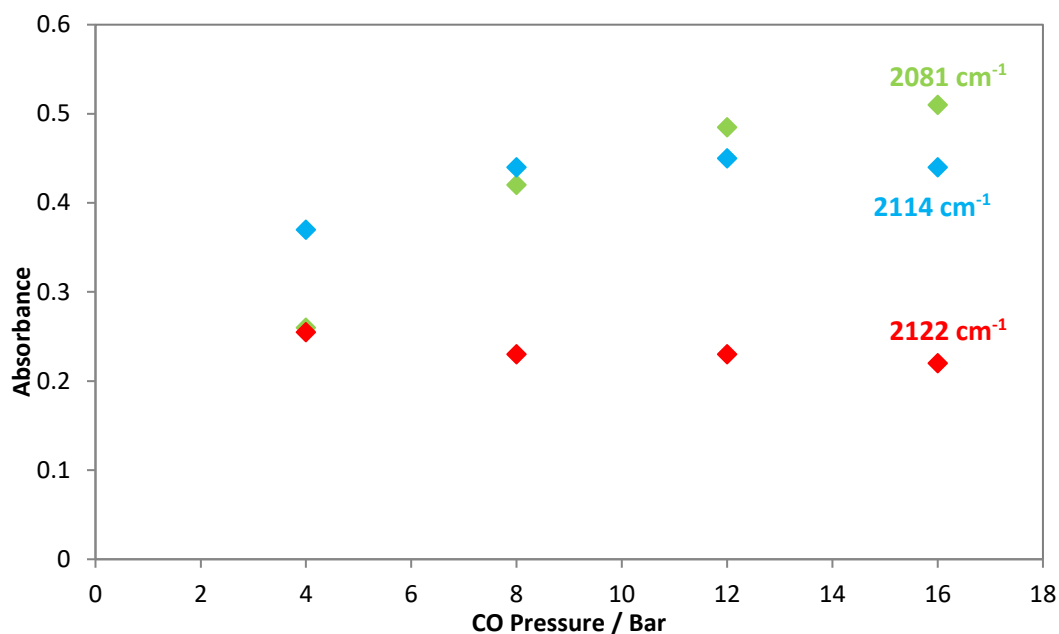
The higher  $\nu(\text{CO})$  values ( $> 2100 \text{ cm}^{-1}$ ) for these carbonyl complexes would suggest relatively weak Cu-CO bonding and hence CO dissociation was expected to be more facile than for the halide systems which required about 100 °C to fully remove the bound CO.<sup>19</sup> However, the temperature required for full desorption was comparable, and even higher in some cases, for the triflyl systems. Full desorption of CO from the OTf/NTf<sub>2</sub> system required about 100 °C and the bis(OTf) system required about 140 °C, an observation also noted by Repper.<sup>6</sup> Partial desorption of one of the CO ligands to form the monocarbonyl was facile as this could be done by releasing the pressure without the need for heating.

The ability of the triflyl systems to form dicarbonyl complexes means that the amount of CO that could be absorbed is potentially double the copper concentration of the IL.

For comparison, a HPIR experiment was performed on a 0.1 M COSORB-type solution (CuCl + AlCl<sub>3</sub> in toluene). IR data for the COSORB system has not previously been reported in the literature. The spectra (included in the appendix Figure 8.1 and 8.2) show the rapid appearance of a  $\nu(\text{CO})$  absorption at 2128 cm<sup>-1</sup> along with a slightly weaker and broader band at 2118 cm<sup>-1</sup>, suggesting formation of at least two Cu(CO) species. The measured peak absorbance (~0.25) under 2 bar CO is comparable to that typically found for the IL systems at higher pressures (~10 bar), suggesting that CO complexation is more favourable in the CuCl/AlCl<sub>3</sub>/toluene system.<sup>24</sup> This is consistent with data from Hogendoorn et al that show CO uptake by a COSORB solution (1.7 M [Cu]) giving ~70% occupancy of Cu sites at 1 bar CO.<sup>25</sup>

### 3.8.2 CO Uptake at equilibrium

Figure 3.15 shows the equilibrium IR absorbances of the monocarbonyl  $\nu(\text{CO})$  band recorded at pressures 4, 8, 12 and 16 bar. The equilibrium position was determined after no increase in absorbance was seen after 30 minutes. Data for the [C<sub>6</sub>minm]Br system are added for reference.



**Figure 3.15.** Equilibrium absorbances of the monocarbonyl peak for different ILs at various CO pressures at 25 C. The position of the  $\nu(\text{CO})$  for each respective IL is quoted on the graph. When Red =  $[\text{C}_6\text{mim}][\text{Cu}(\text{NCMe})(\text{OTf})(\text{NTf}_2)]$ ; Blue =  $[\text{C}_6\text{mim}][\text{Cu}(\text{NCMe})(\text{OTf})_2]$ ; Green =  $[\text{C}_6\text{mim}][\text{CuBr}_2]$

Figure 3.15 shows that the OTf/NTf<sub>2</sub> system forms the dicarbonyl more readily since the decline of the peak attributed to the monocarbonyl occurs at lower pressures. Dicarbonyl formation can be seen as low as 4 bar equilibrium for NTf<sub>2</sub> compared to 12 bar for the OTf system.

In order to correlate the amount of CO absorbed to the observed IR absorbance, the CIR cell was initially pressurised to a given CO pressure and sealed. As the IL absorbed the CO, the pressure of the cell headspace dropped. At regular intervals, the depletion of the headspace pressure was noted, along with the absorbance of the monocarbonyl  $\nu(\text{CO})$  band. Given the volume of the CIR cell was measured to be 60 cm<sup>3</sup>, and the amount of IL loaded into the cell approximately 8 cm<sup>3</sup>, this leads to a headspace volume of ~52 cm<sup>3</sup>. Knowing the pressure of CO absorbed and the volume of the headspace, the number of moles of CO absorbed by the IL can be calculated from the ideal gas law

(eq 4), where  $P$  = the pressure drop in Pascals,  $V$  = volume of the headspace,  $5.2 \times 10^{-5} \text{ m}^3$ ,  $R$  = universal gas constant,  $8.314 \text{ J K}^{-1} \text{ mol}^{-1}$  and  $T$  = temperature, 293 K.

$$n = \frac{PV}{RT} \quad (\text{eq 4})$$

Figure 3.16 shows a plot of the absorbance of the monocarbonyl  $\nu(\text{CO})$  peak, against the amount of CO absorbed by the IL. From this, the amount of CO absorbed at any given point can be determined from the absorbance. For the OTf and NTf<sub>2</sub> systems, this approach was only applied before the formation of the dicarbonyl and it is assumed no dicarbonyl was formed during this period. This assumption seems reasonable as there was no evidence of dicarbonyl peaks until the monocarbonyl peaks began to decline.

It is notable that the gradients of the different systems are quite similar, showing that the extinction coefficients do not differ too much.

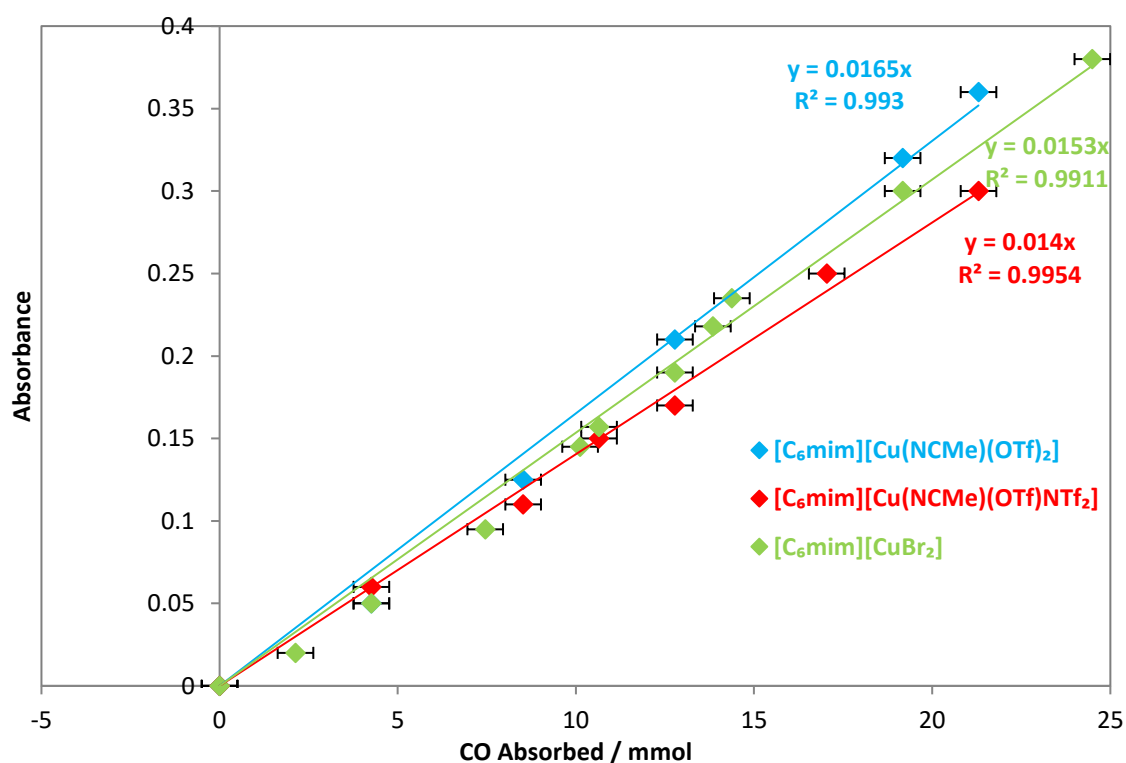


Figure 3.16. Plot of IR absorbance of the copper monocarbonyl against amount of CO absorbed by 8 cm<sup>3</sup> of IL at 293 K.

Pressure drop experiments were also investigated to determine the amount of CO that could be absorbed at 12 bar equilibrium. Similarly to the previous experiment, the cell was initially pressurised to 12 bar and sealed. As the IL absorbed the CO, the headspace pressure decreased. The difference in pressure was noted, and then the cell was repressurised to 12 bar and the IL allowed to continue to absorb CO. These steps were repeated until no drop in pressure was recorded after 30 minutes when repressurised to 12 bar. Table 3.7 gives the sum of all the decreases in pressure and the corresponding amount of CO absorbed at 12 bar equilibrium at 293 and 353 K. The data confirm that the triflyl systems are capable of absorbing more than 1 equivalent of CO per Cu centre, consistent with the dicarbonyl formation observed by HPIR. At the higher temperature less CO was absorbed, consistent with the observation that heating encourages desorption of CO. For  $[\text{C}_2\text{mim}][\text{Cu}(\text{NCMe})(\text{OTf})(\text{NTf}_2)]$  more than 1 equivalent of CO is absorbed even at the higher temperature, and the IR spectrum in Figure 3.17 confirms the presence of some dicarbonyl under these conditions.

**Table 3.7.** Calculations for the molar ratio of CO to Cu at 12 bar equilibrium pressure at a given temperature.

Ionic Liquid	Temperature / K	Pressure of CO absorbed / bar	n(CO) / mmol	n(Cu) / mmol	CO:Cu ratio
$[\text{C}_6\text{mim}][\text{CuBr}_2]$	293	15	32.0	34	0.94
$[\text{C}_6\text{mim}][\text{CuBr}_2]$	353	2	3.5	34	0.10
$[\text{C}_6\text{mim}][\text{Cu}(\text{NCMe})(\text{OTf})_2]$	293	12	25.6	20	1.28
$[\text{C}_6\text{mim}][\text{Cu}(\text{NCMe})(\text{OTf})_2]$	353	10	17.7	20	0.89
$[\text{C}_2\text{mim}][\text{Cu}(\text{NCMe})(\text{OTf})(\text{NTf}_2)]$	293	16	34.2	20	1.71
$[\text{C}_2\text{mim}][\text{Cu}(\text{NCMe})(\text{OTf})(\text{NTf}_2)]$	353	13	23.0	20	1.15

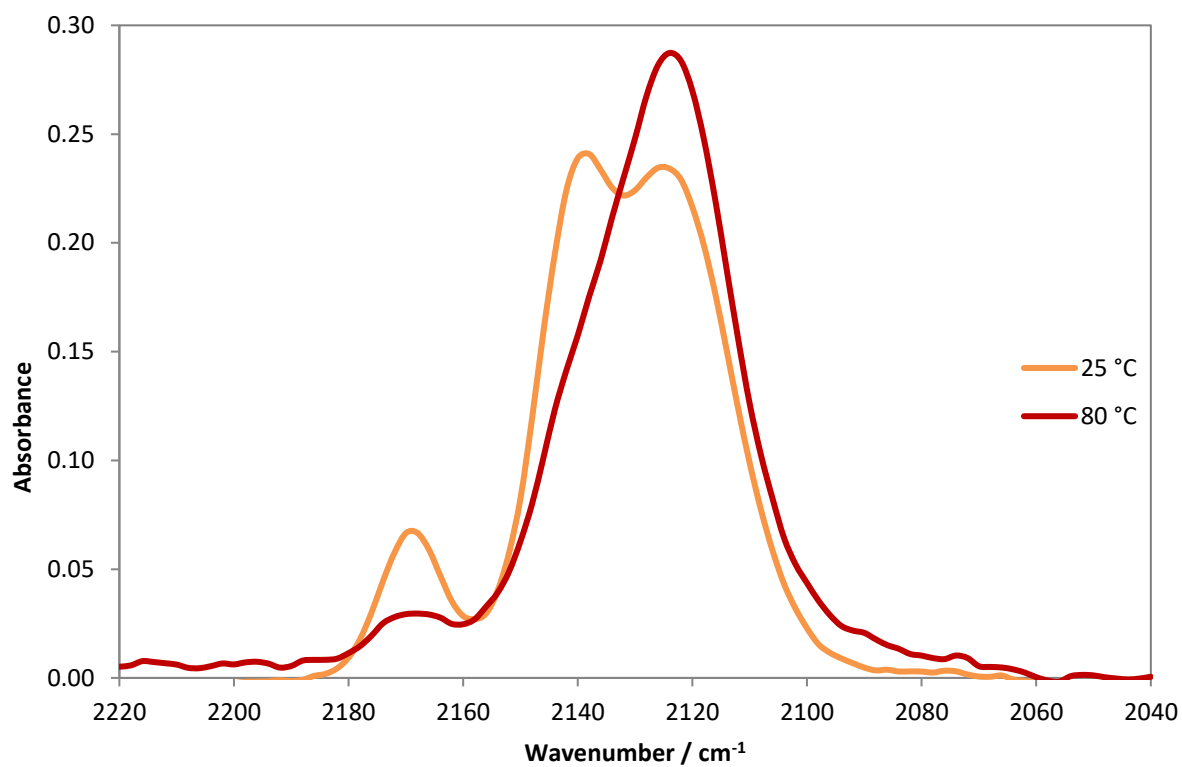
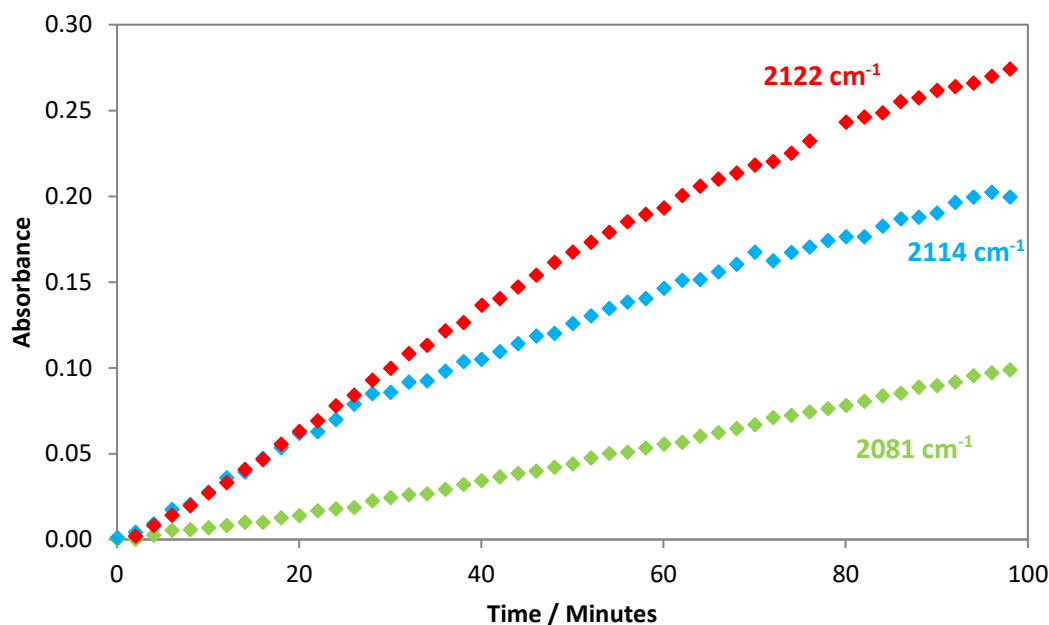


Figure 3.17. IR spectra of [C<sub>2</sub>mim][Cu(NCMe)(OTf)(NTf<sub>2</sub>)] at 12 bar CO pressure orange = 25 °C and red = 80 °C.

### 3.8.3 Rate of CO Uptake

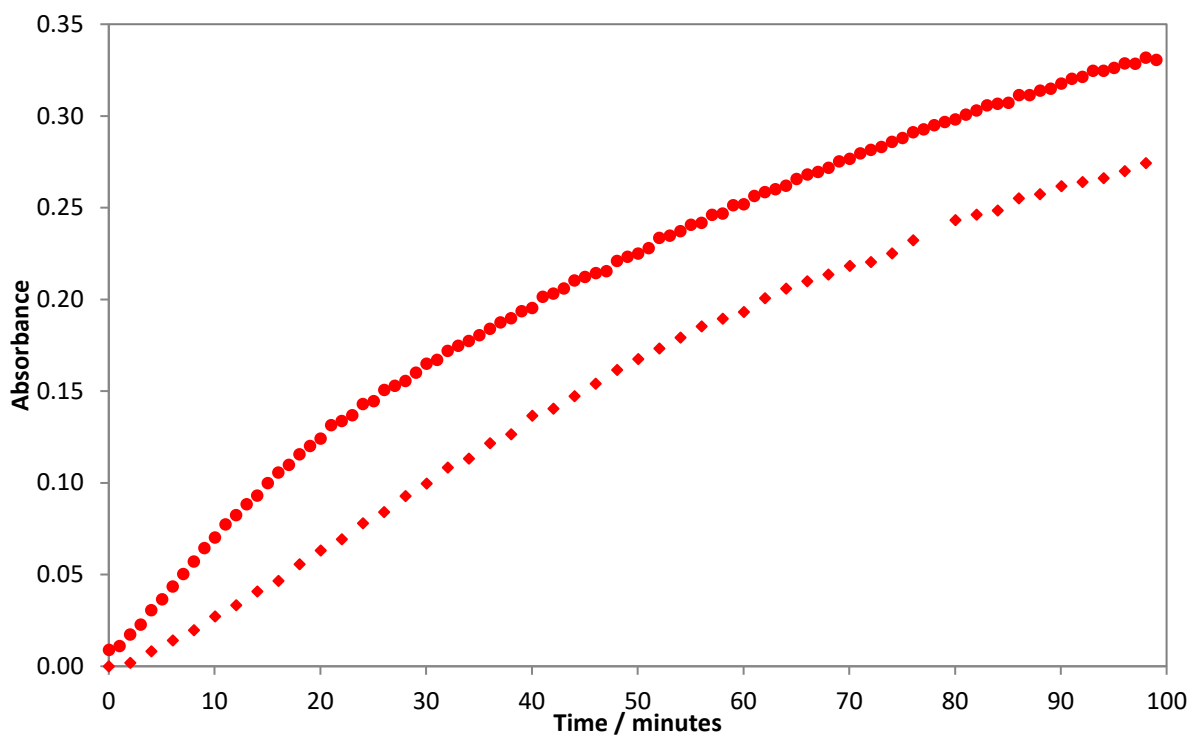
Figure 3.18 shows the growth in intensity of the monocarbonyl  $\nu(\text{CO})$  band during the first 100 minutes of CO absorption at 12 bar CO pressure.



**Figure 3.18.** Plot of absorbance vs. time for the initial uptake of CO by different ILs on exposure to 12 bar CO at 25 °C and stirrer speed 214 rpm. When Red =  $[\text{C}_6\text{mim}][\text{Cu}(\text{NCMe})(\text{OTf})(\text{NTf}_2)]$ ; Blue =  $[\text{C}_6\text{mim}][\text{Cu}(\text{NCMe})(\text{OTf})_2]$ ; Green =  $[\text{C}_6\text{mim}][\text{CuBr}_2]$

After 100 minutes, the bis(OTf) and OTf/NTf<sub>2</sub> systems have, respectively twice and three times the stronger absorbance than the Br<sup>-</sup> system. Assuming similar extinction coefficients (as shown in Figure 3.16), the amount of CO absorbed follows the trend NTf<sub>2</sub> > OTf > Br. This trend also follows the trend in viscosity suggesting that a less viscous IL may aid the transport of CO to the copper sites.

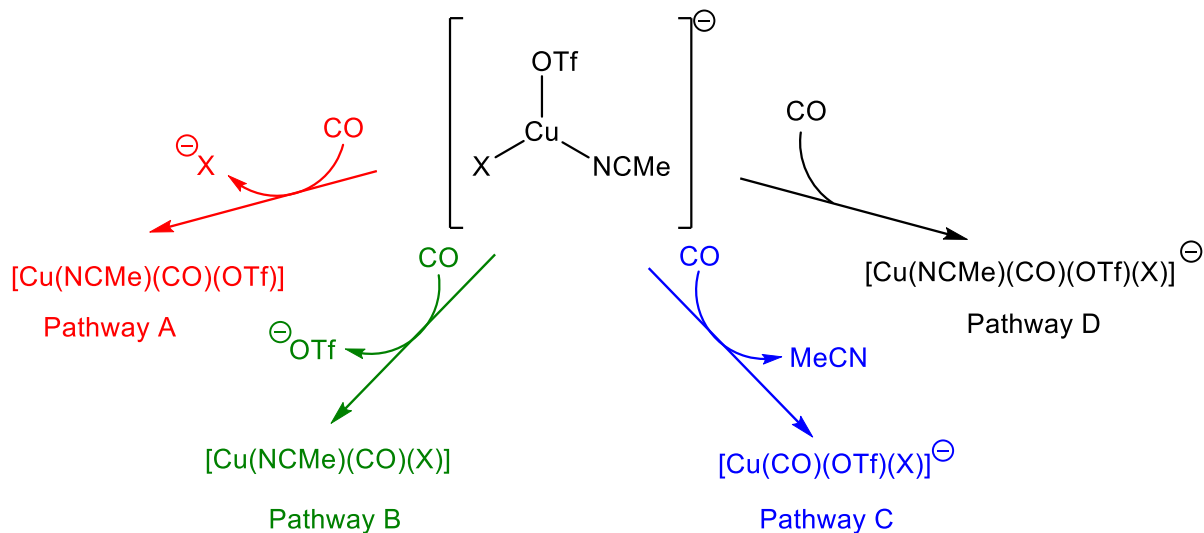
Figure 3.19 compares the rate of CO uptake for  $[\text{C}_n\text{mim}][\text{Cu}(\text{NCMe})(\text{OTf})(\text{NTf}_2)]$  ILs with different size C<sub>n</sub>mim cations (n = 2, 6). The shorter alkyl chain length resulted in a higher copper concentration (Table 3.2) and lower viscosity (Figure 3.6) which probably explain the superior rate and higher v(CO) absorbance at equilibrium over the C<sub>6</sub>mim system.



**Figure 3.19.** Plot of absorbance vs. time for the initial uptake of CO by different  $[C_n\text{mim}][\text{Cu}(\text{NCMe})(\text{OTf})(\text{NTf}_2)]$  ILs when exposed to 4 bar CO at 25 °C and stirrer speed 214 rpm. When  $n$ ; 2 = circle; 6 = diamond

### 3.8.4 Speciation of Copper Carbonyl Complexes

Scheme 3.6 proposes a number of potential  $\text{Cu}(\text{CO})$  species which could represent the monocarbonyl species formed on reacting  $[C_n\text{mim}][\text{Cu}(\text{NCMe})(\text{OTf})(\text{X})]$  with CO. Carbon monoxide could substitute one of the ligands bound to Cu (pathways A-C) or simply associate to give a tetra-coordinate complex (pathway D).



**Scheme 3.6.** Potential Cu(CO) species formed upon reaction of  $[\text{Cu}(\text{NCMe})(\text{OTf})(\text{X})]$  based ILs with CO (X = OTf or NTf<sub>2</sub>).

Pathway A leads to the same copper species regardless of the initial starting species i.e.  $[\text{Cu}(\text{NCMe})(\text{OTf})_2]^{-}$  or  $[\text{Cu}(\text{NCMe})(\text{OTf})(\text{NTf}_2)]^{-}$ . Since the  $\nu(\text{CO})$  recorded when using bis(OTf) and OTf/NTf<sub>2</sub> systems differed, pathway A does not seem likely.

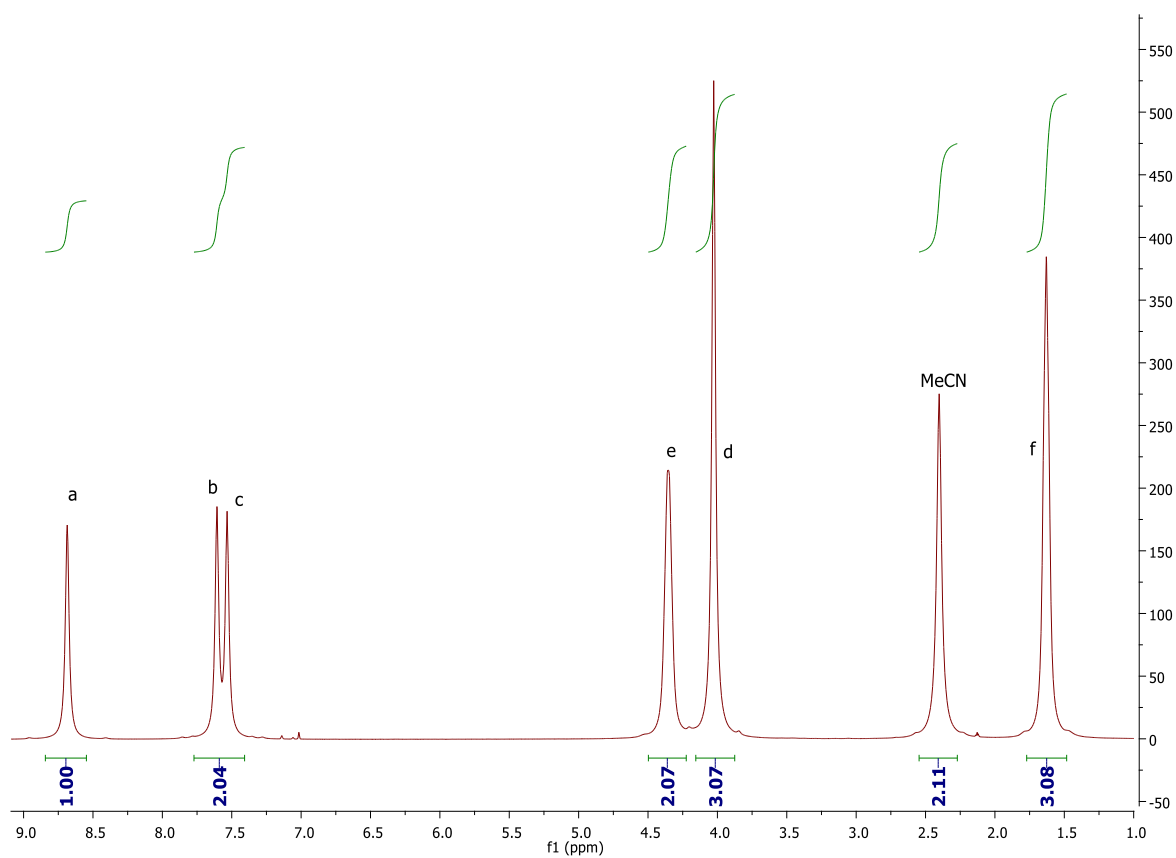
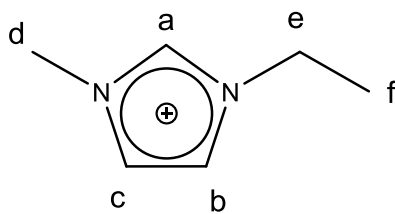
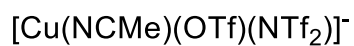
Literature data reports the  $\nu(\text{CO})$  for Cu(CO)OTf as 2131 cm<sup>-1</sup> and Cu(CO)NTf<sub>2</sub> as 2162 cm<sup>-1</sup>.<sup>5,26</sup> Given the  $\nu(\text{CO})$  recorded for  $[\text{C}_6\text{mim}][\text{Cu}(\text{NCMe})(\text{OTf})_2]$  and  $[\text{C}_n\text{mim}][\text{Cu}(\text{NCMe})(\text{OTf})(\text{NTf}_2)]$  were 2114 cm<sup>-1</sup> and 2122 cm<sup>-1</sup> respectively, it seems unlikely that a MeCN ligand would cause such a dramatic effect on the  $\nu(\text{CO})$ . An anionic species would be more consistent with the lower  $\nu(\text{CO})$  therefore, pathway B seems unlikely.

This leaves pathways C and D most likely. <sup>1</sup>H NMR analysis of  $[\text{C}_n\text{mim}][\text{Cu}(\text{NCMe})(\text{OTf})(\text{X})]$ , after reaction with CO, showed there still to be one MeCN present. However, this MeCN could still possibly remain in solution and therefore pathway C could be viable.

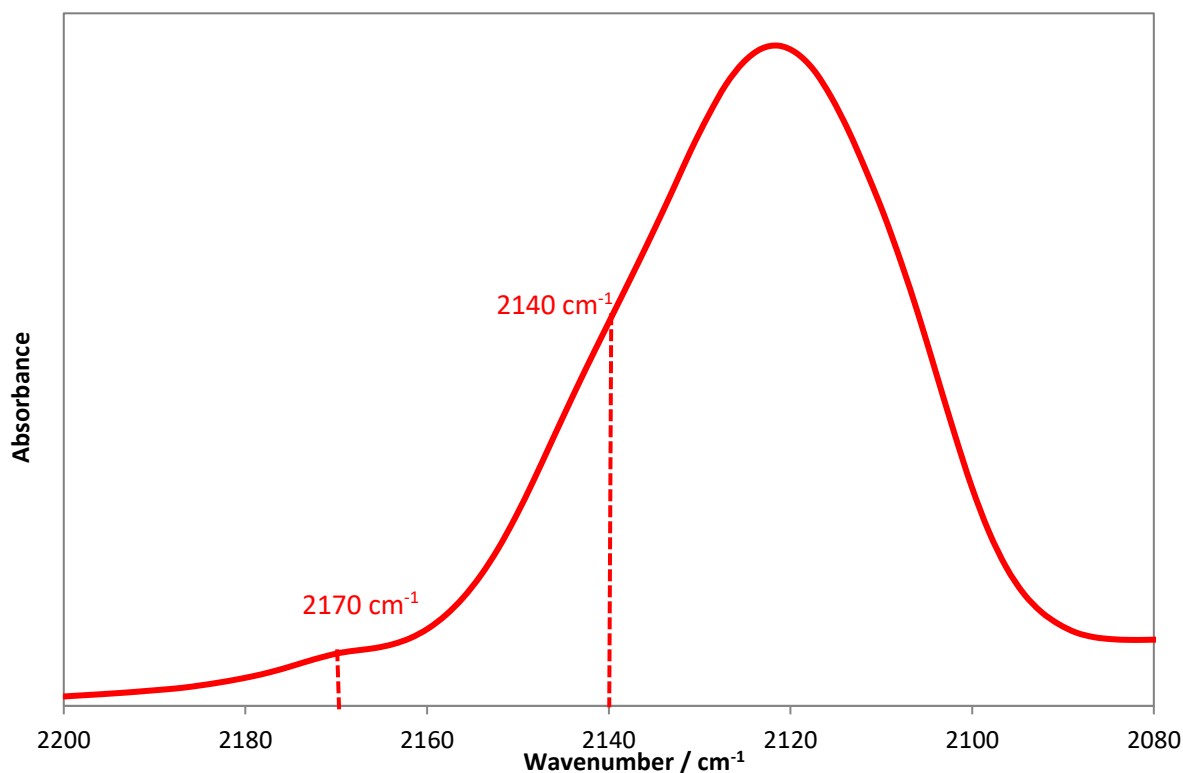
Pathway D gives a four coordinate, anionic copper species. This would particularly explain the disparity between the literature  $\nu(\text{CO})$  frequency for Cu(CO)NTf<sub>2</sub> and  $[\text{C}_n\text{mim}][\text{Cu}(\text{NCMe})(\text{CO})(\text{OTf})(\text{NTf}_2)]$ .

However, the added complication is that these systems also display dicarbonyl behaviour. Therefore, more experiments were conducted to determine the nature of the copper species, when a second CO molecule binds.

Figure 3.20 shows a follow up experiment from the experiment performed in section 3.4, where this time a stream of CO, rather than argon, was passed through a sample of  $[\text{C}_2\text{mim}][\text{Cu}(\text{NCMe})(\text{OTf})(\text{NTf}_2)]$  in an attempt to remove the MeCN. After 16 hours, the NMR spectrum showed that the MeCN peak had reduced to 70 % of its original value suggesting the CO was able to displace the MeCN, and subsequently evaporated. The broadness of the peaks in Figure 3.20 is likely due to some oxidation occurring during manipulation and set up of the experiment.



**Figure 3.20.** NMR spectrum of  $[\text{C}_2\text{mim}][\text{Cu}(\text{NCMe})(\text{OTf})(\text{NTf}_2)] + \text{CO}$  in  $d^8$  toluene after passing CO through the sample for 16 hours.



**Figure 3.21.** Infrared spectrum of  $[\text{C}_2\text{mim}][\text{Cu}(\text{NCMe})_x(\text{CO})_x(\text{OTf})(\text{NTf}_2)]$  after being exposed to a stream CO for 16 hours.

Figure 3.21 shows that the sample was also analysed by infrared spectroscopy, and it was found that the dicarbonyl could be formed under these conditions. From these experiments, it seems as though the MeCN is displaced by CO to form the carbonyl species. Whether the MeCN is lost during the coordination of the first or second CO is unclear, however, it does indicate the final dicarbonyl species does not accommodate any MeCN.

A sample of  $[\text{C}_2\text{mim}][\text{Cu}(\text{NCMe})(\text{OTf})(\text{NTf}_2)]$  was also mixed with one volume equivalent of MeCN and CO was passed through the sample. When analysed by IR, no absorption was observed in the region  $2100\text{ cm}^{-1} - 2200\text{ cm}^{-1}$  showing no copper carbonyl was formed. This suggests the MeCN is competing with CO for the coordination to the copper species.

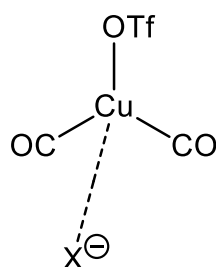
Table 3.8 gives the  $\nu(\text{CO})$  frequencies for some relevant copper(I) dicarbonyls and shows that the copper dicarbonyl formed in the ILs, is similar to that of the neutral CuOTf.

**Table 3.8.**  $\nu(\text{CO})$  data for some selected copper(I) dicarbonyls.

Copper Species	$\nu \text{Cu}(\text{CO})_2 / \text{cm}^{-1}$
$[\text{C}_6\text{mim}][\text{Cu}(\text{NCMe})(\text{OTf})_2]$	2136, 2168
$[\text{C}_n\text{mim}][\text{Cu}(\text{NCMe})(\text{OTf})(\text{NTf}_2)]$	2140, 2170
$\text{CuOTf}$	2143, 2171 <sup>26</sup>

To transition to the neutral species, an anion must be lost from the copper. During high pressure IR studies, it was the mixed  $\text{NTf}_2/\text{OTf}$  system which showed the greatest affinity for dicarbonyl formation. Since  $\text{NTf}_2$  is a weaker base, it should be easier to displace during coordination of the second CO and thus form the dicarbonyl more readily. Given OTf is a more strongly coordinating anion, the coordination of the second CO would be more difficult in the bis(OTf) system and this is exactly the observation seen in our experiments where the dicarbonyl is only formed at high pressures and much less favourably compared to  $\text{NTf}_2$ .

However, there are some discrepancies in  $\nu(\text{CO})$  for the dicarbonyls reported in Table 3.8. Given that the literature data corresponds to solid-state structures, a direct comparison is complicated. Another suggestion is provided in Figure 3.22. This may be due to the anion, which is being lost to coordinate the second CO, still having some slight interaction with the copper centre. This may be a result of the system being liquid, and the active species not able to be fully defined as it would be if it were a solid-state system.

**Figure 3.22.** Proposed copper dicarbonyl species formed on reaction of  $[\text{C}_n\text{mim}][\text{Cu}(\text{NCMe})(\text{OTf})(\text{X})]$  with CO.

### 3.9 Conclusions

Moving away from ILs based on  $\text{Cl}^-$  and  $\text{Br}^-$ , a number of ILs with more weakly coordinating anions have been synthesised, along with the corresponding copper(I) salts. These in turn have been utilised to generate room-temperature copper-containing ILs based on  $\text{OTf}^-$  and  $\text{NTf}_2^-$  anions. The ILs outlined in this chapter have been shown to dramatically reduce the viscosity, whilst the absence of free halides avoids potential issues with corrosion. Such attributes make them more appealing for commercial use.

These ILs have been shown to absorb CO more quickly than the halide systems, although the conditions required for CO desorption are harsher. Based on the  $v(\text{CO})$  values, this was not expected and the reasons are not presently fully understood. HPIR spectroscopy and CO uptake measurements gave evidence for formation of copper(I) dicarbonyl species, which suggests potential for greater CO absorption capacity which should aid in gas separations.

The most appealing properties were shown by the  $[\text{C}_n\text{mim}]\text{NTf}_2/\text{Cu}(\text{NCMe})_2\text{OTf}$  systems, with respect to their lower viscosity, quicker CO uptake, more favourable dicarbonyl formation and less forcing conditions to remove the bound CO. Overall, this makes them promising for use in CO gas separations.

### 3.10 References

- 1 E. Alcalde, I. Dinarès, A. Ibáñez and N. Mesquida, *Chem. Commun.*, 2011, **47**, 3266.
- 2 I. Dinarès, C. Garcia de Miguel, A. Ibáñez, N. Mesquida and E. Alcalde, *Green Chem.*, 2009, **11**, 1507.
- 3 F. A. Cotton, A. Evgeny V. Dikarev and M. A. Petrukhina, *Inorg. Chem.*, 2000, **39**, 6072–6079.
- 4 P. F. Rodesiler and E. L. Amma, *J. Chem. Soc. Chem. Commun.*, 1974, 599.
- 5 Oleg G. Polyakov, Svetlana M. Ivanova, Christine M. Gaudinski, Susie M. Miller, A. Oren P. Anderson and S. H. Strauss\*, *Organometallics*, 1999, **18**, 3769–3771.
- 6 S. Repper PhD Thesis, University of Sheffield, 2014.
- 7 N. R. Brooks, S. Schaltin, K. Van Hecke, L. Van Meervelt, K. Binnemans and J. Fransaer, *Chem. A Eur. J.*, 2011, **17**, 5054–5059.
- 8 C. Fehr, M. Vuagnoux, A. Buzas, J. Arpagaus and H. Sommer, *Chem. A Eur. J.*, 2011, **17**, 6214–6220.
- 9 J. Kagimoto, S. Taguchi, K. Fukumoto and H. Ohno, *J. Mol. Liq.*, 2010, **153**, 133–138.
- 10 J. A. Hogendoorn, W. P. M. van Swaaij and G. F. Versteeg, *Chem. Eng. J. Biochem. Eng. J.*, 1995, **59**, 243–252.
- 11 G. Zarca, M. Fernández, A. Santamaría, I. Ortiz and A. Urtiaga, *Sep. Purif. Technol.*, 2015, **155**, 96–100.
- 12 J.-G. Li, Y.-F. Hu, S.-F. Sun, Y.-S. Liu and Z.-C. Liu, *J. Chem. Thermodyn.*, 2010, **42**, 904–908.
- 13 H. Shirota, T. Mandai, H. Fukazawa and T. Kato, *J. Chem. Eng. Data*, 2011, **56**, 2453–2459.

- 14 J. T. Bolkan, S. A.; Yoke III, *J. Chem. Eng. Data*, 1986, **31**, 194.
- 15 A. Takada, K. Imaichi, T. Kagawa and Y. Takahashi, *J. Phys. Chem. B*, 2008, **112**, 9660–9662.
- 16 G. Zarca, I. Ortiz and A. Urriaga, *Sep. Purif. Technol.*, 2018, **196**, 47–56.
- 17 N. V. Ignat'ev, U. Welz-Biermann, A. Kucheryna, G. Bissky and H. Willner, *J. Fluor. Chem.*, 2005, **126**, 1150–1159.
- 18 H. Tokuda, K. Hayamizu, K. Ishii, A. Md. Abu Bin Hasan Susan and Masayoshi Watanabe, *J. Phys. Chem. B*, 2005, **109**, 6103–6110.
- 19 S. E. Repper, A. Haynes, E. J. Ditzel and G. J. Sunley, *Dalton. Trans.*, 2017, **46**, 2821–2828.
- 20 W. R. Moser, J. E. Clossen, A. W. Wang and S. A. Krouse, *J. Catal.*, 1985, **95**, 21–32.
- 21 J. M. Birbeck, A. Haynes, H. Adams, L. Damoense and S. Otto, *ACS Catal.*, 2012, **2**, 2512–2523.
- 22 J. J. Rack, J. D. Webb and S. H. Strauss, *Inorg. Chem.*, 1996, **35**, 277–278.
- 23 J. J. Rack, O. G. Polyakov, C. M. Gaudinski, J. W. Hammel, P. Kasperbauer, H. D. Hochheimer and S. H. Strauss, *Appl. Spectrosc.*, 1998, **52**, 1035–1038.
- 24 R. V. Gholap and R. V. Chaudhari, *Can. J. Chem. Eng.*, 2009, **70**, 505–510.
- 25 J. A. Hogendoorn, W. P. M. van Swaaij and G. F. Versteeg, *Chem. Eng. J. Biochem. Eng. J.*, 1995, **59**, 243–252.
- 26 J. J. Rack, J. D. Webb and S. H. Strauss, *Inorg. Chem.*, 1996, **35**, 277–278.

## **4. Functionalised Imidazolium Ionic Liquids**

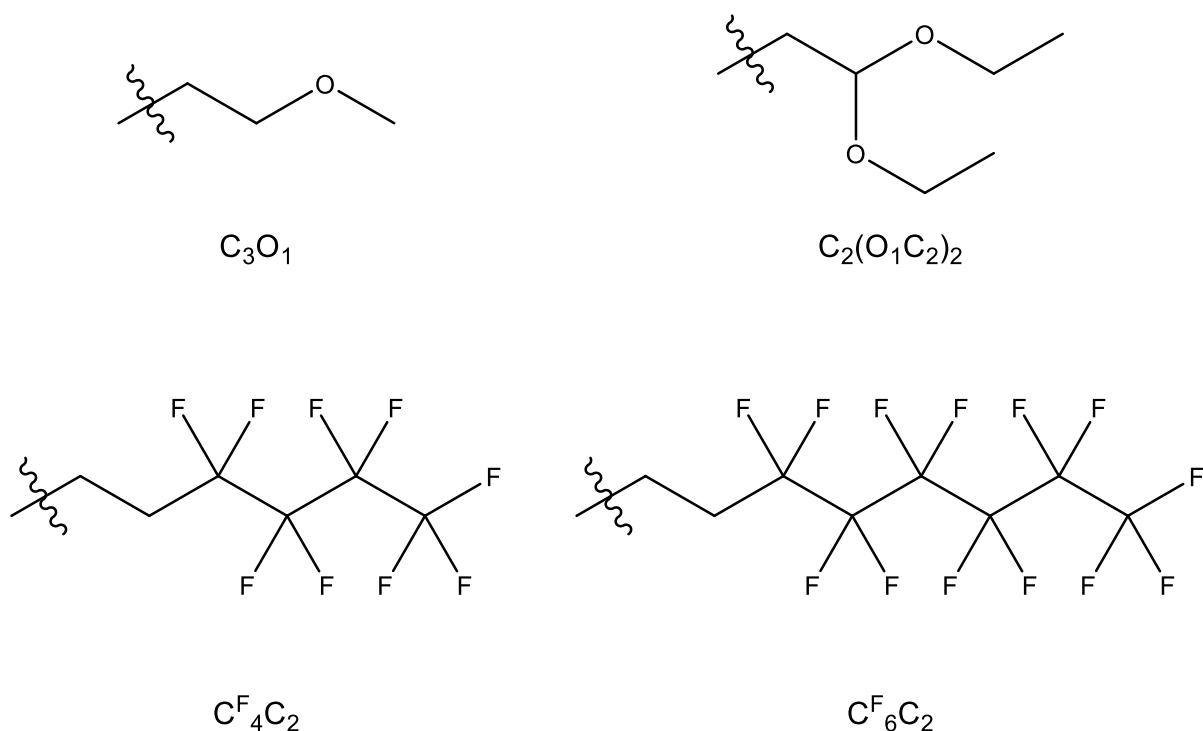
## 4.1 Introduction

It has been shown that introducing functionality to the imidazolium cation can influence the physical solubility of gases in ILs.<sup>1</sup> Literature on CO solubility in ILs is quite limited, relative to that for CO<sub>2</sub>.<sup>2-6</sup> Fortunately, there appears to be a relation between CO<sub>2</sub> and CO solubility, in that families of ILs that show high CO<sub>2</sub> solubility, also show high CO solubility. For example, ILs with highly fluorinated anions tend to exhibit increased solubility of CO as well as CO<sub>2</sub>.<sup>7</sup> Bara *et al.* showed that CO<sub>2</sub>/N<sub>2</sub> and CO<sub>2</sub>/CH<sub>4</sub> solubility selectivities increased by 30 – 75 % when an ether group was introduced onto the imidazolium cation.<sup>8</sup> A similar improvement in selectivity for CO might therefore be expected for related systems.

This chapter describes the synthesis of ILs with ether and fluorinated side chains, and their subsequent reaction with Cu(I) salts to produce copper-containing ILs. Physical properties and CO absorption behaviour were then compared to the non-functionalised systems.

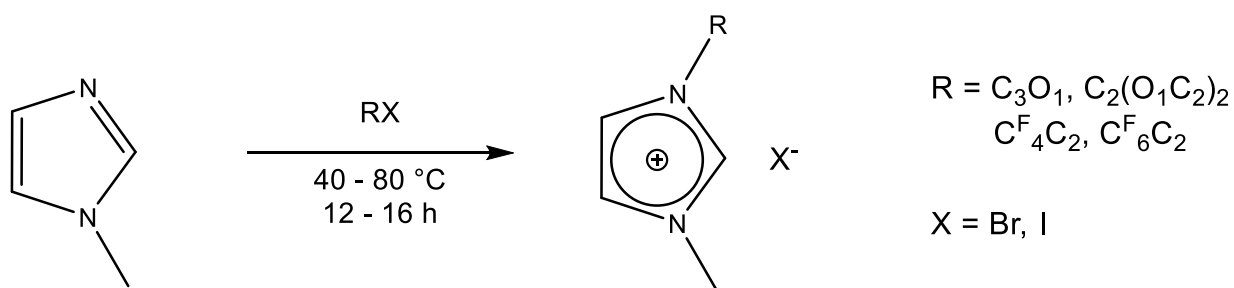
## 4.2 Synthesis and Characterisation of Functionalised Imidazolium Ionic Liquids

Figure 4.1 displays the types of ether and fluorinated side chains investigated in this section, along with their abbreviations. The variety of functionalisation was chosen to exploit their promising behaviour outlined in the literature i.e. better selectivity or improved CO solubility.



**Figure 4.1.** Ether and fluorinated side chains used for imidazolium cations.

Scheme 4.1 shows how the functionalised imidazolium halide salts were prepared by the reaction of 1-methyl imidazole with the necessary alkyl halide.

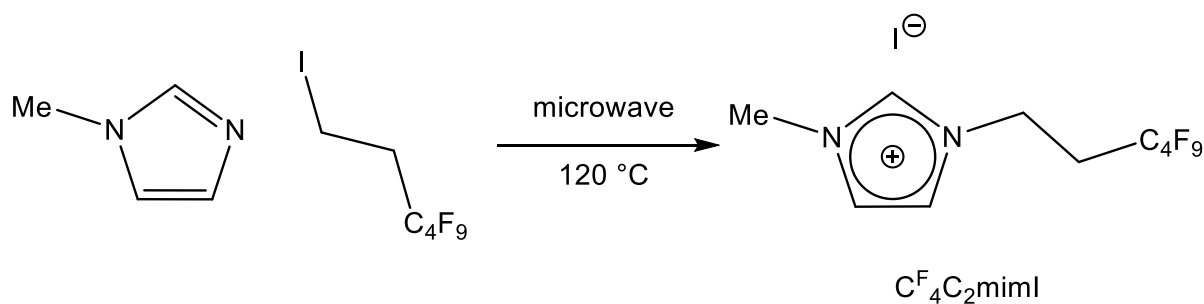


**Scheme 4.1.** General reaction scheme for the synthesis of imidazolium halide salts.

All the imidazolium salts made were hygroscopic crystalline solids or viscous liquids, necessitating the storage under dry N<sub>2</sub>. Yields for the bromide salts were close to quantitative, whereas the iodide salts gave significantly lower yields (20-30 %). Presumably the instability of the alkyl iodide and the

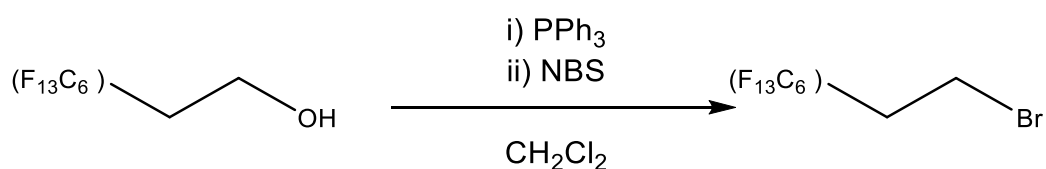
relatively harsh synthetic conditions resulted in some decomposition of the starting material. Moreover, to remove the iodine generated from the decomposition of the starting material, purification by flash column chromatography was necessary.

Scheme 4.2 shows a microwave synthesis approach taken in an attempt to improve the yield.<sup>9</sup> Microwave synthesis has been found to improve the yields of reaction, due to the ability to rapidly heat the reaction solution to high temperatures. This leads to cleaner reactions and higher yields in shorter time periods.<sup>10</sup> Two fundamental mechanisms of energy transfer from the microwave to heating of the substrate are dipole rotation and ionic conduction. ILs are ideal candidates for microwave synthesis, due to both mechanisms being active. This allows for energy transfer to occur quickly and efficiently, which limits the amount of decomposition of the starting material.

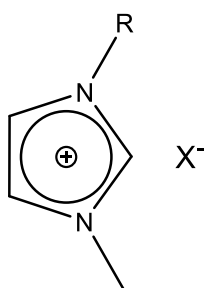


**Scheme 4.2.** Microwave synthesis of the highly fluorinated imidazolium iodide salts.

Scheme 4.3 shows how  $\text{C}_6\text{F}_{13}\text{C}_2\text{H}_4\text{Br}$  was synthesised from the alcohol via the Appel reaction in a yield of 53%.<sup>11,12</sup> Subsequent reaction of the bromide with methyl imidazole gave the imidazolium salt with an overall yield for the two steps of 35 %. Table 4.1 shows the physical states and yields of all the halide salts synthesised.



**Scheme 4.3.** Synthesis of C<sub>6</sub>F<sub>13</sub>C<sub>2</sub>H<sub>4</sub>Br via the Appel reaction.



**Table 4.1.** Yields and physical states for the overall synthesis of the functionalised imidazolium halides

R	X	Abbreviation	Yield / %	Physical State at 25 °C
n-C <sub>6</sub> H <sub>13</sub>	Br	[C <sub>6</sub> mim]Br	99	Liquid
C <sub>2</sub> H <sub>4</sub> OCH <sub>3</sub>	Br	[C <sub>3</sub> O <sub>1</sub> mim]Br	96	Solid
C <sub>2</sub> H <sub>3</sub> (OC <sub>2</sub> H <sub>5</sub> ) <sub>2</sub>	Br	[C <sub>2</sub> (O <sub>1</sub> C <sub>2</sub> ) <sub>2</sub> mim]Br	98	Solid
C <sub>2</sub> H <sub>4</sub> C <sub>4</sub> F <sub>9</sub>	I	[C <sup>F</sup> <sub>4</sub> C <sub>2</sub> mim]I	68	Solid
C <sub>2</sub> H <sub>4</sub> C <sub>6</sub> F <sub>13</sub>	Br	[C <sup>F</sup> <sub>6</sub> C <sub>2</sub> mim]Br	35	Solid
C <sub>2</sub> H <sub>4</sub> C <sub>6</sub> F <sub>13</sub>	I	[C <sup>F</sup> <sub>6</sub> C <sub>2</sub> mim]I	45	Solid

As for the alkyl imidazolium ILs, the halide anion could be exchanged for carboxylates, OTf<sup>-</sup> or NTf<sub>2</sub><sup>-</sup> using an anion exchange column, or by metathesis depending on the hydrophobicity of the anion, as discussed in chapter 3. Table 4.2 gives the yields of the products, which were isolated as viscous liquids.

**Table 4.2.** Percentage yields of a range of functionalised imidazolium ILs.

Cation	Anion	Yield / %
[C <sub>3</sub> O <sub>1</sub> mim] <sup>+</sup>	AcO <sup>-</sup>	71
[C <sub>3</sub> O <sub>1</sub> mim] <sup>+</sup>	CF <sub>3</sub> CO <sub>2</sub> <sup>-</sup>	76
[C <sub>3</sub> O <sub>1</sub> mim] <sup>+</sup>	OTf <sup>-</sup>	89
[C <sub>3</sub> O <sub>1</sub> mim] <sup>+</sup>	NTf <sub>2</sub> <sup>-</sup>	78
[C <sub>2</sub> (O <sub>1</sub> C <sub>2</sub> ) <sub>2</sub> mim] <sup>+</sup>	AcO <sup>-</sup>	88
[C <sub>2</sub> (O <sub>1</sub> C <sub>2</sub> ) <sub>2</sub> mim] <sup>+</sup>	CF <sub>3</sub> CO <sub>2</sub> <sup>-</sup>	82
[C <sub>2</sub> (O <sub>1</sub> C <sub>2</sub> ) <sub>2</sub> mim] <sup>+</sup>	OTf <sup>-</sup>	75
[C <sub>2</sub> (O <sub>1</sub> C <sub>2</sub> ) <sub>2</sub> mim] <sup>+</sup>	NTf <sub>2</sub> <sup>-</sup>	89
[C <sup>F</sup> <sub>4</sub> C <sub>2</sub> mim] <sup>+</sup>	OTf <sup>-</sup>	74
[C <sup>F</sup> <sub>4</sub> C <sub>2</sub> mim] <sup>+</sup>	NTf <sub>2</sub> <sup>-</sup>	76
[C <sup>F</sup> <sub>6</sub> C <sub>2</sub> mim] <sup>+</sup>	OTf <sup>-</sup>	80
[C <sup>F</sup> <sub>6</sub> C <sub>2</sub> mim] <sup>+</sup>	NTf <sub>2</sub> <sup>-</sup>	77

The ILs synthesised in this section were characterised by <sup>1</sup>H, <sup>13</sup>C and <sup>19</sup>F NMR spectroscopy, where appropriate, and mass spectrometry.

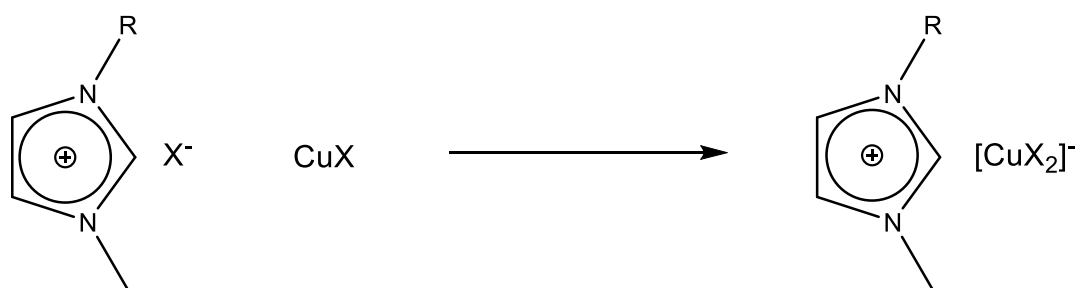
These salts were again stored under an inert atmosphere due to their hygroscopic nature. Their stability, even after months, was confirmed by <sup>1</sup>H, <sup>13</sup>C and <sup>19</sup>F NMR spectroscopy.

### 4.3 Copper-Containing Functionalised Imidazolium Ionic Liquids

As for the alkyl imidazolium salts, copper(I) was incorporated by reacting with the corresponding copper(I) salt in a 1:1 ratio, as shown in Scheme 4.4. In all cases, a homogeneous melt was formed

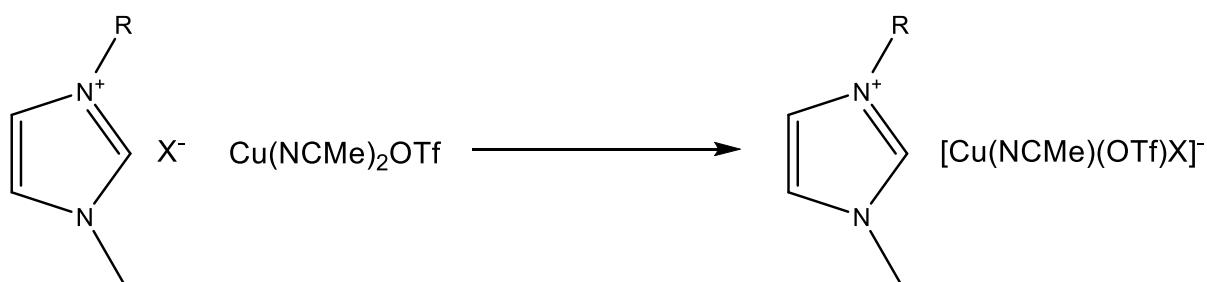
with the products remaining liquid at room temperature. The ether-functionalised copper-containing materials were qualitatively similar in viscosity to the alkyl imidazolium systems. However, the highly fluorinated cations were much more viscous and were deemed inappropriate to be taken forward to CO binding studies.

Although the carboxylate copper containing ILs were subjected to low pressure CO binding studies, they were found to be very air sensitive. Even when taking great caution setting up for high-pressure studies, the sample would quickly oxidise to a dark green/ blue colour.



**Scheme 4.4.** Synthesis of functionalised imidazolium copper containing ILs. Where R = [C<sub>3</sub>O<sub>1</sub>], [C<sub>2</sub>(O<sub>1</sub>C<sub>2</sub>)<sub>2</sub>], [C<sub>2</sub>F<sub>4</sub>C<sub>2</sub>], [C<sub>6</sub>F<sub>6</sub>C<sub>2</sub>] and X = Br, I, OAc, CF<sub>3</sub>CO<sub>2</sub>.

Scheme 4.5 shows the synthesis of the triflyl copper-containing ILs. In each case, a homogeneous mixture was formed at elevated temperatures, which in all but one case remained liquid on cooling to room-temperature. Only [C<sub>6</sub>F<sub>6</sub>C<sub>2</sub>mim][Cu(NCMe)(OTf)<sub>2</sub>] solidified, most likely due to the long fluorinated alkyl side chain. In both cases, the OTf and NTf<sub>2</sub> systems were qualitatively less viscous than the halide systems.



**Scheme 4.5.** Synthesis of functionalised imidazolium copper containing ILs. Where R = [C<sub>3</sub>O<sub>1</sub>], [C<sub>2</sub>(O<sub>1</sub>C<sub>2</sub>)<sub>2</sub>], [C<sup>F</sup><sub>4</sub>C<sub>2</sub>], [C<sup>F</sup><sub>6</sub>C<sub>2</sub>] and X = OTf and NTf<sub>2</sub>.

The copper-containing ILs synthesised in this section were analysed by <sup>1</sup>H, <sup>13</sup>C and <sup>19</sup>F NMR spectroscopy. However, unfortunately the carboxylate systems were too air sensitive to obtain adequate NMR spectra. <sup>1</sup>H NMR analysis of the triflyl systems showed the presence of a single MeCN, as observed for the products formed from reaction of [C<sub>n</sub>mim]X with Cu(NCMe)<sub>2</sub>OTf, discussed in chapter 3. Therefore, the species formed in this section are considered to also have a MeCN ligand coordinated to the copper.

Mass spectrometry showed that the cation was the desired imidazolium species and [Cu(X)<sub>2</sub>]<sup>-</sup> was detected by negative electrospray mass spectrometry for each respective anion. Therefore, the species formed is proposed to be analogous to that in chapter 3, [C<sub>n</sub>mim][Cu(NCMe)(OTf)(X)].

#### 4.4 Density Measurements

Table 4.3 shows the density of each IL measured at 20 °C and the copper-concentration calculated.

**Table 4.3.** Densities of functionalised imidazolium ILs at 293 K.

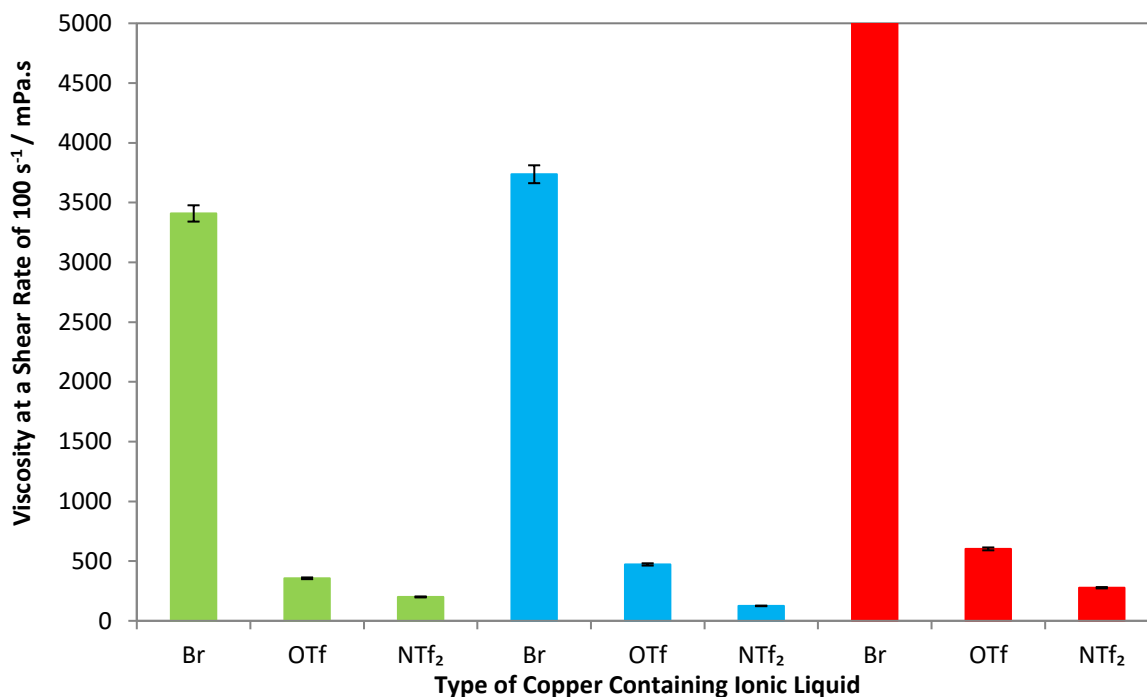
Copper-Containing Ionic Liquid	Density / g cm <sup>-3</sup>	[Cu] / M
[C <sub>6</sub> mim][CuBr <sub>2</sub> ]	1.65	4.2
[C <sub>3</sub> O <sub>1</sub> mim][CuBr <sub>2</sub> ]	1.90	5.2
[C <sub>2</sub> (O <sub>1</sub> C <sub>2</sub> ) <sub>2</sub> mim][CuBr <sub>2</sub> ]	1.70	4.0
[C <sub>6</sub> mim][Cu(NCMe)(OTf) <sub>2</sub> ]	1.40	2.5
[C <sub>3</sub> O <sub>1</sub> mim][Cu(NCMe)(OTf) <sub>2</sub> ]	1.54	2.8
[C <sub>2</sub> (O <sub>1</sub> C <sub>2</sub> ) <sub>2</sub> mim][Cu(NCMe)(OTf) <sub>2</sub> ]	1.46	2.4
[C <sub>6</sub> mim][Cu(NCMe)(OTf)(NTf <sub>2</sub> )]	1.50	2.1
[C <sub>3</sub> O <sub>1</sub> mim][Cu(NCMe)(OTf)(NTf <sub>2</sub> )]	1.61	2.4
[C <sub>2</sub> (O <sub>1</sub> C <sub>2</sub> ) <sub>2</sub> mim][Cu(NCMe)(OTf)(NTf <sub>2</sub> )]	1.54	2.1

Both of the ether-functionalised ILs exhibited higher densities than the alkyl imidazolium ILs. This was expected, as both modifications, adding ether functionality or branching, has been shown to increase density of ILs.<sup>13,14</sup> The [C<sub>2</sub>(O<sub>1</sub>C<sub>2</sub>)<sub>2</sub>mim] cation has a branched chain, which results in a small decrease in density compared with the linear C<sub>3</sub>O<sub>1</sub> chain.

#### 4.5 Viscosity Measurements

The viscosity of each copper-containing IL was measured in the same manner as described in chapter 3. Figure 4.2 shows the effect of changing the cation on viscosity. For a given anion, the alkyl and monoether functionalised cations showed similar viscosities, whereas the branched ether cation, [C<sub>2</sub>(O<sub>1</sub>C<sub>2</sub>)<sub>2</sub>mim]<sup>+</sup>, gave a higher viscosity. This effect has previously been reported in the literature, with higher viscosities of the branched ILs resulting from relatively more stable packing between cations

and anions, and therefore stronger intermolecular interactions.<sup>15</sup> The branched IL could have a less flexible chain which would therefore be harder to move in response to shear stress and therefore have a higher viscosity.



**Figure 4.2.** Viscosities of ether functionalised imidazolium ILs where green = [C<sub>6</sub>mim]; blue = [C<sub>3</sub>O<sub>1</sub>mim]; red = [C<sub>2</sub>(O<sub>1</sub>C<sub>2</sub>)<sub>2</sub>mim] cations.

Noticeably, the viscosity dependence on the anion is the same as described in the previous chapter regardless of the cation used, with viscosity decreasing in the order Br<sup>-</sup> >> OTf<sup>-</sup> > NTf<sub>2</sub><sup>-</sup>. This reinforces the idea that although the cation does have an effect on the viscosity, it is the anion which has the dominating effect.

## 4.6 Low-Pressure CO Reactions

Table 4.4 and Table 4.5 give the  $\nu(\text{CO})$  values for a range of functionalised imidazolium copper-containing ILs after a stream of CO, at atmospheric pressure, was passed through the sample for a few minutes. This was initially to test whether the sample was capable of binding CO. In all cases a single  $\nu(\text{CO})$  band was observed, consistent with the formation of a copper(I) monocarbonyl species. Simply passing a stream of  $\text{N}_2$  or applying reduced pressure was sufficient to reverse the reaction, after a couple of minutes.

Table 4.4 and Table 4.5 are arranged such that the effect of functionalising the cation, for each respective anion, on the  $\nu(\text{CO})$  can be seen.

**Table 4.4.** IR spectroscopic data for Cu(CO) species formed on reaction of  $[\text{C}_n\text{mim}][\text{CuX}_2]$  with 1 atmosphere of CO.

[Cation]X	Copper Source	$\nu(\text{CO}) / \text{cm}^{-1}$
$[\text{C}_6\text{mim}]\text{Br}$	CuBr	2081
$[\text{C}_3\text{O}_1\text{mim}]\text{Br}$	CuBr	2080
$[\text{C}_2(\text{O}_1\text{C}_2)_2\text{mim}]\text{Br}$	CuBr	2086
$[\text{C}_6\text{mim}]\text{OAc}$	CuOAc	2086
$[\text{C}_3\text{O}_1\text{mim}]\text{OAc}$	CuOAc	2081
$[\text{C}_2(\text{O}_1\text{C}_2)_2\text{mim}]\text{OAc}$	CuOAc	2088
$[\text{C}_6\text{mim}]\text{CF}_3\text{CO}_2$	$\text{Cu}(\text{CF}_3\text{CO}_2)$	2099
$[\text{C}_3\text{O}_1\text{mim}]\text{CF}_3\text{CO}_2$	$\text{Cu}(\text{CF}_3\text{CO}_2)$	2084
$[\text{C}_2(\text{O}_1\text{C}_2)_2\text{mim}]\text{CF}_3\text{CO}_2$	$\text{Cu}(\text{CF}_3\text{CO}_2)$	2105

Table 4.4 shows that the complexes with halide and carboxylate anions, in the form  $[\text{C}_n\text{mim}][\text{CuX}_2]$ , show a moderate dependence of  $\nu(\text{CO})$  on the cation R group. Particularly when using the branched

ether side chain,  $[\text{C}_2(\text{O}_1\text{C}_2)_2\text{mim}]$ , it is notable that the  $\nu(\text{CO})$  is shifted to a higher wavenumber suggesting there is a change to the local environment of the copper complex. However, a full explanation for this observation is not presently understood.

**Table 4.5.** IR spectroscopic data for  $\text{Cu}(\text{CO})$  species formed on reaction of  $\text{CO}$   $[\text{C}_n\text{mim}][\text{Cu}(\text{NCMe})_2\text{X}_2]$ .

[Cation]X	Copper Source	1 atm CO $\nu(\text{CO})$ / $\text{cm}^{-1}$
$[\text{C}_6\text{mim}]\text{OTf}$	$\text{Cu}(\text{NCMe})_2\text{OTf}$	2114
$[\text{C}_3\text{O}_1\text{mim}]\text{OTf}$	$\text{Cu}(\text{NCMe})_2\text{OTf}$	2114
$[\text{C}_2(\text{O}_1\text{C}_2)_2\text{mim}]\text{OTf}$	$\text{Cu}(\text{NCMe})_2\text{OTf}$	2116
$[\text{C}^{\text{F}}_4\text{C}_2\text{mim}]\text{OTf}$	$\text{Cu}(\text{NCMe})_2\text{OTf}$	2117
$[\text{C}_6\text{mim}]\text{NTf}_2$	$\text{Cu}(\text{NCMe})_2\text{OTf}$	2122
$[\text{C}_3\text{O}_1\text{mim}]\text{NTf}_2$	$\text{Cu}(\text{NCMe})_2\text{OTf}$	2121
$[\text{C}_2(\text{O}_1\text{C}_2)_2\text{mim}]\text{NTf}_2$	$\text{Cu}(\text{NCMe})_2\text{OTf}$	2120
$[\text{C}^{\text{F}}_4\text{C}_2\text{mim}]\text{NTf}_2$	$\text{Cu}(\text{NCMe})_2\text{OTf}$	2123
$[\text{C}^{\text{F}}_6\text{C}_2\text{mim}]\text{NTf}_2$	$\text{Cu}(\text{NCMe})_2\text{OTf}$	2120

Table 4.5 shows the effect of changing the alkyl side chain is less dramatic for the triflyl copper-containing ILs. The variation of  $\nu(\text{CO})$  for each respective anion is about  $2\text{-}3\text{ cm}^{-1}$ , suggesting that the same copper carbonyl species is forming in each case and cation-anion interactions have little effect.

#### 4.7 In Situ High-Pressure Infrared Studies

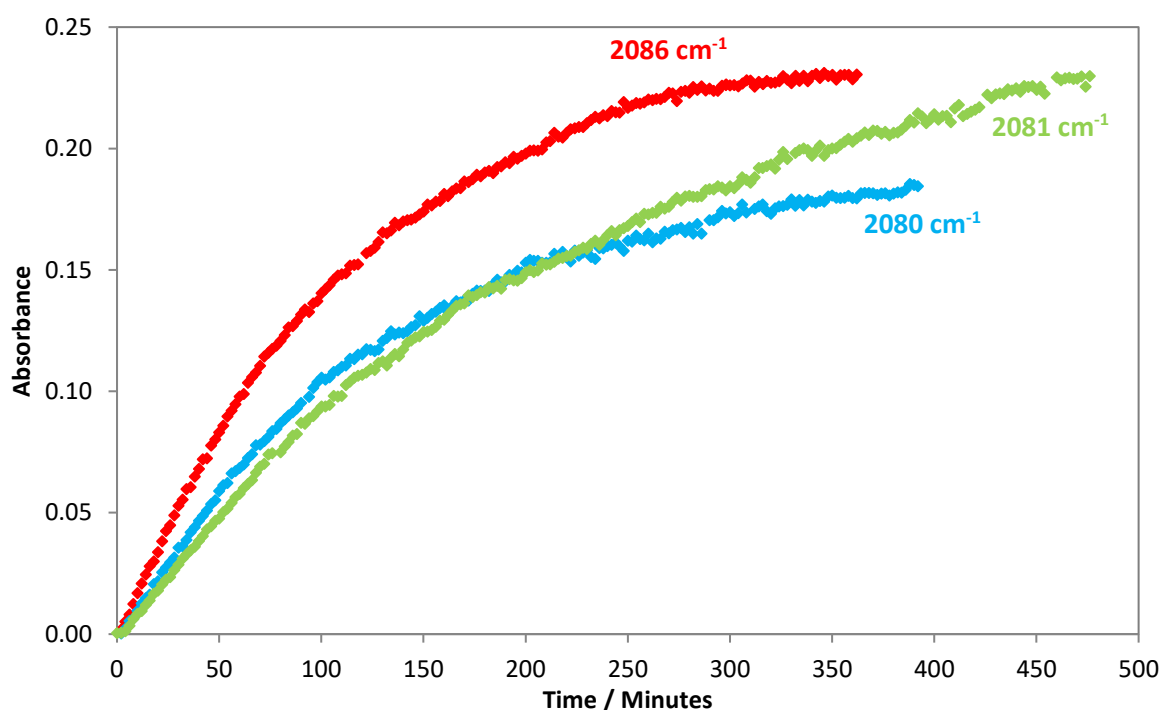
Absorption of  $\text{CO}$  by the copper(I)-containing ILs at elevated pressure was monitored by in situ high pressure infra-red (HPIR) spectroscopy using a cylindrical internal reflectance (CIR) cell,<sup>16,17</sup> allowing

the effects of CO pressure, temperature, and the rate of gas/liquid mixing to be probed as described in chapter 3.

#### 4.7.1 $[C_n\text{mim}][\text{CuBr}_2]$

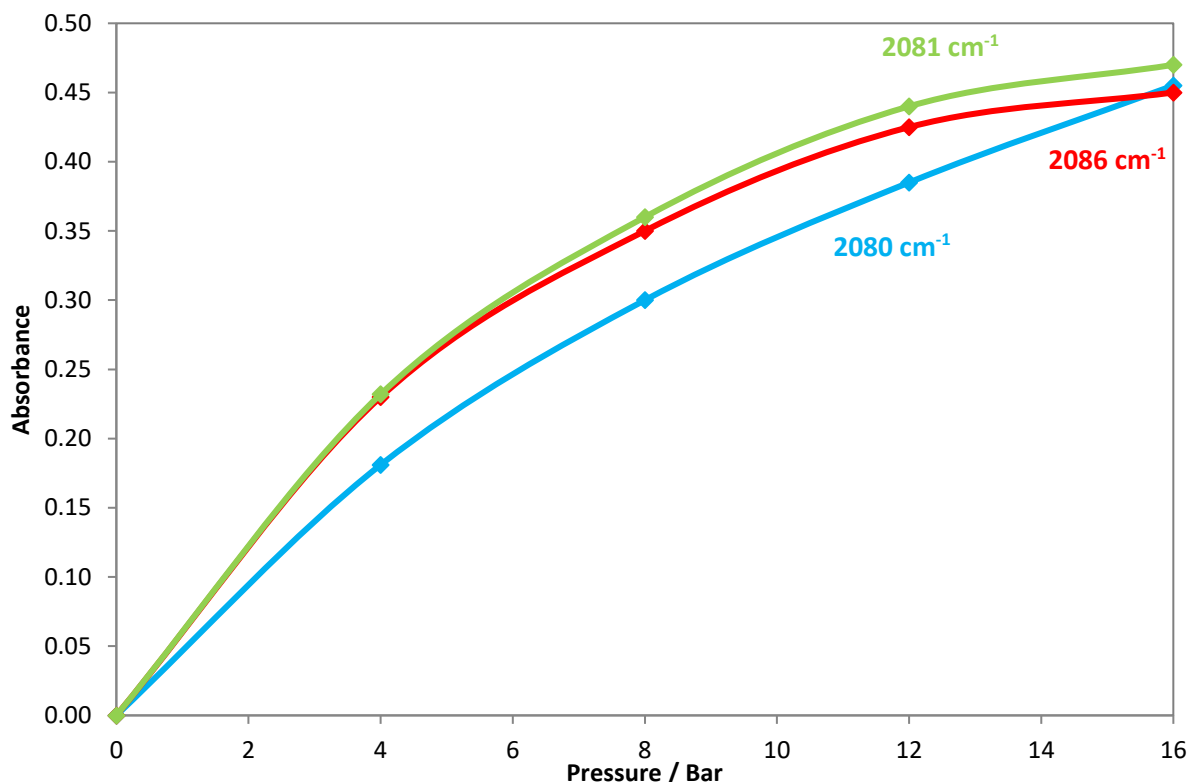
CO absorption experiments for the  $[C_n\text{mim}][\text{CuBr}_2]$  type ILs were performed in the same manner as discussed in chapter 3 under identical conditions. The three liquids tested,  $[C_6\text{mim}][\text{CuBr}_2]$ ,  $[C_3\text{O}_1\text{mim}][\text{CuBr}_2]$  and  $[C_2(\text{O}_1\text{C}_2)_2\text{mim}][\text{CuBr}_2]$  were found to take up CO reversibly and over a period of many cycles without loss of performance. Inspection of samples after a series of runs showed no evidence of discolouration or solid deposits, which was encouraging.

Figure 4.3 shows plots of the growth of the  $\nu(\text{CO})$  absorption when each sample was subjected to 4 bar CO pressure, in order to determine how adding an ether functional group affects the rate of CO uptake.



**Figure 4.3.** Absorbance vs time plot showing the growth of the  $\nu(\text{CO})$  band at a given wavenumber when  $[C_6\text{mim}][\text{CuBr}_2]$  = green;  $[C_3\text{O}_1\text{mim}][\text{CuBr}_2]$  = blue;  $[C_2(\text{O}_1\text{C}_2)_2\text{mim}][\text{CuBr}_2]$  = red was exposed to 4 bar CO pressure at 298 K and a stir rate of 214 rpm.

The plots in Figure 4.3 suggest that  $[\text{C}_2(\text{O}_1\text{C}_2)_2\text{mim}][\text{CuBr}_2]$  has the quickest rate of CO uptake with the  $[\text{C}_6\text{mim}]^+$  and  $[\text{C}_3\text{O}_1\text{mim}]^+$  cations showing similar rates. This does assume that the extinction coefficients for the respective  $\nu(\text{CO})$  bands do not differ significantly. The  $[\text{C}_3\text{O}_1\text{mim}]^+$  cation reached a slightly lower equilibrium position relative to the other two, suggesting the ether functionality may hinder the physical solubility of CO into these copper containing ILs.



**Figure 4.4.** Plot of equilibrium  $\nu(\text{CO})$  intensity against pressure of CO for  $[\text{C}_6\text{mim}][\text{CuBr}_2]$  = green;  $[\text{C}_3\text{O}_1\text{mim}][\text{CuBr}_2]$  = blue;  $[\text{C}_2(\text{O}_1\text{C}_2)_2\text{mim}][\text{CuBr}_2]$  = red

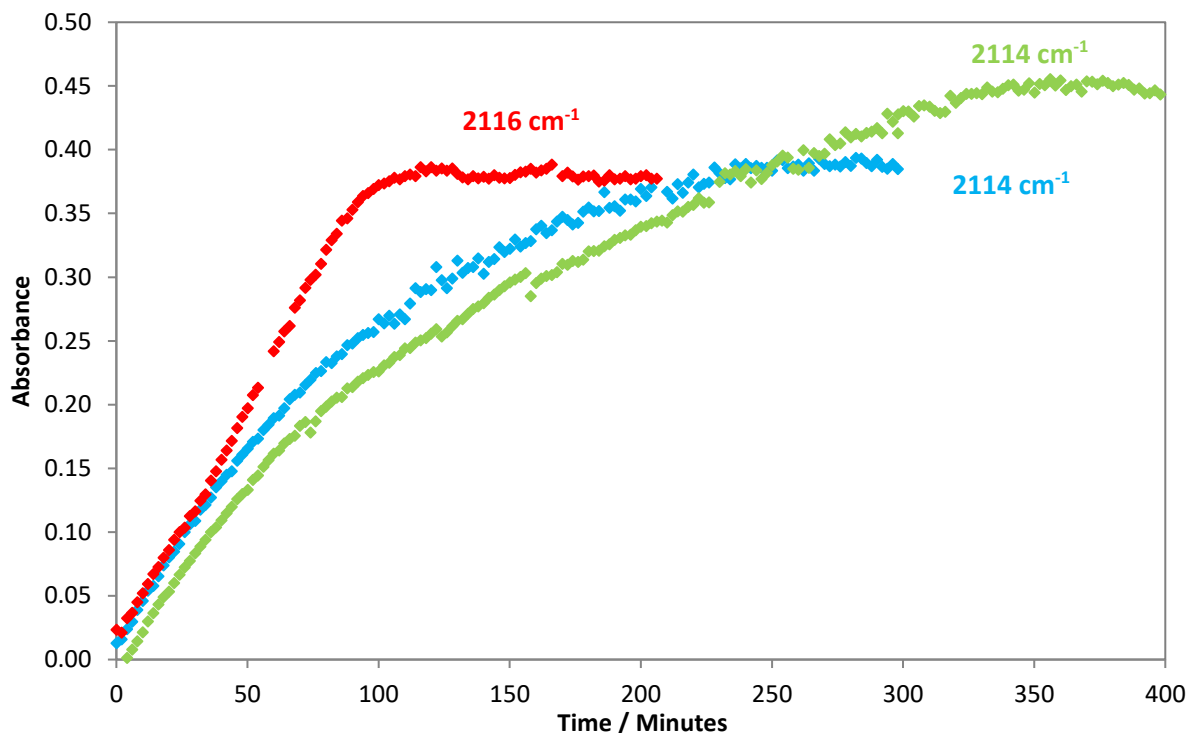
Figure 4.4 shows the equilibrium  $\nu(\text{CO})$  absorbances, at a given pressure for each respective cation. At a given pressure, the  $[\text{C}_3\text{O}_1\text{mim}]$  system gives a slightly lower equilibrium absorbance compared to the other two cations, which are approximately the same. The  $[\text{C}_2(\text{O}_1\text{C}_2)_2\text{mim}]^+$  cation starts to reach saturation first at an absorbance around 0.45 with the  $[\text{C}_6\text{mim}]^+$  cation slightly higher. The  $\nu(\text{CO})$  for the  $[\text{C}_3\text{O}_1\text{mim}]^+$  cation appears to be continuing to increase and will reach the highest saturation point.

This would be consistent with the copper concentration calculated for each system, where the trend was  $[\text{C}_2(\text{O}_1\text{C}_2)_2\text{mim}]^+ < [\text{C}_6\text{mim}]^+ < [\text{C}_3\text{O}_1\text{mim}]^+$ . However, overall the shape of the curves and height of the equilibria at 16 bar were similar in each case, further suggesting any effect caused from changing the cation is small.

#### 4.7.2 $[\text{C}_n\text{mim}][\text{Cu}(\text{NCMe})(\text{OTf})_2]$

Figure 4.5 shows plots of the growth of  $\nu(\text{CO})$  bands for the  $[\text{C}_n\text{mim}][\text{Cu}(\text{NCMe})(\text{OTf})_2]$  ILs under 12 bar CO pressure. Again the system with the  $[\text{C}_2(\text{O}_1\text{C}_2)_2\text{mim}]^+$  cation showed the fastest rate of CO uptake, reaching an equilibrium position first. The rates of uptake for the  $[\text{C}_6\text{mim}]^+$  and  $[\text{C}_3\text{O}_1\text{mim}]^+$  cations are again similar, with the latter reaching a lower equilibrium position.

The shape of the curve for  $[\text{C}_2(\text{O}_1\text{C}_2)_2\text{mim}][\text{Cu}(\text{NCMe})(\text{OTf})_2]$  is slightly different than for the other systems. The growth of the  $\nu(\text{CO})$  band is more linear and reaches equilibrium earlier. Experiments were repeated on the same sample, and with a second sample of this type, to test the reproducibility of this curve and in each case a similar trace was observed. The reasons for this behaviour are not presently understood.

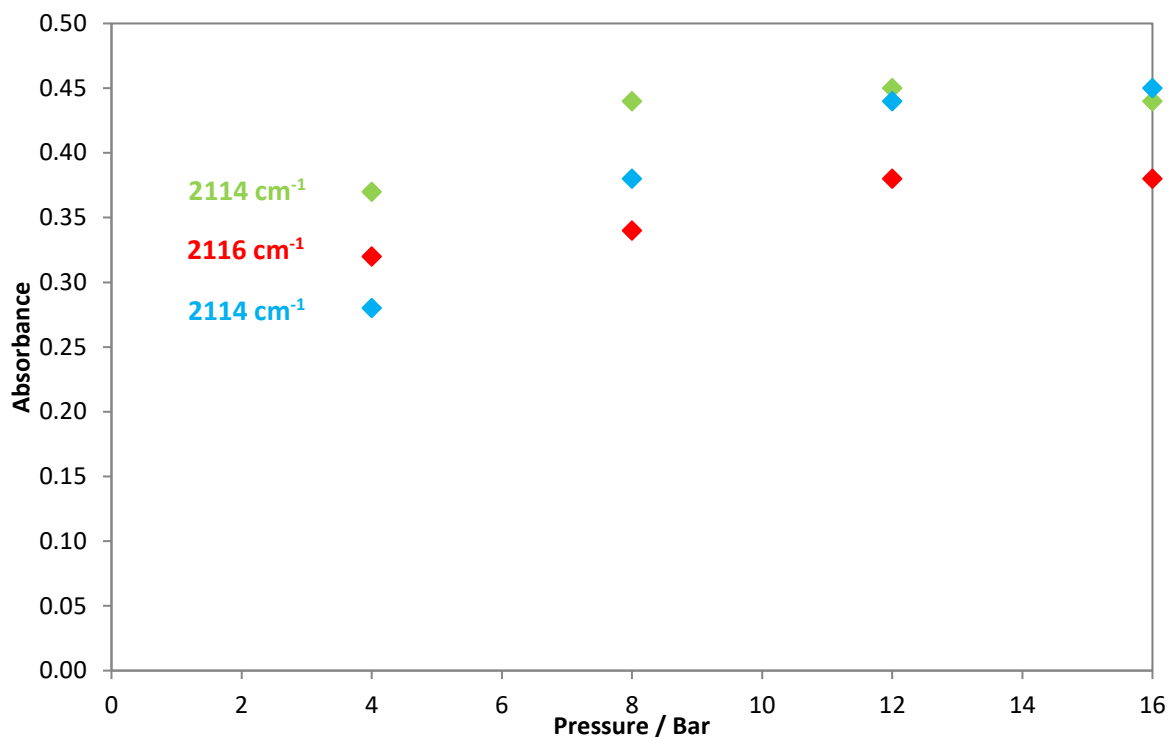


**Figure 4.5.** Absorbance vs time plot showing the growth of the  $\nu(\text{CO})$  monocarbonyl band at a given wavenumber where green =  $[\text{C}_6\text{mim}][\text{Cu}(\text{NCMe})(\text{OTf})_2]$ ; blue =  $[\text{C}_3\text{O}_1\text{mim}][\text{Cu}(\text{NCMe})(\text{OTf})_2]$ ; red =  $[\text{C}_2(\text{O}_1\text{C}_2)_2\text{mim}][\text{Cu}(\text{NCMe})(\text{OTf})_2]$  was exposed to 12 bar CO pressure at 298 K and a stir rate of 214 rpm.

Figure 4.6 shows the equilibrium absorbances of  $\nu(\text{CO})$  intensity at a given pressure for each cation. The differences in the position of the equilibria at a given pressure are small suggesting they are absorbing similar amounts of CO. Without knowledge of the extinction coefficients it is difficult to say with certainty if any absorbed more CO than another.

It was found that the functionalisation did not hinder dicarbonyl formation and all systems investigated exhibited dicarbonyl formation. Dicarbonyl formation became apparent at about 12 bar CO pressure where small peaks at  $2168\text{ cm}^{-1}$  and  $2136\text{ cm}^{-1}$  were observed. These peaks were in the same position as recorded for  $[\text{C}_6\text{mim}][\text{Cu}(\text{NCMe})(\text{OTf})_2]$ . The amount of dicarbonyl formed also seemed to be comparable regardless of the cation species used as the absorbance at  $2168\text{ cm}^{-1}$  was

small, about 0.01 – 0.02. None of the systems investigated exhibited stronger dicarbonyl formation as observed for the mixed OTf/NTf<sub>2</sub> anion systems.

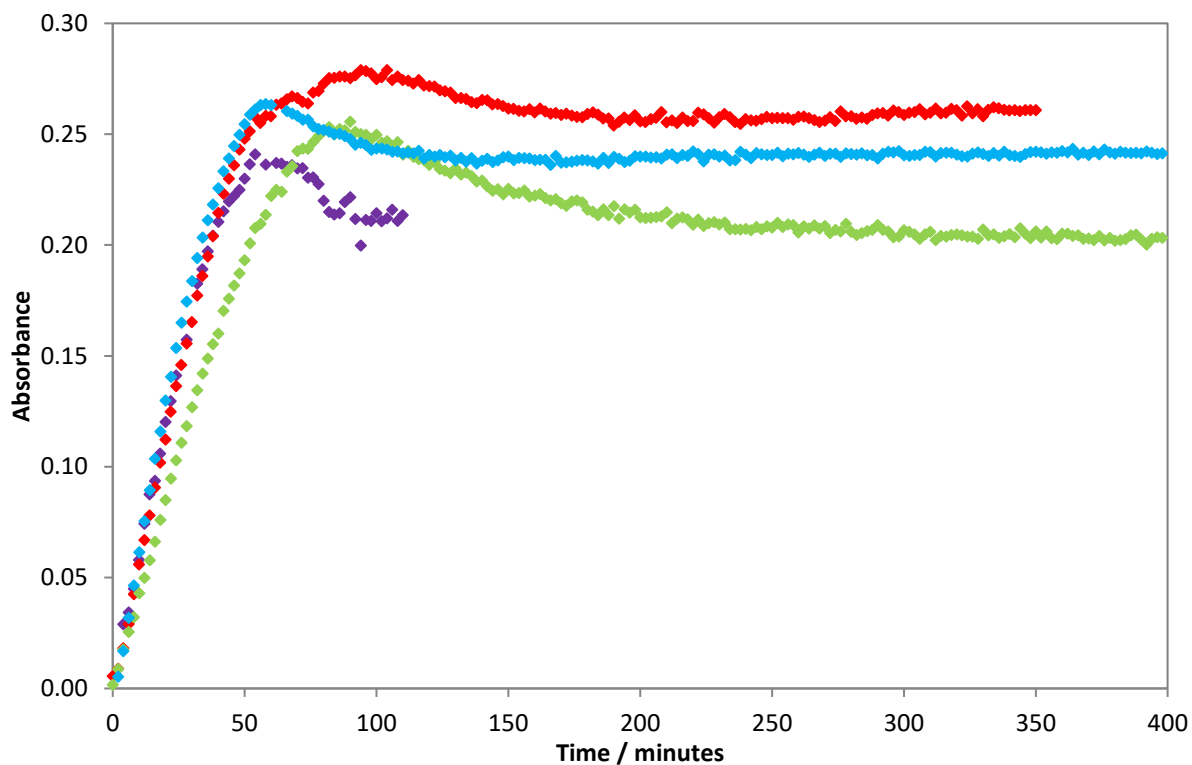


**Figure 4.6.** Plot of equilibrium  $\nu(\text{CO})$  intensity against pressure of CO for [C<sub>6</sub>mim][Cu(NCMe)(OTf)<sub>2</sub>] = green;

[C<sub>3</sub>O<sub>1</sub>mim][Cu(NCMe)(OTf)<sub>2</sub>] = blue; [C<sub>2</sub>(O<sub>1</sub>C<sub>2</sub>)<sub>2</sub>mim][Cu(NCMe)(OTf)<sub>2</sub>] = red

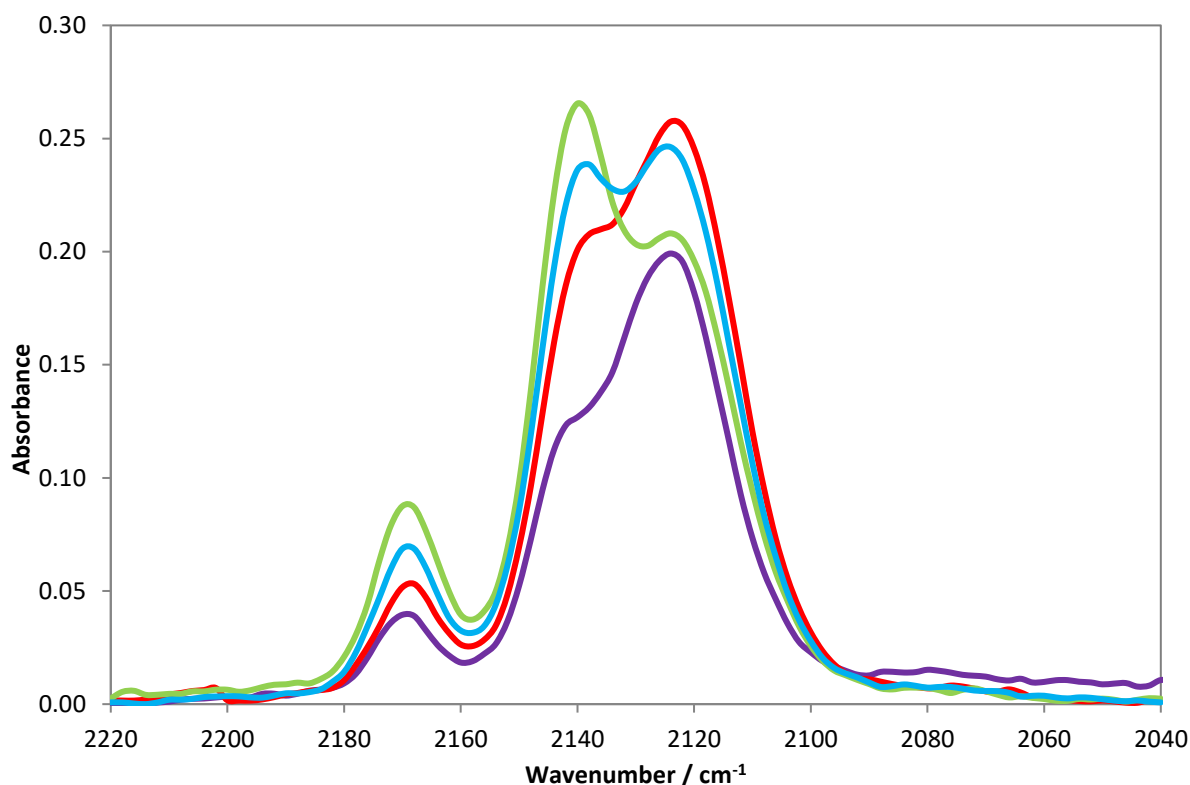
#### 4.7.3 [C<sub>n</sub>mim][Cu(NCMe)(OTf)(NTf<sub>2</sub>)]

Figure 4.7 shows plots of the growth of  $\nu(\text{CO})$  bands for the [C<sub>n</sub>mim][Cu(NCMe)(OTf)(NTf<sub>2</sub>)]<sup>-</sup> systems under 12 bar CO pressure. It was found that the initial rate was quite similar when varying the cation, with only the [C<sub>6</sub>mim]<sup>+</sup> cation showing a slightly lower rate. It was hoped that the highly fluorinated cation, [C<sup>F</sup><sub>6</sub>C<sub>2</sub>mim]<sup>+</sup> would increase the physical solubility of the CO into the IL. However, it gave a very similar rate and equilibrium absorbance to the other cations.



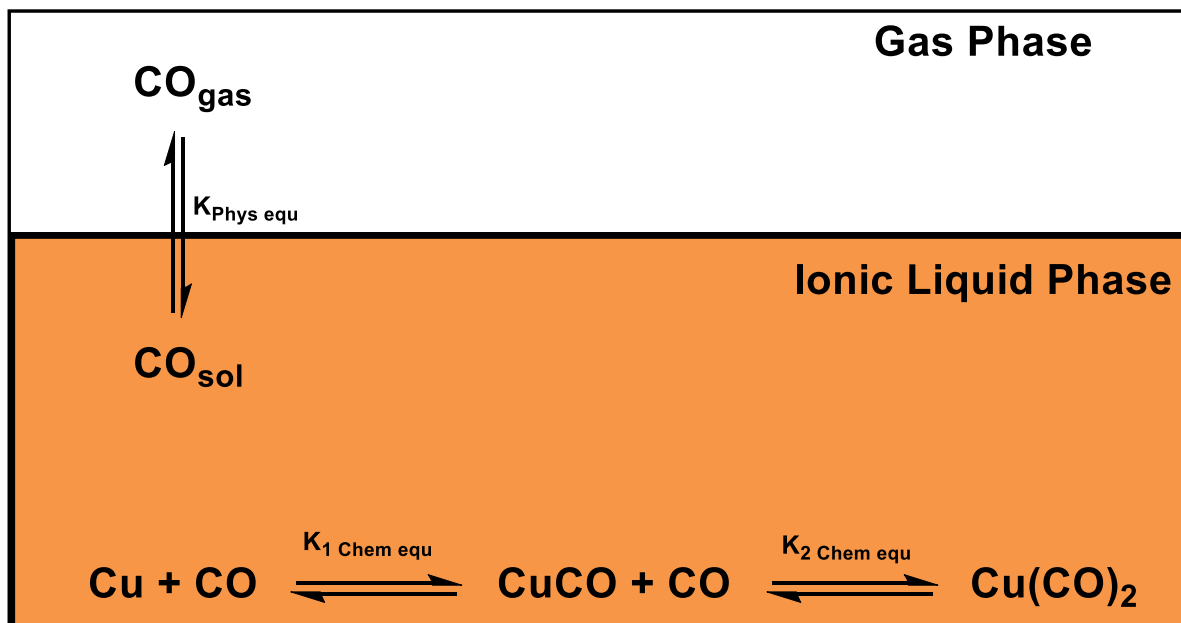
**Figure 4.7.** Plot of absorbance vs time showing the growth of the  $\nu(\text{CO})$  band at a given wavenumber where green =  $[\text{C}_6\text{mim}][\text{Cu}(\text{NCMe})(\text{OTf})(\text{NTf}_2)]$ ; blue =  $[\text{C}_3\text{O}_1\text{mim}][\text{Cu}(\text{NCMe})(\text{OTf})(\text{NTf}_2)]$ ; red =  $[\text{C}_2(\text{O}_1\text{C}_2)_2\text{mim}][\text{Cu}(\text{NCMe})(\text{OTf})(\text{NTf}_2)]$ ; purple =  $[\text{C}^{\text{F}}_6\text{C}_2\text{mim}][\text{Cu}(\text{NCMe})(\text{OTf})(\text{NTf}_2)]$  was exposed to 12 bar CO pressure at 298 K and a stir rate of 214 rpm.

As for the parent  $[\text{C}_6\text{mim}][\text{Cu}(\text{NCMe})(\text{OTf})(\text{NTf}_2)]$  system, all these liquids showed evidence for formation of a dicarbonyl complex. Figure 4.8 shows IR spectra recorded at 12 bar CO pressure for the four liquids. The intensity of the two higher frequency IR bands shows that dicarbonyl formation could be influenced by the choice of cation. The dependence for dicarbonyl formation on the cation proceeds in the order  $[\text{C}_6\text{mim}]^+ > [\text{C}_3\text{O}_1\text{mim}]^+ > [\text{C}_2(\text{O}_1\text{C}_2)_2\text{mim}]^+ > [\text{C}^{\text{F}}_6\text{C}_2\text{mim}]^+$ .



**Figure 4.8.** Profiles showing the extent of dicarbonyl formation at 12 bar CO equilibrium pressure where green =  $[\text{C}_6\text{mim}][\text{Cu}(\text{NCMe})(\text{OTf})(\text{NTf}_2)]$ ; blue =  $[\text{C}_3\text{O}_1\text{mim}][\text{Cu}(\text{NCMe})(\text{OTf})(\text{NTf}_2)]$ ; red =  $[\text{C}_2(\text{O}_1\text{C}_2)_2\text{mim}][\text{Cu}(\text{NCMe})(\text{OTf})(\text{NTf}_2)]$ ; purple =  $[\text{C}^{\text{F}}_6\text{C}_2\text{mim}][\text{Cu}(\text{NCMe})(\text{OTf})(\text{NTf}_2)]$ .

Figure 4.9 shows several equilibria which describes the transport of CO into solution ( $K_{\text{Phys equ}}$ ) and binding of the CO to the copper(I) species ( $K_{1 \text{ Chem equ}}$  and  $K_{2 \text{ Chem equ}}$ ). Functionalisation of the cation should not have a large effect on the CO binding equilibria and much more likely to effect the physical solubility of the CO into the IL (i.e. Henry's law constant). A greater physical solubility of CO will increase the concentration of CO in the liquid phase. Consequently, this will drive the equilibria for CO complexation to the right, thus forming more dicarbonyl.



**Figure 4.9.** Physical CO solubility equilibrium and CO binding equilibria to show the pathway to  $\text{Cu}(\text{CO})_2$  in solution

The IL gas/liquid interface could also be the cause of the slightly higher rate of CO uptake from the  $[\text{C}_2(\text{O}_1\text{C}_2)\text{mim}]^+$  cation relative to the  $[\text{C}_6\text{mim}]^+$  and  $[\text{C}_3\text{O}_1\text{mim}]$ . The surface interface of an IL can differ from the bulk IL.<sup>18</sup> The bulky branched nature of the  $[\text{C}_2(\text{O}_1\text{C}_2)\text{mim}]^+$  cation could cause the side chain to stick out from the IL which could encourage more CO molecules to become absorbed into the IL. Following the argument described in Figure 4.9, more CO absorbed by the IL would reach the copper sites more quickly, hence the slightly quicker rate of copper carbonyl formation.

## 4.8 Conclusions

In an attempt to influence the physical solubility of CO, copper containing imidazolium ILs with ether and highly fluorinated side chains were synthesised. Although there were some differences in properties such as CO uptake and viscosity when compared to the  $[\text{C}_6\text{mim}]^+$  cation, on the whole their behaviour was quite similar to the non-functionalised analogue. This reinforces the view that it is the anion which has the dominating effect on gas solubility in ILs.

Formation of copper(I) dicarbonyl complexes was again observed with the OTf and NTf<sub>2</sub> systems. Interestingly, there appears to be a cation effect on the formation of the dicarbonyl which can be exploited through careful choice of cation.

## 4.9 References

- 1 M. Hasib-ur-Rahman, M. Sijaj and F. Larachi, *Chem. Eng. Process. Process Intensif.*, 2010, **49**, 313–322.
- 2 Z.-Z. Yang, Y.-N. Zhao and L.-N. He, *RSC Adv.*, 2011, **1**, 545.
- 3 Y. Xu, J. Zhao, W. Wu and B. Jin, *Int. J. Greenh. Gas Control*, 2015, **42**, 454–460.
- 4 L. Zhou, X. Shang, J. Fan and J. Wang, *J. Chem. Thermodyn.*, 2016, **103**, 292–298.
- 5 F. Llovel, M. B. Oliveira, J. A. P. Coutinho and L. F. Vega, *Catal. Today*, 2015, **255**, 87–96.
- 6 L. R. Field, E. Wilhelm and R. Battino, *J. Chem. Thermodyn.*, 1974, **6**, 237–243.
- 7 S. Raeissi, L. J. Florusse and C. J. Peters, *AIChE J*, 2013, **59**, 3886–3891.
- 8 J. E. Bara, C. J. Gabriel, S. Lessmann, T. K. Carlisle, A. Finotello, D. L. Gin and R. D. Noble, *Ind. Eng. Chem. Res.*, 2007, **46**, 5380–5386.
- 9 J. M. Breen, S. Olejarz and K. R. Seddon, *ACS Sustain. Chem. Eng.*, 2016, **4**, 387–391.
- 10 C. R. Strauss and D. W. Rooney, *Green Chem.*, 2010, **12**, 1340.
- 11 K. Das, B., Damodar, *Tetrahedron Lett.*, 2009, **50**, 2072.
- 12 R. Appel, *Angew. Chem. Int. Ed. Engl.*, 1975, **14**, 801.
- 13 L. Xue, E. Gurung, G. Tamas, Y. P. Koh, M. Shadeck, S. L. Simon, M. Maroncelli and E. L. Quitevis, *J. Chem. Eng. Data*, 2016, **61**, 1078–1091.
- 14 Z.-B. Zhou, H. Matsumoto and K. Tatsumi, *Chem. - A Eur. J.*, 2004, **10**, 6581–6591.
- 15 L. Xue, E. Gurung, G. Tamas, Y. P. Koh, M. Shadeck, S. L. Simon, M. Maroncelli and E. L. Quitevis, *J. Chem. Eng. Data*, 2016, **61**, 1078–1091.

- 16 W. R. Moser, J. E. Clossen, A. W. Wang and S. A. Krouse, *J. Catal.*, 1985, **95**, 21–32.
- 17 J. M. Birbeck, A. Haynes, H. Adams, L. Damoense and S. Otto, *ACS Catal.*, 2012, **2**, 2512–2523.
- 18 D. W. Bruce, C. P. Cabry, N. Canongia Lopes, M. L. Costen, I. Grillo, B. C. Marshall, K. G. McKendrick, T. K. Minton, S. M. Purcell, S. Rogers, J. M. Slattery, K. Shimizu, E. Smoll and M. A. Tesa-Serrate,

## **5. Separation of CO from N<sub>2</sub> and H<sub>2</sub> Using Copper(I) Containing Ionic Liquids**

## 5.1 Introduction

As demonstrated in the previous chapters and in the literature, the potential for copper-containing ILs to reversibly bind CO makes them attractive candidates for use in separation of CO-containing gas mixtures.

In a previous PhD project at Sheffield, Repper *et al.* demonstrated that 1-alkyl-3-methylimidazolium dihalocuprate(I) ILs can selectively purify CO from a 50:50 mixture with either H<sub>2</sub> or N<sub>2</sub> to a CO purity of 89 % and 95 % respectively after one absorption/desorption cycle.<sup>1</sup>

This chapter discusses the potential of copper-containing ILs with weakly coordinating anions to separate CO from H<sub>2</sub> and N<sub>2</sub>, for comparison with the free halide systems.

## 5.2 Analysis of composition of gas mixtures

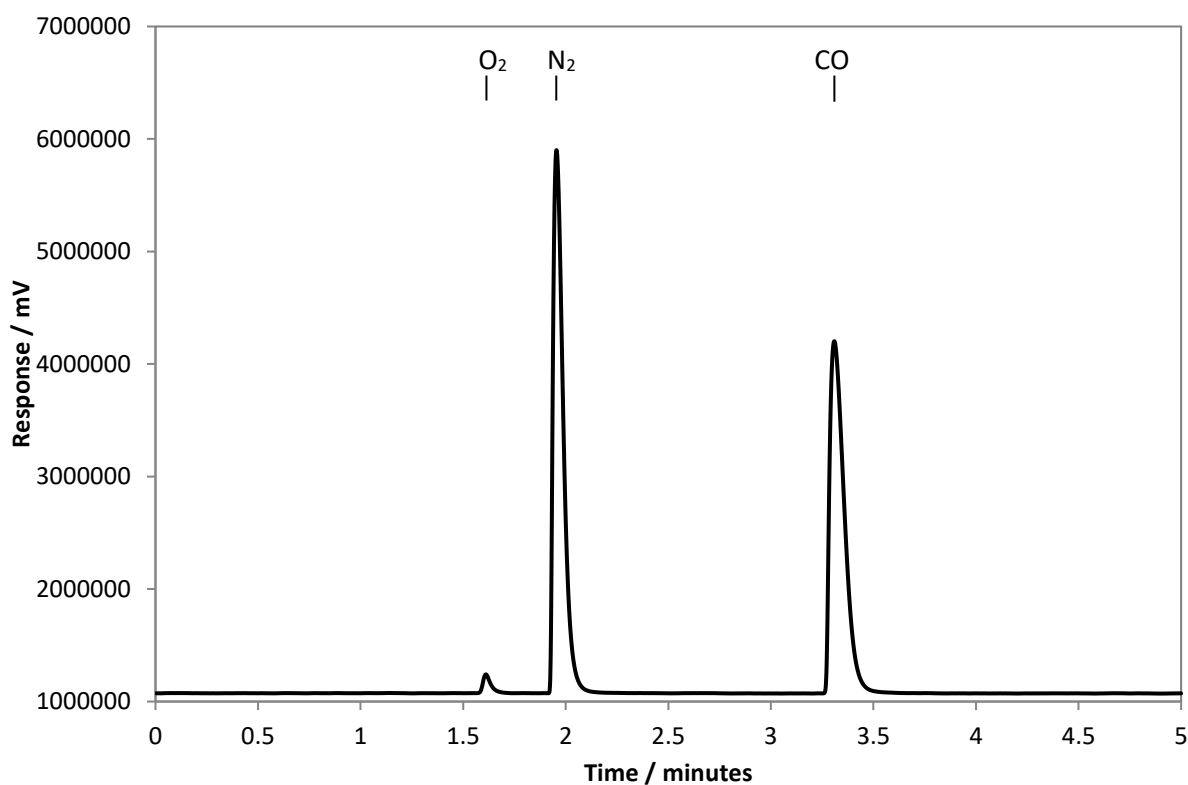
In previous CO/X<sub>2</sub> separation studies performed by Repper, gas mixtures were analysed using a gas phase IR cell.<sup>1</sup> Samples of gas were collected into a pre-evacuated IR cell and the amount of CO was quantified via its IR absorption, based on a calibration plot for gas mixtures of known CO content. The N<sub>2</sub> or H<sub>2</sub> components could not be measured directly using this method since they are not IR active.

In the experiments described in this chapter, gas mixtures were analysed by gas chromatography (GC) so that N<sub>2</sub> and H<sub>2</sub> content could be quantified, as well as CO. In order to determine whether the gas mixture composition could be quantified with reasonable accuracy by GC, known ratios of CO:N<sub>2</sub> and CO:H<sub>2</sub> from commercially supplied cylinders were used as references to build calibration plots.

For CO/N<sub>2</sub> separations, a hydrogen carrier gas was used and the peaks for CO and N<sub>2</sub> were integrated to determine the amount present. For CO/H<sub>2</sub> separations, both nitrogen and helium were tested as

carrier gases. However, conflicts in thermal conductivities between CO and N<sub>2</sub> and between H<sub>2</sub> and He meant that neither was appropriate to detect both CO and H<sub>2</sub> in a single run. Therefore, each sample had to be run twice using a different carrier gas in order to determine how much of each component was present.

To this end, known proportions of CO:X<sub>2</sub> from gas cylinders were used to fill the CIR cell to 10 bar. A sample of this gas was then collected in a pre-evacuated Schlenk tube and a 100  $\mu$ L syringe was then used to extract a sample from the Schlenk tube and injected into the GC. Figure 5.1 shows an example gas chromatogram obtained for a CO/N<sub>2</sub> mixture. By integrating the area under each peak, the amount of each gas present can be calculated.



**Figure 5.1.** Typical gas chromatogram of a CO:N<sub>2</sub> sample.

Figure 5.2 and Figure 5.3 show plots of integrated intensity of the GC peak, against proportion of that gas in the sample. Figure 5.2 shows the calibration graph used when analysing CO/N<sub>2</sub> mixtures. Due to the method of collecting the gas from the high pressure infrared cell, it was difficult to entirely

exclude traces of air. Since air contains N<sub>2</sub> this had to be corrected for. Therefore, O<sub>2</sub> was also measured and from that the amount of N<sub>2</sub> contamination from the air could be determined. This amount was then subtracted from the overall amount of N<sub>2</sub> in the Schlenk tube to give the amount of N<sub>2</sub> in the sample transferred from the CIR cell. In most cases, the amount of air contamination was small with the amount of O<sub>2</sub> present in a typical sample around 1 %.

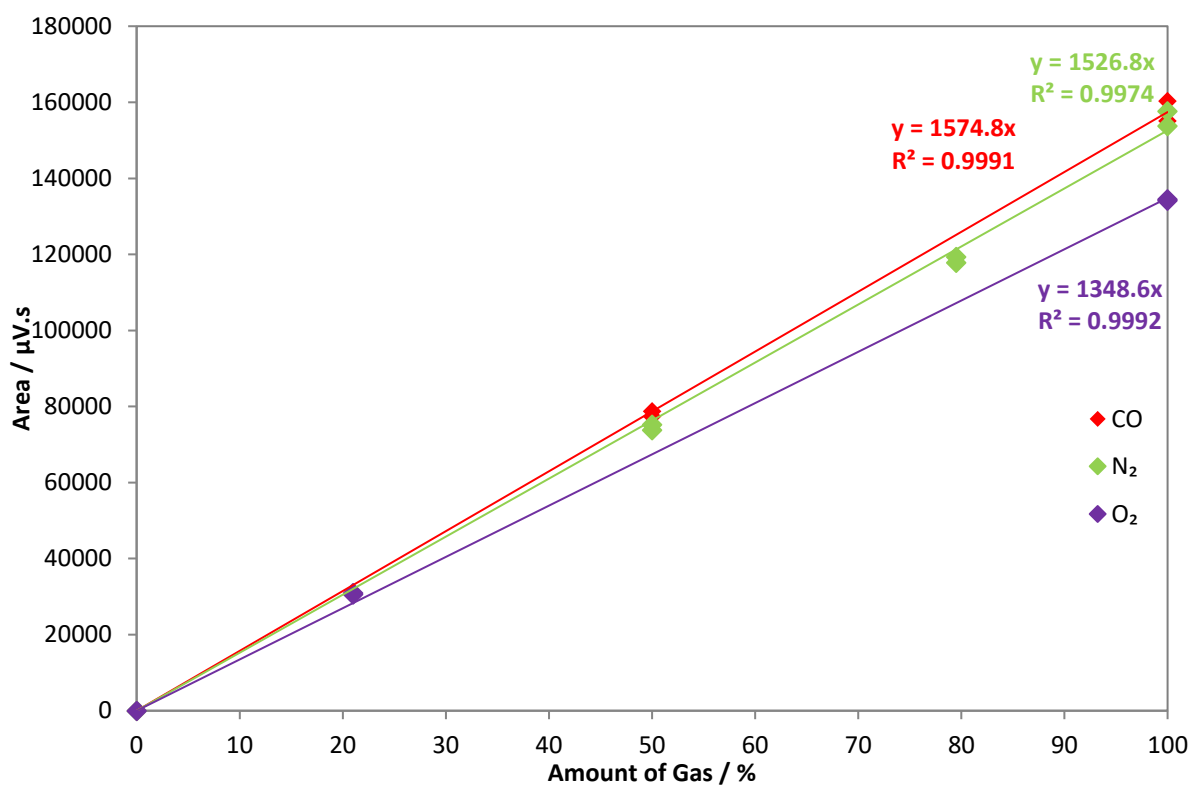


Figure 5.2. Calibration graph for CO/N<sub>2</sub> mixtures.

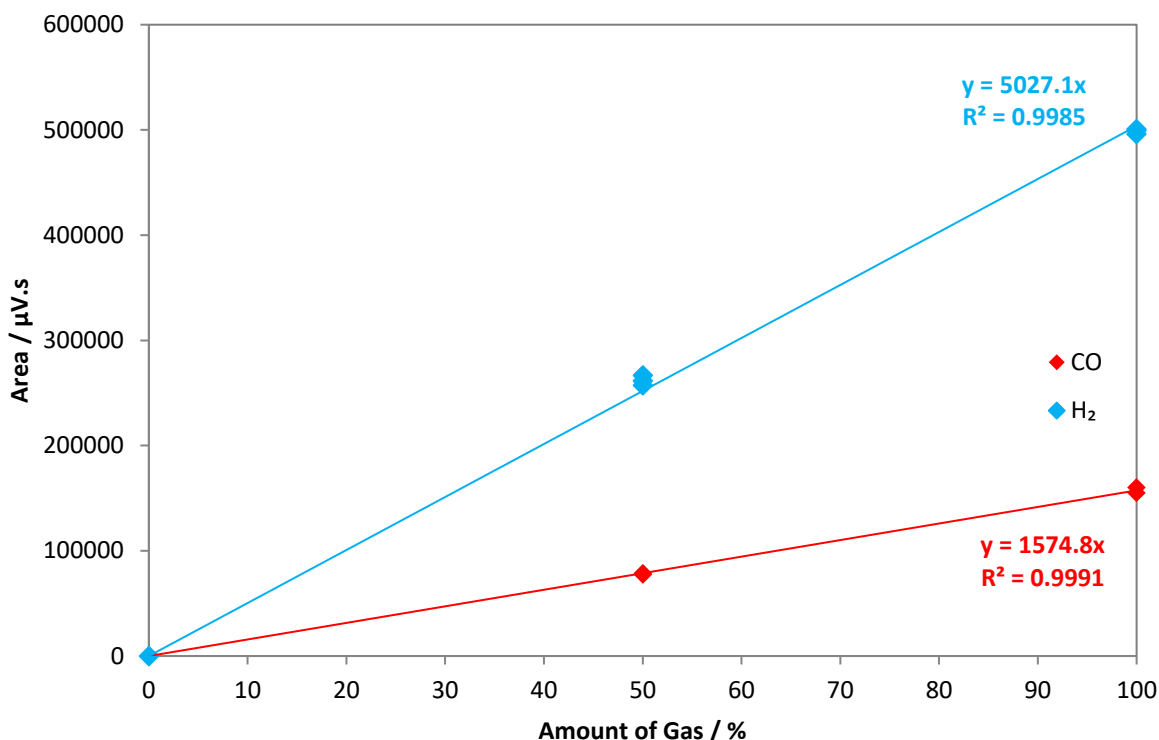


Figure 5.3. Calibration graph for CO/H<sub>2</sub> mixtures.

### 5.3 CO Enrichment Studies using Copper(I) Containing Ionic Liquids

Initially, tests were performed to determine whether analysing the mixtures by GC gave comparable results to gas-phase IR spectroscopy. To do this, experiments were performed on the [C<sub>6</sub>mim][CuBr<sub>2</sub>] IL to compare with the results obtained by Repper *et al.*<sup>1</sup> Using a 50:50 mixture of either CO/N<sub>2</sub> or CO/H<sub>2</sub>, the CIR cell was pressurised to 8 bar and the absorption of CO was tracked by IR spectroscopy. The formation of a  $\nu(\text{CO})$  band at 2081 cm<sup>-1</sup> was observed, as when using pure CO. When equilibrium had been reached, the headspace was vented (with a gas sample taken for analysis) and resealed. The cell was then heated to 100 °C to drive off the absorbed gas and a sample of the headspace gas was collected after desorption. All measurements were repeated several times to check reproducibility. Table 5.1 shows that the data obtained are in good agreement with the results reported by Repper.

**Table 5.1.** Headspace CO content in CO/X<sub>2</sub> enrichment experiments on the [C<sub>6</sub>mim][CuBr<sub>2</sub>] IL. In each experiment, the initial total pressure was 8 bar at 25 °C. The % CO values are averages of several measurements.

Ionic Liquid	X <sub>2</sub>	% CO			
		At equilibrium <sup>1</sup> (IR)	At equilibrium (GC)	After Desorption <sup>1</sup> (IR)	After Desorption (GC)
[C <sub>6</sub> mim][CuBr <sub>2</sub> ]	H <sub>2</sub>	37	40	89	89
	N <sub>2</sub>	33	33	95	94

#### 5.4 Enrichment Studies Using [C<sub>2</sub>mim][Cu(NCMe)(OTf)(NTf<sub>2</sub>)]

In previous chapters, [C<sub>2</sub>mim][Cu(NCMe)(OTf)(NTf<sub>2</sub>)] was singled out as the best performing IL in a number of properties such as high copper concentration, low viscosity and high dicarbonyl formation. Therefore, [C<sub>2</sub>mim][Cu(NCMe)(OTf)(NTf<sub>2</sub>)] was ideal to test in separation studies as this was the most promising candidate to use in a commercial process and a good benchmark for other systems tested.

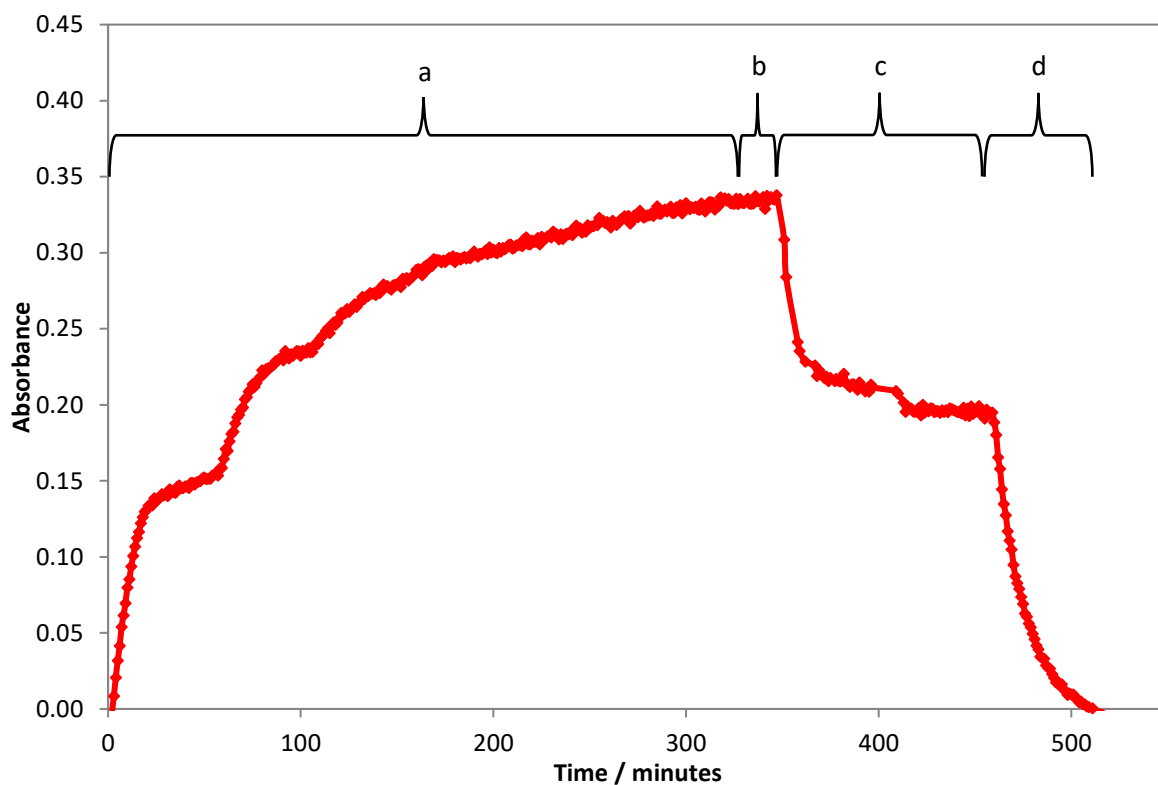
The [C<sub>6</sub>mim]<sup>+</sup> cation has also been used in separation studies with other anions such as Br<sup>-</sup> and OTf<sup>-</sup>. As demonstrated in chapter 4, the cation has a secondary small effect on CO uptake with the anion having the dominating effect. Therefore, although the cation used in this section is the [C<sub>2</sub>mim]<sup>+</sup> cation, results would likely be similar for the [C<sub>6</sub>mim]<sup>+</sup> analogue.

##### 5.4.1 CO Enrichment from CO/N<sub>2</sub>

Figure 5.4 shows in situ high pressure IR data from a typical enrichment experiment which was performed in the same manner as for the pure CO uptake experiments. About 8 cm<sup>3</sup> of copper-

containing IL was loaded into the CIR cell and pressurised to 10 bar of 50:50 CO:N<sub>2</sub>. The absorption of CO was tracked by monitoring the intensity of the  $\nu(\text{CO})$  band. As CO was absorbed, the pressure dropped and the headspace was repressurised up to 10 bar and left to absorb several times, until no further drop in pressure was recorded. The repressurisation was done in stages in order to limit diffusion effects that could occur if the line was left open to the cylinder.

Once equilibrium was reached, as determined from a plateau in the  $\nu(\text{CO})$  band intensity, stirring was stopped and the headspace vented before being resealed. The cell was then heated to between 80 °C – 140 °C, depending on the experiment, and the absorbed gas was driven back into the headspace. This new headspace was then sampled and the procedure repeated as many times as necessary.



**Figure 5.4.** Plot of the intensity of the 2122  $\text{cm}^{-1}$  band vs time for  $[\text{C}_2\text{mim}][\text{Cu}(\text{NCMe})(\text{OTf})(\text{NTf}_2)]$  under 50:50 CO:N<sub>2</sub>. (a) growth of  $\nu(\text{CO})$  band as CO is absorbed under 10 bar and repressurised accordingly, (b) stirring is ceased and the headspace vented and collected, (c) CO is driven out of the solvent into the sealed headspace at 140 °C and collected, (d) 140 °C desorb with a purge of N<sub>2</sub> to remove all CO absorbed by solvent.

Experiments were repeated several times and multiple samples of the headspace were taken to determine the average composition. Figure 5.4 shows the stages of a typical experiment where period a is the absorption of CO and b is the point where the headspace was collected at 10 bar equilibrium. During period c, two desorptions occurred at 140 °C with the cell sealed and then collected for analysis.

Table 5.2 summarises the data collected during enrichment experiments using [C<sub>2</sub>mim][Cu(NCMe)(OTf)(NTf<sub>2</sub>)] starting from an initial mixture of 50:50 CO:N<sub>2</sub>. Evidently, an appreciable increase in the CO content after a single absorption/partially desorption cycle is observed, with a mean CO content of 79 % measured after the second desorption.

**Table 5.2.** Final % measurements from the CIR cell for multiple enrichment experiments performed with [C<sub>2</sub>mim][Cu(NCMe)(OTf)(NTf<sub>2</sub>)] at 10 bar 50:50 CO:N<sub>2</sub> gas mixture.

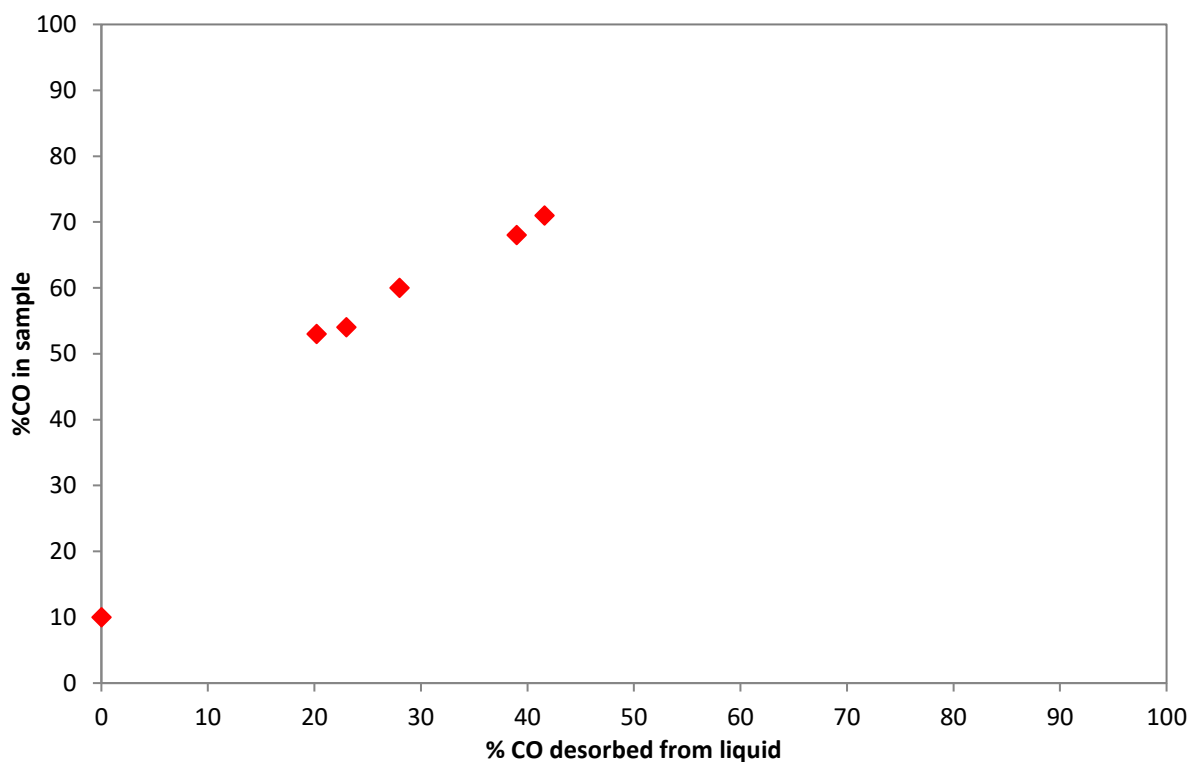
		% Gas from Cell						Mean
Headspace	CO	8	8	10	11	11	11	<b>10 ± 1</b>
	N <sub>2</sub>	92	92	90	89	89	89	<b>90 ± 1</b>
1 <sup>st</sup> Desorption	CO	71	71	62	66	69		<b>68 ± 3</b>
	N <sub>2</sub>	29	29	38	34	31		<b>32 ± 3</b>
2 <sup>nd</sup> Desorption	CO	82	83	71	78			<b>79 ± 4</b>
	N <sub>2</sub>	18	17	29	22			<b>21 ± 4</b>

The initial headspace sample that was taken at 10 bar equilibrium, before any desorption had occurred, gave a mean CO content of 10 %, consistent with preferential absorption of CO over N<sub>2</sub>. This was a larger depletion of CO compared to [C<sub>6</sub>mim][CuBr<sub>2</sub>], which gave a CO content of 33 % showing that [C<sub>2</sub>mim][Cu(NCMe)(OTf)(NTf<sub>2</sub>)] is more selective for CO.

The residual headspace after venting and before desorption will still contain 1 atmosphere of the unabsorbed gas after venting i.e. 10 % CO. Consequently, the % CO values displayed in Table 5.2 will

be the result of mixing the residual headspace with the gas evolved from the IL. Therefore, any % CO values recorded will be 'diluted' and so will need to be normalised to give the true value for CO content of the desorbed gas. Given that the residual headspace was measured to be 10 % CO, we can calculate the % CO that was driven out of the IL in the 1<sup>st</sup> desorption to be 80 %. Similarly, applying this to the 2<sup>nd</sup> desorption, gives a normalised value of 90 % CO.

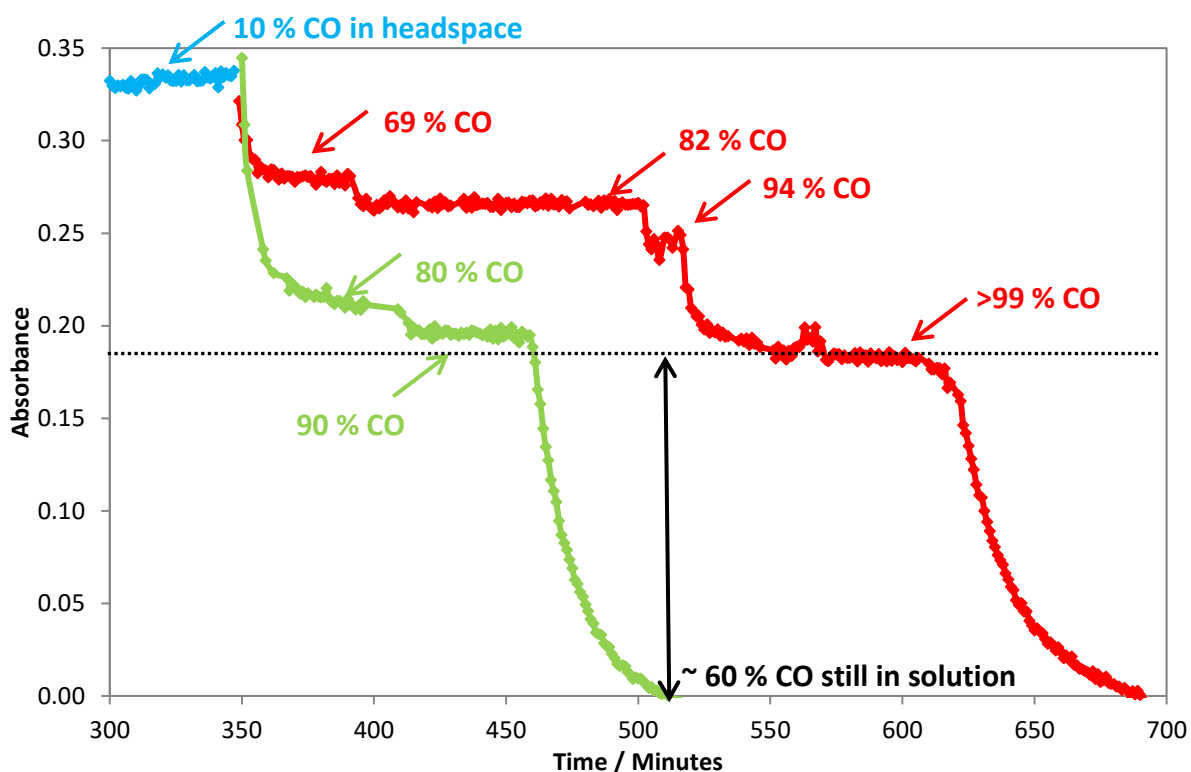
These results show that from a 50:50 CO:N<sub>2</sub> mixture, [C<sub>2</sub>mim][Cu(NCMe)(OTf)(NTf<sub>2</sub>)] can effectively enrich CO even after only a partial desorption. It was found that heating to 140 °C was not sufficient to desorb all the bound CO unless the system was open with an N<sub>2</sub> purge, as shown in Figure 5.4. Based on the change in  $\nu(\text{CO})$  intensity during period c, only 40 % of the absorbed CO was liberated from the liquid phase which suggests the selectivity for CO absorption is higher than apparent from the data in Table 2. However, to achieve full desorption of CO with the cell sealed, temperatures in excess of 200 °C would have been required. This is problematic as it would pose a significant hazard to the CIR cell and therefore was not attempted. In order to estimate the final % CO content in the headspace if full desorption had occurred, desorptions were undertaken at different temperatures. A lower temperature desorption would liberate less CO from the IL and therefore the headspace would have a lower % CO content. A higher temperature desorption would liberate more CO from the IL and therefore the headspace would have a higher % CO content. Figure 5.5 plots the % CO desorbed from the IL against % CO in the GC sample, and suggests that complete desorption of CO at a higher temperature would give a higher CO content.



**Figure 5.5.** Plot of % CO desorbed from the [C<sub>2</sub>mim][Cu(NCMe)(OTf)(NTf<sub>2</sub>)] against % CO recorded in gas chromatograph sample.

#### ***Stepwise Increasing Temperature Desorption vs Constant High Temperature Desorption***

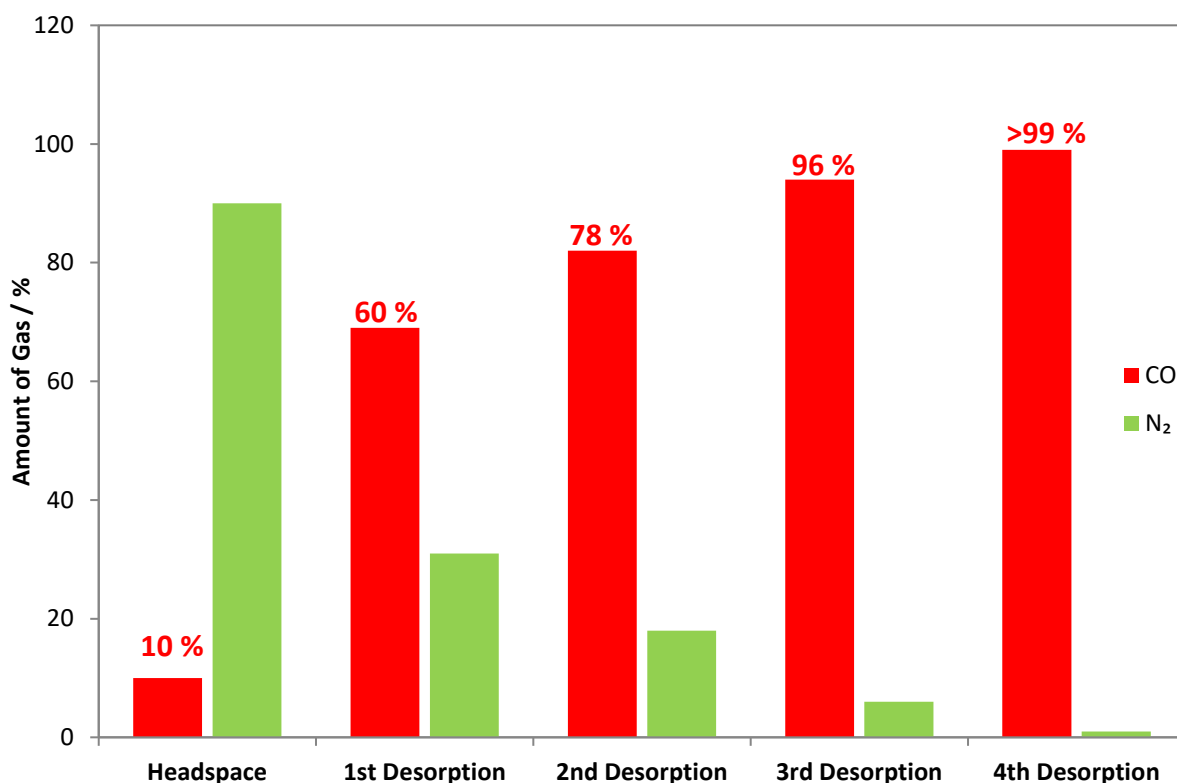
Figure 5.6 shows two different approaches to the desorption of gas from [C<sub>2</sub>mim][Cu(NCMe)(OTf)(NTf<sub>2</sub>)] during enrichment experiments. One procedure used a constant high temperature of 140 °C (green profile) and another used a stepwise desorption starting at a lower temperature of 80 °C and increasing the temperature to 100 °C, 120 °C and finally 140 °C on each subsequent desorption (red profile). Due to the stronger absorption of CO over N<sub>2</sub>, it was thought that by starting at a low temperature and slowly ramping up the temperature on each desorption, mostly N<sub>2</sub> would be lost initially, as it is less strongly bound through physisorption. This would leave a higher proportion of CO in solution to be collected on a later desorption.



**Figure 5.6.** Plot of the intensity of the 2124  $\text{cm}^{-1}$  band vs time for  $[\text{C}_2\text{mim}][\text{Cu}(\text{NCMe})(\text{OTf})(\text{NTf}_2)]$  during desorption, after equilibrating under 10 bar 50:50  $\text{CO}:\text{N}_2$ . For the green profile the system was closed and heated to 140 °C and gas samples collected twice. For the red profile the system was closed and initially heated to 80 °C. The temperature was then ramped up in 20 °C increments and the headspace sampled after equilibrium was reached again. The numbers given next to each trace are the normalised % CO values calculated from corresponding headspace measurements.

Figure 5.6 shows how after two high temperature desorptions at 140 °C, the CO has been enriched from 50 % to 90 % (green profile). However, the enrichment measured during the stepwise procedure (red profile) showed the CO had increased from 50 % to >99 %, compared to 90 % given by the green profile. This highlights how starting from a lower desorption temperature to preferentially remove the  $\text{N}_2$ , leads to larger enrichment values overall (individual values in appendix 8.3).

Figure 5.7 represents the same data to fully illustrate the gas enrichment after each desorption step. The first two desorptions give similar, lower % CO values, as most of the physically absorbed  $\text{N}_2$  is lost during this period, in addition to CO. By the third and fourth desorption, most of the absorbed  $\text{N}_2$  is lost, and therefore the % CO values start to increase.



**Figure 5.7.** Stepwise desorption gas enrichment values for the [C<sub>2</sub>mim][Cu(NCMe)(OTf)(NTf<sub>2</sub>)] IL starting from a 50:50 mixture of CO:N<sub>2</sub>. The system was closed and initially heated to 80 °C and the headspace sampled. The temperature was then ramped up to 100 °C during the 2<sup>nd</sup> desorption, 120 °C for the 3<sup>rd</sup> desorption and finally 140 °C during the 4<sup>th</sup> desorption and the headspace sampled after equilibrium was reached.

#### 5.4.2 CO Enrichment from CO/H<sub>2</sub>

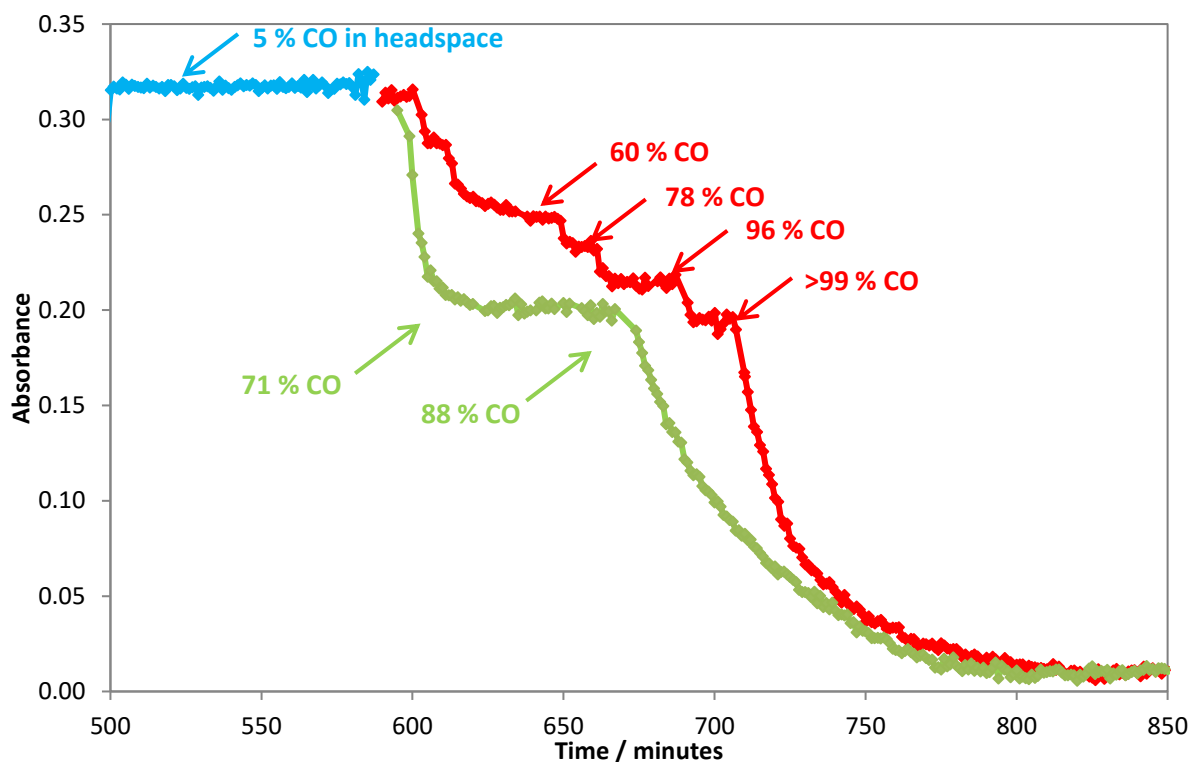
Enrichment experiments for CO/H<sub>2</sub> mixtures were conducted in the same manner and on the same sample of [C<sub>2</sub>mim][Cu(NCMe)(OTf)(NTf<sub>2</sub>)] as for the CO/N<sub>2</sub> mixtures. Therefore, starting from a 50:50 mixture of CO:H<sub>2</sub>, the sample was exposed to 10 bar pressure until equilibrium was reached. Table 5.3 summarises the results of the experiment (individual values in appendix 8.3). Again, there is an appreciable increase in the % CO after the 2<sup>nd</sup> desorption to 71 % after one absorption/partial desorption. When the residual headspace is accounted for, this value is calculated to be 88 % CO.

## Separation of CO from N<sub>2</sub> and H<sub>2</sub> Using Copper(I) Containing Ionic Liquids

**Table 5.3.** Final % CO measurements from the CIR cell for multiple enrichment experiments performed with [C<sub>2</sub>mim][Cu(NCMe)(OTf)(NTf<sub>2</sub>)] at 10 bar 50:50 CO:H<sub>2</sub> gas mixture.

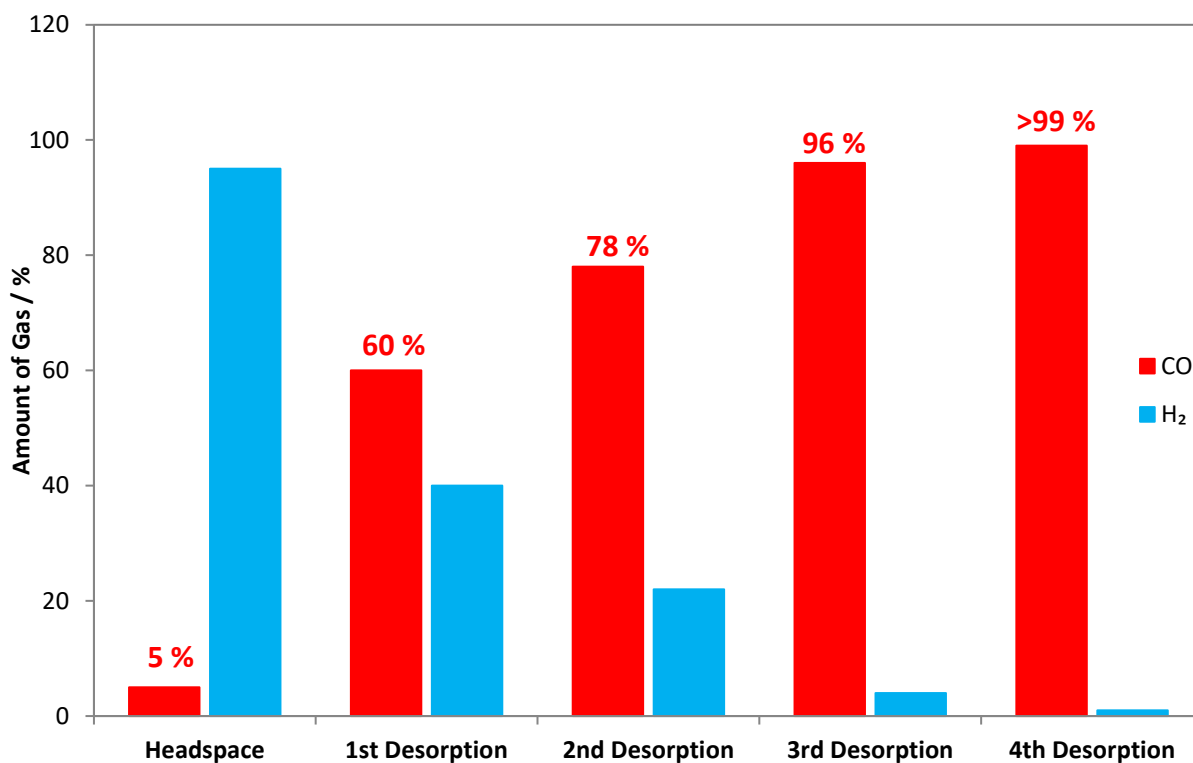
Ionic Liquid		% CO		
		Headspace	After 1 <sup>st</sup> Desorption	After 2 <sup>nd</sup> Desorption
[C <sub>2</sub> mim][Cu(NCMe)(OTf)(NTf <sub>2</sub> )]	Measured	5 ± 1	58 ± 4	68 ± 3
	Normalised		71 ± 4	88 ± 3

Compared to the CO/N<sub>2</sub> experiments, the 5 % CO recorded for the residual headspace in the CO/H<sub>2</sub> experiments suggested that the [C<sub>2</sub>mim][Cu(NCMe)(OTf)(NTf<sub>2</sub>)] IL was more selective for CO over H<sub>2</sub> than N<sub>2</sub>. This is given the 10 % recorded during the CO/N<sub>2</sub> experiments. This is consistent with the Henry's law constants for N<sub>2</sub> and H<sub>2</sub> in [C<sub>2</sub>mim]NTf<sub>2</sub> being 140 MPa and 260 MPa respectively.<sup>2</sup> Overall, the % CO collected during desorptions was comparable to the CO/N<sub>2</sub> separations, showing [C<sub>2</sub>mim][Cu(NCMe)(OTf)(NTf<sub>2</sub>)] is effective at purifying CO from mixtures containing either N<sub>2</sub> or H<sub>2</sub>.



**Figure 5.8.** Plot of the intensity of the 2124 cm<sup>-1</sup> band vs time for [C<sub>2</sub>mim][Cu(NCMe)(OTf)(NTf<sub>2</sub>)] during desorption, after equilibrating under 10 bar 50:50 CO:H<sub>2</sub>. For the green profile the system was closed and heated to 140 °C and gas samples collected twice. For the red profile the system was closed and initially heated to 80 °C. The temperature was then ramped up in 20 °C increments and the headspace sampled after equilibrium was reached again. The numbers given next to each trace are the normalised % CO values calculated from corresponding headspace measurements.

Figure 5.8 shows in situ high pressure IR data during the desorption steps and the % CO in the headspace gas sampled at each stage. Again it is found that by performing stepwise desorptions, better CO enrichment can be reached whilst still having significant amounts of CO available in the solvent (individual values in appendix 8.3).



**Figure 5.9.** Stepwise desorption gas enrichment values for the  $[\text{C}_2\text{mim}][\text{Cu}(\text{NCMe})(\text{OTf})(\text{NTf}_2)]$  IL starting from a 50:50 mixture of CO:H<sub>2</sub>. The system was closed and initially heated to 80 °C and the headspace sampled. The temperature was then ramped up to 100 °C during the 2<sup>nd</sup> desorption, 120 °C for the 3<sup>rd</sup> desorption and finally 140 °C during the 4<sup>th</sup> desorption and the headspace sampled after equilibrium was reached.

## 5.5 Enrichment Studies Using $[\text{C}_6\text{mim}][\text{Cu}(\text{NCMe})(\text{OTf})_2]$

### 5.5.1 CO Enrichment from CO/N<sub>2</sub>

The enrichment studies for  $[\text{C}_6\text{mim}][\text{Cu}(\text{NCMe})(\text{OTf})_2]$  were performed in the same manner as for  $[\text{C}_2\text{mim}][\text{Cu}(\text{NCMe})(\text{OTf})(\text{NTf}_2)]$ . Therefore, about 8 cm<sup>3</sup> of copper-containing IL was loaded into the CIR cell and pressurised to 10 bar of 50:50 CO:N<sub>2</sub>. The absorption proceeded until 10 bar equilibrium was reached. The  $v(\text{CO})$  observed was the same as that when performing the pure CO uptake

experiments. Two 140 °C desorptions were performed and the headspace was sampled once the new equilibrium was formed. Likewise for the NTf<sub>2</sub> system, 140°C was not sufficient enough to totally remove all the bound CO, unless the cell remained open during desorption.

The amount of gas evolved from this partial desorption from [C<sub>6</sub>mim][Cu(NCMe)(OTf)<sub>2</sub>] was comparable to that of [C<sub>2</sub>mim][Cu(NCMe)(OTf)(NTf<sub>2</sub>)], as noted from the headspace pressure. This shows that both copper-containing ILs are absorbing similar amounts of gas.

Table 5.4 shows that the selectivity for CO over N<sub>2</sub> in both [C<sub>6</sub>mim][Cu(NCMe)(OTf)<sub>2</sub>] and [C<sub>2</sub>mim][Cu(NCMe)(OTf)(NTf<sub>2</sub>)] were comparable, given the residual headspace sampled recorded at about 10 % CO. The data also shows that [C<sub>6</sub>mim][Cu(NCMe)(OTf)<sub>2</sub>] can effectively enrich CO to excellent levels of > 99% after the second desorption.

**Table 5.4.** Final % CO measurements from the CIR cell for multiple enrichment experiments performed with [C<sub>6</sub>mim][Cu(NCMe)(OTf)<sub>2</sub>] and [C<sub>2</sub>mim][Cu(NCMe)(OTf)(NTf<sub>2</sub>)] at 10 bar 50:50 CO:N<sub>2</sub> gas mixture.

Ionic Liquid		% CO		
		Headspace	After 1 <sup>st</sup> Desorption	After 2 <sup>nd</sup> Desorption
[C <sub>6</sub> mim][Cu(NCMe)(OTf) <sub>2</sub> ]	Measured	9 ± 2	70 ± 2	78 ± 5
	Normalised		87 ± 2	>99 ± 5
[C <sub>2</sub> mim][Cu(NCMe)(OTf)(NTf <sub>2</sub> )]	Measured	10 ± 1	68 ± 3	79 ± 5
	Normalised		80 ± 3	90 ± 5

### 5.5.2 CO Enrichment from CO/H<sub>2</sub>

Table 5.5 shows that the selectivity of CO/H<sub>2</sub> separations using [C<sub>6</sub>mim][Cu(NCMe)(OTf)<sub>2</sub>] was quite similar compared to separations using [C<sub>2</sub>mim][Cu(NCMe)(OTf)(NTf<sub>2</sub>)] based on the % CO of the headspace after absorption. However, the % CO values recorded for [C<sub>6</sub>mim][Cu(NCMe)(OTf)<sub>2</sub>] after desorption were slightly higher than for [C<sub>2</sub>mim][Cu(NCMe)(OTf)(NTf<sub>2</sub>)]. In both cases, [C<sub>6</sub>mim][Cu(NCMe)(OTf)<sub>2</sub>] consistently showed good CO enrichment values regardless of the X<sub>2</sub> gas used (individual measurements are given in appendix 8.3).

**Table 5.5.** Final % CO measurements from the CIR cell for multiple enrichment experiments performed with [C<sub>6</sub>mim][Cu(NCMe)(OTf)<sub>2</sub>] and [C<sub>2</sub>mim][Cu(NCMe)(OTf)(NTf<sub>2</sub>)] at 10 bar 50:50 CO:H<sub>2</sub> gas mixture

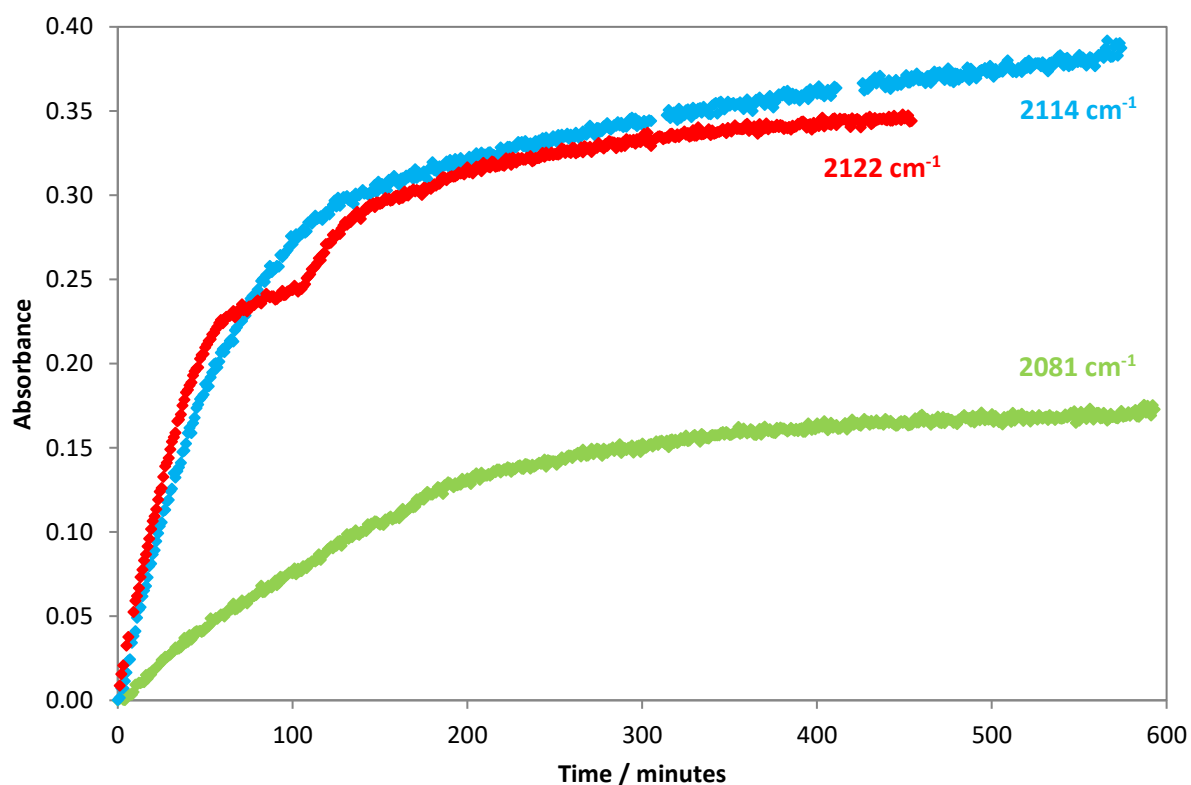
Ionic Liquid		% CO		
		Headspace	After 1 <sup>st</sup> Desorption	After 2 <sup>nd</sup> Desorption
[C <sub>6</sub> mim][Cu(NCMe)(OTf) <sub>2</sub> ]	Measured	11 ± 1	74 ± 2	84 ± 2
	Normalised		88 ± 2	>99 ± 2
[C <sub>2</sub> mim][Cu(NCMe)(OTf)(NTf <sub>2</sub> )]	Measured	5 ± 1	58 ± 4	68 ± 3
	Normalised		71 ± 4	88 ± 3

### 5.6 Comparisons with Halide Ionic Liquids and Implications for Commercial Use

Figure 5.10 compares *in situ* high-pressure IR data for the uptake of CO from a mixture of 50:50 CO:N<sub>2</sub> at 10 bar in various ILs. Clearly, the amount of CO taken up by the [C<sub>6</sub>mim][CuBr<sub>2</sub>] IL is less than that of the other two. This is assuming the extinction coefficients are similar, which is a reasonable assumption given the results from pressure drop experiments in chapter 3 (Figure 3.15). Similar

observations were made during CO/H<sub>2</sub> separations. Since the partial pressure of CO is low in these experiments, and the OTf<sup>-</sup> and NTf<sub>2</sub><sup>-</sup> systems have a strong affinity for CO given the higher desorption conditions required, this is expected. Based on the relative ν(CO) intensities at equilibrium, the OTf and NTf<sub>2</sub> systems absorb approximately double the amount of CO compared to the Br system. Assuming the amount of either N<sub>2</sub> or H<sub>2</sub> absorbed in each IL is comparable, the OTf and NTf<sub>2</sub> systems should have better selectivity for CO.

Table 5.6 compared data for CO content of the headspace at equilibrium, which support the conclusion that more CO is absorbed by the OTf and NTf<sub>2</sub> systems than by the Br system.



**Figure 5.10.** Plot of absorbance vs. time for the uptake of CO by different ILs on exposure to 10 bar of 50:50 CO:N<sub>2</sub> at 25 °C and stirrer speed 214 rpm. When Red = [C<sub>2</sub>mim][Cu(NCMe)(OTf)(NTf<sub>2</sub>)]; Blue = [C<sub>6</sub>mim][Cu(NCMe)(OTf)<sub>2</sub>]; Green = [C<sub>6</sub>mim][CuBr<sub>2</sub>].

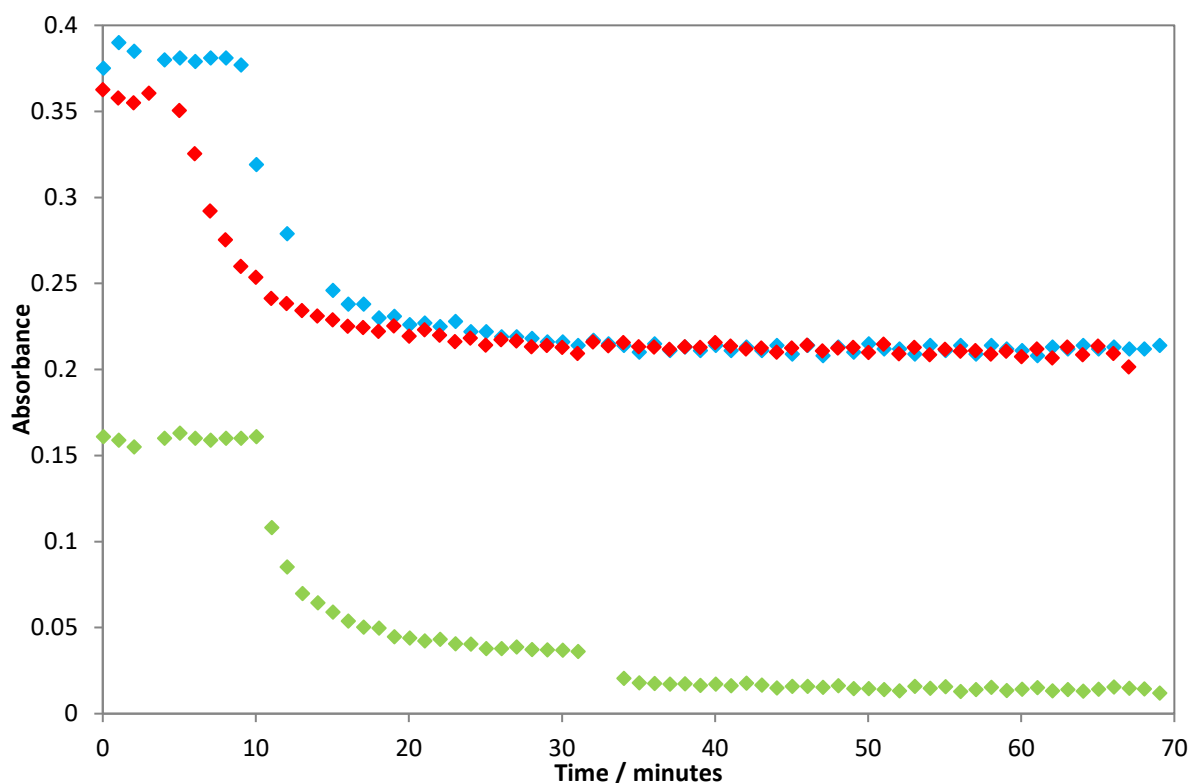
Since the halide copper-containing ILs fully desorb the bound CO more easily than in the weakly coordinating anion systems, it is difficult to compare their desorption behaviour directly. However,

even with a partial desorption in the OTf and NTf<sub>2</sub> systems, the values for CO enrichment are quite similar, as shown in Table 5.6.

**Table 5.6.** CO/X<sub>2</sub> enrichment experiments on various IL. Each experiment the pressure was 10 bar at 25 °C. The % CO values are averages of several measurements.

Ionic Liquid	X <sub>2</sub>	% CO	
		At Equilibrium	After Desorption
[C <sub>6</sub> mim][CuBr <sub>2</sub> ]	H <sub>2</sub>	40 ± 0	93 ± 3
	N <sub>2</sub>	33 ± 3	>99 ± 1
[C <sub>6</sub> mim][Cu(NCMe)(OTf) <sub>2</sub> ]	H <sub>2</sub>	11 ± 1	>99 ± 2
	N <sub>2</sub>	9 ± 1	>99 ± 5
[C <sub>2</sub> mim][Cu(NCMe)(OTf)(NTf <sub>2</sub> )	H <sub>2</sub>	10 ± 1	88 ± 3
	N <sub>2</sub>	5 ± 1	90 ± 5

Therefore, it can be concluded that the OTf and NTf<sub>2</sub> systems are at least performing as well as the Br system at this pressure. Moreover, Figure 5.11 shows there is still a high proportion of CO bound to copper(I) after a single desorption at 140 °C. Subsequent desorption of this CO will primarily give a very high % CO, as demonstrated in stepwise desorption experiments.



**Figure 5.11.** Plot of absorbance vs. time for the desorption of CO by different ILs on heating to 100 °C for green = [C<sub>6</sub>mim][CuBr<sub>2</sub>] and 140 °C for red = [C<sub>2</sub>mim][Cu(NCMe)(OTf)(NTf<sub>2</sub>)] and blue = [C<sub>6</sub>mim][Cu(NCMe)(OTf)<sub>2</sub>] at a stirrer speed of 214 rpm.

Whether these copper-containing ILs could be economically viable will be determined by both the cost of the IL itself and the cost of running the process. For example, the [C<sub>6</sub>mim][CuBr<sub>2</sub>] IL would be cheaper to synthesise, but its CO uptake ability is lower. Moreover, its relatively high viscosity would be problematic. However, desorption conditions are much milder in this case, where desorption can be done as low as 40 °C. Another issue for the copper(I) dihalide ILs is the potential formation of HX which would require the system to have expensive anti-corrosive metals installed.

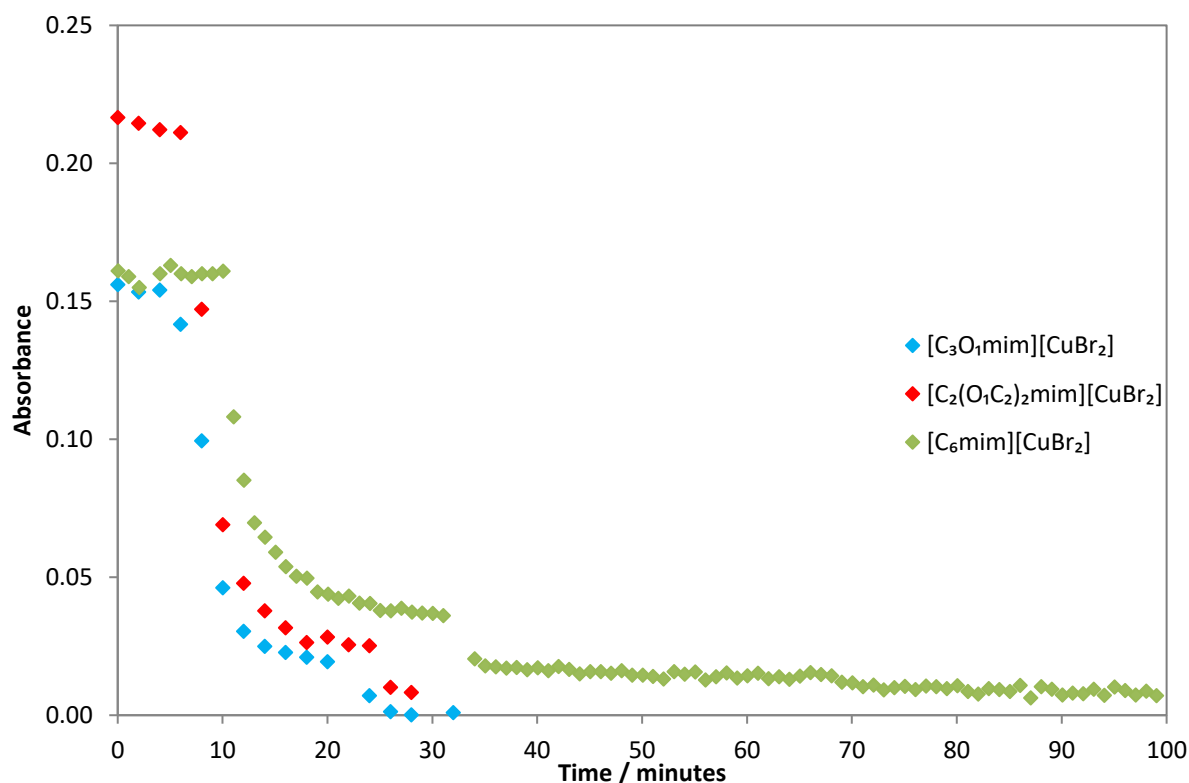
The [C<sub>n</sub>mim][Cu(NCMe)(OTf)(X)] ILs, would be more expensive to synthesise, but they have higher CO uptake at low pressures. They are less viscous than the [C<sub>6</sub>mim][CuBr<sub>2</sub>] IL but the desorption temperature required is higher.

## 5.7 CO Enrichment Studies Using Functionalised Imidazolium Copper Containing Ionic Liquids

Enrichment studies discussed up until this point have investigated the effect of changing the anion and thus copper speciation, leading to some notable differences. This section explores the use of the ether-functionalised imidazolium copper containing ILs discussed in chapter 4, and their influence on CO separations from mixtures of N<sub>2</sub> and H<sub>2</sub>.

### 5.7.2 CO Enrichment from CO/X<sub>2</sub>

Enrichment studies were performed in the same manner as described previously in this chapter. Therefore, about 8 cm<sup>3</sup> of [C<sub>n</sub>mim][CuBr<sub>2</sub>] IL was subjected to 10 bar CO:N<sub>2</sub> or CO:H<sub>2</sub> until equilibrium was reached. The desorption conditions required to fully desorb all the bound CO were the same as for the [C<sub>6</sub>mim][CuBr<sub>2</sub>] IL. This was expected as the anion has the dominant effect. Figure 5.12 shows the in situ high pressure IR data recorded during desorption at 100 °C



**Figure 5.12.** Plot of absorbance vs. time for the desorption of CO by different ILs on heating to 100 °C for green = [C<sub>6</sub>mim][CuBr<sub>2</sub>] red = [C<sub>2</sub>(O<sub>1</sub>C<sub>2</sub>)<sub>2</sub>mim][CuBr<sub>2</sub>] and blue = [C<sub>3</sub>O<sub>1</sub>mim][CuBr<sub>2</sub>] at a stirrer speed of 214 rpm.

[C<sub>2</sub>(O<sub>1</sub>C<sub>2</sub>)<sub>2</sub>mim][CuBr<sub>2</sub>] reached a slightly higher equilibrium absorbance, which suggests that it absorbed more CO than the other two. This was reflected in the headspace pressure on desorption i.e. the amount of gas driven from the IL. This was recorded at 6 bar for [C<sub>2</sub>(O<sub>1</sub>C<sub>2</sub>)<sub>2</sub>mim][CuBr<sub>2</sub>], whereas the headspace pressure for the other two systems was 5 bar.

Table 5.7 gives the headspace % CO values before and after desorption. The results are similar for each cation, demonstrating effective enrichment of CO in a single absorption/desorption cycle. Therefore there appears to be little benefit in using an ether-functionalised cation over the simpler [C<sub>6</sub>mim]<sup>+</sup>

**Table 5.7.** Enrichment results for [C<sub>n</sub>mim][CuBr<sub>2</sub>] ILs at 10 bar 50:50 CO:N<sub>2</sub> or CO:H<sub>2</sub> gas mixture.

Ionic Liquid	X <sub>2</sub>	Mean CO % in Headspace	Mean CO % After Enrichment (measured)	Actual CO % Absorbed (normalised)
[C <sub>6</sub> mim][CuBr <sub>2</sub> ]	N <sub>2</sub>	33 ± 3	91 ± 1	>99 ± 1
	H <sub>2</sub>	40 ± 0	85 ± 3	94 ± 3
[C <sub>3</sub> O <sub>1</sub> mim][CuBr <sub>2</sub> ]	N <sub>2</sub>	31 ± 3	87 ± 1	>99 ± 1
[C <sub>2</sub> (O <sub>1</sub> C <sub>2</sub> ) <sub>2</sub> mim][CuBr <sub>2</sub> ]	N <sub>2</sub>	36 ± 0	88 ± 0	98 ± 0
	H <sub>2</sub>	37 ± 0	88 ± 2	97 ± 2

## 5.8 Discussion of Potential Separation of CO/X mixtures

It has been shown that the CO content can be enriched from 50:50 CO:N<sub>2</sub> and CO:H<sub>2</sub> mixtures. Using Henry's law constants for the closely related IL [C<sub>6</sub>mim]NTf<sub>2</sub>, it gives some insight as to the selectivity of CO against other gases.<sup>2,3</sup>

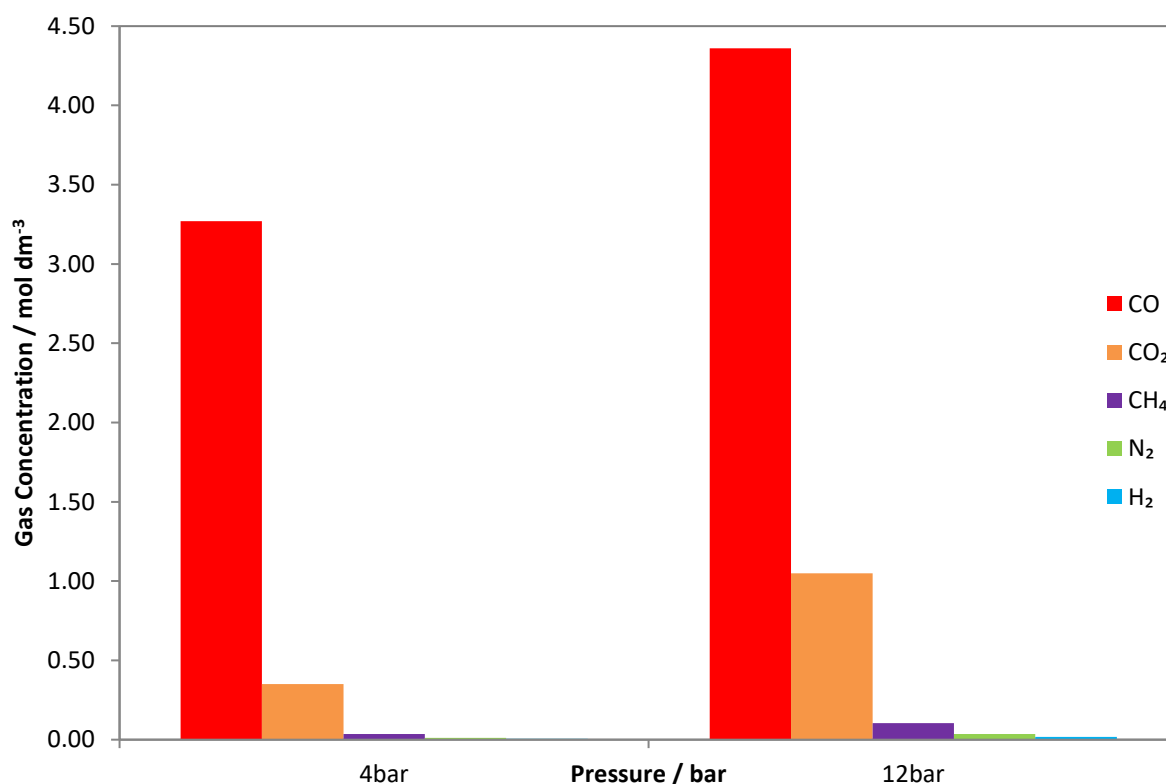
**Table 5.8.** Henry's law constants for different gases in the IL [C<sub>6</sub>mim]NTf<sub>2</sub>

Ionic Liquid	K <sub>H</sub> (CO) / MPa	K <sub>H</sub> (H <sub>2</sub> ) / MPa	K <sub>H</sub> (N <sub>2</sub> ) / MPa	K <sub>H</sub> (CH <sub>4</sub> ) / MPa	K <sub>H</sub> (CO <sub>2</sub> ) / MPa
[C <sub>6</sub> mim]NTf <sub>2</sub>	76	200	101	35	3.5

Table 5.8 gives the Henry's law volatilities of CO, N<sub>2</sub>, H<sub>2</sub>, CH<sub>4</sub> and CO<sub>2</sub> in [C<sub>6</sub>mim]NTf<sub>2</sub> where a lower value corresponds to a higher solubility of the gas in the liquid. It shows a high Henry's law constant

for H<sub>2</sub>, which suggests H<sub>2</sub> is less soluble than N<sub>2</sub> and explains the even higher depleted headspace in the CO/H<sub>2</sub> separations.

Table 5.8 also highlights the high solubility of CO<sub>2</sub> over the other common gases. It is an order of magnitude more soluble in [C<sub>6</sub>mim]NTf<sub>2</sub> than the next most soluble, CH<sub>4</sub>, and even more so for CO which suggests CO/CO<sub>2</sub> separation may be challenging. In the copper containing IL systems however, rather than just the physical absorption, there is an extra component the chemical complexation of the CO to the copper(I). Therefore, the overall CO dissolution will be the sum of the physical CO solubility and the chemical complexation of the CO to the copper(I). Since the solubility of N<sub>2</sub>, H<sub>2</sub>, CH<sub>4</sub> and CO<sub>2</sub> increases linearly with pressure, and the copper sites will eventually become saturated at high pressures, the selectivity will be greatest at low pressures.



**Figure 5.13.** Gas solubility data for CO<sub>2</sub>, CH<sub>4</sub>, N<sub>2</sub> and H<sub>2</sub> plotted from the literature value of the Henry's law constant at 298 K at 4 bar and 12 bar pressure. CO solubility plotted from pressure drop experiments at 298 K.

Figure 5.13 gives the gas solubility of N<sub>2</sub>, H<sub>2</sub>, CH<sub>4</sub> and CO<sub>2</sub> in [C<sub>6</sub>mim]NTf<sub>2</sub> as predicted from the Henry's law constants.<sup>3</sup> The CO uptake measured by experiment in the pressure drop experiments in chapter 3. Simply taking the ratio of the amount of absorbed gases at the equilibrium pressure available, an estimate of the selectivity can be made.

**Table 5.9.** Gas solubility data for CO, CO<sub>2</sub>, CH<sub>4</sub>, N<sub>2</sub> and H<sub>2</sub> in [C<sub>6</sub>mim]NTf<sub>2</sub> at 4 and 12 bar pressure. CO/X gas selectivities are given in bold.

Gas, X	Partial Pressure	Absorbed [X] / M	Absorbed [CO] / M	CO/X Absorbed
CO <sub>2</sub>	4	0.35	3.3	<b>~10</b>
CO <sub>2</sub>	12	1.05	4.3	<b>~4</b>
CH <sub>4</sub>	4	0.035	3.3	<b>~94</b>
CH <sub>4</sub>	12	0.105	4.3	<b>~41</b>
N <sub>2</sub>	4	0.012	3.3	<b>~275</b>
N <sub>2</sub>	12	0.036	4.3	<b>~119</b>
H <sub>2</sub>	4	0.006	3.3	<b>~550</b>
H <sub>2</sub>	12	0.018	4.3	<b>~239</b>

The data in Table 5.9 suggests there is some scope to achieve some separation between CO and CO<sub>2</sub> if the CO<sub>2</sub> content in the mixture is low. It may not be detrimental if a little CO<sub>2</sub> was present during a separation cycle. CO/CH<sub>4</sub> separation looks to be achievable depending on the pressure used. Large selectivities are observed when CO/N<sub>2</sub> and CO/H<sub>2</sub> separations are modelled which shows why this approach to CO separations looks promising. Again, it also reiterates how the selectivity is better at lower pressures due to the chemical complexation of CO to copper(I) having a larger influence. It is worth noting that during this modelling it is assumed that the Henry's law constant does not change too much when copper is added to the IL.

## 5.9 Conclusions

Copper-containing ILs with weakly coordinating anions, OTf<sup>-</sup> and NTf<sub>2</sub><sup>-</sup>, were used to separate CO from gas mixtures containing H<sub>2</sub> or N<sub>2</sub>. The use of these types of anions is both novel and highly desirable. Using [C<sub>2</sub>mim][Cu(NCMe)(OTf)(NTf<sub>2</sub>)], a 50:50 CO:N<sub>2</sub> or CO:H<sub>2</sub> mixture can be enriched to around 90 % after one absorption/partial desorption. [C<sub>6</sub>mim][Cu(NCMe)(OTf)<sub>2</sub>] was particularly adept at separating CO from gas mixtures containing either N<sub>2</sub> or H<sub>2</sub>, with enrichment values of > 99 % recorded after one absorption/partial desorption cycle.

Stepwise desorptions starting at lower temperatures provide a convenient way to remove some of the physisorbed N<sub>2</sub> or H<sub>2</sub> initially, without losing much CO. By doing this, the levels of enrichment at a given equilibrium during desorption can be enhanced. The amount of IL needed to effectively enrich CO may be less for the OTf and NTf<sub>2</sub> systems due to their higher affinity for CO even at low pressures.

The systems with weakly coordinating anions OTf<sup>-</sup> and NTf<sub>2</sub><sup>-</sup> have shown they are at least capable to match the copper(I) dihalide systems in their ability to purify a 50:50 mixture of CO:X<sub>2</sub> (X<sub>2</sub> = N<sub>2</sub> or H<sub>2</sub>). Since full desorption of CO could not be analysed, plot of % CO desorbed from the IL against % CO in the GC sample was used to estimate the % CO collected if complete desorption was achieved. This suggested a higher CO content could be obtained upon full desorption of CO which shows they have the potential to be an even more effective absorbent for CO separation.

One shortcoming is the high binding affinity of CO to the copper(I) in these systems which results in harsher desorption conditions of 140 °C. However, desorption times were short with most of the bound CO driven out of the liquid in around 100 minutes if the cell remained open.

Functionalising the cation did not result in any significant improvements in CO enrichment emphasising that it is the anion which has the dominant effect.

## 5.9 References

- 1 S. E. Repper, A. Haynes, E. J. Ditzel and G. J. Sunley, *Dalton. Trans.*, 2017, **46**, 2821–2828.
- 2 A. Finotello, J. E. Bara, A. Dean Camper and Richard D. Noble, *Ind. Eng. Chem. Res*, 2008, **47**, 3453–3459.
- 3 C. A. Ohlin, P. J. Dyson and G. Laurenczy, *Chem. Commun.*, 2004, **9**, 1070–1071.

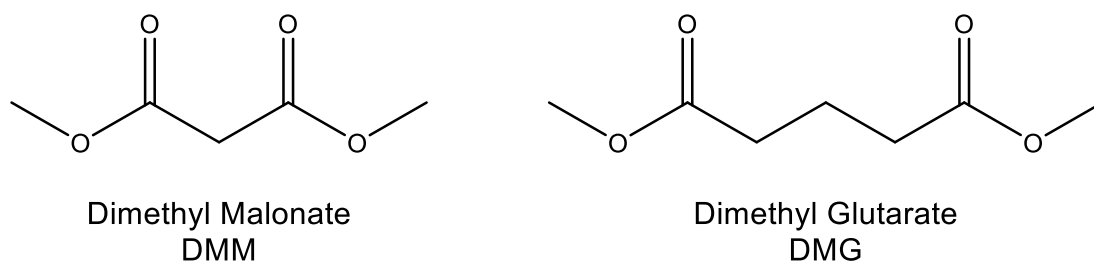
## **6. Ionic Liquid Co-Solvent Mixtures**

## 6.1 Introduction

As described in the previous chapters, copper-containing ILs are able to bind CO reversibly and could potentially be applied to separate CO from gas mixtures. However the relatively high viscosity of these liquids means that their usefulness in an industrial process would be limited, as discussed in Chapter 1. A reasonable viscosity to work with in a process like this would be about 20 mPa.s. None of the ILs studied meet this target at room temperature, although  $[\text{C}_2\text{mim}][\text{Cu}(\text{NCMe})(\text{OTf})(\text{NTf}_2)]$  was found to have a viscosity below 20 mPa.s at temperatures  $> 60\text{ }^\circ\text{C}$ .

An alternative way to reduce viscosity is by ‘cutting’ the IL with a co-solvent. An ideal co-solvent would have low viscosity, high boiling point, low molecular weight and high density. The family of organic solvents that were selected to meet these criteria are dibasic esters (DBEs), which are dicarboxylic acid dimethyl esters.

This chapter details the use of the DBEs, dimethyl malonate (DMM) and dimethyl glutarate (DMG), as shown in Figure 6.1, in combination with copper-containing ILs. Properties such as viscosity, copper concentration and CO uptake behaviour have been investigated to determine whether such a combination is a viable option for use in CO separation. Selected relevant properties of dimethyl malonate and dimethyl glutarate are given in Table 6.1.



**Figure 6.1.** Structures of dimethyl malonate and dimethyl glutarate.

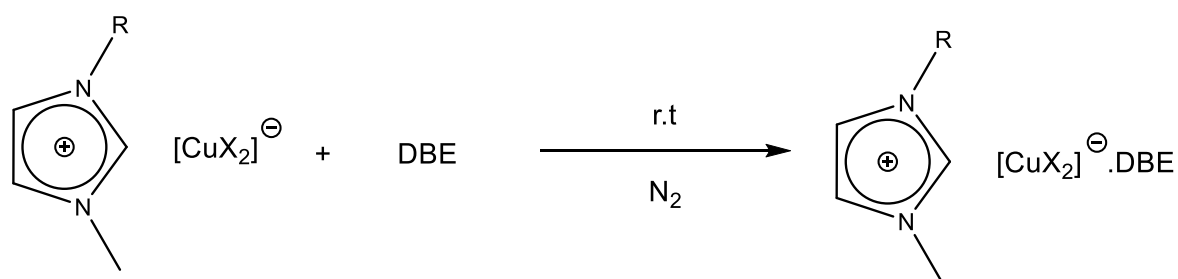
**Table 6.1.** Selected relevant properties of dimethyl malonate and dimethyl glutarate under standard temperature and pressure.<sup>1-4</sup>

Dibasic Ester	Boiling Point / °C	Viscosity / mPa.s	Molecular Weight / g mol <sup>-1</sup>	Density / g cm <sup>-3</sup>
Dimethyl Glutarate	214	2.75	160.17	1.09
Dimethyl Malonate	181	1.8	132.11	1.15

## 6.2 Copper Containing Ionic Liquid / Dibasic Ester Co-Solvent Mixtures

### 6.2.1 Synthesis and Copper Stability

Scheme 6.1 shows how the preparation of the copper-containing IL/DBE mixtures was performed by mixing a 1:1 molar ratio of the two liquids at room temperature under N<sub>2</sub> for 1 hour until a homogeneous solution was formed.

**Scheme 6.1.** Synthesis of copper-containing IL/DBE mixtures where R = C<sub>6</sub>H<sub>13</sub>, Et and X = Br, OAc, CF<sub>3</sub>CO<sub>2</sub>, OTf or NTf<sub>2</sub>

In most cases, the two liquids were miscible and the homogeneous mixture formed quickly. The only exception was [C<sub>2</sub>mim][CuBr<sub>2</sub>] which was immiscible with both DBEs, even when longer stirring times and higher temperatures were implemented. When X = OAc or TFA, the IL was miscible with the DBEs and formed low viscosity mixtures. However, properties such as density or viscosity were difficult to measure due to air sensitivity. Of the IL/DBE mixtures that were stable enough to be taken forward to further study, <sup>1</sup>H, <sup>13</sup>C and <sup>19</sup>F NMR analysis was consistent with a 1:1 mixture of each component. Furthermore, mass spectrometry gave the same main ES<sup>+</sup> and ES<sup>-</sup> peaks, as observed for the neat ILs.

The systems that were miscible remained the same colour as the parent IL and showed no evidence of oxidation, as long as they were kept under an inert atmosphere. Oxidation occurred when exposed to air, at a rate similar to that of the neat IL. Addition of the co-solvent resulted in a significant decrease in viscosity compared to the neat ILs. Quantitative viscosity measurements will be discussed in section 6.2.3.

Mixtures with higher ratios of copper were also investigated to determine whether it was possible to achieve higher copper loading without decomposition of the copper(I) salt. Up to two equivalents of the corresponding copper(I) salt could be incorporated into a mixture without degradation of the copper(I) species.

### 6.2.2 Density Measurements

Table 6.2 gives the density of each mixture measured at 20 °C and the calculated copper concentration. Unsurprisingly, the densities of the mixtures are lower than those of the parent ILs. Rather than being an average of the two component densities, the mixtures have densities that are closer to that of the neat IL rather than the DBE.

**Table 6.2.** Densities of neat IL and IL/DBE mixtures at 293 K.

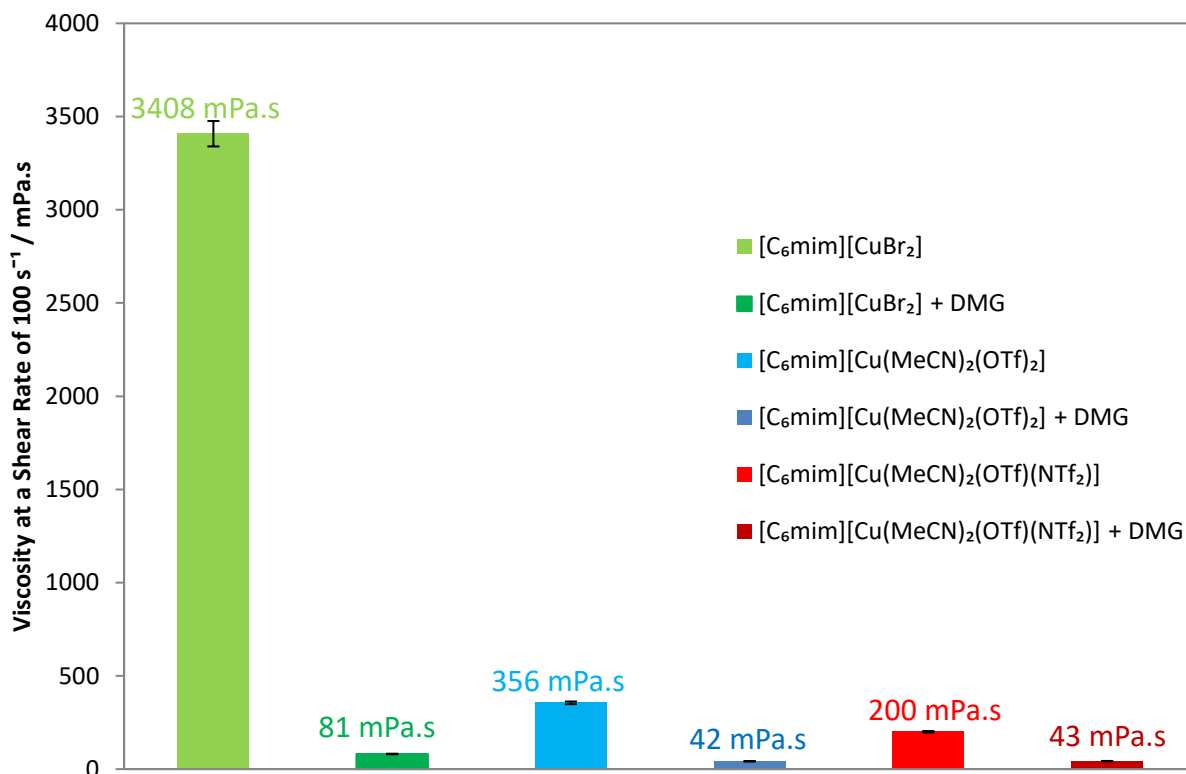
Ionic Liquid	Copper Equivalents	Co-solvent	Density, $\rho$ / g cm <sup>-3</sup>	Calculated [Cu] / M
[C <sub>6</sub> mim]Br	1	-	1.65	4.2
[C <sub>6</sub> mim]Br	1	DMG	1.39	2.5
[C <sub>6</sub> mim]Br	2	DMG	1.63	4.7
[C <sub>6</sub> mim]Br	1	DMM	1.43	2.7
[C <sub>6</sub> mim]OTf	1	-	1.40	2.5
[C <sub>6</sub> mim]OTf	1	DMG	1.29	1.8
[C <sub>6</sub> mim]OTf	2	DMG	1.47	3.0
[C <sub>6</sub> mim]OTf	1	DMM	1.35	1.9
[C <sub>2</sub> mim]NTf <sub>2</sub>	1	-	1.60	2.5
[C <sub>2</sub> mim]NTf <sub>2</sub>	1	DMG	1.42	1.7
[C <sub>2</sub> mim]NTf <sub>2</sub>	1	DMM	1.50	2.0
[C <sub>6</sub> mim]NTf <sub>2</sub>	1	-	1.50	2.1
[C <sub>6</sub> mim]NTf <sub>2</sub>	1	DMG	1.38	1.6
[C <sub>6</sub> mim]NTf <sub>2</sub>	2	DMG	1.40	2.5
[C <sub>6</sub> mim]NTf <sub>2</sub>	1	DMM	1.41	1.7

When 'cutting' the IL with a co-solvent it was inevitable that the copper concentration would be lowered. However, copper concentrations (calculated from the measured density) are comparable to that reported for the COSORB process ( $[\text{Cu}] \sim 1.7 \text{ M}$ ), which is encouraging.<sup>5</sup> Adding a second equivalent of the appropriate copper(I) source allowed the copper concentration to surpass that of the neat IL. Although this did noticeably increase the viscosity, it remained qualitatively low, and less than that of the neat IL system. Quantitative viscosity measurements will be discussed in section 6.2.3.

Given that DMM has a lower molecular weight and a higher density compared to DMG, it was expected that 1:1 mixtures of IL with DMM would give higher copper concentrations. In all cases, the IL / DMM mixtures gave slightly higher copper concentrations compared to the analogous DMG systems.

### 6.2.3 Viscosity Measurements

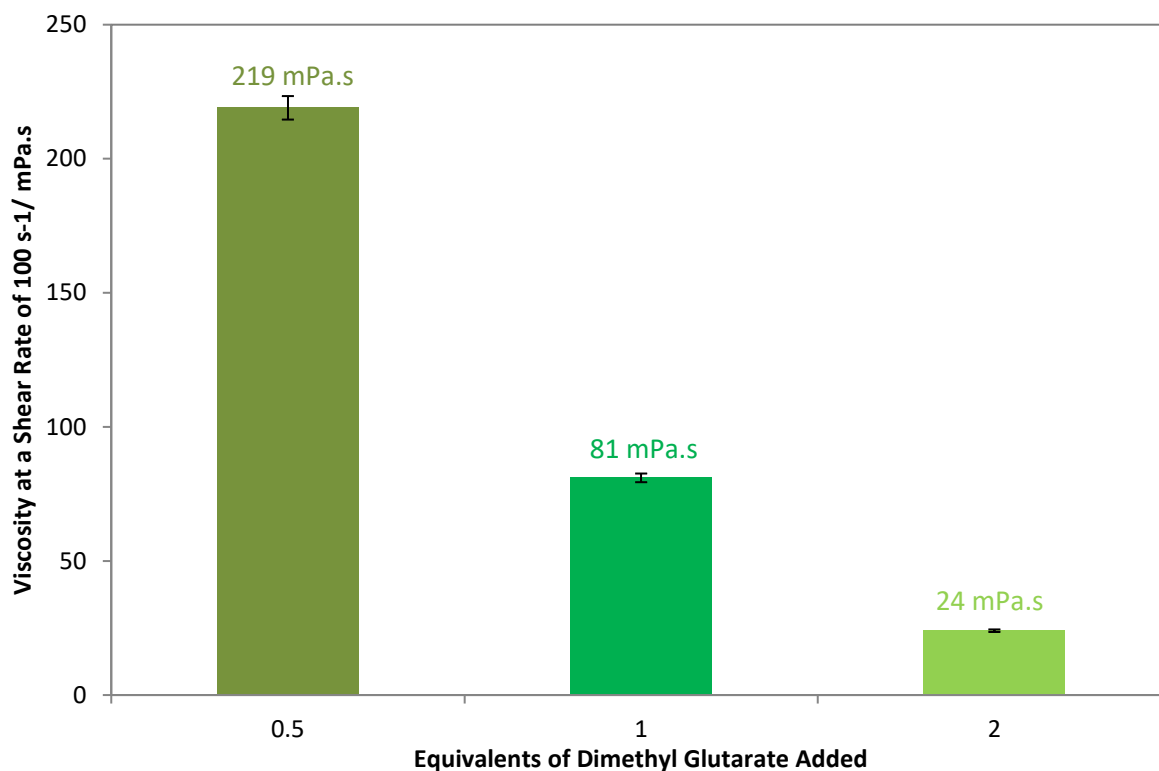
The viscosities of the IL/DBE mixtures were measured in the same manner as described in chapter 3. Figure 6.2 shows the dramatic reduction in viscosity on addition of one equivalent of DMG to three copper-containing ILs. Regardless of the starting viscosity of the neat liquid, the viscosity of the mixture is lowered to a value which is closer to the viscosity of that of DMG,  $\eta = 2.75 \text{ mPa}\cdot\text{s}$ , rather than that of the IL.



**Figure 6.2.** Viscosities of various ILs and IL/DMG mixtures at a shear rate of  $100 \text{ s}^{-1}$  and 298 K when adding 1 mole equivalent of dimethylglutarate.

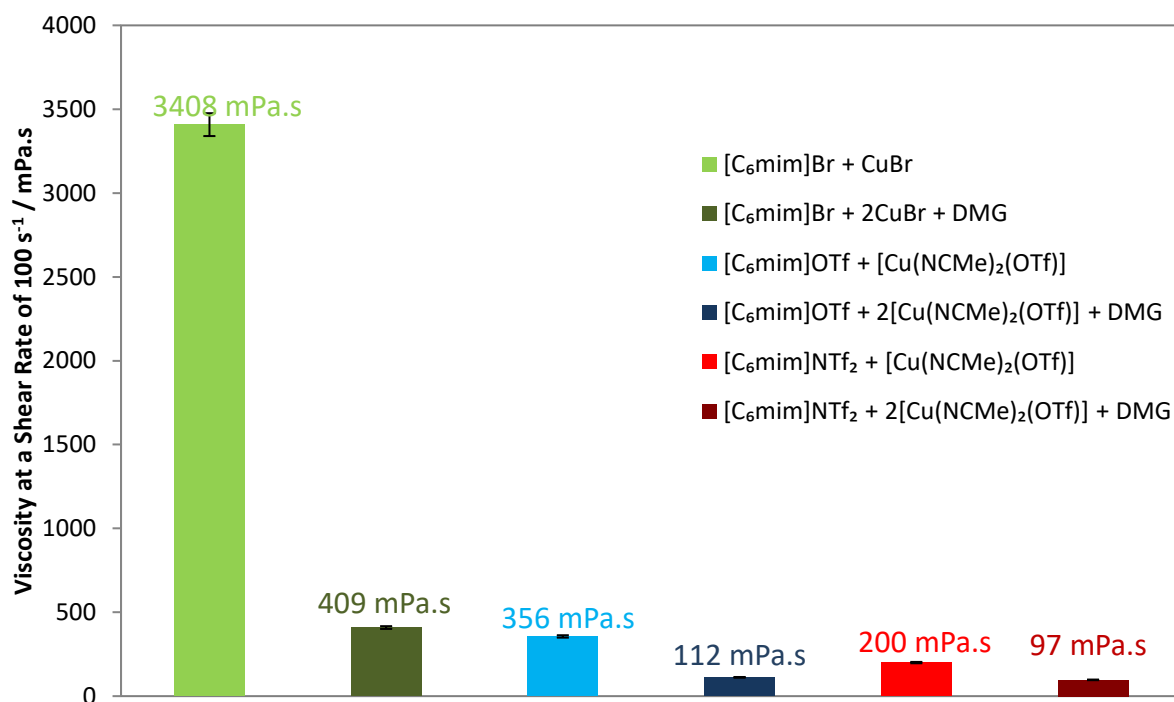
The observation that the lower viscosity component, in this case DMG, has the dominating effect on overall viscosity is one that has been reported in the literature, albeit for hydrocarbons. Gambill *et al.* proposed a model that had good agreement with experiment which states that the cube root of the kinematic viscosity is additive.<sup>6</sup> This implies that the lower viscosity component has a larger effect in a mixture, consistent with the results in Figure 6.2.

Addition of a second equivalent of DMG lowered the viscosity further as shown in Figure 6.3. This demonstrates that these co-solvent systems can achieve viscosities close to that required in an industrial process.

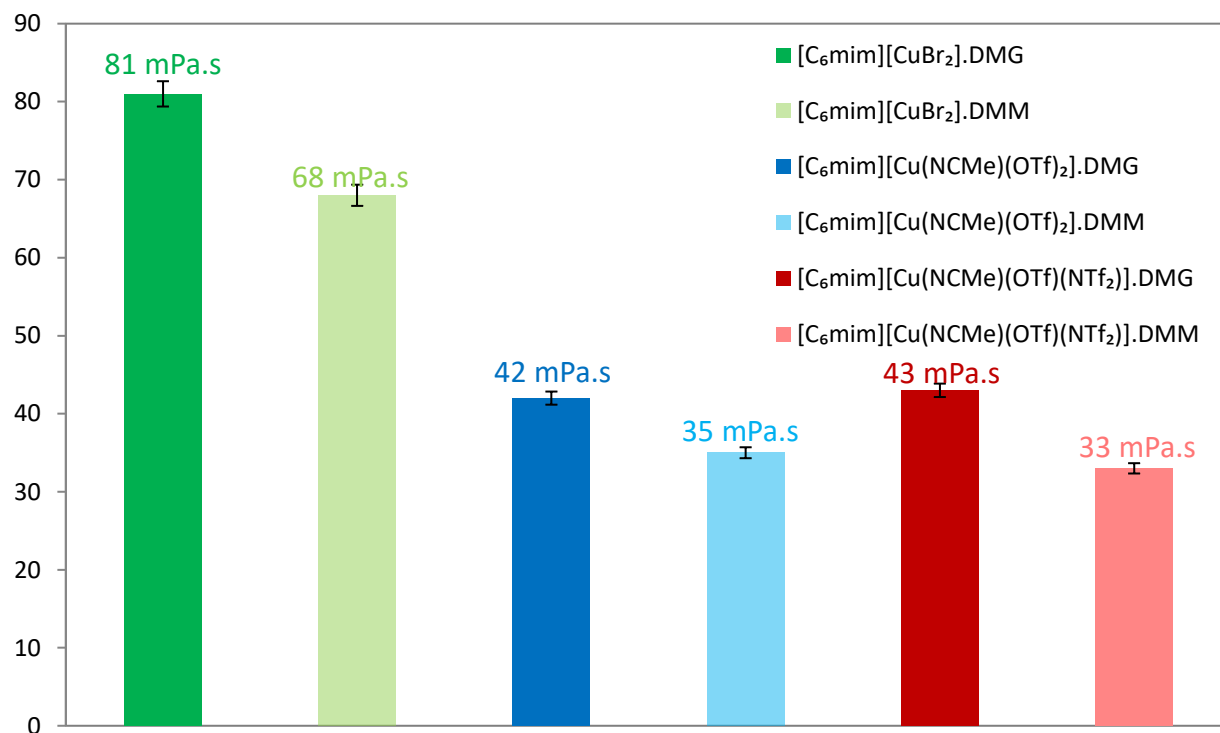


**Figure 6.3.** Viscosities of various [C<sub>6</sub>mim][CuBr<sub>2</sub>]/DMG systems at a shear rate of 100 s<sup>-1</sup> and 298 K

Although reducing the viscosity is important, introducing a co-solvent will lower the copper concentration. In section 6.2.2, it was observed that a second equivalent of copper can be incorporated to increase the copper concentration, but this resulted in an increase in viscosity. The data in Figure 6.4 confirm this but show that the viscosity is still low relative to the neat IL. Consequently, by combining different ratios of DMG and copper(I) salt, solutions could be tailored to give optimum viscosity and copper concentration. Figure 6.5 shows that lower viscosities can be obtained by addition of 1 equivalent of DMM rather than DMG to the ILs, as expected since DMM possesses a lower viscosity than DMG.

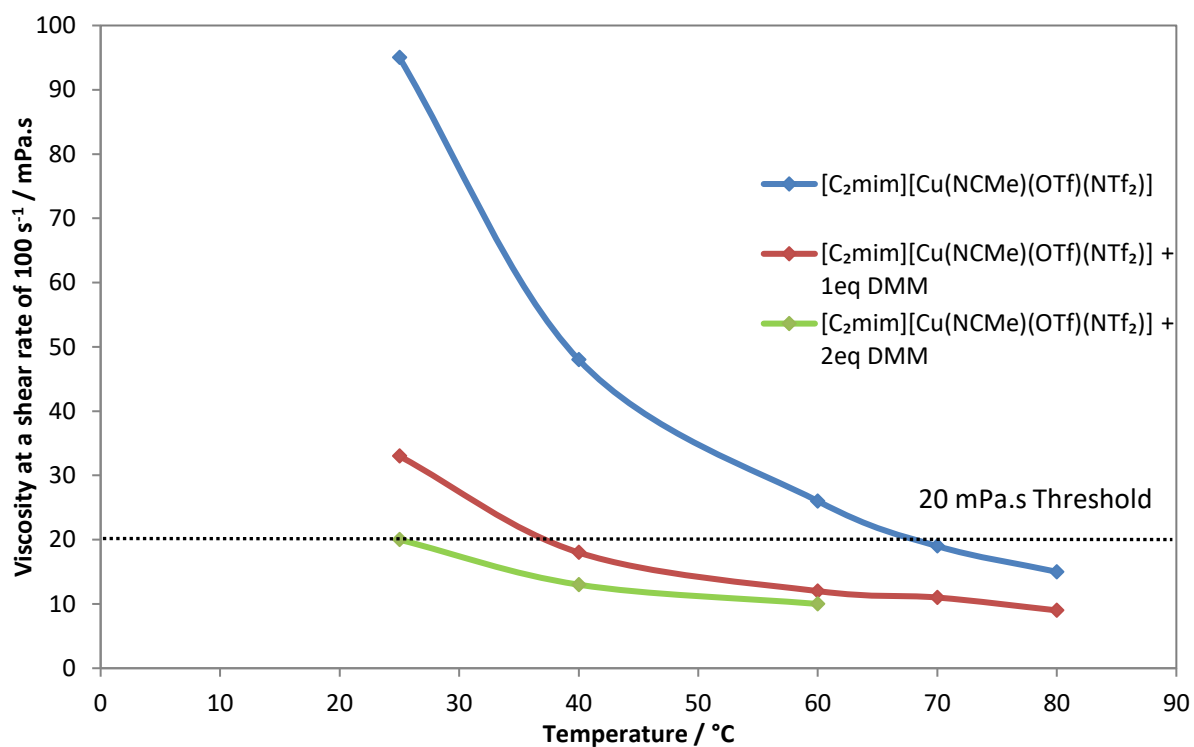


**Figure 6.4.** Viscosities of various neat [C<sub>6</sub>mim] copper containing IL compared with [C<sub>6</sub>mim]X/DMG mixtures with 2 mole equivalents of the corresponding copper(I) source at a shear rate of 100 s<sup>-1</sup> and 298 K where green = Br; blue = OTf; red = NTf<sub>2</sub>



**Figure 6.5.** Viscosities of various IL/DMM and IL/DMG mixtures at a shear rate of 100 s<sup>-1</sup> and 298 K when adding 1 mole equivalent of the appropriate DBE.

Different combinations of temperature and solvent dilution were investigated for  $[\text{C}_2\text{mim}][\text{Cu}(\text{NCMe})(\text{OTf})(\text{NTf}_2)]$ , with DMM as the co-solvent, as this combination gave the lowest overall preliminary viscosity of 30 mPa.s. Figure 6.6 that viscosity decreases with increasing temperature and DMM content, as would be expected.



**Figure 6.6.** Viscosities of various  $[\text{C}_2\text{mim}][\text{Cu}(\text{NCMe})(\text{OTf})(\text{NTf}_2)]/\text{DMM}$  mixtures at various temperatures at a shear rate of  $100 \text{ s}^{-1}$ .

#### 6.2.4 Low-Pressure CO Reactions

To determine whether the co-solvent systems were able to absorb CO, the samples were subjected to a stream of CO for a few minutes and a thin-film IR spectrum taken to check the presence of a  $\nu(\text{CO})$  absorption. The results are shown in Table 6.3 along with the  $\nu(\text{CO})$  values for the corresponding neat ILs.

**Table 6.3.** IR spectroscopic data for Cu(CO) species formed on reaction of 1 atm CO with [C<sub>n</sub>mim][CuX<sub>2</sub>].DBE mixtures

Ionic Liquid	Copper Equivalents	Co-solvent	$\nu(\text{CO}) / \text{cm}^{-1}$
[C <sub>6</sub> mim]Br	1	-	2081
[C <sub>6</sub> mim]Br	1	DMG	2080
[C <sub>6</sub> mim]Br	2	DMG	2093
[C <sub>6</sub> mim]Br	1	DMM	2081
[C <sub>6</sub> mim]OTf	1	-	2114
[C <sub>6</sub> mim]OTf	1	DMG	2114
[C <sub>6</sub> mim]OTf	1	DMM	2114
[C <sub>2</sub> mim]NTf <sub>2</sub>	1	-	2122
[C <sub>2</sub> mim]NTf <sub>2</sub>	1	DMG	2122
[C <sub>2</sub> mim]NTf <sub>2</sub>	1	DMM	2122
[C <sub>6</sub> mim]NTf <sub>2</sub>	1	-	2122
[C <sub>6</sub> mim]NTf <sub>2</sub>	1	DMG	2122
[C <sub>6</sub> mim]NTf <sub>2</sub>	1	DMM	2122

Formation of a copper carbonyl was observed in all the co-solvent systems mixtures and the position of the  $\nu(\text{CO})$  absorption was the same as for the neat IL, suggesting that the interaction of the solvent with the copper species is negligible. An appreciably higher  $\nu(\text{CO})$  is seen for the [C<sub>6</sub>mim]Br system with two equivalents of CuBr added. In this scenario, the copper speciation is thought to be [Cu<sub>2</sub>Br<sub>3</sub>]<sup>-</sup> rather than [CuBr<sub>2</sub>]<sup>-</sup> as discussed in chapter 1.

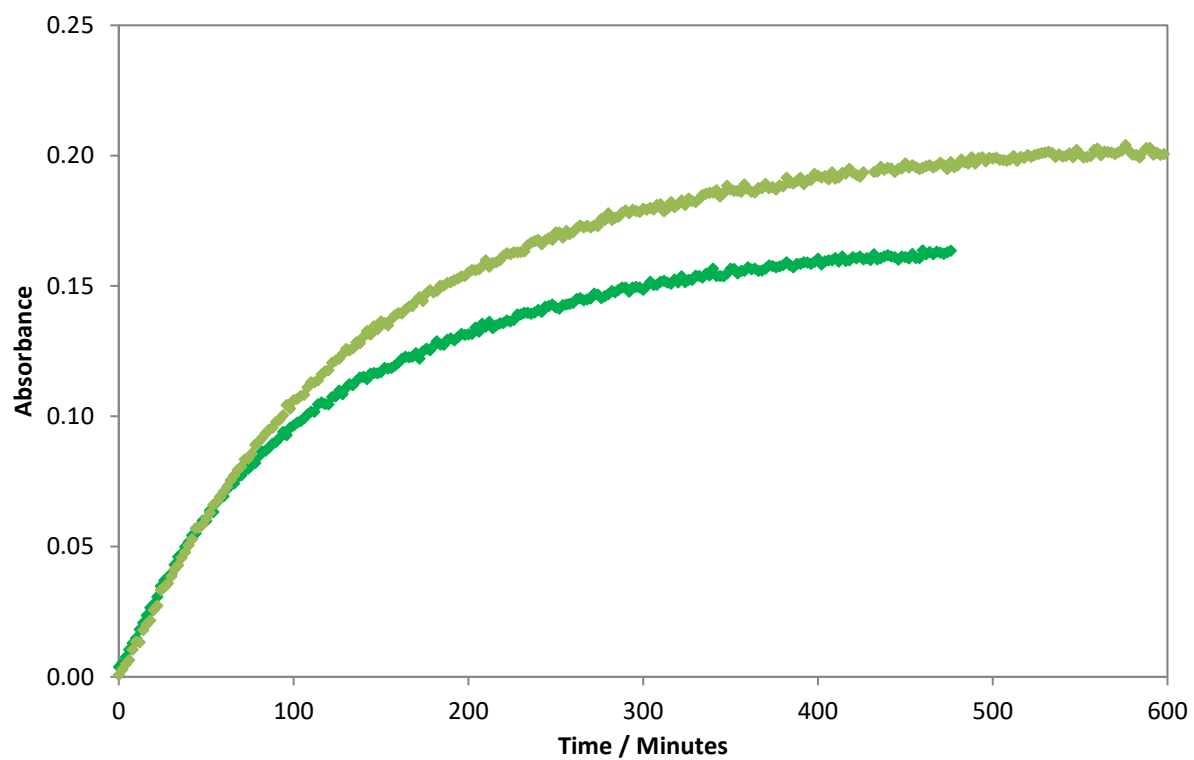
### 6.2.5 *In Situ* High-Pressure Infrared Studies

Absorption of CO by the copper(I)-containing IL/co-solvent mixtures at elevated pressure was monitored by *in situ* high-pressure infra-red (HPIR) spectroscopy using the cylindrical internal reflectance (CIR) cell,<sup>7,8</sup> allowing the effects of CO pressure, temperature, and the rate of gas/liquid mixing to be probed as described in chapter 3. These results were then compared against each other as well as the 'neat' IL systems.

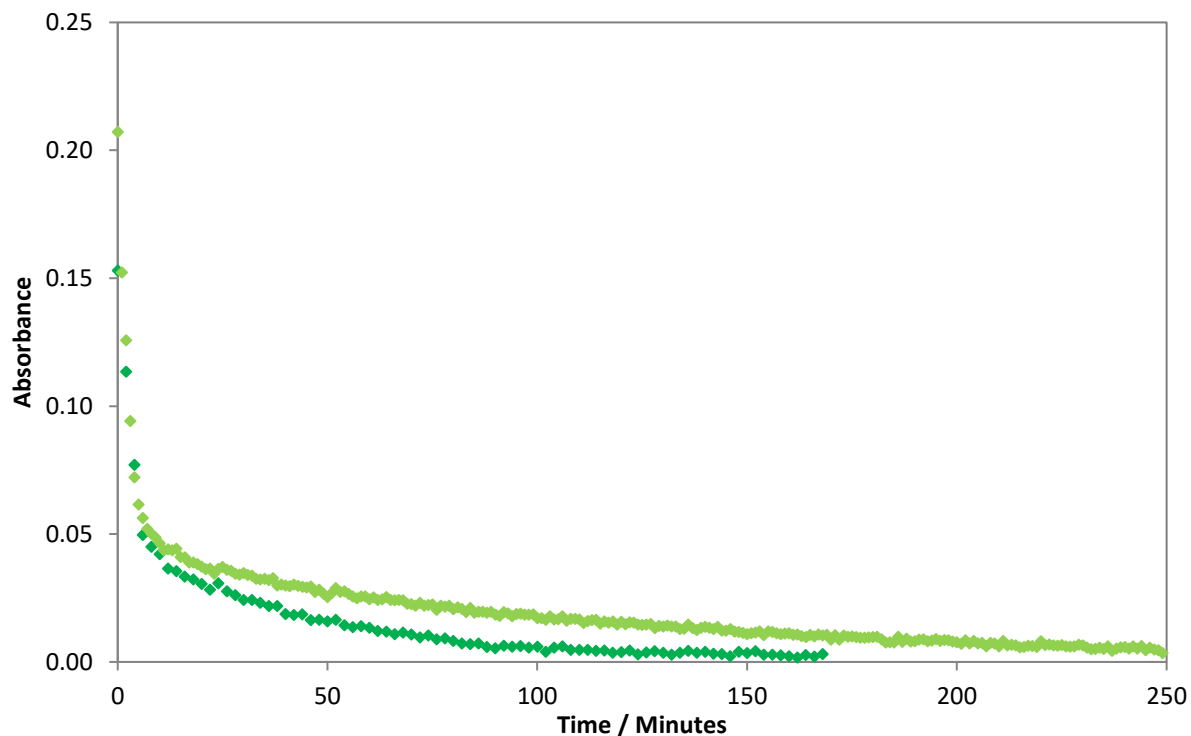
#### [C<sub>6</sub>mim][CuBr<sub>2</sub>] vs [C<sub>6</sub>mim][CuBr<sub>2</sub>].DMG

A sample of [C<sub>6</sub>mim][CuBr<sub>2</sub>].DMG was loaded into the CIR cell and subjected to a range of CO pressures. Figure 6.7 compares plots of the growth of the  $\nu(\text{CO})$  band under 3 bar CO pressure for this mixed system and neat [C<sub>6</sub>mim][CuBr<sub>2</sub>]. The initial rates over the first 50 minutes are almost identical for both samples which shows that the introduction of DMG does not hinder the uptake of CO. As time progressed, however, the  $\nu(\text{CO})$  intensity reached a higher equilibrium position for [C<sub>6</sub>mim][CuBr<sub>2</sub>], which is expected as it has a higher copper concentration (Table 6.2).

Given that the equilibrium absorbance of the mixed system is about 80 % that of the neat IL [C<sub>6</sub>mim][CuBr<sub>2</sub>] and the copper concentration is about 60 %, this suggests that the percentage of copper sites occupied for the co-solvent system is higher.



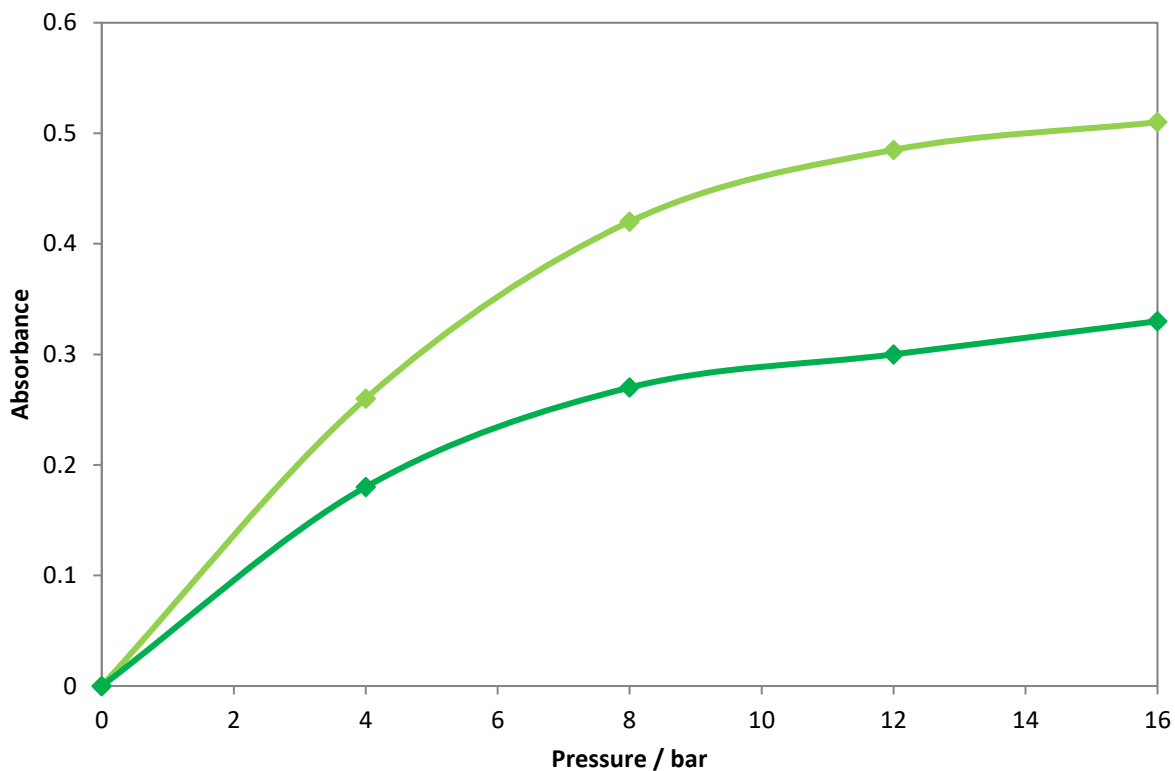
**Figure 6.7.** Absorbance vs time plot showing the growth of the  $\nu(\text{CO})$  band at a given wavenumber when  $[\text{C}_6\text{mim}][\text{CuBr}_2]$  = green;  $[\text{C}_6\text{mim}][\text{CuBr}_2].\text{DMG}$  = dark green was exposed to 3 bar CO pressure at 298 K and at a stir rate of 214 rpm



**Figure 6.8.** Absorbance vs time plot showing the decay of the  $\nu(\text{CO})$  band at a given wavenumber when  $[\text{C}_6\text{mim}][\text{CuBr}_2]$  = green;  $[\text{C}_6\text{mim}][\text{CuBr}_2].\text{DMG}$  = dark green was heated to 40 °C and purged with  $\text{N}_2$  at a stir rate of 214 rpm.

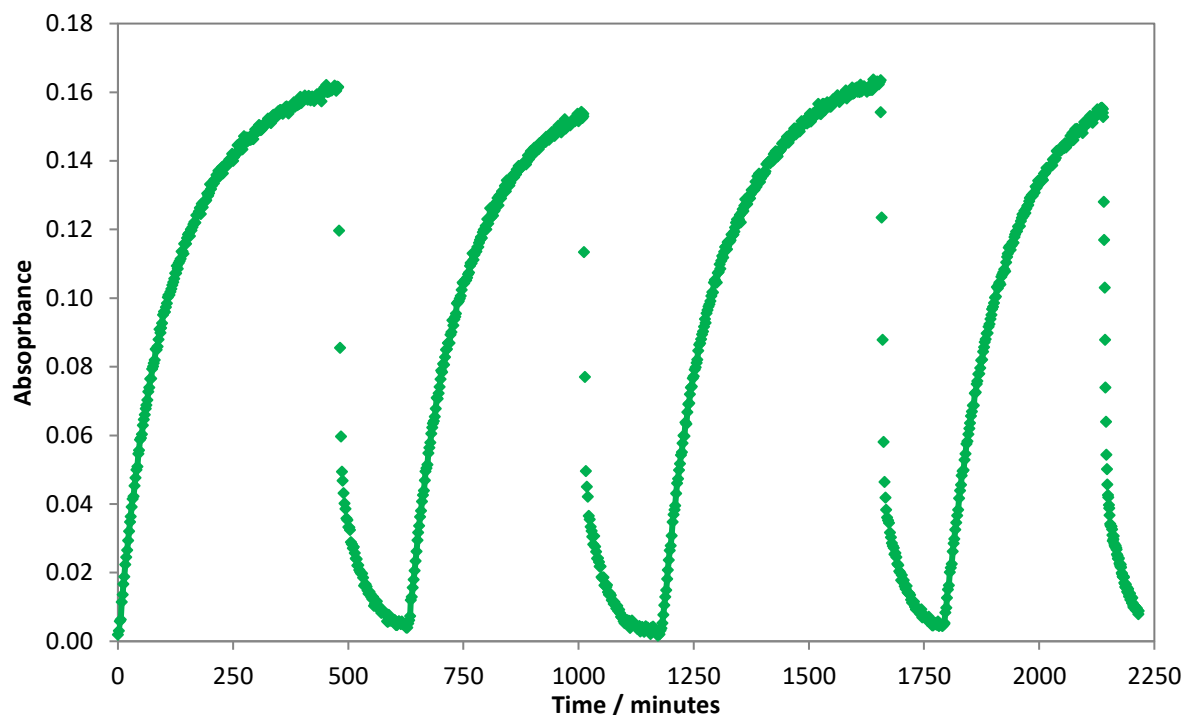
Figure 6.8 shows the decay of the  $\nu(\text{CO})$  intensity on heating each sample to 40 °C and purging with  $\text{N}_2$ . It was found that the bound CO was removed at similar rates which shows that the introduction of the DMG does not hinder CO desorption. About 80 % of the bound CO at equilibrium could be desorbed at this mild temperature in as little as 10 minutes. Moreover, the co-solvent system does appear to desorb the bound CO completely in a shorter time.

Figure 6.9 shows that at a given CO pressure, the equilibrium  $\nu(\text{CO})$  absorbance is lower for the co-solvent mixture compared to the neat IL. This is expected, due to the lower copper concentration of the former.



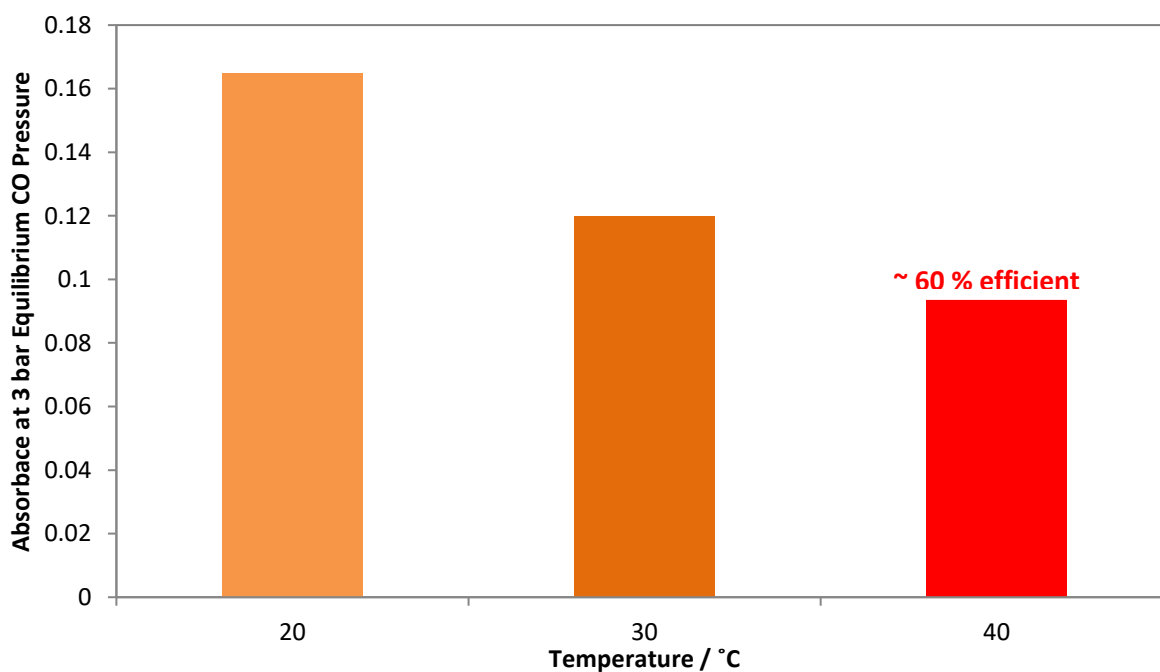
**Figure 6.9.** Plot of equilibrium  $\nu(\text{CO})$  intensity against pressure of CO for  $[\text{C}_6\text{mim}][\text{CuBr}_2]$  = green;  $[\text{C}_6\text{mim}][\text{CuBr}_2].\text{DMG}$  = dark green

As a large scale process would need to work over multiple cycles and for a long period of time, it was important to examine the stability of the co-solvent system. Figure 6.10 shows a plot of the IR data for four successive absorption/desorption cycles, demonstrating good reversibility and reproducibility. In other experiments, it was shown that a sample could be subjected to different CO pressures and desorption temperatures for up to a month with no significant change in CO absorption behaviour.



**Figure 6.10.** Absorbance vs time plot showing the growth and decay of the  $\nu(\text{CO})$  band at  $2081\text{ cm}^{-1}$  of a sample of  $[\text{C}_6\text{mim}][\text{CuBr}_2].\text{DMG}$ . The absorption cycles were done by exposing the sample to 3 bar CO pressure and the desorption cycles were done by heating the sample up to  $40\text{ }^\circ\text{C}$  and purging with  $\text{N}_2$  with all runs done at a stir rate of 214 rpm.

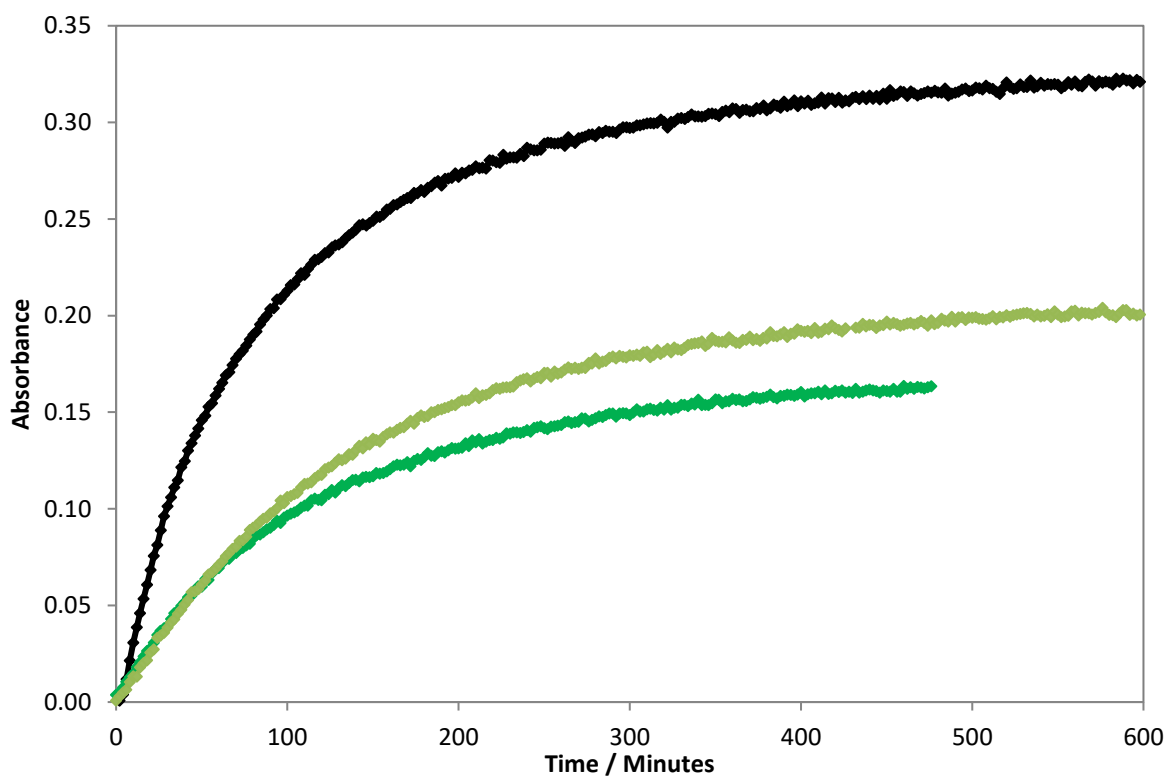
Figure 6.11 shows the equilibrium absorbance at temperatures ranging from  $20\text{ }^\circ\text{C}$  –  $40\text{ }^\circ\text{C}$ . The data suggest that about 40 % less CO was absorbed at  $40\text{ }^\circ\text{C}$  than at  $20\text{ }^\circ\text{C}$ .



**Figure 6.11.** Equilibrium absorbances of  $[\text{C}_6\text{mim}][\text{CuBr}_2].\text{DMG}$  at 3 bar CO pressure and a given temperature.

### Higher Copper Equivalentents

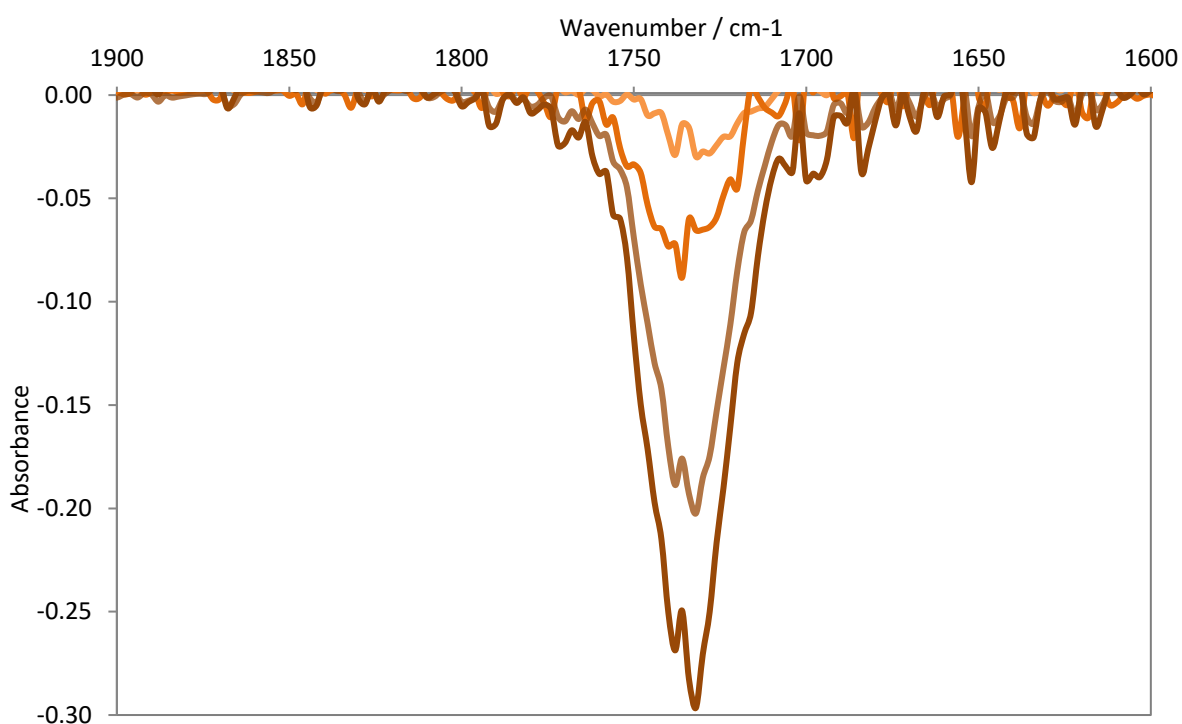
High-pressure infrared spectroscopy was used to probe the co-mixtures with higher copper ratios. Figure 6.12 shows the initial uptake of CO by the Br systems compared at 3 bar CO pressure. Assuming the extinction coefficients do not vary too much, it appears that the  $[\text{C}_6\text{mim}][\text{Cu}_2\text{Br}_3].\text{DMG}$  system has a quicker rate of CO uptake compared to the neat system even though their copper concentrations are quite similar (Table 6.2). Moreover, the equilibrium position is much higher, indicating that this system has the potential to absorb more CO



**Figure 6.12.** Absorbance vs time plot showing the growth of the  $\nu(\text{CO})$  band at a given wavenumber when  $[\text{C}_6\text{mim}][\text{CuBr}_2] =$  green;  $[\text{C}_6\text{mim}][\text{CuBr}_2].\text{DMG} =$  dark green;  $[\text{C}_6\text{mim}][\text{Cu}_2\text{Br}_3].\text{DMG} =$  black was exposed to 3 bar CO pressure at 298 K and at a stir rate of 214 rpm.

### Loss of Dibasic Esters on Desorption

Although dimethylglutarate has a high boiling point, it is still relatively volatile when compared to ILs. Figure 6.13 illustrates how during HPIR runs it was common to see negative absorptions at  $1732\text{ cm}^{-1}$  and  $1738\text{ cm}^{-1}$  after multiple desorption cycles, explained by loss of DMG from the solvent mixture.



**Figure 6.13.** Series of IR spectra showing the loss of DMG from  $[\text{C}_6\text{mim}][\text{CuBr}_2]\cdot\text{DMG}$  co-mixture over many desorption cycles during a month period.

In order to determine how much DBE was being lost during desorption cycles, a sample of  $[\text{C}_6\text{mim}][\text{CuBr}_2]\cdot\text{DMG}$  or  $[\text{C}_6\text{mim}][\text{CuBr}_2]\cdot\text{DMM}$  was heated at various temperatures and periods of time while a stream of  $\text{N}_2$  was bubbled through it. The sample was weighed before and after the

experiment and the mass difference was assumed to be the loss of DBE. This was reasonable since any loss of IL under these conditions should be negligible as they are considered non-volatile.

**Table 6.4.** Loss of DBE at different temperatures after 24 hours.

Temperature / °C	Time / Hours	Percentage Mass Loss of	Percentage Mass Loss of
		DMM/ %	DMG/ %
40	24	13	3
60	24	26	11
80	24	40	19
100	24	65	37
120	24	87	54
140	24	97	81

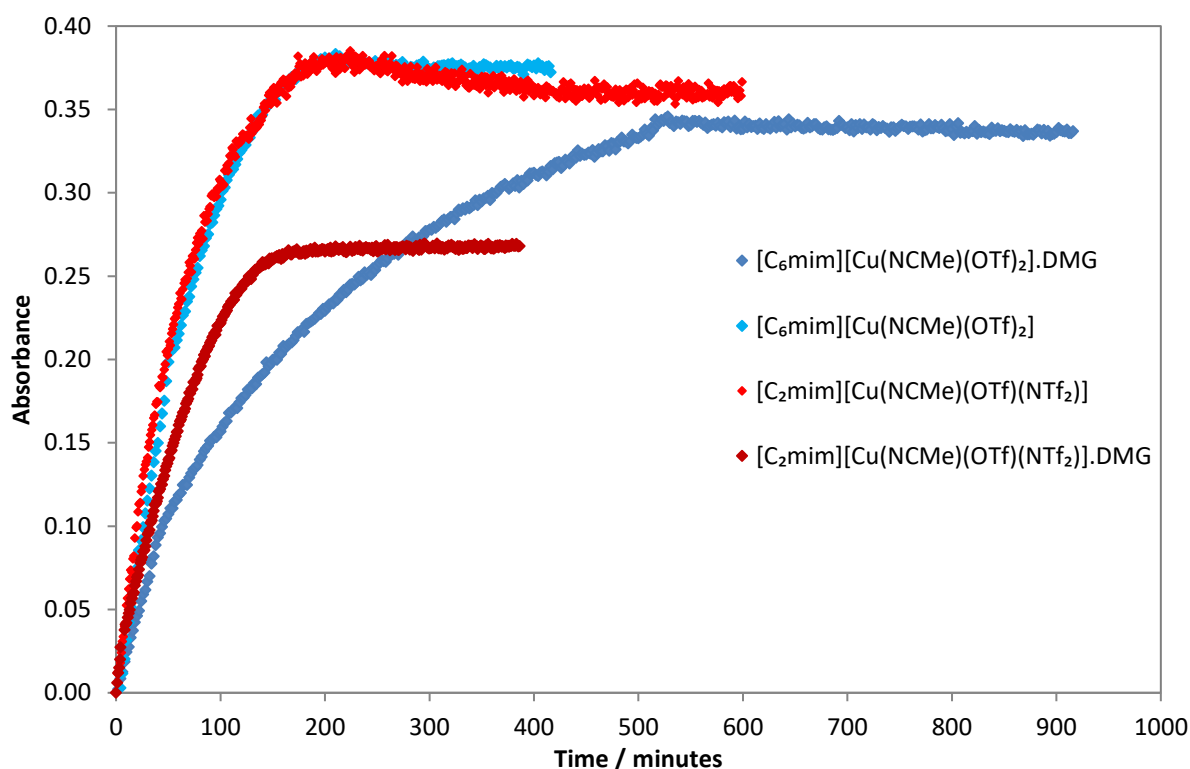
The amount of DBE lost after 24 hours was noticeable, however, in practice desorption times will be much less than 24 hours so loss should be negligible. DMM has a higher vapour pressure so the higher percentage loss observed for DMM mixtures was expected.

#### **[C<sub>n</sub>mim][Cu(NCMe)(OTf)(X)] vs [C<sub>n</sub>mim][Cu(NCMe)(OTf)(X)].DMG co-mixtures**

Figure 6.14 shows in situ high pressure IR data during absorption of CO by the [C<sub>n</sub>mim][Cu(NCMe)(OTf)(X)].DMG systems and the respective neat ILs. The uptake of CO was found to be reversible and could be run over multiple cycles without loss of efficiency in both cases (See appendix 8.2). For example, the reversibility of CO from a sample of

$[\text{C}_2\text{mim}][\text{Cu}(\text{NCMe})(\text{OTf})(\text{NTf}_2)]\cdot\text{DMM}$  was investigated over a period of two months without any notable change in CO absorption behaviour.

The rate of CO uptake for  $[\text{C}_6\text{mim}][\text{Cu}(\text{NCMe})(\text{OTf})_2]\cdot\text{DMG}$  was slightly slower than in the neat IL system however the position of the equilibrium absorbance was similar. The  $\text{NTf}_2$  system has rates of CO uptake which were comparable, but the  $[\text{C}_2\text{mim}][\text{Cu}(\text{NCMe})(\text{OTf})(\text{NTf}_2)]\cdot\text{DMG}$  reached a lower equilibrium absorbance compared to the neat IL.

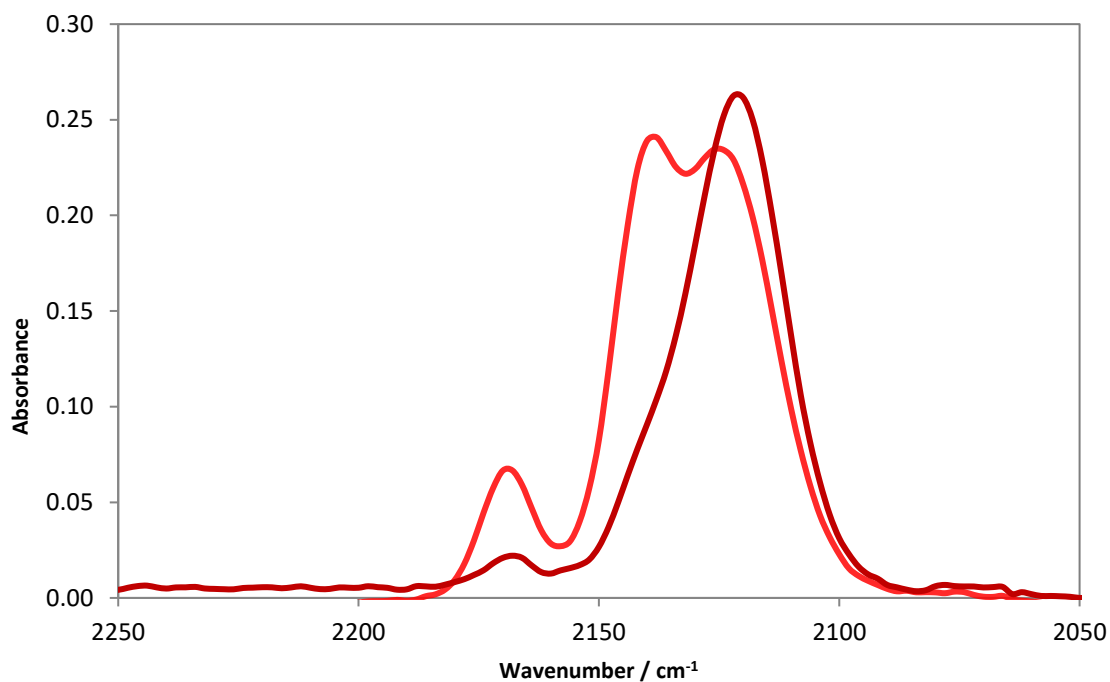


**Figure 6.14.** Absorbance vs time plot showing the growth of the  $\nu(\text{CO})$  band at a given wavenumber when blue =  $[\text{C}_6\text{mim}][\text{Cu}(\text{NCMe})(\text{OTf})_2]$ ; dark blue =  $[\text{C}_6\text{mim}][\text{Cu}(\text{NCMe})(\text{OTf})_2]\cdot\text{DMG}$ ; red =  $[\text{C}_2\text{mim}][\text{Cu}(\text{NCMe})(\text{OTf})(\text{NTf}_2)]$  and dark red =  $[\text{C}_2\text{mim}][\text{Cu}(\text{NCMe})(\text{OTf})(\text{NTf}_2)]\cdot\text{DMG}$  was exposed to 4 bar CO pressure at 298 K and at a stir rate of 214 rpm.

Overall the  $[\text{C}_6\text{mim}][\text{Cu}(\text{NCMe})(\text{OTf})_2]\cdot\text{DMG}$  mixture behaved similarly to the neat IL. The equilibrium absorbances at a given pressure for the  $\nu(\text{CO})$  band at  $2114\text{ cm}^{-1}$ , were similar in the neat and mixed systems. Moreover, there were signals in the IR at  $2136\text{ cm}^{-1}$  and  $2168\text{ cm}^{-1}$  consistent with the

formation of copper dicarbonyl (Both observations are found in appendix 8.2). The amount of dicarbonyl formed in  $[\text{C}_6\text{mim}][\text{Cu}(\text{NCMe})(\text{OTf})_2].\text{DMG}$  was low like in the neat IL system.

Figure 6.15 shows that dicarbonyl behaviour was also observed in  $[\text{C}_n\text{mim}][\text{Cu}(\text{NCMe})(\text{OTf})(\text{NTf}_2)].\text{DMG}$  mixtures at pressures as low as 4 bar CO.



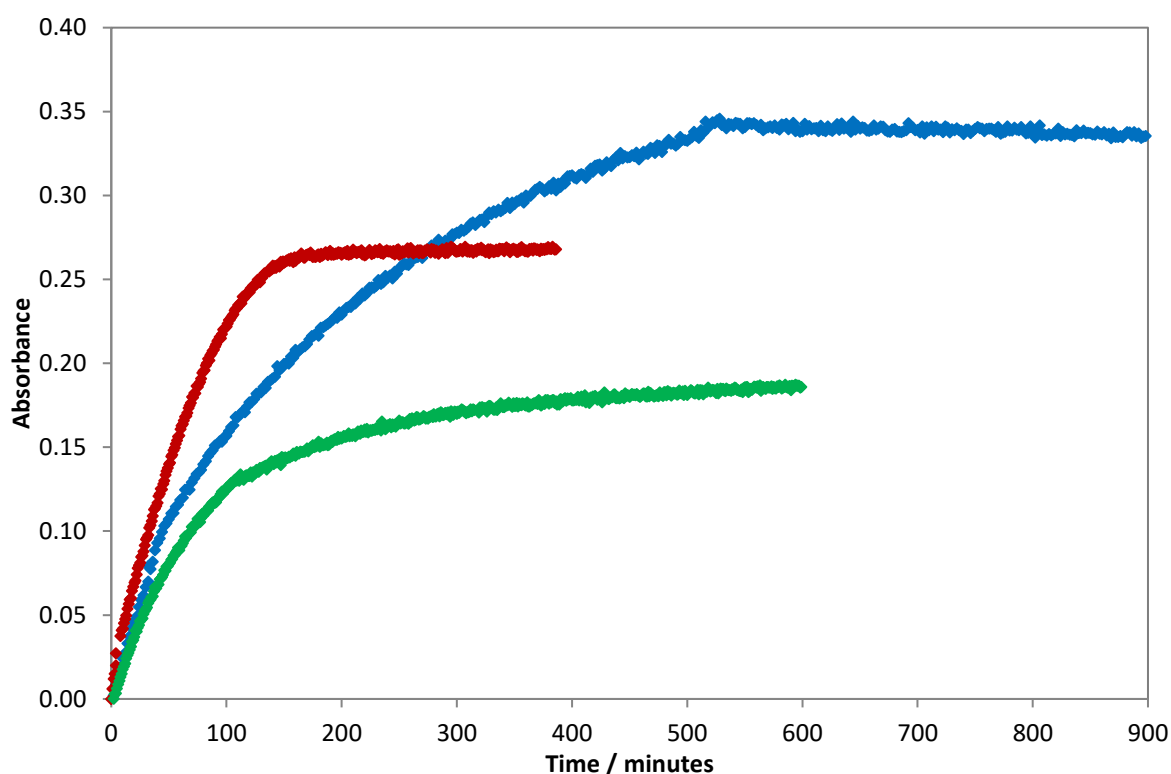
**Figure 6.15.** IR spectra of  $[\text{C}_2\text{mim}][\text{Cu}(\text{NCMe})(\text{OTf})(\text{NTf}_2)]$  with and without 1 equivalent of DMG at 12 bar CO pressure and 25 °C showing the extent of dicarbonyl formation. Where red =  $[\text{C}_2\text{mim}][\text{Cu}(\text{NCMe})(\text{OTf})(\text{NTf}_2)]$  and dark red =  $[\text{C}_2\text{mim}][\text{Cu}(\text{NCMe})(\text{OTf})(\text{NTf}_2)].\text{DMG}$ .

However, the introduction of DMG hinders formation of the dicarbonyl. Possible reasons for the hindrance could be the reduction of the physical solubility of CO into the solvent. Less CO in solution would result in less CO available to form the copper dicarbonyl.

The desorption conditions required to drive off CO from  $[\text{C}_n\text{mim}][\text{Cu}(\text{NCMe})(\text{OTf})(\text{X})].\text{DMG}$  mixtures was the same as that of the neat ILs. In the  $\text{NTf}_2$  systems, the required temperature was 100 °C and for the OTf systems 140 °C. Therefore, the lower temperature desorption would favour  $\text{NTf}_2$  mixtures due to the volatility of the DBE.

### 6.2.6 $[\text{C}_6\text{mim}][\text{CuBr}_2].\text{DMG}$ vs $[\text{C}_n\text{mim}][\text{Cu}(\text{NCMe})(\text{OTf})(\text{X})].\text{DMG}$ vs co-mixtures

The CO absorption behaviour observed for the co-solvent systems was generally very similar to that of the neat IL systems. The  $\text{Br}^-$  systems only ever produced a monocarbonyl whereas the  $\text{OTf}^-$  and  $\text{NTf}_2^-$  systems showed evidence for a dicarbonyl. Moreover, the rate of CO uptake followed the trend  $\text{Br}^- < \text{OTf}^- < \text{NTf}_2^-$  as shown in Figure 6.16. The DMG also did not affect the rate of desorption with the required temperature for full desorption being largely determined by the choice of anion.



**Figure 6.16.** Absorbance vs time plot showing the growth of the  $\nu(\text{CO})$  band at a given wavenumber when  $[\text{C}_6\text{mim}][\text{CuBr}_2].\text{DMG}$  = dark green  $[\text{C}_6\text{mim}][\text{Cu}(\text{NCMe})(\text{OTf})_2].\text{DMG}$  = dark blue;  $[\text{C}_2\text{mim}][\text{Cu}(\text{NCMe})(\text{OTf})(\text{NTf}_2)].\text{DMG}$  = dark red was exposed to 4 bar CO pressure at 298 K and at a stir rate of 214 rpm.

### 6.3 Enrichment Studies Using [C<sub>6</sub>mim][CuBr<sub>2</sub>].DMM Mixtures

Studies of CO enrichment from CO:N<sub>2</sub> and CO:H<sub>2</sub> mixtures were carried out using IL/DMM systems, in view of their lower viscosity and higher copper concentration. A disadvantage of DMM is its higher vapour pressure.

#### 6.3.1 CO Enrichment from CO/X<sub>2</sub>

Enrichment studies were conducted in the same manner as described in chapter 5. A 10 cm<sup>3</sup> sample of [C<sub>6</sub>mim][CuBr<sub>2</sub>].DMM was used to keep the amount of copper during separation studies at similar levels as for the neat systems. This sample was subjected to a 50:50 mixture of CO:N<sub>2</sub> or CO:H<sub>2</sub> until equilibrium was reached at 10 bar. The experiments were run numerous times and the mean enrichment values are shown in Table 6.5 as well as a comparison with the analogous 'neat' system (individual values in appendix 8.3).

**Table 6.5.** Enrichment results for [C<sub>6</sub>mim][CuBr<sub>2</sub>] and [C<sub>6</sub>mim][CuBr<sub>2</sub>].DMM at 10 bar 50:50 CO:N<sub>2</sub> or CO:H<sub>2</sub> gas mixture

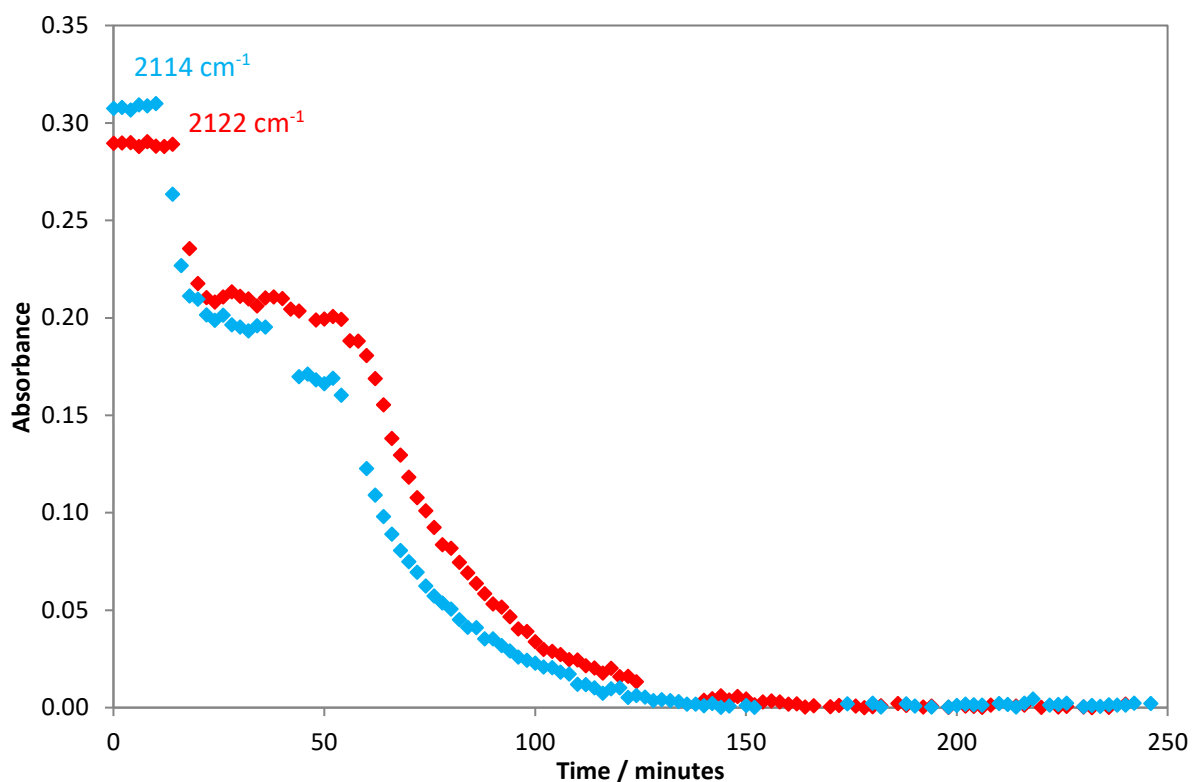
	X <sub>2</sub>	Mean CO % in Headspace	Mean CO % After Enrichment (measured)	Actual CO % Absorbed (normalised)
[C <sub>6</sub> mim][CuBr <sub>2</sub> ]	N <sub>2</sub>	33 ± 3	91 ± 1	>99 ± 1
[C <sub>6</sub> mim][CuBr <sub>2</sub> ].DMM	N <sub>2</sub>	31 ± 1	88 ± 1	99 ± 1
[C <sub>6</sub> mim][CuBr <sub>2</sub> ]	H <sub>2</sub>	40 ± 0	85 ± 3	94 ± 3
[C <sub>6</sub> mim][CuBr <sub>2</sub> ].DMM	H <sub>2</sub>	36 ± 3	91 ± 3	99 ± 3

As for to the neat IL, one absorption/desorption cycle was sufficient to effectively enrich a 50:50 mixture of CO from either N<sub>2</sub> or H<sub>2</sub>, with the gas being liberated from the liquid being composed of 99 % CO. Table 6.5 shows that the results for the neat and mixed systems are similar to each other, even given the differences in the CO uptake (Figure 6.9).

## 6.4 CO Enrichment Using [C<sub>n</sub>mim][Cu(NCMe)(OTf)(X)].DMM Where X = OTf, NTf<sub>2</sub>

### 6.4.1 CO/X<sub>2</sub> Separations

As for [C<sub>6</sub>mim][CuBr<sub>2</sub>].DMM, 10 cm<sup>3</sup> of [C<sub>n</sub>mim][Cu(NCMe)(OTf)(X)].DMM was loaded into the CIR cell so the total amount of copper in the cell was similar to that in the neat IL experiments. During desorption of CO from the [C<sub>n</sub>mim][Cu(NCMe)(OTf)(X)].DMM mixture, 140 °C was again not sufficient to completely drive off all the absorbed CO whilst the cell was sealed. Therefore, samples were collected once equilibrium had been reached (Figure 6.17). However, the CO could be completely driven off at 140 °C in about 100 minutes if the cell was open.



**Figure 6.17.** Plot of the intensity of the monocarbonyl band vs time for IL/DMM under 50:50 CO:N<sub>2</sub>. The profile shows when the system was closed and heated to 140 °C and gas samples collected twice when equilibrium was reached. After 50 minutes the cell was heated to 140 °C whilst open to remove all the bound CO. Where red = [C<sub>2</sub>mim][Cu(NCMe)(OTf)(NTf<sub>2</sub>)].DMM and blue = [C<sub>6</sub>mim][Cu(NCMe)(OTf)<sub>2</sub>].DMM

The recorded headspace pressure upon desorption of CO:X<sub>2</sub> from [C<sub>n</sub>mim][Cu(NCMe)(OTf)(X)].DMM, showed that the amount of gas liberated was less than that for the neat IL. The results from the CO:N<sub>2</sub> and CO:H<sub>2</sub> separation experiments along with comparisons with the neat IL are shown in Table 6.6 and Table 6.7 respectively.

**Table 6.6.** Enrichment results for various IL and IL/DMM mixtures at 10 bar 50:50 CO:N<sub>2</sub> gas mixture.

Ionic Liquid		% CO		
		Headspace	After 1 <sup>st</sup>	After 2 <sup>nd</sup>
			Desorption	Desorption
[C <sub>2</sub> mim][Cu(NCMe)(OTf)(NTf <sub>2</sub> )]	Measured	10 ± 1	68 ± 3	79 ± 5
	Normalised	-	80 ± 3	90 ± 5
[C <sub>2</sub> mim][Cu(NCMe)(OTf)(NTf <sub>2</sub> ).DMM]	Measured	12 ± 2	55 ± 3	70 ± 3
	Normalised	-	68 ± 3	>99 ± 3
[C <sub>6</sub> mim][Cu(NCMe)(OTf) <sub>2</sub> ]	Measured	9 ± 2	70 ± 2	78 ± 5
	Normalised	-	87 ± 2	>99 ± 5
[C <sub>6</sub> mim][Cu(NCMe)(OTf) <sub>2</sub> .DMM]	Measured	10 ± 1	65 ± 0	80 ± 2
	Normalised	-	93 ± 0	>99 ± 2

**Table 6.7.** Enrichment results for [C<sub>2</sub>mim][Cu(NCMe)(OTf)(NTf<sub>2</sub>)] and [C<sub>2</sub>mim][Cu(NCMe)(OTf)(NTf<sub>2</sub>).DMM] at 10 bar 50:50 CO:H<sub>2</sub> gas mixture.

Ionic Liquid		% CO		
		Headspace	After 1 <sup>st</sup>	After 2 <sup>nd</sup>
			Desorption	Desorption
[C <sub>2</sub> mim][Cu(NCMe)(OTf)(NTf <sub>2</sub> )]	Measured	5 ± 1	58 ± 4	68 ± 3
	Normalised	-	71 ± 4	88 ± 3
[C <sub>2</sub> mim][Cu(NCMe)(OTf)(NTf <sub>2</sub> ).DMM]	Measured	12 ± 1	52 ± 1	70 ± 0
	Normalised	-	65 ± 1	93 ± 0
[C <sub>6</sub> mim][Cu(NCMe)(OTf) <sub>2</sub> ]	Measured	11 ± 1	74 ± 2	84 ± 2
	Normalised	-	88 ± 2	>99 ± 2
[C <sub>6</sub> mim][Cu(NCMe)(OTf) <sub>2</sub> .DMM]	Measured	14 ± 1	58 ± 3	71 ± 3
	Normalised	-	87 ± 3	92 ± 3

For CO:N<sub>2</sub> separations, in both mixed systems, by the second desorption the composition of the evolved gas is almost entirely CO, suggesting the mixed system can perform as well as the neat IL.

As seen previously, the CO/H<sub>2</sub> separations were less successful than CO/N<sub>2</sub>, however, there is still significant enrichment of >90 % CO evolved from the mixed liquid upon the second headspace sample.

Like the CO/N<sub>2</sub> separations, the DMM IL mixture gave similar enrichment values to the pure IL.

## 6.5 Conclusions

Addition of 1 mole equivalent of DBE to copper containing IL led to a less viscous mixture than the neat IL. The stability of the copper(I) in solution was demonstrated through NMR spectroscopy and the reversible binding of CO. Copper concentrations were reduced when the solvents were mixed, however remained relatively high and comparable to the established COSORB process. The dramatic reduction in viscosity is a major breakthrough with regards the viability of this technology to upscale for commercial use. Although the viscosity is not ideally as low as required, the reduction is, in some cases, two orders of magnitude lower which is a significant step.

The mixed systems showed some dicarbonyl behaviour, however, it was not as prominent as in the neat ILs. This was particularly noticeable during CO uptake experiments using the NTf<sub>2</sub> systems.

Selective absorption of CO in IL/DMM from gas mixtures containing N<sub>2</sub> and H<sub>2</sub> have been shown to be effective in only one absorption desorption cycle. Starting from a 50:50 mixture of CO/X<sub>2</sub> mixtures can be enriched to excellent levels. Although IL/DMM mixtures have shown to have a lower concentration of CO absorbed during these experiments, the % CO enrichment values remain high. Overall, the % CO values in CO:X<sub>2</sub> separation studies were similar using the neat or the mixed IL. The similarity in % CO enrichment values could be due to the large difference in solubility of CO to other

gases such as  $N_2$  and  $H_2$ . Since the CO absorption has been shown to be a lot higher than  $N_2$  and  $H_2$  in these ILs, a slight reduction in CO absorption will still result in a high net difference in solubility between the two gases. Therefore, enrichment values stay relatively similar.

## 6.6 References

- 1 Ş. İ. Kırbaşlar, S. Şahin and M. Bilgin, *J. Chem. Thermodyn.*, 2007, **39**, 284–290.
- 2 Dimethyl glutarate CAS 1119-40-0 | 814659,  
[http://www.merckmillipore.com/GB/en/product/Dimethyl-glutarate,MDA\\_CHEM-814659](http://www.merckmillipore.com/GB/en/product/Dimethyl-glutarate,MDA_CHEM-814659),  
(accessed 3 July 2019).
- 3 C. Wohlfarth, *Viscosity of dimethyl malonate*, Springer, Berlin, Heidelberg, 2017.
- 4 Dimethyl malonate 98% | Sigma-Aldrich,  
[https://www.sigmaaldrich.com/catalog/product/aldrich/136441?lang=en&region=GB&gclid=EAlalQobChMIrveDiYaZ4wIVU4fVCh345wP9EAAAYASAAEgKX0PD\\_BwE](https://www.sigmaaldrich.com/catalog/product/aldrich/136441?lang=en&region=GB&gclid=EAlalQobChMIrveDiYaZ4wIVU4fVCh345wP9EAAAYASAAEgKX0PD_BwE), (accessed 3 July 2019).
- 5 J. A. Hogendoorn, W. P. M. van Swaaij and G. F. Versteeg, *Chem. Eng. J. Biochem. Eng. J.*, 1995, **59**, 243–252.
- 6 M. L. Druin and S. I. Kreps, *Ind. Eng. Chem. Fundam.*, 1970, **9**, 79–83.
- 7 W. R. Moser, J. E. Clossen, A. W. Wang and S. A. Krouse, *J. Catal.*, 1985, **95**, 21–32.
- 8 J. M. Birbeck, A. Haynes, H. Adams, L. Damoense and S. Otto, *ACS Catal.*, 2012, **2**, 2512–2523.
- 9 A. Finotello, J. E. Bara, A. Dean Camper and Richard D. Noble, *Ind. Eng. Chem. Res.*, 2008, **47**, 3453–3459.

## **7. Overall Conclusions and Future Work**

## 7.1 Conclusions

To further investigate the scope of copper(I) containing ionic liquids to purify CO containing gas mixtures, a number of ionic liquids with the weakly coordinating anions  $\text{OTf}^-$  and  $\text{NTf}_2^-$  were synthesised. These types of ionic liquid showed enhanced properties over the copper halide systems such as lower viscosity, they were less hygroscopic and had the ability to coordinate a second CO molecule.

The ability to coordinate a second CO molecule to the copper presents an exciting opportunity not observed in other copper(I) based CO separation techniques. This should give a higher CO absorption capacity and the potential for a more selective purification process.

Compared to the copper(I) dihalide systems, the binding of CO was reversible over a wider temperature range of 25 °C – 140 °C. The release of CO required higher temperatures but was comparable over a short time scale. The samples were also robust under the operating conditions where over the course of months, with many absorption-desorption cycles performed and no loss of efficiency.

The potential for these liquids to separate a 50:50 mixture of  $\text{CO}:\text{X}_2$  ( $\text{X} = \text{N}_2$  or  $\text{H}_2$ ) was studied by high pressure IR spectroscopy and gas chromatography. It was shown that the  $\text{OTf}^-$  and  $\text{NTf}_2^-$  ionic liquids are at least capable of matching the copper(I) dihalide systems in their ability to purify CO gas mixtures after one absorption/partial desorption cycle. Since full desorption was not achieved, higher % CO values are expected and suggest they are a more effective absorbent.

By estimating the amount of CO absorbed at a given pressure, predictions were made regarding the effectiveness of these materials to purify  $\text{CO}/\text{CH}_4$  and  $\text{CO}/\text{CO}_2$  gas mixtures. It appears there is scope to separate  $\text{CO}/\text{CH}_4$  mixtures given the predicted selectivities. For  $\text{CO}/\text{CO}_2$  separations, there could be some selectivity if the separation is done at low pressures and the  $\text{CO}_2$  content was low.

Addition of a dibasic ester co-solvent (either DMM or DMG) led to a less viscous mixture than the neat ionic liquid, whilst the copper species remained stable. The dramatic reduction in viscosity is a notable observation and a significant step if this technology is to be commercialised. Selective absorption of CO from mixtures of N<sub>2</sub> and H<sub>2</sub> was also possible using these ionic liquid/DBE mixtures and the % CO remained high. This shows how this approach is viable and feasible to take forward.

Expanding the scope of the cations was also explored by incorporating ether and highly fluorinated substituents. CO absorption was still achieved, as well as selectivity from other gases such as N<sub>2</sub> and H<sub>2</sub>. The selectivity was similar to the alkyl imidazolium cations, showing adding functionality does not hinder the purification process. It also reinforced the notion that the anion has the dominating effect in these cases.

### 7.2 Future Work

The work performed throughout this project has been based on high pressure in-situ IR spectroscopy as a convenient way to monitor copper carbonyl formation. In addition to this, pressure changes in the headspace of the reactor were also monitored to estimate the amount of CO absorbed. A more accurate method to improve the analysis could be achieved by monitoring CO uptake by gravimetric or volumetric methods.

The formation of the copper carbonyl and copper dicarbonyl from the [Cu(NCMe)(OTf)(X)]<sup>-</sup> (X = OTf or NTf<sub>2</sub>) type ionic liquids has been proposed to coincide with the loss of MeCN. Further characterisation is necessary to determine the speciation. If the copper anionic species was paired with a small, symmetrical cation eg Et<sub>4</sub>N<sup>+</sup>, then upon cooling the system could crystallise forming a solid. If this could be reacted with CO and isolated in a crystalline form the structure could be characterised using X-ray crystallography.

The viscosities achieved using combinations of ionic liquid and DBE are approaching levels which would be viable for commercial use. Combining different ratios of ionic liquid to copper source to DBE is required to find an ideal system that possesses high copper concentration, as well as low viscosity.

Since these systems have been shown to purify CO gas mixtures and have properties that could work commercially, the next step would be to design a small test rig based on how the technology would operate on an industrial scale. This would optimise the absorption of CO into the liquid and give an indication as to how much sample is required to purify a certain volume of gas. From this more accurate comparisons could be drawn to more established methods such as the COSORB process to determine this technologies advantages and disadvantages.

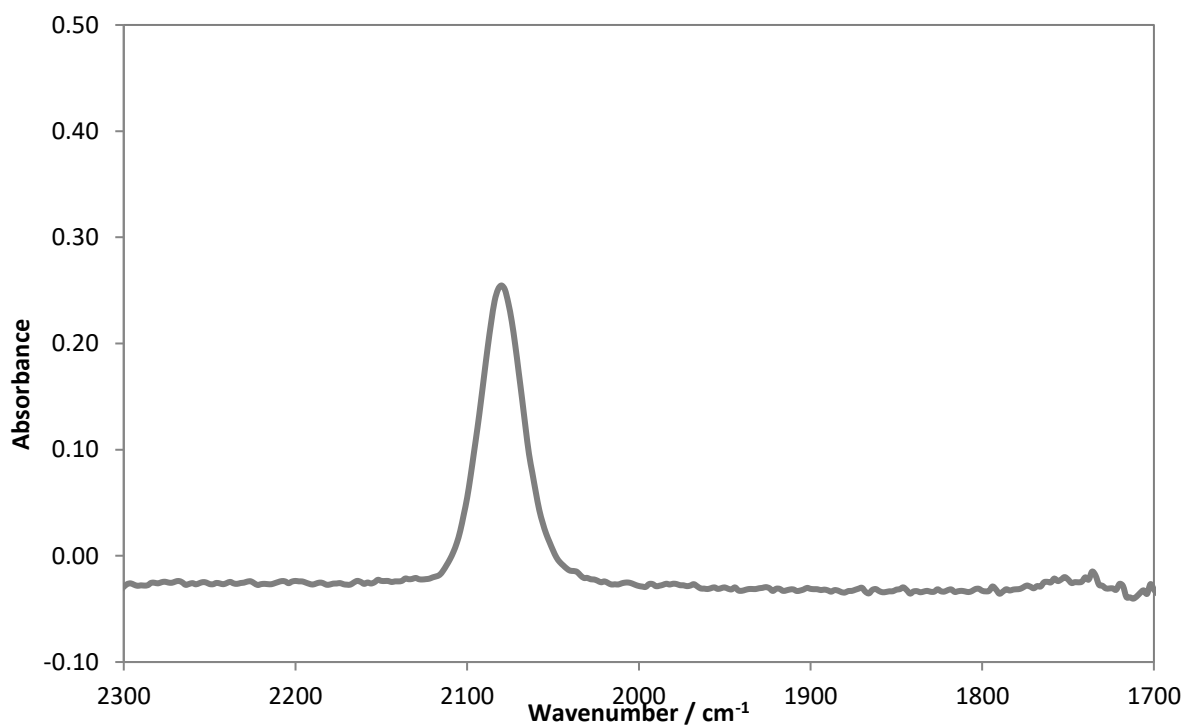
## **8. Appendix**

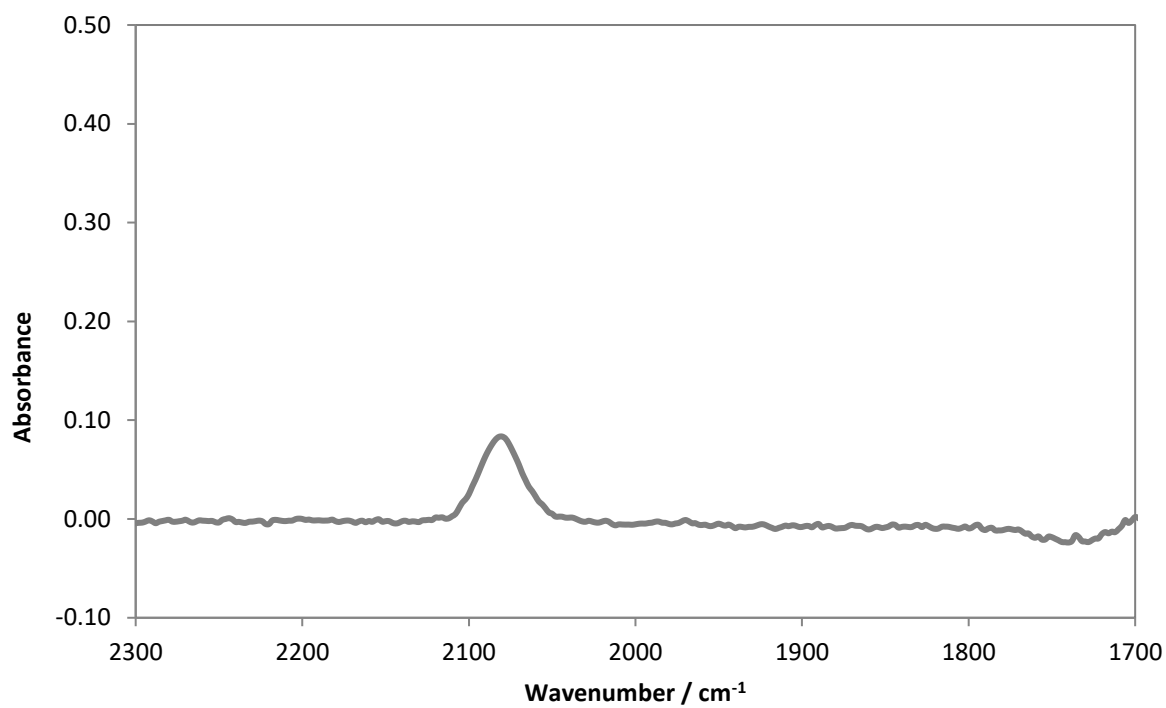
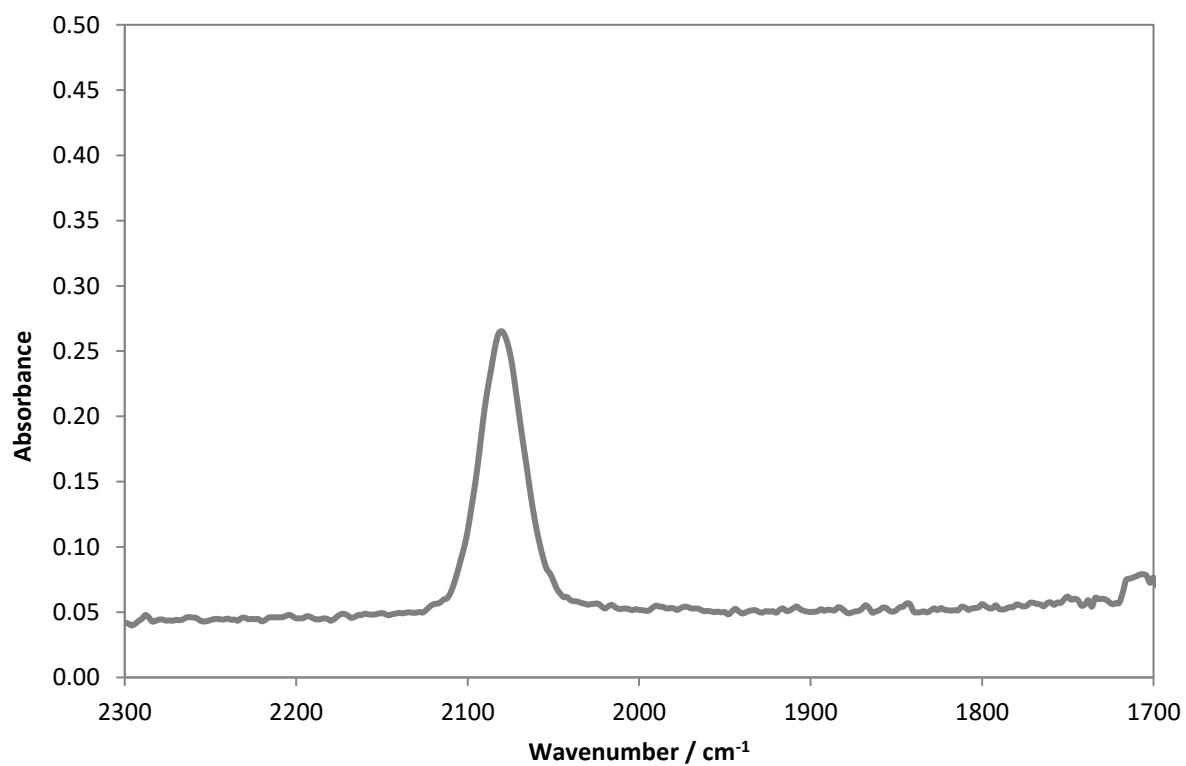
## 8.1 Sample IR Spectra

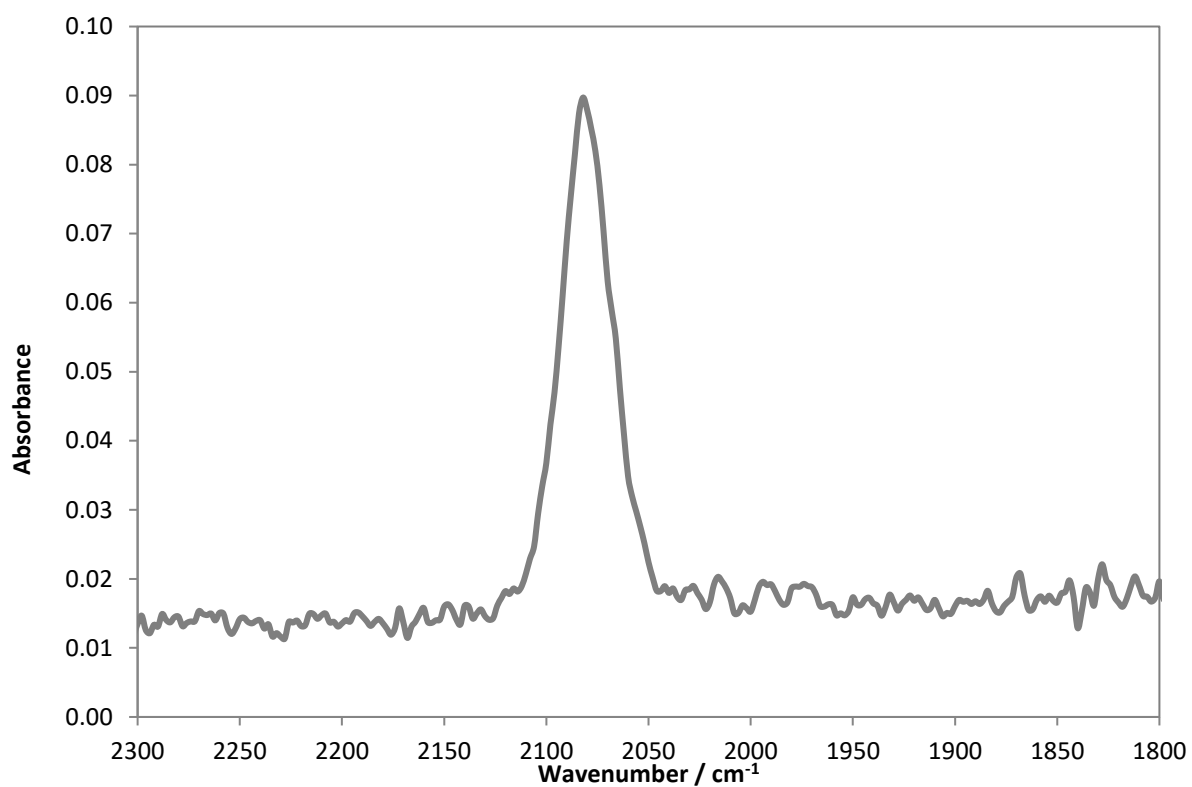
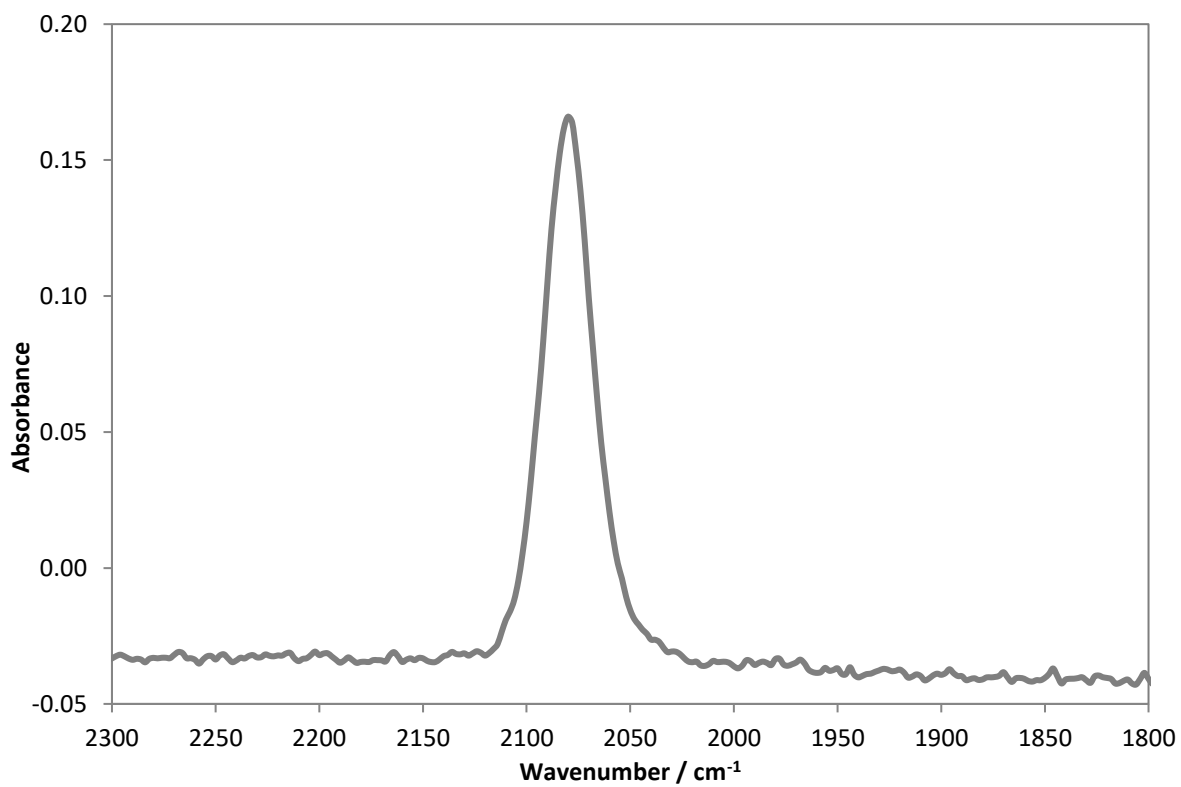
Example spectra showing the  $\nu(\text{CO})$  band(s) formed when the copper-containing ILs were reacted with CO.

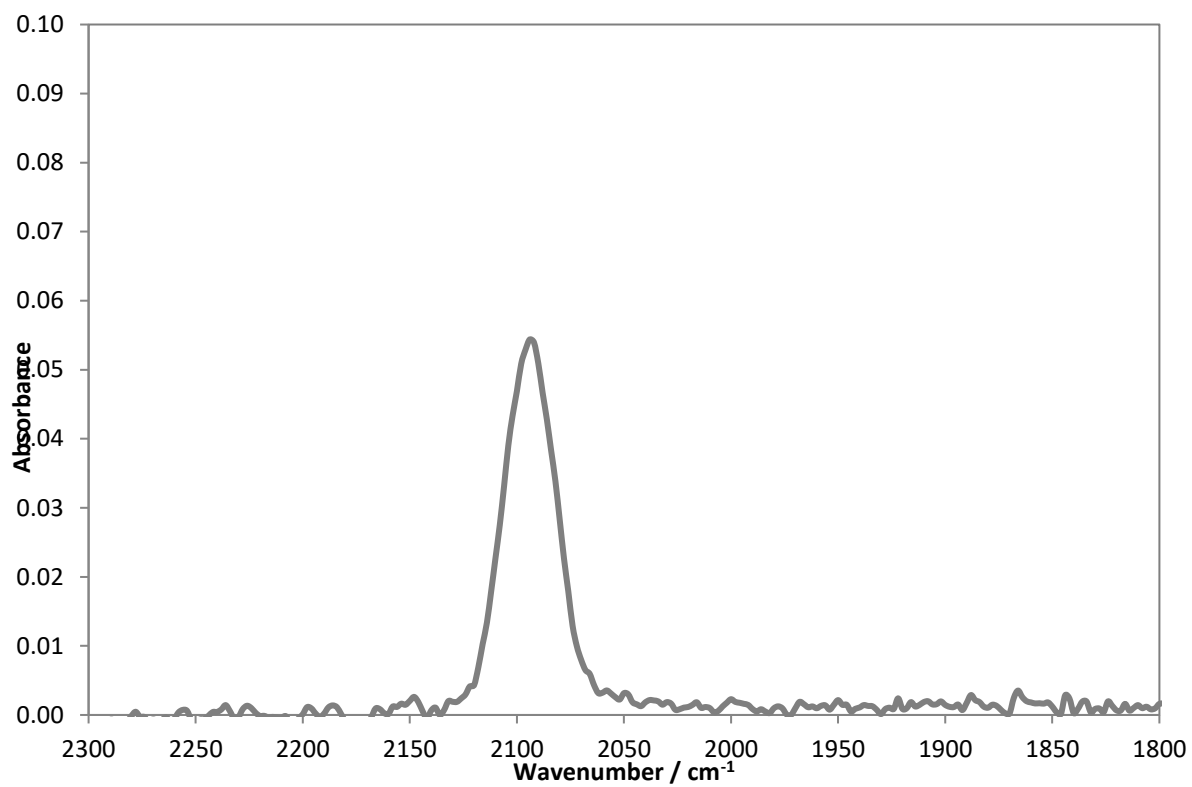
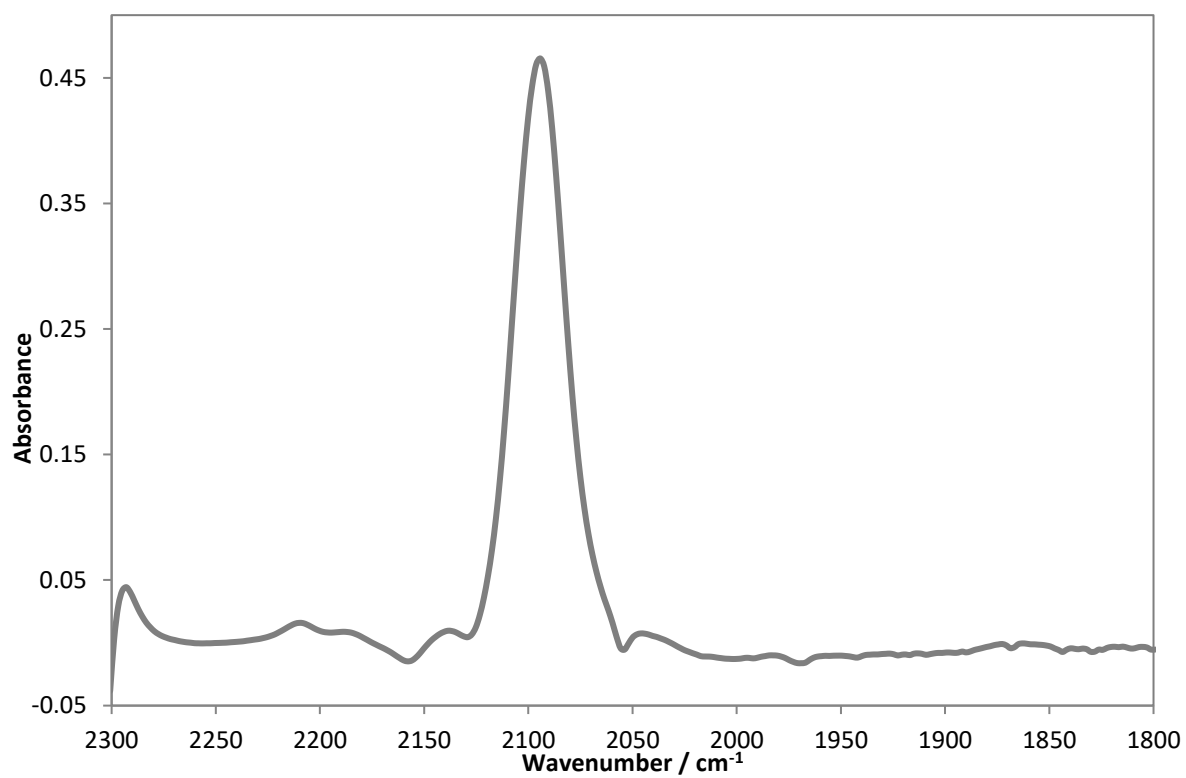
### 8.1.1 Neat Copper-Containing Ionic Liquids

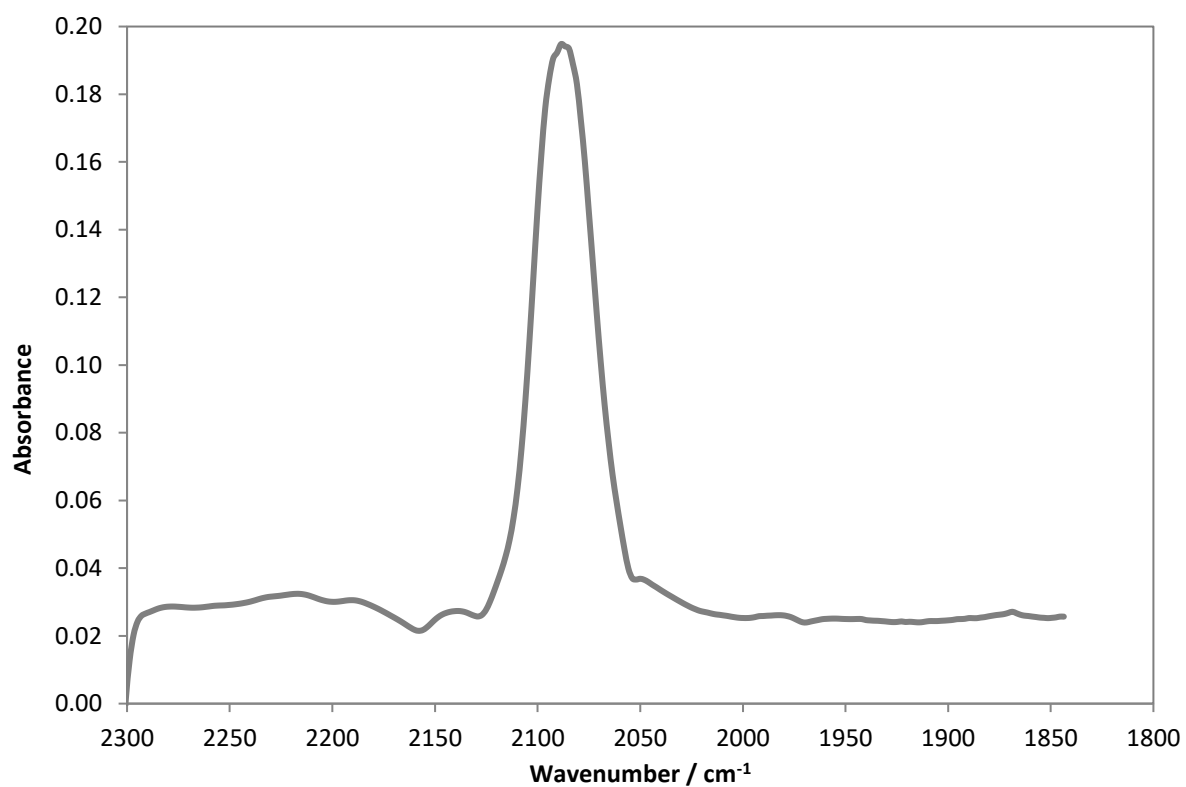
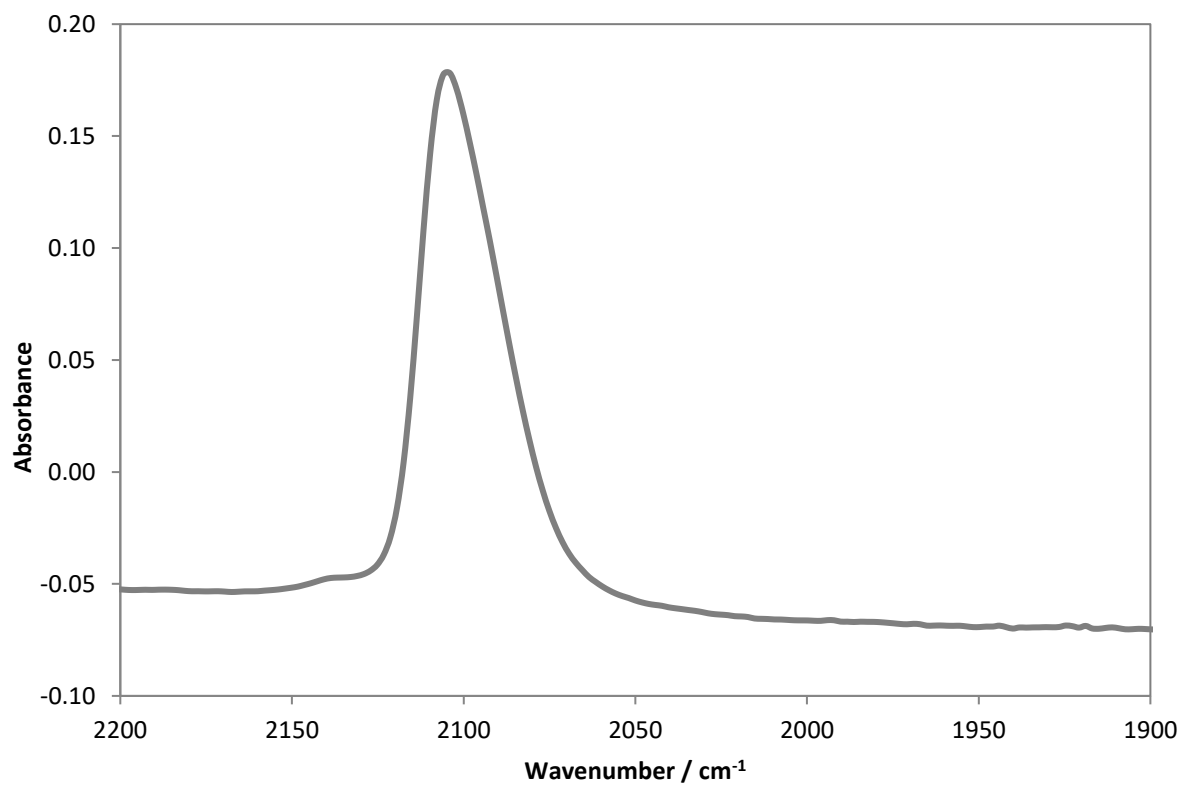
#### $[\text{C}_6\text{mim}][\text{CuBr}_2]$

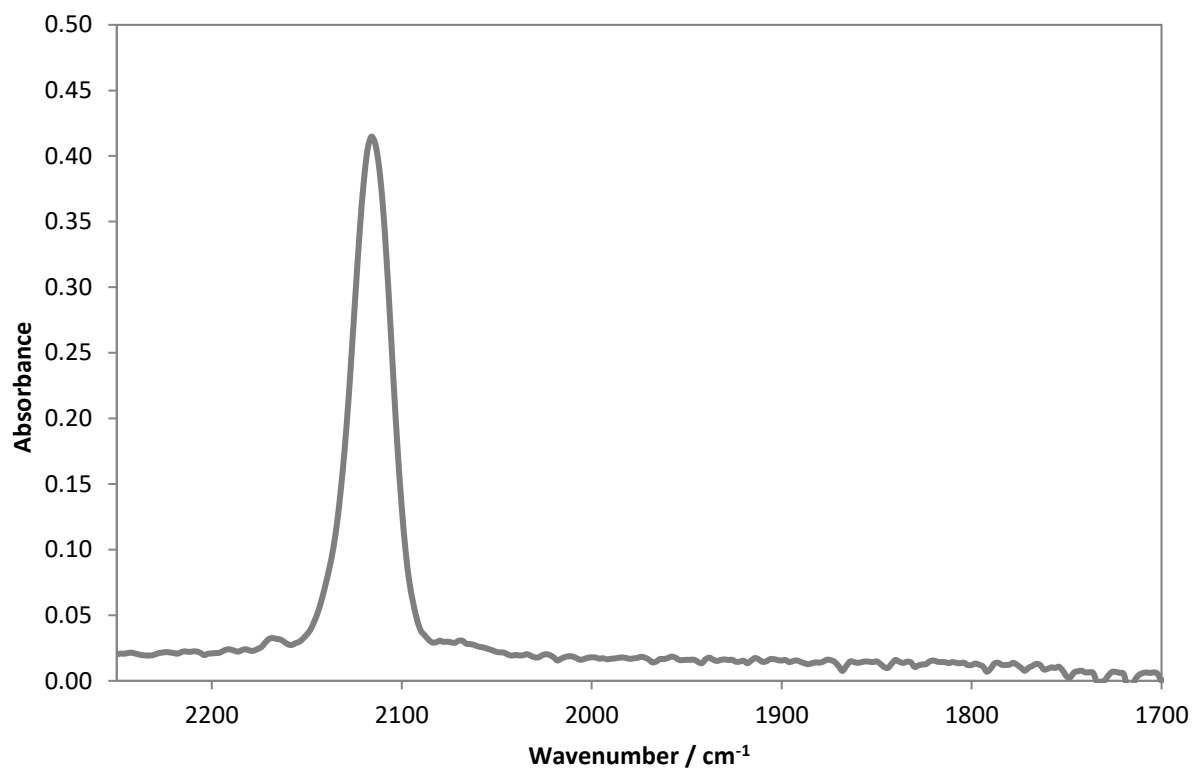
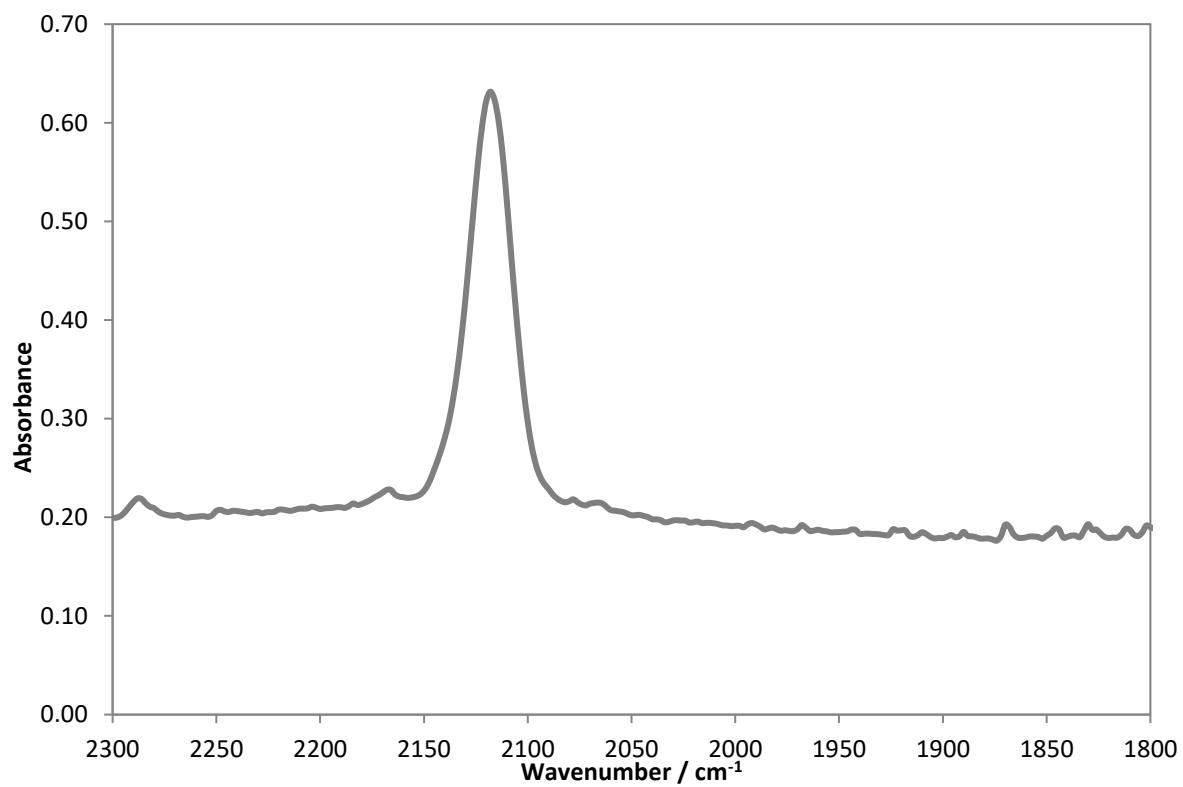


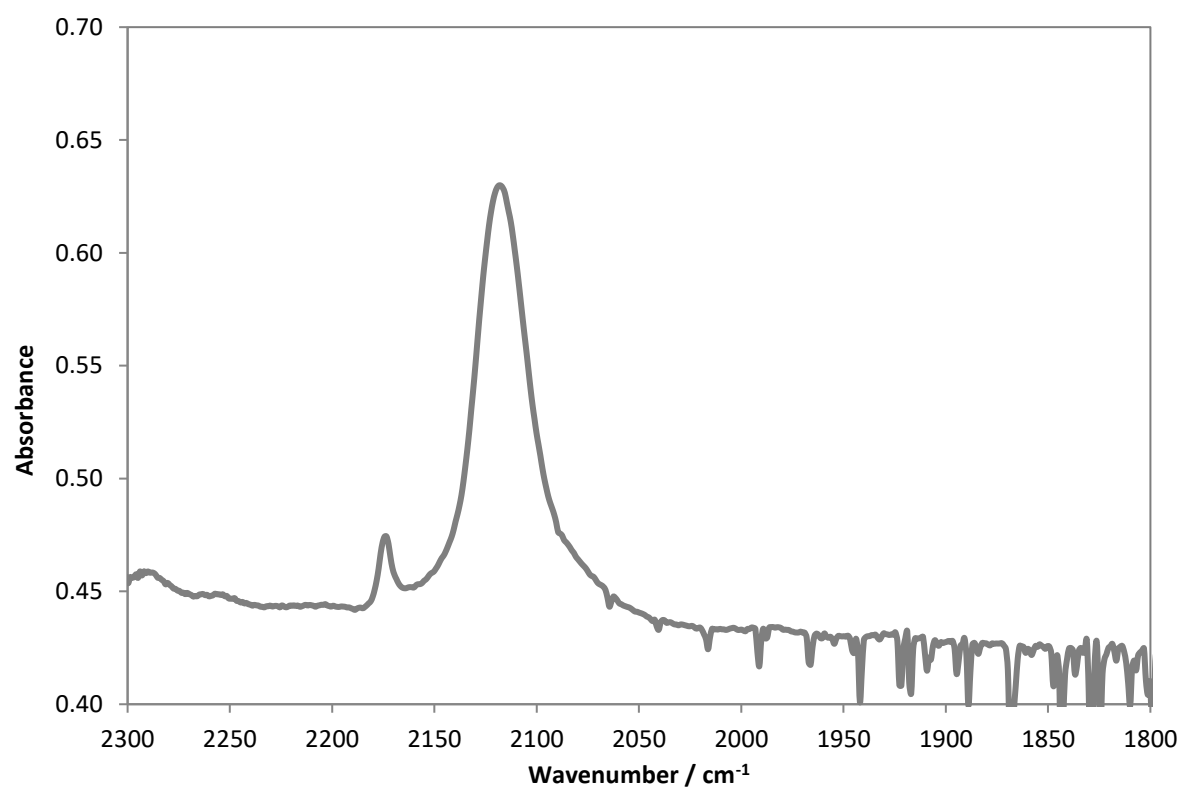
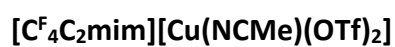
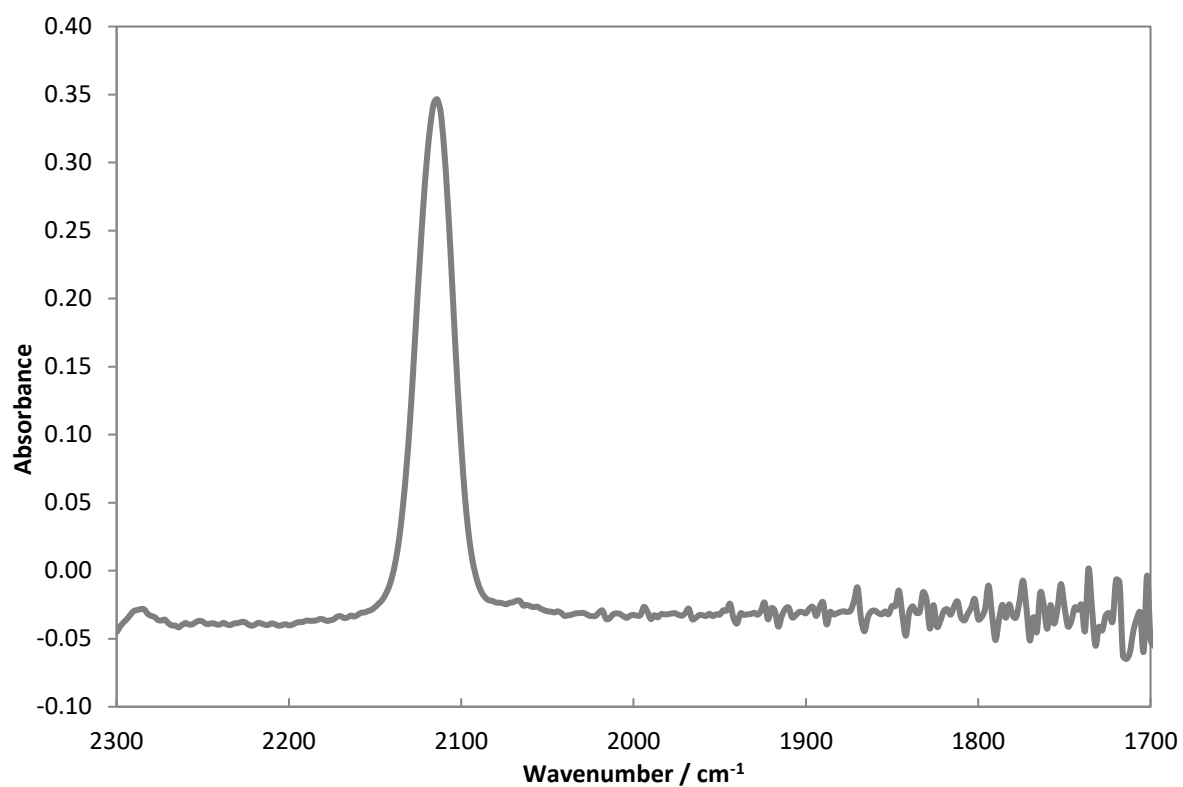
**[C<sub>3</sub>O<sub>1</sub>mim][CuBr<sub>2</sub>]****[C<sub>2</sub>(O<sub>1</sub>C<sub>2</sub>)<sub>2</sub>mim][CuBr<sub>2</sub>]**

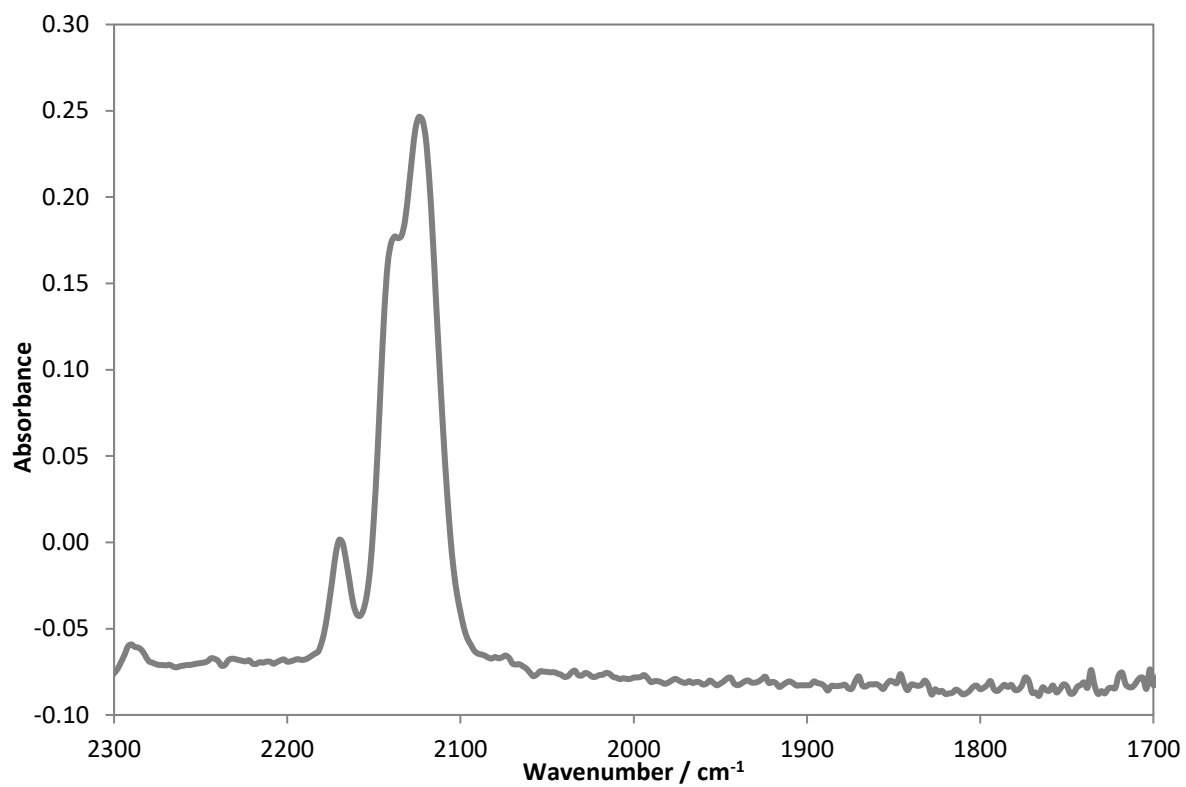
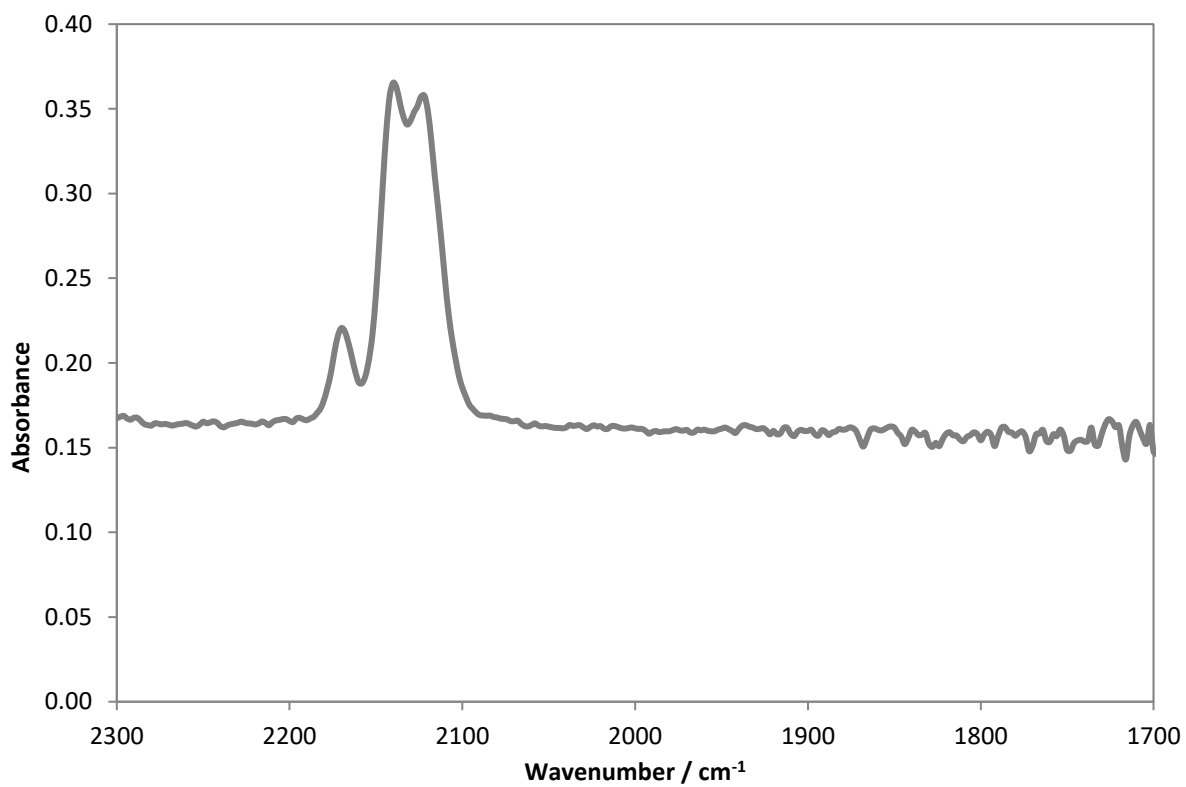
**[C<sub>6</sub>mim][Cu(OAc)<sub>2</sub>]****[C<sub>3</sub>O<sub>1</sub>mim][Cu(OAc)<sub>2</sub>]**

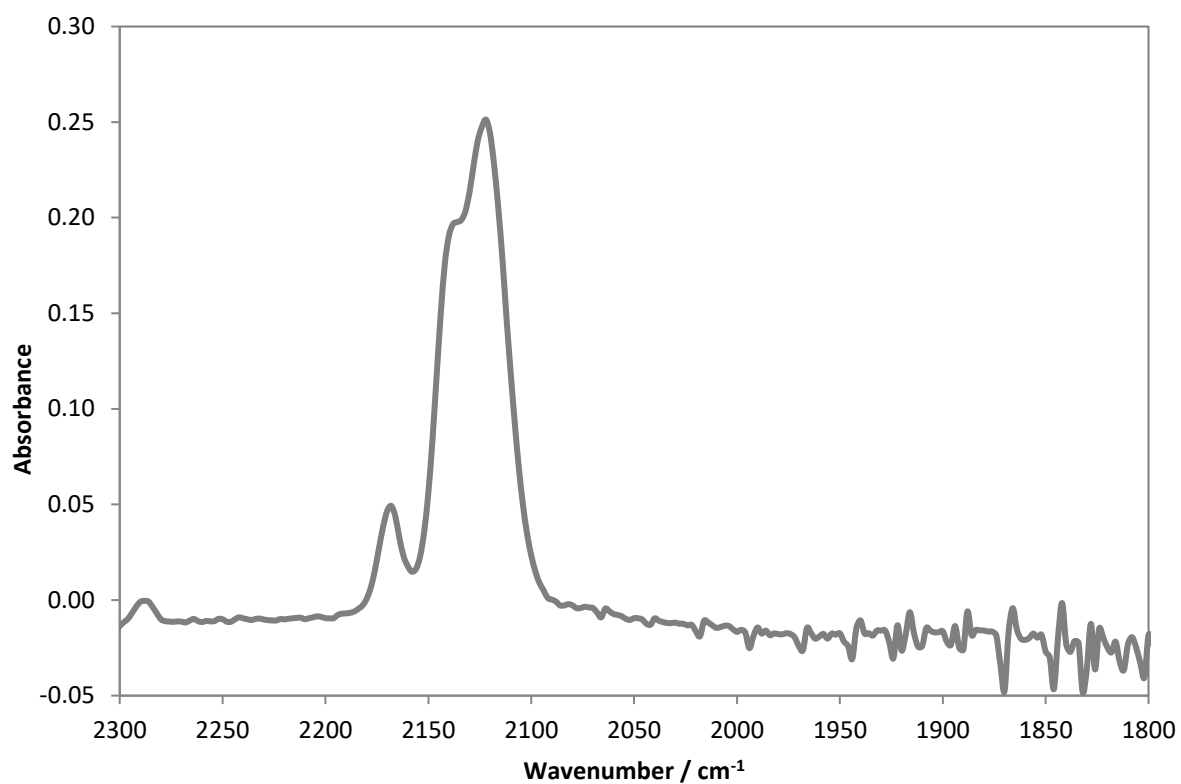
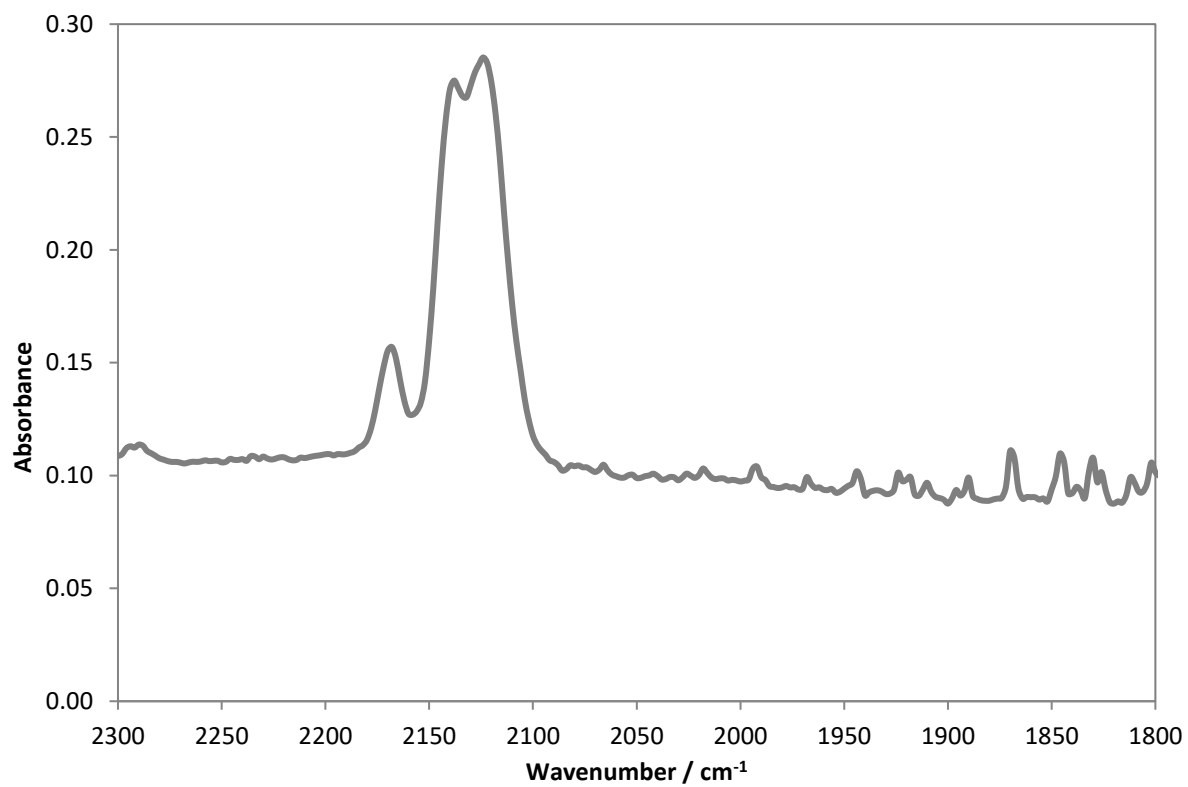
**[C<sub>2</sub>(O<sub>1</sub>C<sub>2</sub>)<sub>2</sub>mim][Cu(OAc)<sub>2</sub>]****[C<sub>6</sub>mim][Cu(TFA)<sub>2</sub>]**

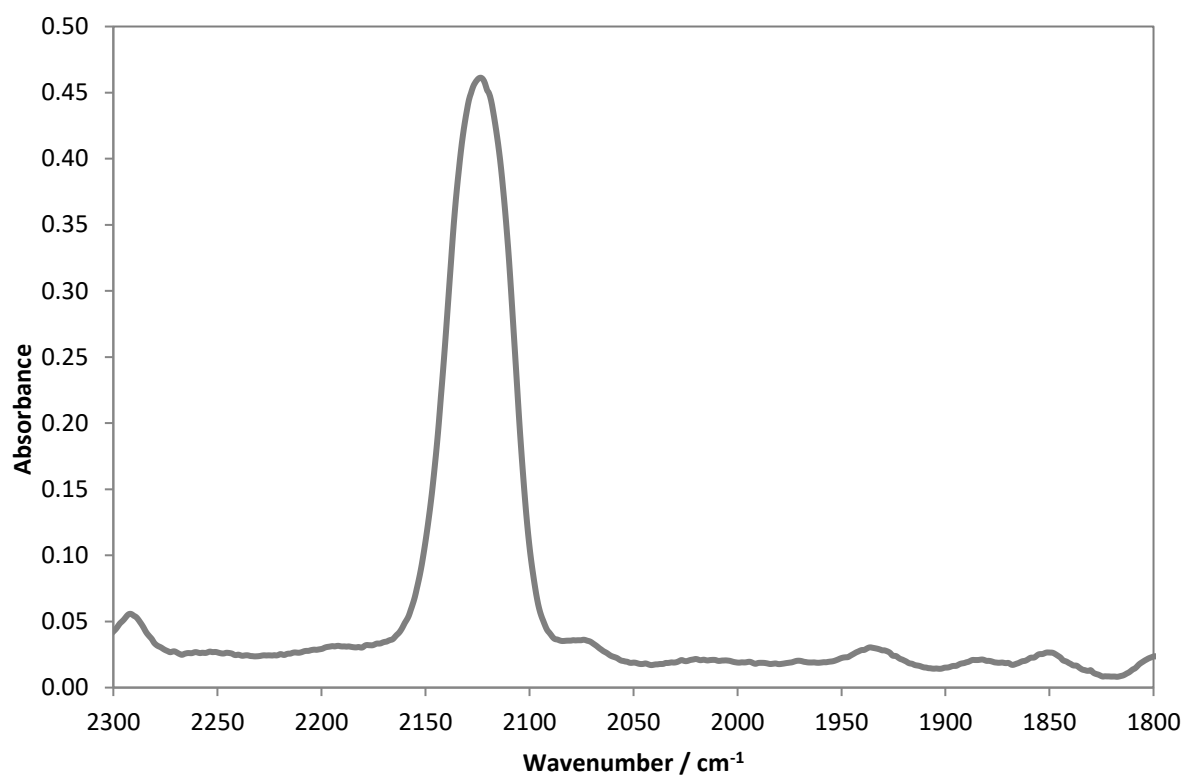
**[C<sub>3</sub>O<sub>1</sub>mim][Cu(TFA)<sub>2</sub>]****[C<sub>2</sub>(O<sub>1</sub>C<sub>2</sub>)<sub>2</sub>mim][Cu(TFA)<sub>2</sub>]**

**[C<sub>6</sub>mim][Cu(NCMe)(OTf)<sub>2</sub>]****[C<sub>3</sub>O<sub>1</sub>mim][Cu(NCMe)(OTf)<sub>2</sub>]**



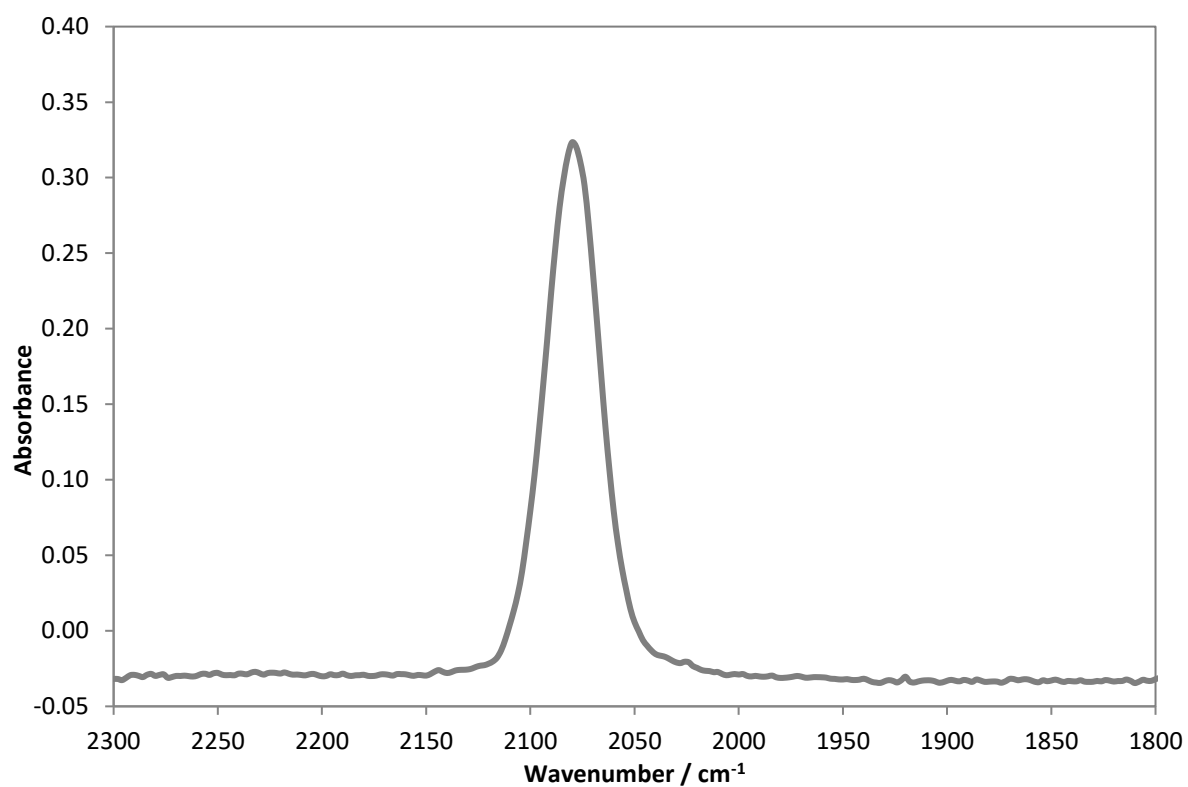
**[C<sub>2</sub>mim][Cu(NCMe)(OTf)(NTf<sub>2</sub>)]****[C<sub>6</sub>mim][Cu(NCMe)(OTf)(NTf<sub>2</sub>)]**

**[C<sub>3</sub>O<sub>1</sub>mim][Cu(NCMe)(OTf)(NTf<sub>2</sub>)]****[C<sub>2</sub>(O<sub>1</sub>C<sub>2</sub>)<sub>2</sub>mim][Cu(NCMe)(OTf)(NTf<sub>2</sub>)]**

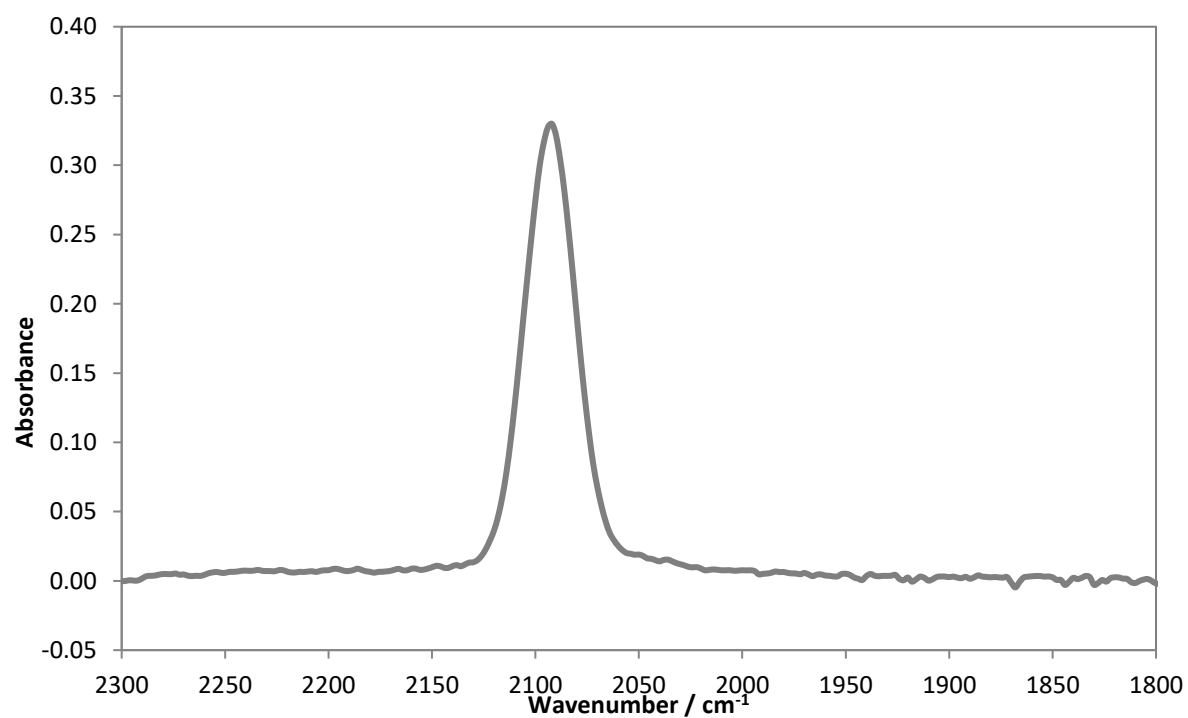
**[C<sup>F4</sup>C<sub>2</sub>mim][Cu(NCMe)(OTf)(NTf<sub>2</sub>)]**

### 8.1.2. Copper-Containing Ionic Liquid/DBE Mixtures

#### $[\text{C}_6\text{mim}][\text{CuBr}_2]\cdot\text{DMM}$



#### $[\text{C}_6\text{mim}][\text{Cu}_2\text{Br}_3]\cdot\text{DMM}$



## 8.2 HPIR Spectra

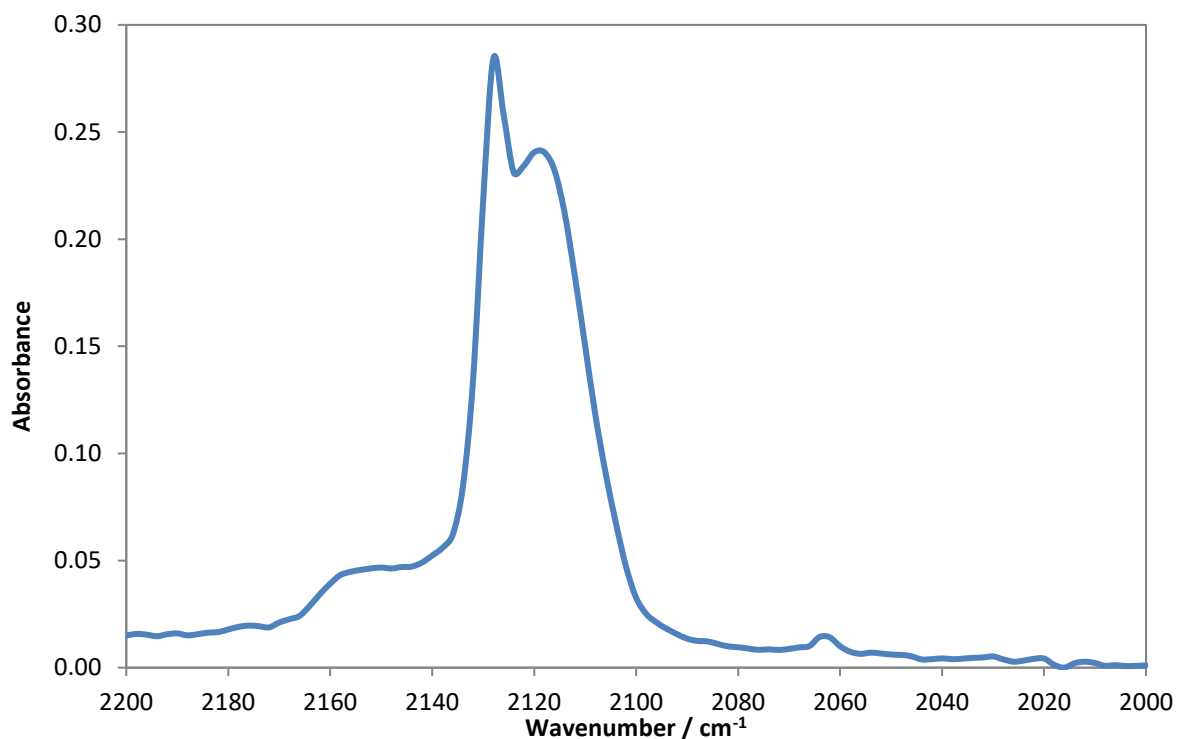


Figure 8.1. IR spectrum of the COSORB solution (0.1 M [Cu]) at 2 bar CO pressure and 25 °C.

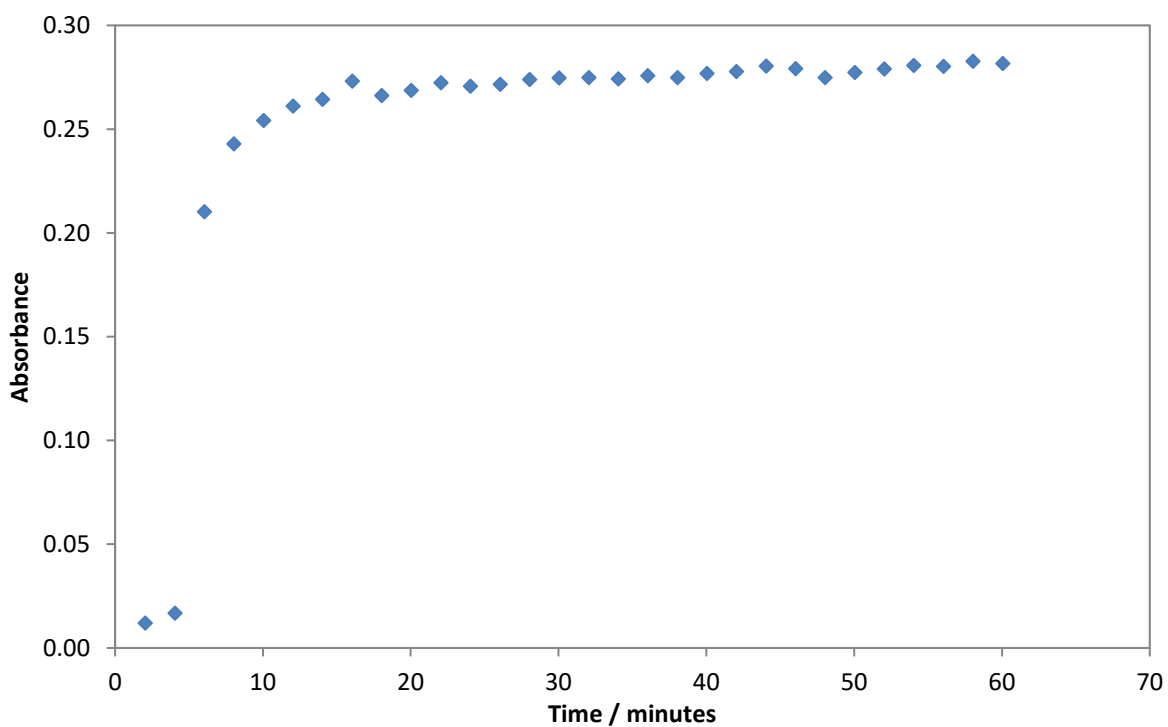
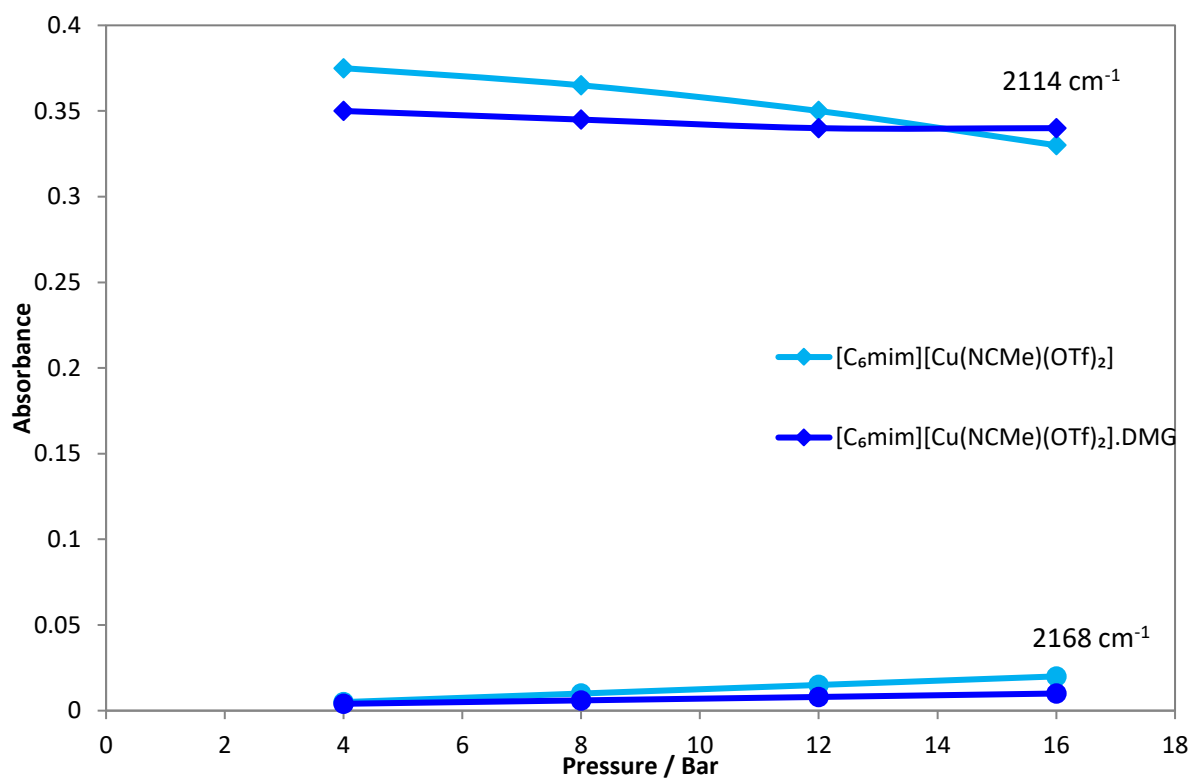
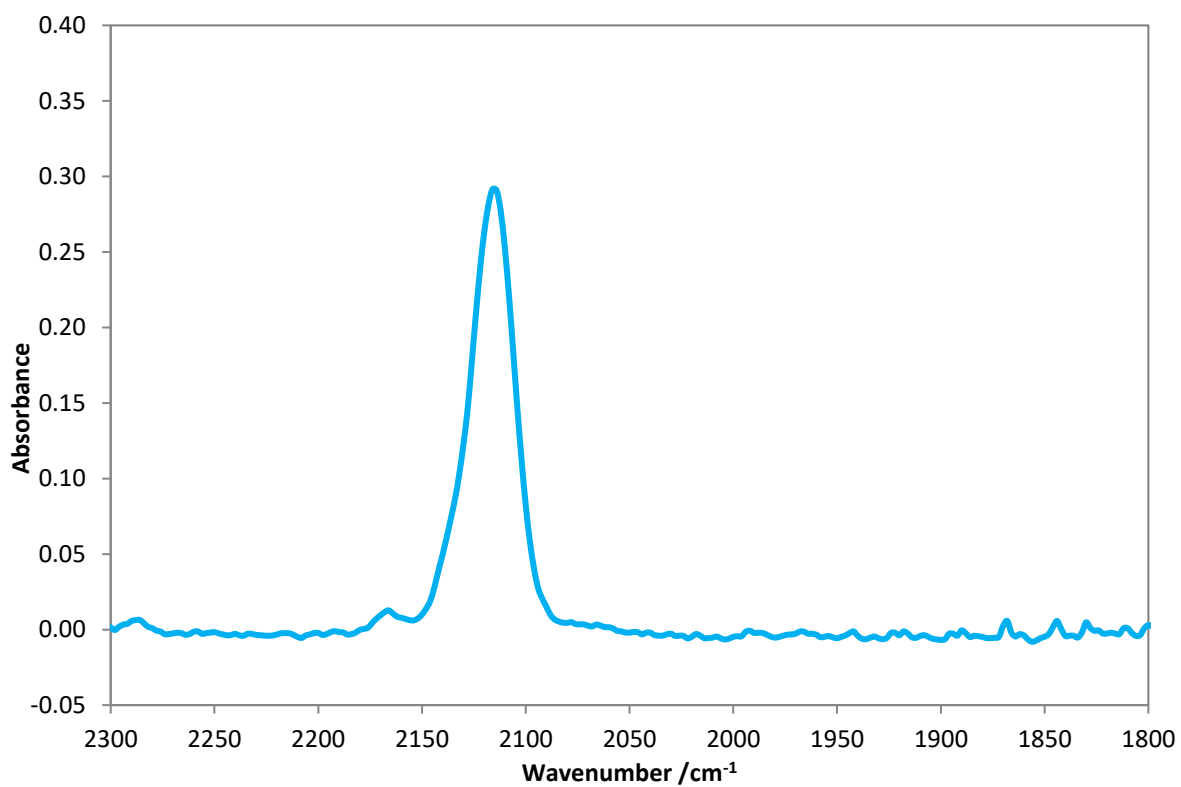


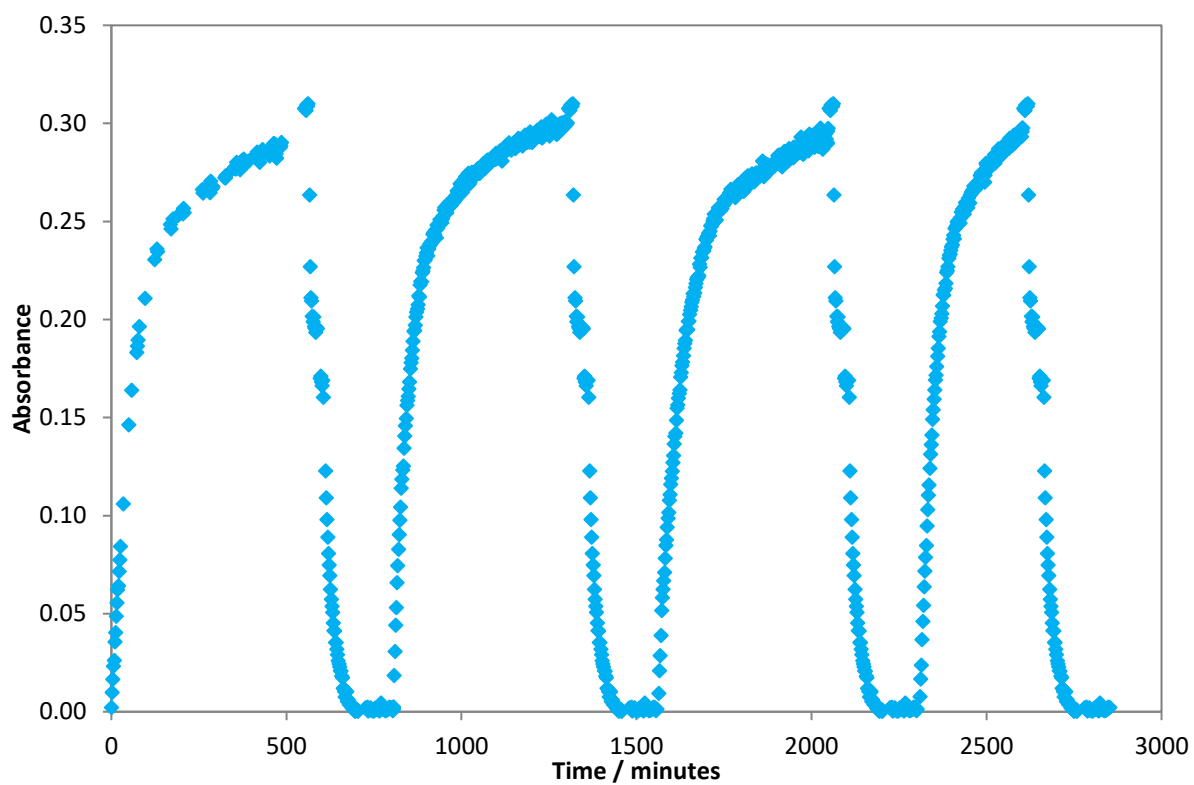
Figure 8.2. Plot of absorbance vs. time for the uptake of CO at 2128 cm<sup>-1</sup> by the COSORB solution (0.1 M [Cu]) on exposure to 2 bar CO at 25 °C and stirrer speed 214 rpm.



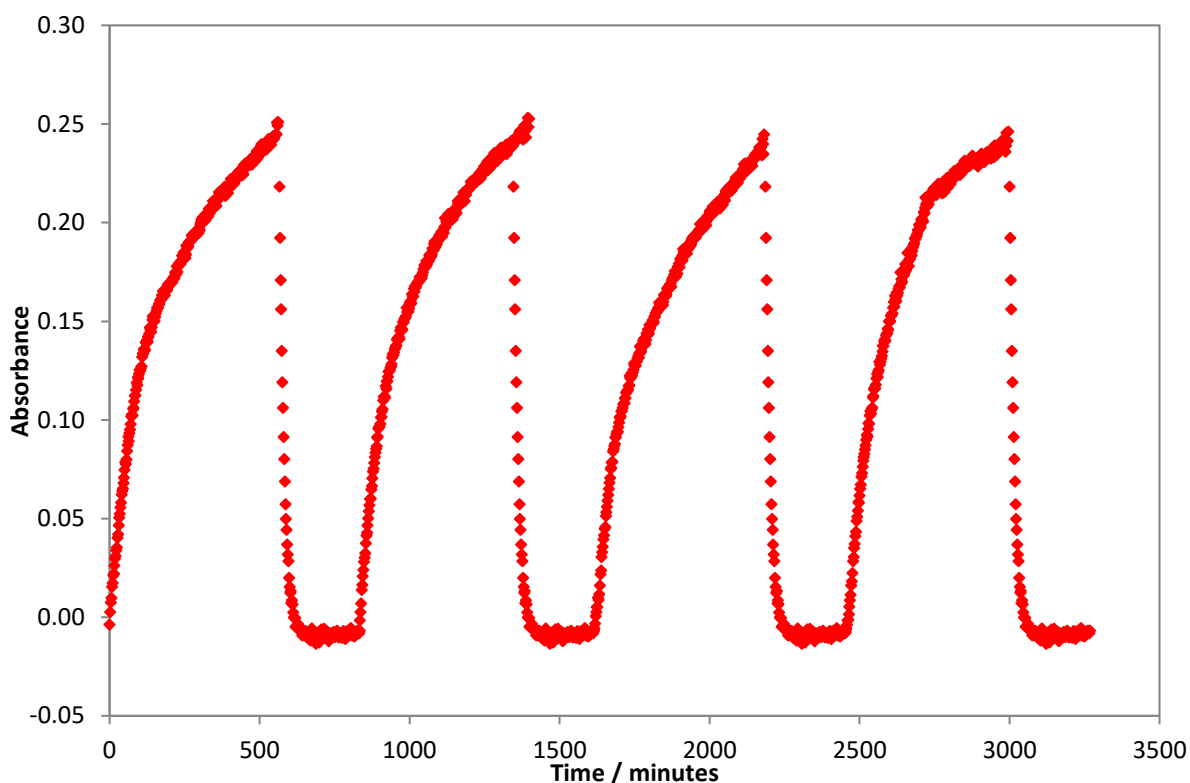
**Figure 8.3.** Equilibrium absorbances of [C<sub>6</sub>mim][Cu(NCMe)(OTf)<sub>2</sub>] with and without 1 equivalent of DMG at different pressures. Where blue = [C<sub>6</sub>mim][Cu(NCMe)(OTf)<sub>2</sub>] and dark blue = [C<sub>6</sub>mim][Cu(NCMe)(OTf)<sub>2</sub>].DMG; Squares = monocarbonyl peak at 2114 cm<sup>-1</sup> and circles = dicarbonyl peak at 2168 cm<sup>-1</sup>



**Figure 8.4.** Profile of [C<sub>6</sub>mim][Cu(NCMe)(OTf)<sub>2</sub>].DMM under 12 bar CO shows evidence of dicarbonyl formation through peak at 2136 cm<sup>-1</sup>.



**Figure 8.5.** Absorbance vs time plot showing the growth and decay of the  $\nu(\text{CO})$  band at  $2114\text{ cm}^{-1}$  of a sample of  $[\text{C}_6\text{mim}][\text{Cu}(\text{NCMe})(\text{OTf})_2]\cdot\text{DMM}$ . The absorption cycles were done by exposing the sample to 8 bar CO pressure and the desorption cycles were done by heating the sample up to  $140\text{ }^\circ\text{C}$  and purging with  $\text{N}_2$  at a stir rate of 214 rpm.



**Figure 8.6.** Absorbance vs time plot showing the growth and decay of the  $\nu(\text{CO})$  band at  $2122\text{ cm}^{-1}$  of a sample of  $[\text{C}_6\text{mim}][\text{Cu}(\text{NCMe})(\text{OTf})(\text{NTf}_2)]\cdot\text{DMM}$ . The absorption cycles were done by exposing the sample to 8 bar CO pressure and the desorption cycles were done by heating the sample up to  $140\text{ }^\circ\text{C}$  and purging with  $\text{N}_2$  at a stir rate of 214 rpm.

### 8.3 CO/ $\text{X}_2$ Enrichment Data

In a typical experiment, the CIR cell was pressurised to 10 bar with the appropriate mixture of 50:50 gas and sealed. The reaction was CO with copper(I) was tracked by IR until equilibrium was reached. At this point the stirring was ceased and the headspace gas was vented and sampled, this is termed 'LW-### at equilibrium'. Once vented, the cell was resealed and heated to drive off the absorbed CO until a new equilibrium formed or complete desorption occurred. At this point the headspace was sampled again to determine the % CO and %  $\text{X}_2$  by using the calibration plots described in chapter 5. These individual results were used to calculate a mean final % CO which were discussed in chapters 5 and 6.

**[C<sub>6</sub>mim][CuBr<sub>2</sub>]****Table 8.1.** Enrichment results for [C<sub>6</sub>mim][CuBr<sub>2</sub>] at 10 bar 50:50 CO:N<sub>2</sub> or CO:H<sub>2</sub> gas mixture

Experiment Number	Headspace % CO (measured)	Headspace % N <sub>2</sub> (measured)
LW-887g at equilibrium	34	66
LW-887g at equilibrium	34	66
LW-887i at equilibrium	40	60
LW-887i at equilibrium	40	60
LW-887g 1st desorb	92	8
LW-887i 1st desorb	90	10
LW-887i 1st desorb	91	9
Experiment Number	Headspace % CO (measured)	Headspace % H <sub>2</sub> (measured)
LW-887b at equilibrium	40	60
LW-887b at equilibrium	40	60
LW-887f at equilibrium	40	60
LW-887b 1st desorb	83	17
LW-887b 1st desorb	83	17
LW-887f 1st desorb	89	11

**[C<sub>3</sub>O<sub>1</sub>mim][CuBr<sub>2</sub>]****Table 8.2.** Enrichment results for [C<sub>3</sub>O<sub>1</sub>mim][CuBr<sub>2</sub>] at 10 bar 50:50 CO:N<sub>2</sub> gas mixture

Experiment Number	Headspace % CO (measured)	Headspace % N <sub>2</sub> (measured)
LW-898b at equilibrium	27	73
LW-898b at equilibrium	26	74
LW-898d at equilibrium	34	66
LW-898d at equilibrium	34	66
LW-898f at equilibrium	32	68
LW-898f at equilibrium	32	68
LW-898b desorb	87	13
LW-898b desorb	88	12
LW-898d desorb	87	13
LW-898d desorb	87	13
LW-898f desorb	86	14
LW-898f desorb	86	14

**[C<sub>2</sub>(O<sub>1</sub>C<sub>2</sub>)<sub>2</sub>mim][CuBr<sub>2</sub>]****Table 8.3.** Enrichment results for [C<sub>2</sub>(O<sub>1</sub>C<sub>2</sub>)<sub>2</sub>mim][CuBr<sub>2</sub>] at 10 bar 50:50 CO:N<sub>2</sub> gas mixture

Experiment Number	Headspace % CO (measured)	Headspace % N <sub>2</sub> (measured)
LW-899h at equilibrium	36	64
LW-899h at equilibrium	36	64
LW-899j at equilibrium	36	64
LW-899h desorb	88	12
LW-899h desorb	88	12
LW-899j desorb	88	12

**Table 8.4.** Enrichment results for [C<sub>2</sub>(O<sub>1</sub>C<sub>2</sub>)<sub>2</sub>mim][CuBr<sub>2</sub>] at 10 bar 50:50 CO:H<sub>2</sub> gas mixture

Experiment Number	Headspace % CO (measured)	Headspace % H <sub>2</sub> (measured)
LW-899b at equilibrium	18	82
LW-899b at equilibrium	18	82
LW-899d at equilibrium	37	63
LW-899d at equilibrium	37	63
LW-899b desorb	82	18
LW-899b desorb	88	12
LW-899d desorb	87	13
LW-899d desorb	87	13

**[C<sub>6</sub>mim][Cu(NCMe)(OTf)<sub>2</sub>]****Table 8.5.** Enrichment results for [C<sub>6</sub>mim][Cu(NCMe)(OTf)<sub>2</sub>] at 10 bar 50:50 CO:N<sub>2</sub> gas mixture

Experiment Number	Headspace % CO (measured)	Headspace % N <sub>2</sub> (measured)
LW-888b at equilibrium	11	89
LW-888i at equilibrium	6	94
LW-900b at equilibrium	11	89
LW-900b at equilibrium	11	89
LW-888b 1st desorb	72	28
LW-888i 1st desorb	67	33
LW-900b 1st desorption	72	28
LW-900b 1st desorption	72	28
LW-888b 2nd desorb	93	7
LW-888i 2nd desorb	78	22
LW-900b 2nd desorption	88	12
LW-900b 2nd desorption	88	12

**Table 8.6.** Enrichment results for [C<sub>6</sub>mim][Cu(NCMe)(OTf)<sub>2</sub>] at 10 bar 50:50 CO:H<sub>2</sub> gas mixture

Experiment Number	Headspace % CO (measured)	Headspace % H <sub>2</sub> (measured)
LW-888d at equilibrium	11	89
LW-888g at equilibrium	11	89
LW-888d 1st desorb	71	29
LW-888g 1st desorb	77	23
LW-888d 2nd desorb	82	18
LW-888g 2nd desorb	86	14

**[C<sub>2</sub>mim][Cu(NCMe)(OTf)(NTf<sub>2</sub>)]****Table 8.7.** Enrichment results for [C<sub>2</sub>mim][Cu(NCMe)(OTf)(NTf<sub>2</sub>)] at 10 bar 50:50 CO:N<sub>2</sub> gas mixture

Experiment Number	Headspace % CO (measured)	Headspace % N <sub>2</sub> (measured)
LW-881t at equilibrium	8	92
LW-881t at equilibrium	8	92
LW-881v at equilibrium	10	90
LW-881x at equilibrium	11	89
LW-881x at equilibrium	11	89
LW-881x at equilibrium	11	89
LW-881t 1st desorb	71	29
LW-881t 1st desorb	71	29
LW-881v 1st desorb	62	38
LW-881x 1st desorb	66	34
LW-881x 1st desorb	69	31
LW-881t 2nd desorb	82	18
LW-881t 2nd desorb	83	17
LW-881v 2nd desorb	71	29
LW-881x 2nd desorb	78	22

**Table 8.8.** Enrichment results for [C<sub>2</sub>mim][Cu(NCMe)(OTf)(NTf<sub>2</sub>)] at 10 bar 50:50 CO:H<sub>2</sub> gas mixture

Experiment Number	Headspace % CO (measured)	Headspace % H <sub>2</sub> (measured)
LW-881ab at equilibrium	17	83
LW-881ab at equilibrium	17	83
LW-881ad at equilibrium	5	95
LW-881ad at equilibrium	5	95
LW-881af at equilibrium	7	93
LW-881af at equilibrium	7	93
LW-881aj at equilibrium	3	97
LW-881ab 1st desorb	63	37
LW-881ab 1st desorb	63	37
LW-881ad 1st desorb	60	40
LW-881ad 1st desorb	60	40
LW-881af 1st desorb	52	48
LW-881af 1st desorb	52	48
LW-881aj 1st desorb	58	42
LW-881ab 2nd desorb	70	30
LW-881ad 2nd desorb	71	29
LW-881ad 2nd desorb	71	29
LW-881af 2nd desorb	63	37
LW-881af 2nd desorb	63	37
LW-881aj 2nd desorb	69	31

### [C<sub>2</sub>mim][Cu(NCMe)(OTf)(NTf<sub>2</sub>)] Stepwise Desorptions

**Table 8.9.** Enrichment results for [C<sub>2</sub>mim][Cu(NCMe)(OTf)(NTf<sub>2</sub>)] at 10 bar 50:50 CO:N<sub>2</sub> gas mixture

Experiment Number	Headspace % CO (measured)	Headspace % N <sub>2</sub> (measured)
LW-881k at equilibrium	11	89
LW-881k at equilibrium	11	89
LW-881o at equilibrium	13	87
LW-881o at equilibrium	12	87
LW-881r at equilibrium	13	87
LW-881r at equilibrium	11	89
LW-881r at equilibrium	11	89
LW-881k 1st desorb	54	46
LW-881k 1st desorb	54	46
LW-881o 1st desorb	56	44
LW-881o 1st desorb	56	44
LW-881r 1st desorb	45	55
LW-881r 1st desorb	45	55
LW-881k 2nd desorb	66	34
LW-881k 2nd desorb	66	34
LW-881o 2nd desorb	67	33
LW-881o 2nd desorb	67	33
LW-881r 2nd desorb	59	41
LW-881r 2nd desorb	59	41
LW-881k 3rd desorb	84	16
LW-881k 3rd desorb	85	15

LW-881o 3rddesorb	89	11
LW-881o 3rd desorb	90	10
LW-881r 3rd desorb	80	20
LW-881r 3rd desorb	80	20
LW-881k 4th desorb	90	10
LW-881k 4th desorb	90	10
LW-881o 4th desorb	97	3
LW-881r 4th desorb	93	7
LW-881r 4th desorb	93	7

**Table 8.10.** Enrichment results for [C<sub>2</sub>mim][Cu(NCMe)(OTf)(NTf<sub>2</sub>)] at 10 bar 50:50 CO:H<sub>2</sub> gas mixture

Experiment Number	Headspace % CO (measured)	Headspace % H <sub>2</sub> (measured)
LW-881al at equilibrium	5	95
LW-881al 1st desorb	42	58
LW-881al 2nd desorb	54	46
LW-881al 3rd desorb	73	27
LW-881al 4thdesorb	85	15

**[C<sub>6</sub>mim][CuBr<sub>2</sub>].DMM****Table 8.11.** Enrichment results for [C<sub>6</sub>mim][CuBr<sub>2</sub>].DMM at 10 bar 50:50 CO:N<sub>2</sub> gas mixture

Experiment Number	Headspace % CO (measured)	Headspace % N <sub>2</sub> (measured)
LW-892b at equilibrium	30	70
LW-892b at equilibrium	30	70
LW-892d at equilibrium	31	69
LW-892d at equilibrium	31	69
LW-892m at equilibrium	32	68
LW-892m at equilibrium	32	68
LW-892b desorb	87	13
LW-892b desorb	87	13
LW-892d desorb	89	11
LW-892d desorb	89	11
LW-892m desorb	89	11

**Table 8.12.** Enrichment results for [C<sub>6</sub>mim][CuBr<sub>2</sub>].DMM at 10 bar 50:50 CO:H<sub>2</sub> gas mixture

Experiment Number	Headspace % CO (measured)	Headspace % H <sub>2</sub> (measured)
LW-892f at equilibrium	33	67
LW-892f at equilibrium	33	67
LW-892h at equilibrium	40	60
LW-892h at equilibrium	39	61
LW-892f desorb	93	7
LW-892f desorb	93	7
LW-892h desorb	88	12
LW-892h desorb	88	12

**[C<sub>6</sub>mim][Cu(NCMe)(OTf)<sub>2</sub>].DMM****Table 8.13.** Enrichment results for [C<sub>6</sub>mim][Cu(NCMe)(OTf)<sub>2</sub>].DMM at 10 bar 50:50 CO:N<sub>2</sub> gas mixture

Experiment Number	Headspace % CO (measured)	Headspace % N <sub>2</sub> (measured)
LW-901b at equilibrium	9	91
LW-901b at equilibrium	9	91
LW-901d at equilibrium	10	90
LW-901d at equilibrium	10	90
LW-901b 1st desorb	65	35
LW-901b 1st desorb	65	35
LW-901d 1st desorb	65	35
LW-901d 1st desorb	65	35
LW-901b 2nd desorb	82	18
LW-901b 2nd desorb	82	18
LW-901d 2nd desorb	77	23
LW-901d 2nd desorb	77	23

**Table 8.14.** Enrichment results for [C<sub>6</sub>mim][Cu(NCMe)(OTf)<sub>2</sub>].DMM at 10 bar 50:50 CO:H<sub>2</sub> gas mixture

Experiment Number	Headspace % CO (measured)	Headspace % H <sub>2</sub> (measured)
LW-901f at equilibrium	13	87
LW-901f at equilibrium	13	87
LW-901h at equilibrium	14	86
LW-901h at equilibrium	14	86
LW-901f 1st desorb	59	41
LW-901f 1st desorb	64	36
LW-901h 1st desorb	55	45
LW-901h 1st desorb	55	45
LW-901f 2nd desorb	76	24
LW-901f 2nd desorb	76	24
LW-901h 2nd desorb	66	34
LW-901h 2nd desorb	66	34

**[C<sub>2</sub>mim][Cu(NCMe)(OTf)(NTf<sub>2</sub>)].DMM****Table 8.15.** Enrichment results for [C<sub>2</sub>mim][Cu(NCMe)(OTf)(NTf<sub>2</sub>)].DMM at 10 bar 50:50 CO:N<sub>2</sub> gas mixture

Experiment Number	Headspace % CO (measured)	Headspace % N <sub>2</sub> (measured)
LW-891d at equilibrium	10	90
LW-891d at equilibrium	10	90
LW-891h at equilibrium	13	87
LW-891h at equilibrium	13	87
LW-891j at equilibrium	14	86
LW-891j at equilibrium	14	86
LW-891d 1st desorb	55	45
LW-891d 1st desorb	55	45
LW-891d 1st desorb	58	42
LW-891d 1st desorb	58	42
LW-891d 1st desorb	51	49
LW-891d 1st desorb	51	49
LW-891d 2nd desorb	69	31
LW-891d 2nd desorb	69	31
LW-891d 2nd desorb	74	26
LW-891d 2nd desorb	74	26
LW-891d 2nd desorb	67	33
LW-891d 2nd desorb	67	33

**Table 8.16.** Enrichment results for [C<sub>2</sub>mim][Cu(NCMe)(OTf)(NTf<sub>2</sub>)]<sub>2</sub>.DMM at 10 bar 50:50 CO:H<sub>2</sub> gas mixture

Experiment Number	Headspace % CO (measured)	Headspace % H <sub>2</sub> (measured)
LW-891l at equilibrium	11	89
LW-891l at equilibrium	12	88
LW-891q at equilibrium	11	89
LW-891q headspace	12	88
LW-891l 1st desorb	51	49
LW-891l 1st desorb	50	50
LW-891q 1st desorb	53	47
LW-891l 2nd desorb	70	30
LW-891l 2nd desorb	70	30
LW-891q 2nd desorb	70	30